Naval Surface Warfare Center

Carderock Division

West Bethesda, MD 20817-5700

NSWCCD-80-TR-2029/??? **February 2020**

Naval Architecture and Engineering Department

Technical Report

CONTINUED DEVELOPMENT OF SECOND GENERATION INTACT STABILITY CRITERIA

by

Vadim Belenky
NSWCCD

REPORT DOCUMENTATION PAGE

Form Approved
OMB No. 0704-0188

1. REPORT DATE *(DD-MM-YYYY)*	**2. REPORT TYPE**	**3. DATES COVERED** *(From - To)*
02-03-2020	Final	May 2016-Oct 2017

4. TITLE AND SUBTITLE
Continued Development Of Second Generation Intact Stability Criteria

5a. CONTRACT NUMBER
DCO16XMSR001

5b. GRANT NUMBER

5c. PROGRAM ELEMENT NUMBER

6. AUTHOR(S)
Vadim Belenky

5d. PROJECT NUMBER

5e. TASK NUMBER

5f. WORK UNIT NUMBER

7. PERFORMING ORGANIZATION NAME(S) AND ADDRESS(ES)
NAVSEA Carderock
Naval Surface Warfare Center
Carderock Division (Code 851)
9500 Macarthur Boulevard
West Bethesda, MD 20817-5700

8. PERFORMING ORGANIZATION REPORT NUMBER
NSWCCD-80-TR-2020/0000

9. SPONSORING / MONITORING AGENCY NAME(S) AND ADDRESS(ES)
United States Coast Guard
Office of Design and Engineering Standards
Naval Architecture Division
2703 Martin Luther King, Jr. Ave., SE
Washington DC 20593-7509

10. SPONSOR/MONITOR'S ACRONYM(S)
CG-ENG-2

11. SPONSOR/MONITOR'S REPORT NUMBER(S)

12. DISTRIBUTION / AVAILABILITY STATEMENT
Approved for public release;Distribution unlimited

13. SUPPLEMENTARY NOTES

14. ABSTRACT
The report describes the current U.S. contribution to the development of the second generation IMO intact stability criteria. It includes an evaluation of inconsistency in the vulnerability criteria, a considertion of an alernative formulation, an example of direct stability assessment, a demonstrattion of the development of operational guidance and limitation, and contributions to the explanatory notes.

15. SUBJECT TERMS
IMO, Intact Stability, Criteria, Parametric Roll, Pure Loss of Stability, Dead Ship Condition, Direct Stability Assessment, Operational Guidance

16. SECURITY CLASSIFICATION OF:			**17. LIMITATION OF ABSTRACT**	**18. NUMBER OF PAGES**	**19a. NAME OF RESPONSIBLE PERSON**
					Vadim Belenky
a. REPORT	**b. ABSTRACT**	**c. THIS PAGE**	Unclass.	250	**19b. TELEPHONE NUMBER** *(include area code)* 301-227-1720
Unclassified	Unclassified	Unclassified			

Standard Form 298 (Rev. 8-98)
Prescribed by ANSI Std. Z39.18

THIS PAGE INTENTIONALLY LEFT BLANK

CONTENTS

FIGURES

TABLES

ADMINISTRATIVE INFORMATION

The work described in this report was performed by the Simulations and Analysis Branch (Code 851) of the Surface Ship Hydromechanics Division (Code 85) of the Naval Architecture and Engineering Department at the Naval Surface Warfare Center, Carderock Division (NSWCCD). The work was funded by the U.S. Coast Guard Headquarters, Office of Design and Engineering Standards Naval Architecture Division (CG-ENG-2), in FY 2016-2017.

ACKNOWLEDGEMENTS

The developments in the procedures described in this report were based on the results of research funded by the Office of Naval Research (ONR), under the ongoing research project, "A Probabilistic Procedure for Evaluating the Dynamic Stability and Capsizing of Naval Vessels" under the direction of Dr. Woei-Min Lin.

The author is very grateful for important technical discussions, help and support from Mr. Kenneth Weems, Dr. Arthur Reed, Mr. Timothy Smith, Mr. Bradley Campbell, Dr. Mike Levine (NSWCCD), Prof. Kostas Spyrou (National Technical University of Athens, Greece) and Prof. Vladas Pipiras (University of North Carolina at Chapel Hill). The author would also like to recognize fruitful discussions with Prof. Naoya Umeda (Osaka University, Japan), Prof. Toru Katayama (University of Osaka Prefecture, Japan), Dr. Vladimir Shigunov (DNV-GL, Germany), Dr. Adriana Oliva Remolà (Universidad Politecnica de Madrid, Spain) and Mr. Cleve Wandji (BV, France).

The author would like to extened special gratitude to the technical editor Mr. Shane McCabe for his invaluable help in the prepartaion of this report.

SUMMARY

Significant changes in the design and operation of commercial ships have occurred over the last several decades. These changes, and their impact on the intact stability performance of ships, have motivated the development of a second generation of intact stability criteria by the IMO Sub-Committee on Ship Design and Constriction (SDC) (formerly the Sub-Committee on Stability and Load Lines and on Fishing Vessels Safety (SLF)). Parametric roll resonance, pure loss of stability, broaching-to, stability in dead ship condition and excessive accelerations are among the stability failure modes that are addressed. The second generation intact stability criteria are planned to have a multi-tiered structure. As the direct assessment of dynamic stability may not be necessary for all ships covered by IMO instruments, the first two tiers consist of level 1 and 2 vulnerability criteria that are used as a preliminary design process check of dynamic stability failure risk.

The report describes current U.S. contributions to this development. It includes a study of inconsistency between the levels (when vulnerability is not indicated by level 1 criterion, but indicated by the level 2 criterion). The inconsistency problem is considered for criteria for pure loss of stability, parametric roll and dead ship condition. Alternative vulnerability criteria are proposed. Sample calculations are reported for dead ship condition and excessive accelerations. An example of direct stability assessment for parametric roll is described, including the validation of the simulation tool used in the assessment. Another example of direct assessment includes the application of two methods of extrapolation for pure loss of stability, accompanied by a description of the validation of these extrapolation methods. The report also demonstrates a development of operational guidance for parametric roll based in the information produced by direct stability assessment and from the outcome of the level 2 vulnerability assessment. Contributions are also made to the development of the explanatory notes: a refinement of description of roll damping calculations and a sample data set for vulnerability assessment including final and intermediate results.

1. INTRODUCTION

1.1 The Context of this Work

Sufficient intact stability is one of the most fundamental requirements for any type of vessel. Current international stability regulations are collected inhave been established from the 2008 Intact Stability (IS) Code (Code). The Code was adopted by resolution MSC.267 (85) of the Maritime Safety Committee (MSC) of International Maritime Organization (IMO) and came into force in July 2010.

Stability criteria intended for all types of ships, can be found in two sections of the Code: requirements for GZ curve in section 2.2, and severe wind and rolling criterion (also known as the weather criterion) in section 2.3. The criteria from section 2.2 have originated from works by Rahola (1939), which is embodied in Res. A.167 (ES.IV). The work on the weather criterion that commenced in the 1950s (Kobylinski & Kastner, 2003) is embodied in Res. A.749 (18).

The Code recognizes that the fleet is evolving and the Code "should not remain static" (paragraph 2 of the Preamble). The Code also notes the variety of types of ship and complexity of physical phenomena involved in stability analysis, and recognizes that "...problems of safety against accidents related to stability have generally not yet been solved" (paragraph 2 of the Preamble). Directions for further development are formulated in Chapter 1 of Part A of the Code. Priority is given to development of performance oriented criteria for

- Righting arm variation, resulting in parametric roll resonance and pure loss of stability (paragraph 1.2.1)
- Resonant roll in dead ship conditions (paragraph 1.2.2)
- Broaching and other maneuvering related phenomena (paragraph 1.2.3)

The intact stability working group of IMO Subcommittee on Stability and Load Lines and on Fishing Vessels Safety (SLF) was assigned this task. The working group was re-established in 2002 with the dual purpose of finalizing the IS code and further development.

Performance oriented criterion is essentially a mathematical model of the physical phenomenon "responsible" for possible stability failure. A new framework was envisioned to confront complexity of these physical phenomena and avoid unnecessary costs of analysis performed on irrelevant cases.. The criteria is defined a multi-teared (or multi-leveled) structure, where the first tier defines if the case is relevant, and the second tier determines the loading conditions and environment conditions that are likely to lead to stability failure. The most advanced numerical techniques of analysis are to be used in the third tier. If a possibility of stability failure cannot be eliminated in a design stage, the information produced by the third tier analysis is applied ship-specific operational guidance. This framework was formulated in a paper SLF 50/4/4, discussed on the 50th through 53rd sessions of SLF, taking the final form in Annex 1 of SLF 54/3/1.

In 2010, USCG office of Design and Engineering Standard funded a research effort at US Naval Surface Warfare Center Carderock Division (known as David Taylor Model Basin to develop the framework for operation guidance.. The report was released by NSWCCD in 2011 (Belenky et al. 2011) and was submitted to IMO in its entirety as SLF 54/INF.4, its summary was submitted separately as SLF 54/3/3.

The report provides graphical descriptions of physical phenomena associated with the stability failures, which are cited in the Code. These descriptions have generally been incorporated in the explanatory notes for the second generation intact stability criteria (SDC 4/5/1, annexes 1 through 4). The report also contains proposals for level 1 and 2 criteria for parametric roll and level 2 for surf-riding/broaching, which have been used as a part of the current formulations in Draft Interim Guidelines on Vulnerability Criteria in Annex 3 SDC 6/WP.6.

The report describes a method for calculation of GZ curve in waves, and application of GZ curves in waves to level 2 vulnerability criteria for pure loss of stability. These methods have been incorporated in the current level 2 vulnerability criteria for pure loss of stability in Annex 3 SDC 6/WP.6. The GZ curve-based criterion is applied for detection of variation of stability in waves, but is not sufficient to distinguish between pure loss of stability and parametric roll. While both parametric roll and pure loss of stability are results of large variations of stability in waves (as noted in paragraph 1.2.1 of the IS Code), their dynamics are notably different. Parametric roll is a resonant phenomenon, while pure loss of stability is characterized as a "dynamic angle of heel" problem. The pure loss of stability problem is addressed in this report.

The report (Belenky et al. 2011) reviews the physics of the forces that cause stability failure in dead ship conditions, as well as assumptions involved in current weather criterion. The current level 2 vulnerability criteria for the dead ship condition (Annex 3 SDC 6/WP.6) uses a slightly different set of assumptions, which leads to inconsistencies between the vulnerability criteria and mandatory criteria. This problem is addressed in this p report.

The report (Belenky et al. 2011) provides a rough framework for direct stability assessment. This framework contains formulations for the problems of relationship with time, rarity of stability failure and validation of direct stability assessment. This framework has served as a basis for more detailed specifications of direct stability assessment, which were initially proposed in Annex 21 of SLF 54/INF.12. These detailed specifications provided a basis for draft interim guidance for direct stability assessment in Annex 1 of SDC 6/WP.6. The present report provides examples for direct stability assessment of parametric roll and pure loss of stability, and methods for validation and extrapolation of results.

The report (Belenky et al. 2011) also contains an introduction with the review of key developments up to SLF 53, while work at the sessions SLF 54-55 and SDC sessions are summarized in the following paragraphs of this section.

The SLF 53 session resulted on agreement of the level 1 vulnerability criterion for dead ship condition in terms of application of weather criterion with an extended table for natural roll periods (obtained from MCS.1/Circ. 1200). Proposals were presented at the SLF 53 seesion for both level vulnerability criteria on pure loss of stability, parametric roll and surf-riding / broaching. Discussion has commenced on the direct stability assessment and operational guidance (refer to summary in Annex 1 in SLF 53/ WP. 4. Excessive accelerations were included as the fifth mode of failure in the development of second generation intact stability criteria.

The premise for applying Grim effective wave as method to relate irregular and regular waves with pure loss of stability and parametric roll was introduced to the correspondence group established at SLF 53 (Annex 5, SLF 54/INF.12). The working group report (Annex 1 of SLF 54/WP.3) contains the initial consensus on formulation of level 1 and 2 vulnerability criteria for pure loss, parametric roll and surf-riding / broaching, as well as level 1 on dead ship condition

failure mode. Annex 2 of SLF 54/WP.3 contains agreed upon specifications of vulnerability criteria for excessive accelerations. Other notable results include analysis of suitability of the simplified Ikeda method for estimation of roll damping in SLF 54/3/6 and Annex 1 SLF 54/INF.12. Roll damping is technically difficult to estimate (see e.g. Part IV of Belenky et al. 2019c), but without proper estimation of roll damping criteria for parametric roll, dead ship condition and excessive acceleration cannot be applied in real-world practice.

In the the SLF 54/55 intersessional period and SLF 55th session, most of criteria were developed and agreed, in principle. The focus shifted towards environmental conditions, where the criteria supposed to be applied. Formulation of Grim effective wave was codified (Annex 5 of SLF 55/INF.15). Testing of the criteria became another focus area as number of the sample ships under consideration reached 150, see SLF 55/3/1.

Recognition of the potential significant cost for performing a direct stability assessment on regular basis (SLF 55/INF.14) resulted in the notions of "coarse" ship-specific operational guidance. Such a "coarse" guidance may be developed based on ship-specific information, which is produced during the level 2 vulnerability assessment. This "coarse" guidance was later associated with operational limitations. The criteria for parametric roll and pure loss of stability were formulated as proposed amendments to part B of the 2008 IS Code (Annex 1 and 2 SLF 55/WP.3).

During the SLF 55/SDC 1 intersessional period, pure loss and parametric roll criteria documents were edited (Annexes 1, 2, 5 and 6 of SDC 1/INF.8) and included draft of explanatory notes (Annexes 3 and 4 of SDC1/INF.8). A text on draft amendments for surf-riding / broaching and dead ship condition was developed (Annexes 15 and 16 SDC1/INF.8), Guidelines on direct stability assessment were further edited (Annex 27 SDC 1/INF.8), and sample calculations were incorporated. The draft explanatory notes for dead ship condition (SDC 1/INF.6) and surf-riding broaching (SDC 1/5/4) is drafted and submitted.

Due to reorganization of some IMO sub-committees(the SLF Sub-Committee was amalgamated into the Sub-Committee on Ship Design and Construction (SDC) together with elements of the former DE Sub-Committee), the intact and damage stability working groups were consolidated into a single working group at the 1st session of SDC. Only 1 day was available for discussion of intact stability matters including development of second generation criteria. The remaining time available was not lost – there was an informal meeting of interested parties that included almost all the individuals, who were personally involved in the criteria development. The meeting helped to coordinate further work for the intersessional period leading to SDC 2.

During the intersessional period leading to SDC 2 and at the 2nd SDC session, the first draft text of excessive acceleration was developed (Annex 33 of SDC 2/INF.10), while sample calculations and editing of previously developed documents continued. The notable event was release by the working group of vulnerability criteria for pure loss, parametric roll and surf-riding, which were documented as Annexes 1 through 3 of SDC 2/WP.4. This represented the first delivery of documentation describing the second generation intact stability criteria from the working group to the subcommittee.

During the intersessional period leading to SDC 3 and 3rd SDC session, dead ship conditions and excessive accelerations were completed (Annexes 1 and 2 of SDC 3/WP.5 and SDC 3/INF.10). Explanatory notes for all failure modes documented and released as Annexes 3

through 7 of SDC 3/WP.5 and 16 through 20 of SDC 3/INF.10. Draft Guidelines on operational limitation were developed and documented in Annex 21 of SDC 3/INF.10.

At the same time the results from sample calculations showed inconsistencies between the criteria levels (SDC 3/6/4). The inconsistency occurred when the level 1 criterion had not indicated vulnerability, while for the exact same condition, the level 2 criterion found this ship to be vulnerable for stability failure. This problem became quite apparent for vessels with extended weather deck such as OSVs (SDC 3/6/8). The solution was obtained by increasing the conservatism of the level 1 criteria for pure loss of stability and parametric roll through using simplified formulae (SDC 3/6/9).

While more information was submitted on direct stability assessment and operational guidance, e.g. SDC 3/INF.12, SDC 3/INF.15, the focus shifted towards testing – matrix calculations were proposed (SDC 3/6/2). The development of the second generation intact stability was completed and available documentation was sufficient to support testing.

The intersessional period leading to SDC 4 and 4th SDC session focused on testing of the vulnerability criteria primarily with matrix calculations. The results are encompassed SDC 4/INF.4 (Annexes 1 through 7). Additional sample calculations were submitted directly to the subcommittee: SDC 4/INF.7 SDC 4/INF.9 and SDC 4/INF.10.

As a result of testing, another issue was identified. In addition to consistency issues and applicability of the criteria to OSVs, the problem of the relationship between dead ship condition criteria and mandatory weather criterion was identified (paragraph 2.3 of 2008 IS Code) with extension allowed by the MSC.Circ 1200, see Annex 12 and 16 of SDC 4. INF.4, SDC 4/5/12. Further refinement of explanatory notes was reflected in SDC 4/5/1 and SDC 4/5/6. Some information on differed test approaches of direct stability assessment was submitted SDC 4/INF.8. Draft guidelines on direct stability assessment were documented (Annex 1 of SDC 4 / WP.4).

The focus of intersessional period leading to SDC 5 and papers submitted to SDC 5 was on testing of the vulnerability criteria (Annex 13 of SDC 5/ INF.4, SDC 5/INF.12), direct stability assessment (Annex 18 of SDC 5/ INF.4, SDC 5/INF.7, SDC 5/INF.8), and addressing problems identified during testing (e.g. Annex 1, 11, 16 SDC 5/INF.4, SDC 5/6/4, SDC 5/6/14).

The working group on intact stability did not convened at the 5th session of SDC. The subcommittee noted a number of issues associated with the second generation intact stability criteria in SDC 5/WP.1, listed on paragraph 6.7. In particular, problems associated with the cost of direct stability assessment are cited. The direct stability assessment was not intended to be used on a frequent basis. It was envisioned as a tool for special cases, when dealing with a very new type of vessel or expensive vessel (where the cost of such analysis is well justified). The guidance on direct stability assessment was envisioned as a collection of the best available practices, to set the expectation of a ship-owner and administration. Subsection 5.1 of the present report provides an executive-level review on availability and maturity of these tools.

An assessment with vulnerability criteria provides with a valuable tool for identifying potential problems in dynamic stability for certain loading conditions and environments. This can improve safety, especially when ship-specific information from a vulnerability assessment is shared with a crew. One may expect that ship specific information provides better safety than a generic guidance. See an example in section 6 of the present report.

There was an agreement that the SGISC was nearly completed. As noted in paragraph 6.10.3, documentation for the vulnerability criteria and standard were delivered to the subcommittee at the 2nd and 3rd sessions, while the Guidelines for direct stability assessment were delivered at the 4th session. The document on operational guidance and limitation has not been delivered yet. The eExplanatory notes exist in draft working form and were undergoing active editing. To address maturity issue, it has been proposed to issue the criteria as an MSC circular, which would enable industry to conduct additional testing prior to incorporation into Part B of the IS Code.

Observing the normal work flow of the developers, one can see that editing and discussing of work output takes two-three cycles. For example, the first formulation of vulnerability criteria for parametric roll appeared at SLF 54 and was delivered at SDC 2 (absence of the working group at SDC-1 caused a delay). Some of the items takes longer: the text on direct stability assessment first appeared at SLF 54, but the group did not have sufficient resources to finalize the work product in two cycles.

Perhaps, analysis of the workload and delivery has convinced the subcommittee to continue with finalization but focus on the delivery of documents. This will require postponement of testing and addressing the problems identified during previous testing. Recommendations on how to address a problem will be deferred to future updates (including an alternative for pure loss of stability criteria considered in subsection 2.1 of this report).

The focus of the intersessional period leading to SDC 6 was on the finalization. The coordinator of the corresponding group disseminated two questionnaires to resolve any residual difference in opinions (SDC 6/INF3). The effort of the correspondence group resulted in three guidelines covering direct stability assessment, vulnerability criteria, operational guidance and operational limitation as documented in Annexes 1 through 3 of SDC 6/5. These results facilitated the work of experts' group, finalizing the output in SDC 6/WP.6.

1.2 The Contents of the Work

This report describes the work that was commissioned by the Office of Design and Engineering Standards of the United States Coast Guard (CG ENG) to the Naval Warfare Center Carderock Division (NSWCCD – David Taylor Model Basin, Simulations and Analysis Branch, Code 851) to provide technical support services in FY 16-17, which covered a significant part of the intersessional period between the 3rd and 4th session of SDC (the 3/4 intersessional period), 4th session of SDC, and most of the SDC 4/5 intersessional period. The objective of this R&D work has been to support U.S. participation in the work of the intersessional correspondence group and working groups during the sessions.

In particular, the tasking had included the testing and diagnostic development of the level 1 and 2 vulnerability criteria for stability failure in dead ship condition and excessive accelerations, development of specifications for direct stability assessment, and a methodology for operational guidance based on the results of direct stability assessment. Other tasks included review of other delegation submissions and refinement of explanatory notes. The work also included the development of documents to be submitted to intersessional the correspondence group and to SDC directly.

Based on the work described in this report, the U.S. contributions to the intersessional correspondence group and SDC directly that was developed and submitted encompasses:

- Annex 10 SDC 4/INF.4: “Level 2 vulnerability criteria for the dead ship condition – case study for the C11-class container ship”;
- Annex 12 SDC 4/INF.4: “Observations from sample ship calculations of the vulnerability criteria, levels 1 and 2 for the dead ship condition stability failure mode”;
- Annex 15 SDC 4/INF.4 “On consistency between the mandatory weather criterion and vulnerability criteria to stability failure in dead ship condition”;
- Annex 16 SDC 4/INF.4 “Proposed revision of draft guidelines/specifications for direct stability assessment”;
- Annex IMO SDC 4/INF.7 “Sample ship calculation outcomes”, Submitted by the United States, London, 2016;
- Annex IMO SDC 4/5/6 "Draft consolidated explanatory notes for the second generation intact stability criteria", London, 2016;
- Annex 1 IMO SDC 5/INF.4 “Dead ship condition vulnerability criteria level 2 standard setting and assessment procedure for improved consistency with the vulnerability criteria level 1 and the Weather Criterion (section 2.3 of part A of the 2008 IS Code)”;
- Annex 7 IMO SDC 5/INF.4 “Dead ship condition vulnerability criteria level 2 standard assessment”;
- Annex 11 IMO SDC 5/INF.4 “Pure loss of stability, vulnerability criteria level 2 inconsistency resolution”;
- Annex 12 IMO SDC 5/INF.4 “Reply to comments provided by Japan on assessment in Annex 7 (dead ship condition vulnerability criteria level 2 standard assessment)”;
- Annex 15 IMO SDC 5/INF.4 “Possible sources of inconsistencies in the parametric roll vulnerability assessment”;
- Annex 19 IMO SDC 5/INF.4 “Draft consolidated explanatory notes”.

Section 2 of the present report describes the work performed under task 1, which entailed conducting reviews of other delegation submissions.. The primary focus of Section 2 is on the inconsistency between level 1 and level 2 criteria. The root cause of this inconsistency is addressed in subsection 2.2. The inconsistency issue for the new criteria have been resolved on a theoretical level based on work from Chapter 3 of (Belenky et al. 2011) by incorporation of dynamical behavior that has enabled the criteria to differentiate between vulnerability due to pure loss of stability versus parametric roll. Subsection 2.3 addresses the effect of roll damping on consistency of the criteria for parametric roll, which complements consideration of parametric roll in chapter 2 (Belenky et al. 2011).

Section 3 of the present report is focused on vulnerability criteria for the dead ship condition. The study, described in the section 3, was carried out in fulfillment of Task 2. As requested, special attention was paid to consistency with the mandatory criteria in part A of the

2008 IS Code. Chapter 5 of (Belenky et al. 2011) emphasized complexity of the physical processes associated with stability failure in dead ship condition. The development of a criterion for stability in dead ship condition is based on simplified assumptions. If two criteria for dead ship condition are based on different assumption, they are not going to be consistent. This why SLF 53/3/6 recommended to maintain the existing weather criterion and develop a new weather criterion based on more accurate physical model.

As the development of the second generation intact stability criteria did not take this warning on, the inconsistency between level 2 criterion and mandatory weather criterion cannot be avoided. Given that some inconstancy still exists, a mitigation approached is described in Section 3 that proposes a statistical method to control inconsistency by appropriate choice of a standard.

Section 4 of the present report describes work on Task 3: sample calculation, verification and diagnostic development for vulnerability criteria for excessive accelerations. There was no similar chapter in (Belenky et al. 2011), as the excessive acceleration mode of failure was not in the scope of the previous report.

Section 5 reports completing Task 4 “Development of specifications for direct stability assessment”. The task focuses on further development of the Specifications that were originally submitted to the correspondence group as Annex 21 of SLF 54/INF.12. Proposed revision of the Specifications was submitted to the correspondence group as Annex 16 SDC 4/INF.4. At the fourth session of SDC, the specifications for direct stability assessment were agreed upon and delivered to the Subcommittee as Annex 1 of SDC4/WP.4. Consequently, the version originally developed Task 4 became obsolete and is not reported here.

Section 5 contains an example of application of the Specifications. This example addresses most of the principle elements of the Specifications including wave modeling, qualitative and quantitative validation, and direct counting procedure applied to parametric roll. The example also includes application of two extrapolation procedures described in Chapter 6 of (Belenky et al. 2011), which are comprised of the Peaks-over-threshold method and Split time method. While (Belenky et al. 2011) describes these methods in terms of principle theoretical approaches to extrapolation, the current report contains a practical application for estimation of the rate of failure for pure loss of stability. Section 5 of the present report contains a description of how the Specification for Direct Stability Assessment can be applied. Approaches for improving computational efficiency for the direct stability assessment are also discussed.

Section 6 of this report is focused on operational guidance and operational limitations. The main objective is a methodology of development of operational guidance from the output of direct stability assessment as described by Task 5. The section also contains an example showing how to create a polar plot using data from the direct stability assessment. In addition, Section 6 contains an algorithm and example of development of the operational limitation in a form of a polar plot based on the outcome of level 2 vulnerability assessment. As both examples are performed for the same mode of failure parametric roll for the same sample ship, comparison of the polar plots based on different fidelity provides valuable information for future reference.

Section 7 of the present report describes work performed on the Task 6 entitled “Refinement of the working versions of explanatory notes for all five modes of stability failures”. In fulfilment of this task, a draft with consolidated explanatory notes was developed and submitted directly to SDC 4 (as an Annex IMO SDC 4/5/6) and further to the intersessional

correspondence group as Annex 19 of IMO SDC 5/INF.4. Review of this document has commenced, and the version in Annex 19 has been revised based on comments from Japan and France. Consequently, the documentation developed under this task is obsolete, and not included in the report. Instead, the Section 7 of the present report described the simplified Ikeda Method that was further refined compare to as Annex 19 of IMO SDC 5/INF.4.

The other element, included in the report is the data set for vulnerability assessment for all five modes of failure. The data set includes input data, final results and some intermediate results that may be helpful in future application and benchmarking of the vulnerability criteria.

2. REVIEW OF CURRENT DEVELOPMENT

2.1 General

This section reviews current issues related to the finalization of the second generation IMO intact stability criteria, not covered in other sections of this report. These issues concern consistency of vulnerability criteria for pure loss of stability and parametric roll. The issues of consistency were raised as a result of sample calculations carried out by IMO Intersessional Intact Stability Correspondence Group, while finalizing the development of the second generation intact stability criteria.

The subsection 2.2 summarizes the study on vulnerability criteria on pure loss of stability. As the problem appears to be more difficult, which is to be expected at this stage of development, the analysis starts from the basic physics of the stability failure. Then theoretical reason of inconsistency are examined. Based on the outcome of these studies, a major change in the pure loss criteria is needed in order to achieve consistency between the levels and to avoid excessive conservation. As the current IMO criteria development schedule does not allow changes of this magnitude, it makes sense to consider them for the next round and include them in the upcoming criterial trial and testing as an alternative.

The subsection 2.3 is focused on inconsistencies in parametric roll; where two reasons for the cause of the inconsistency's rise were found. These findings do not require any changes in the vulnerability criteria for parametric roll, nevertheless, they can be useful during the trial application of the criteria.

2.2 Issues Related to Vulnerability Criteria for Pure Loss of Stability

2.2.1 Formulation of the Problem

Consistency between level 1 and level 2 vulnerability assessment was identified as an outstanding issue at the 5th session of SDC; corresponding action item was included in the terms of references of the intersessional correspondence group (paragraph 3.3.5 of SDC 6/5). The inconsistency manifests itself, when a loading condition is identified as "non-vulnerable" by the level 1 assessment and is found to be vulnerable by the level 2 assessment.

The level 1 criterion for pure loss of stability is based on the minimum GM values encountered during the wave pass along the ship. The level 2 criteria are results of averaging of characteristics of GZ curve over a series of waves. Thus, the consistency between the levels are not provided automatically, because the GM values do not define the entire GZ curve.

Two characteristics of GZ curve in waves are included in the level 2 criteria. One characteristic (referred as CR1) is the smallest angle of vanishing stability, encountered during the wave pass. Another one (referred as CR2) is the largest static angle achieved under prescribed heeling moment, encountered during the wave pass.

Inconsistencies between the level 1 and level can be caused by both CR1 and CR2 values. The inconsistency caused by the CR1 level may be alleviated by including weather-tight volumes into calculation of the GZ curves in waves (Peters & Belenky 2016). The inclusion can be justified by a short-time immersion of those volumes in case of pure loss of stability; the immersion of additional volumes creates additional drag, the ship will slow down, and the wave passes and the stability is restored.

Several methods were considered for the resolution of the inconsistencies caused by the CR2 value:

- Level 1 assessment can be made more conservative, in particular:
  - Use of a more conservative way to compute GM value in waves – the choice made by the correspondence group, based on the questionnaire (paragraph 16, SDC 6/5/1)
  - Use of wave steepness, depending on ship length (SDC 5/6/5)
- Have the calculation of CR2 made less conservatively
  - Change of scheme of application of the heeling moment (Annex 11 SDC 5/INF.4)

The solution, chosen by the correspondence group, is supposed to use simplified formula (Paragraph 1.2.2 of Annex 3 SDC 6/5) for calculation of loss of GM on the wave crest exclusively. This simplified formula usually gives significantly more conservative results in comparison with actual calculation of GM changes with the wave pass (see examples in Tables 2.5-2.8)The formula for the heeling moment in Criterion 2 (Paragraph 1.3.4 of Annex 3 SDC 6/5) is also conservative, (see examples in Tables 2.5-2.8). As a result, the vulnerability assessment for pure loss stability may end up being too limiting and identify too many ships as possibly being vulnerable to pure loss of stability, while, in fact, those ships are not vulnerable. See the comment of the United States in paragraph 16 of SDC 6/5/1.

To substantiate this comment, an additional study of inconsistency of vulnerability criteria for pure loss of stability has been carried out and is described below.

2.2.2 On Physics of Pure Loss Stability Failure

Level 2 of vulnerability criterion consists of an assessment of two long-term indices: CR_1 and CR_2, relating to a criterion based on the angle of vanishing stability and the angle of heel under action of a heeling lever specified by a formula for R_{PL3}, respectively. Although not all sample calculations have sufficient detail, those that do show that the CR_2 weighted criterion is the one that is responsible for the inconsistency. As drafted in paragraph 1.3.4 of Annex 3 of SDC 6/ WP.6, the CR_2 assessment assumes that R_{PL3}, a heeling lever related to yaw rate centrifugal force, is applied at all times while the ship is considered to be statically positioned with the wave crest centered at various positions related to amidships.

There are two issues with the aforementioned assumption:

- The centrifugal force supposes occurrence of an involuntary turn that is characteristic for a broaching-to rather than for a pure loss of stability.
- A ship is still situated at wave crest, across the wave front when the maximum moment is created by the centrifugal force; i.e. the centrifugal force is assumed to be created before the turn has started.

The problem of physical correctness of the “centrifugal” assumption was raised during the SDC4-5 intersessional period and documented in the Annex 11 of SDC 5/ INF.4. The immediate solution was sought in a moment of application of the centrifugal moment, considering different schemes of time-averaging. These schemes have eliminated inconsistencies in a number of examples, see Table 2 in Annex 11 of SDC 5/ INF.4. Independent assessment and testing of these application schemes were reported in Annex 16 of SDC 5/ INF.4: 85 % of all the inconsistencies of a sample of RoPax vessels were eliminated.

The idea of time-averaging was criticized in the paper SDC 5/6/12. The point was made that a time-averaged characteristics of stability in waves are close to the characteristics of stability in calm water, defeating the purpose of assessment of vulnerability to pure loss of stability. The paper SDC 5/6/12 does not contain any proposal to improve physical justification of the CR_2 criteria. Instead it reiterates an idea to remove direct calculation of GM in waves in level 1 of the vulnerability criteria leaving a simplified formula, as the only option (paragraph 1.2.1 of Annex 3 of SDC 6/ WP.6). This idea was first described in annexes 14 and 17 of SDC 5/ INF.4. It resolves the inconsistency between the level 1 and 2, by increasing the level of conservatism in the level 1.

The paper SDC 5/6/5 also proposed to resolve inconsistency modifying the level 1 criterion. The essence of the proposal is to use variable wave steepness in the level 1 criterion, depending on the length of a ship. While there were a limited number of example calculations reported, the idea is interesting as a probability of encounter of a long steep wave is much less compared to the probability of encountering a short steep wave. Thus, if one uses the same wave steepness for ships of all lengths, the criterion will be more conservative for longer ships than for shorter ships. The weather criterion in paragraph 2.3 of the IS Code also uses variable wave steepness, that is chosen depending on natural period of roll (i.e. related to ship size), so the idea of variable wave steepness is a conventional one for stability regulations.

The resolution of inconsistency was carried out during the intersessional period of SDC5-6 in a form of a questionnaire, reported in Annex 3 of SDC 6 INF.3, where the majority of members voted for the exclusive use of the simplified formula of GM in waves in the level 1 criterion (paragraph 1.2.1 of Annex 3 of SDC 6/ WP.6), see the table in page 118 of SDC 6 INF.3.

While, perhaps, the inconsistency between the levels decreased, the inconsistency between the criteria and the physics of the pure loss of stability failure have not been resolved. As a result the vulnerability assessment for pure loss of stability becomes overly conservative, providing very little value for the industry. This was recognized in the paper SDC 6/5/6, where the all the results of work on the pure loss of stability were characterized as ‘not mature’ even for test applications by the industry.

While the development of the vulnerability criteria for the pure loss of stability cannot be regarded as successful, the recognition of the failure in SDC 6/5/6 is useful – instead of trying to fix flawed criteria – the problem should be re-examined, starting from the physical mechanism of the pure loss of stability failure mode.

The fact that stability decreases when a ship is located in the wave crest was known to naval architecture well over a century ago (Pollard & Dudebout, 1892). However, practical calculation methods were not available until the 1960s (Paulling, 1961). A decade later, it was recognized as a separate mode of stability failure (Paulling et al. 1975). At the same time, there were few fundamental studies on the basic dynamics of pure loss, with the exception of unpublished work by Spyrou[1]. The focus shifted to probabilistic consideration, using spectral representation of elements of stability Dunwoody (1989). Some insight was gained when an

[1] Spyrou, K.J. (2009) Pure-loss of Stability Revisited: Analytical Design Aid. Internal Report of National Technical University of Athens, Greece.

instantaneous GZ calculation become available for advanced numerical simulation, see Belenky & Weems (2008), Belenky, et al (2013).

One issue never completely resolved: how pure loss of stability can be separated from surf-riding and broaching-to when all six degrees of freedom are considered. None of the studies cited above included surge, sway, and yaw. Also, one may ask the question: if a speed is high enough and a wave is steep enough, would a ship surf-ride and broach in realistic condition rather than suffer from pure loss of stability? Does pure loss of stability still exist as a separate failure mode?

To answer this question consider a coupled-model of nonlinear surging/surf-riding and roll motions with time-dependent stiffness. Assume that a ship sails in exact following regular waves and experiences a sudden action of heeling moment at the initial instant of time:

$$\begin{cases}(m + A_{11})\ddot{\xi}_G + R_x(\dot{\xi}_g) - T_e(\dot{\xi}_g, n) = F_x(\xi_G, t)\\ (I_x + A_{44})\ddot{\varphi} + R_\varphi(\dot{\varphi}) + mgGZ(\varphi, x_c) = mgl_w\end{cases} \tag{2.1}$$

where, ξ_g is a position of the ship's center of gravity in Each-fixed (global) coordinate system, φ is the roll angle of a ship, one or two dots above the symbol signify the first or the second temporal derivative, A_{11} is the added mass in surge; R_x is the ship resistance in calm water; T_e is the ship thrust, achieved with a commanded number of propeller revolutions, n; F_x is the Froude-Krylov wave force in direction of surge, I_x is the moment of inertia in roll; A_{44} are the added mass in roll, and R_φ is the roll damping, m is the mass of the ship, g is gravity acceleration, l_w is a lever of suddenly applied heeling moment. The GZ curve in waves is precomputed and then interpolated for the particular values of the roll angle and position on the wave x_c, which is computed in the ship-fixed (local) coordinate system.

The local coordinate system is assumed to move with a constant speed vs, equal to a speed, a ship will achieve in calm water with the commanded number of revolutions n. Thus the coordinates in global and local system are related as follows:

$$x = \xi_g - v_s t;\ \xi_g = x + v_s t \tag{2.2}$$

The wave is assumed to move in the same direction as the ship with the celerity c. Wave position is identified with the position of wave crest. Thus, at any given instant of time t, a wave crest location in a ship-fixed coordinate system can be expressed as:

$$x_c = (c - \dot{\xi}_g)t \tag{2.3}$$

The nonlinear surging model is taken from paragraph 4.3.3 of Annex 19 of SDC5/INF.4/Add.1, for compatibility with the level 2 surf-riding/broaching vulnerability criterion.

Consider a ship, sailing in regular following seas when both surf-riding and surging co-exist, see Figure 2.1. First, assume a ship is experiencing surging, but surf-riding is not possible without increasing the initial velocity, as shown in Figure 2.2. As shown in Spyrou (1996), surging becomes asymmetric (accelerated part is longer than its decelerated part) in the coexistence mode. It is also known that the asymmetric shape of surging makes a ship spend more time near wave crest, see Figure 2.3. This may be sufficient for capsizing or development of a large roll angle if enough stability is lost near the wave crest, See Figure 2.4. This is why a requirement to model surging was included in the direct stability assessment guidance in Annex

1 of SDC 6/ WP.6.

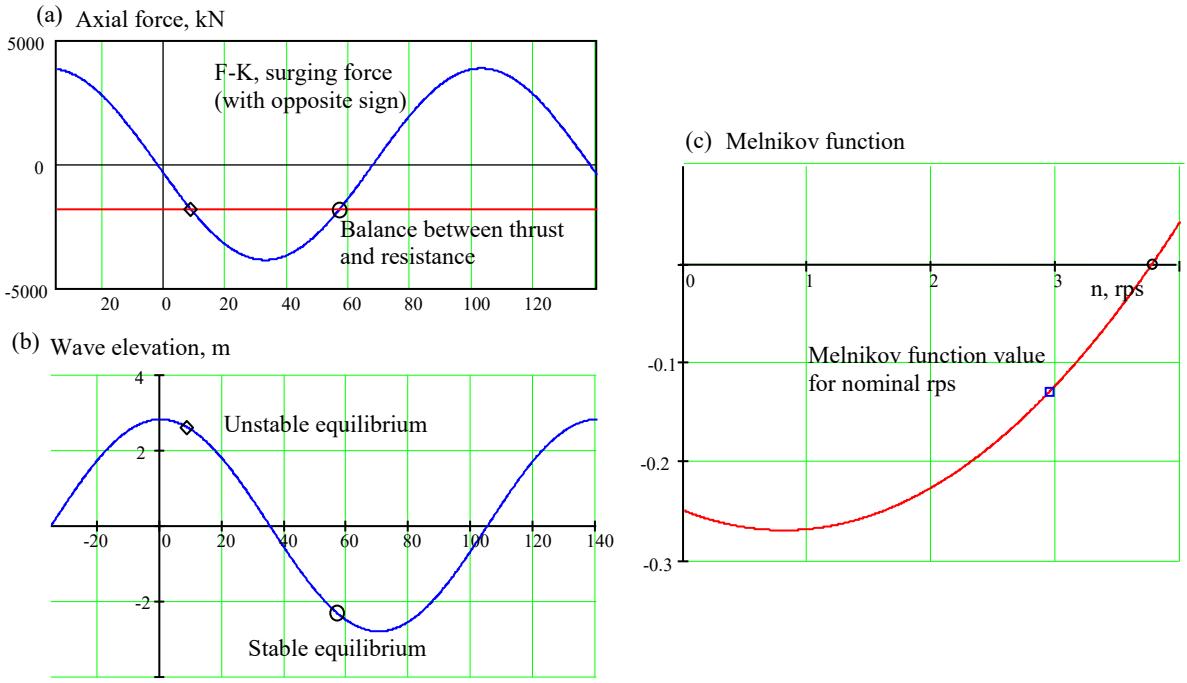

Figure 2.1. Surf Riding Equilibria (a,b) and Melnikov Function (c) Wave Steepness 0.04

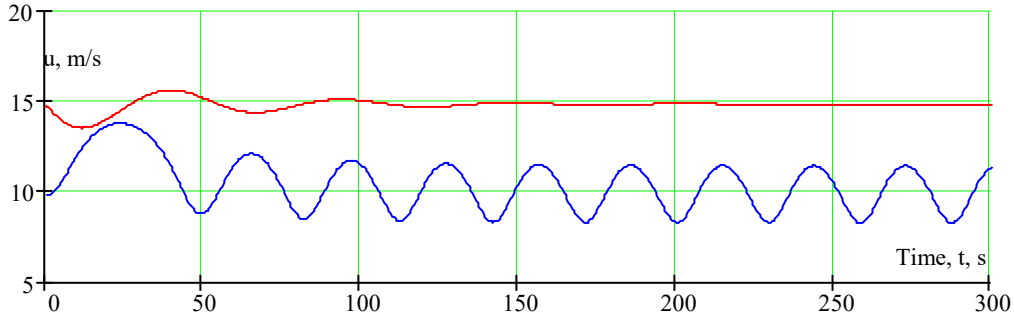

Figure 2.2. Surging and Surfriding from the Same Position on the Wave, but with Different Velocity, Wave Steepness 0.04

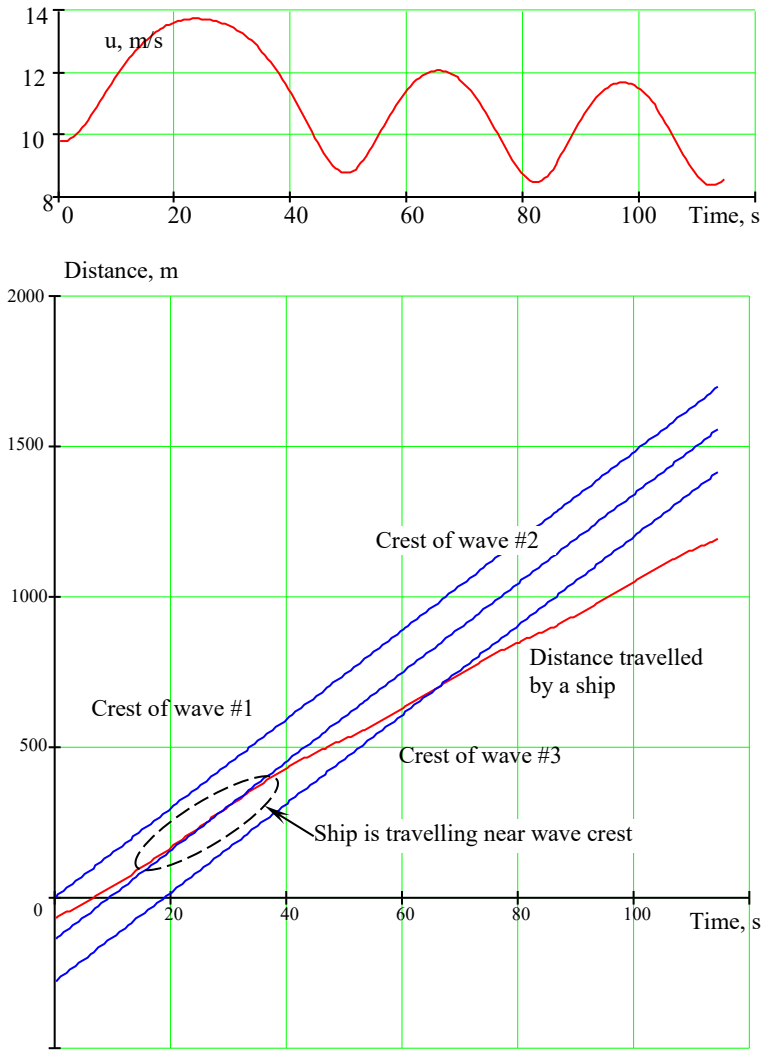

Figure 2.3. Asymmetric Surging and Time near Wave Crest, Wave Steepness 0.04

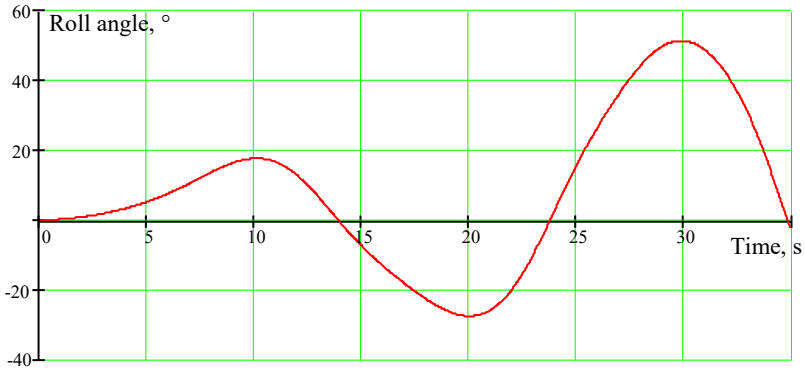

Figure 2.4. Time History of Roll Motion, Wave Steepness 0.04

When the wave steepness is increased, surf-riding becomes possible with the initial velocity equal to service speed if a ship is located at certain position on a wave, see Figure 2.5 and Figure 2.6. Transition to surf-riding in regular seas is essentially attraction to a stable equilibrium. During this transition, a ship spends significant time near the wave crest (Figure 2.7) and is exposed to decreased stability long enough to develop large roll angle (Figure 2.8). The maneuvering forces, resulted from directional instability and causing broaching-to take some time to develop, so the ship is likely to suffer from pure loss of stability before she could broach.

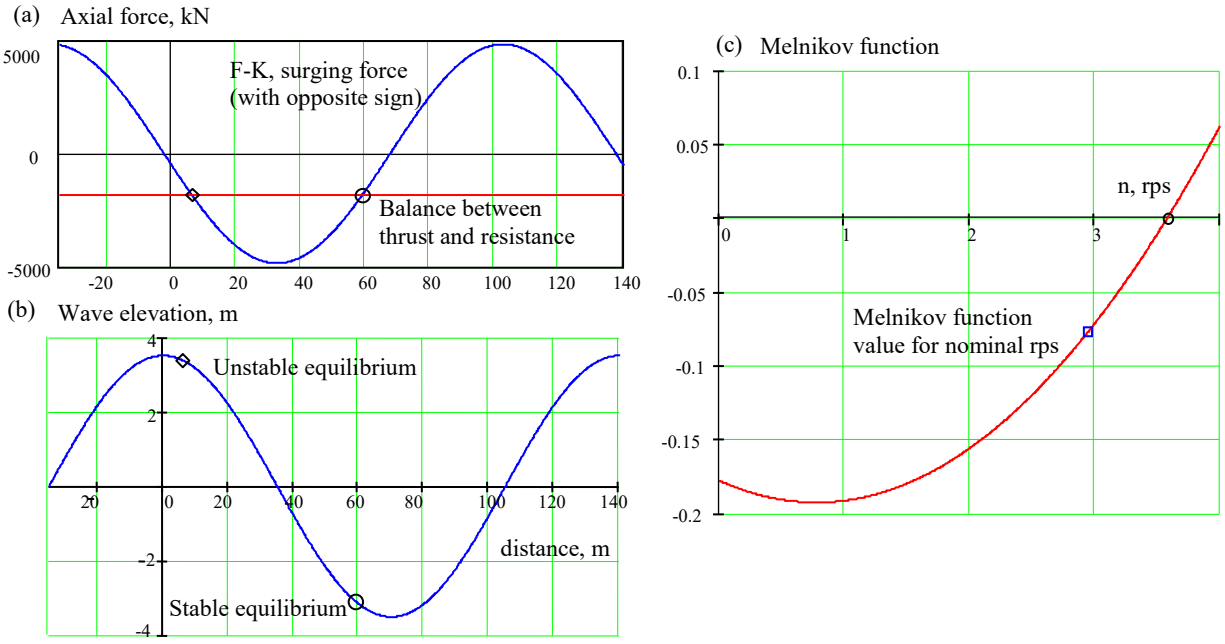

Figure 2.5. Surf Riding Equilibria (a,b) and Melnikov Function (c) Wave Steepness 0.05

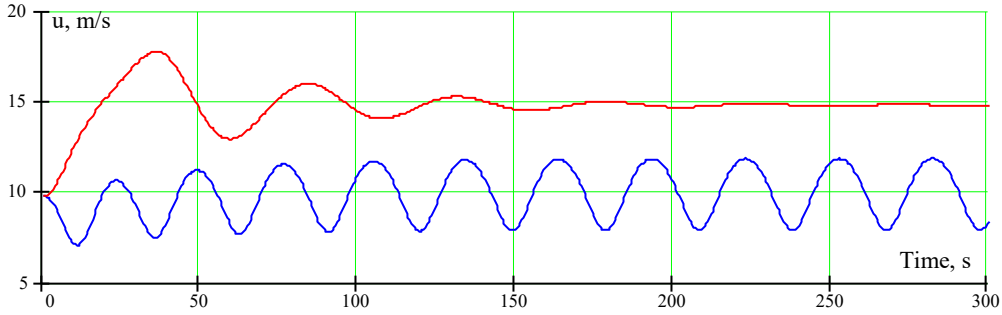

Figure 2.6. Surging and Surfriding from the Different Positions on the Wave, but with the Same Velocity, Wave Steepness 0.05

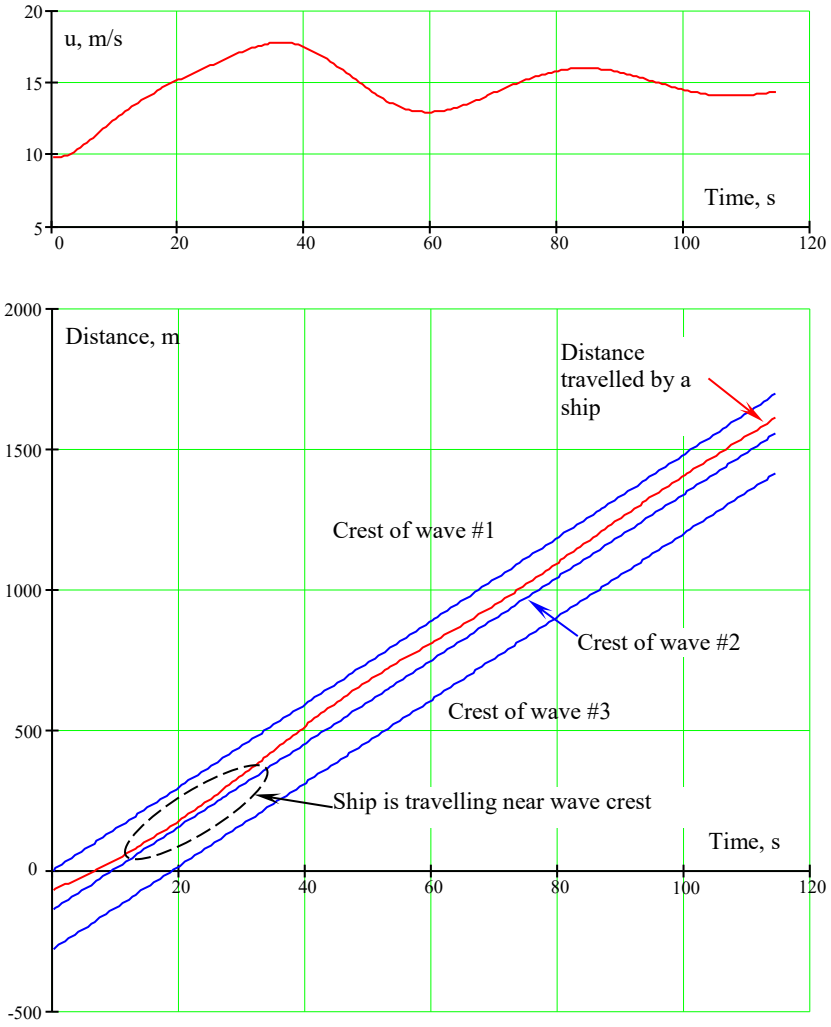

Figure 2.7. Asymmetric Surging and Time near Wave Crest, Wave Steepness 0.05

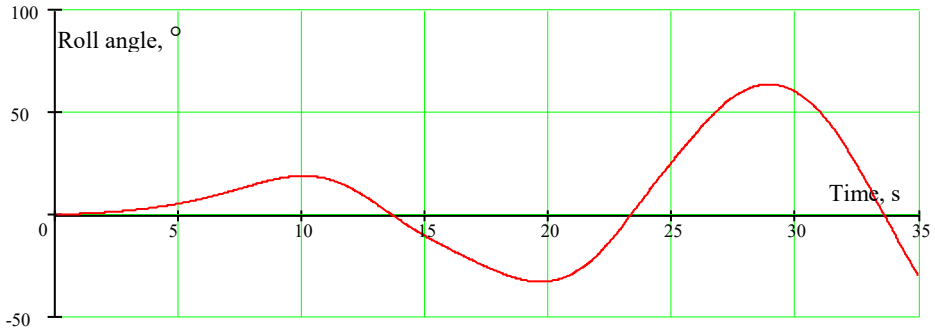

Figure 2.8. Time History of Roll Motion, Wave Steepness 0.05

Finally consider ship sailing in following or quartering irregular waves. As it is shown in a number of recent studies (Belenky, et al. 2019, Kontolefas & Spyrou, 2018), the dynamics of surf-riding in irregular waves are more complex compared to regular waves. As a wave changes in time and space, surf-riding may become a game of "catch-and-release", while development of broaching-to could require encountering several steep waves one after another (Belenky et al, 2016, Andrew, 2012). On the other hand, pure loss of stability may take just one wave acting on a ship from a quarter to one half of a wave period.

These considerations (illustrated with simple simulation examples, Figure 2.1-Figure 2.8) allow a conclusion: pure loss of stability should still be considered as a separate stability failure. It may occur for relatively high speed and relatively steep waves; however, not high and steep enough for surf-riding and broaching.

2.2.3 Methodology

Any ship will lose stability on a wave crest. The possibility of these losses is indirectly reflected in the current regulations through the requirements in paragraph 2.2 of Part A of 2009 IS Code. The criteria in paragraph 2.2 are based on accident statistics gathered by Rahola (1938) of "conventional" ships. Whatever contribution stability variation had in those data sets, were included with the statistics and reflected within the related criteria.

The appearance of new designs introduces hull geometries that were not included in those data. Some of these hull geometries may exhibit a significant propensity towards stability variation in waves. The objective of a vulnerability analysis is to identify those hulls. If a hull is vulnerable to pure loss of stability, the loss of stability in waves is "unacceptably" large. Thus, the study of criteria for pure loss of stability should be done with critical KG for the IS Code.

At the same, time critical KG for IS Code may not be realistic –e.g. the damage stability limit may be governing. Thus, the choice in subject vessel for the study should be done with this consideration in mind, as application of the vulnerability criteria to unrealistic loading conditions may not provide much useful information. For example, IS Code-critical GM value for C11-class container carrier in the "benchmark" draft of 11.5 m is 0.395 m, while realistically minimum GM is about 1 m (France, et al. 2003; Shin, et al. 2004).

2.2.4 Theoretical Considerations

Now consider a theoretical reason for inconsistency between level 1 and 2 of vulnerability criteria. Level 1 criterion is deterministic and the level 2 criterion is probabilistic. This difference, by itself, can lead to inconsistency. To gain insight in the probabilistic aspects of inconsistency consider a static angle of heel achieved under a static heeling moment with the worst GZ curve during the wave pass as a conditional criterion for pure loss of stability for both levels. The heeling lever is assumed to be given. To compute this criterion, one needs to know wave length and wave height.

Following the procedure agreed for the level 2 vulnerability criteria for the pure loss of stability, as described in draft explanatory notes (paragraph 7.3.1 of Annex 19 of SDC 5/INF.4/Add.1), Grim effective wave is used to represent stability variation in a particular sea state. As the length of the Grim effective wave is equal to ship length, only one random variable remains – the wave height. Thus, for a given ship length, each cell of the scatter table (e.g. IACS Recommendation 34, 2001) corresponds to a particular value of the effective wave height H_{eff}:

$$H_{eff} \approx 5.97\sqrt{V_H} \tag{2.4}$$

V_H is the variance of the effective wave:

$$V_H = \int_{\omega_1}^{\omega_2} RAO_{eff}^2(\omega) s(\omega|H_S, T_z) d\omega \tag{2.5}$$

Here, $s(\omega|H_S,T_z)$ is a spectral density of the wave elevations, ω is a frequency, $\omega_{1,2}$ are the limits of integration, H_S is the significant wave height, T_z is the mean wave zero-crossing period and RAO_{eff} is the RAO of the effective wave amplitude:

$$RAO_{eff}(\omega) = \frac{\omega^2 Lg^{-1} \cdot sin(0.5\omega^2 Lg^{-1} \cdot)}{\pi^2 - 0.5\omega^2 Lg^{-1}} \tag{2.6}$$

Where L is a ship length and g is gravity acceleration.

As each cell of the scatter table also corresponds to a statistical frequency, one can easily compute an estimate of cumulative distribution function (CDF) by sorting the effective wave heights in ascending order and integrate all the statistical frequencies below the current value,

$$P(H_{eff}) = P(H_S, T_z) \tag{2.7}$$

$$P_1(H_{eff}) = sort(P(H_{eff}), H_{eff}) \tag{2.8}$$

$$CDF(H_{eff}) = \int_0^{H_{eff}} P_1(h)\, dh \tag{2.9}$$

The resultant CDF is shown in Figure 2.9.

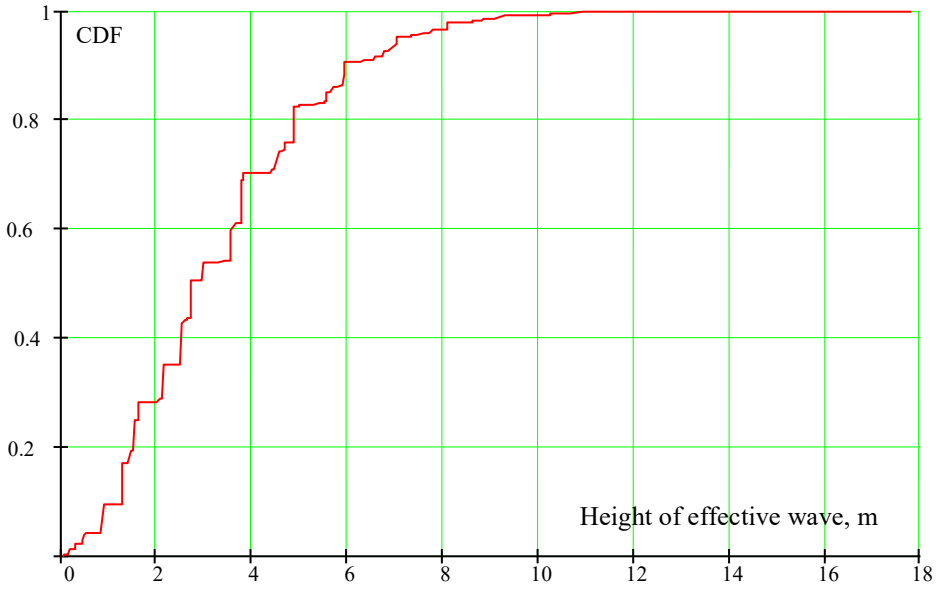

Figure 2.9. Estimate of CDF of the Effective Wave Height Computed for Ship Length L = 260 m

The CDF in Figure 2.9 also can be interpreted as dependence between the safety level for the level 1 criterion and a wave steepness for a ship with length of 260 m. Safety level of a deterministic criterion is a probability that a ship satisfying this criterion will nevertheless suffer from the failure. As the ship stability is a subject of random meteorological factors, the safety level theoretically cannot be zero.

For example, set the safety factor to 1 %. Then effective wave height corresponding to the 99th percentile equals to approximately 9.2 m for a ship of length 260 m. Thus the steepness of the effective wave is 9.2 m/260 m = 0.035. If the ship satisfies the level 1 criterion for the wave steepness 0.035, there is only a 1 % probability over the lifetime that stability will not be sufficient to withstand the pure loss stability failure. Keeping the safety level constant, one will get another wave steepness for another length, coming to an idea of the level-1 wave steepness that depends on a ship length. Originally, this idea was proposed in SDC 5/6/5. Figure 2.10 shows a dependence of wave steepness for level 1 criterion on ship length, computed for the safety level of 1 %. Values of wave steepness, computed for other safety levels, can be found in Table 2.1 and Table 2.2.

It is assumed here that the heeling moment is created by the wind. The relation of mean wind speed U_{Wm} is taken from paragraph 4.3.2.2 of Annex 3 of SDC 6/WP.6:

$$U_{Wm} = \left(\frac{H_S}{0.06717}\right)^{2/3} \tag{2.10}$$

Then the aerodynamic pressure p_A can be computed as:

$$p_A = \frac{\rho_A U_{Wm}^2}{2} \cdot C_m \tag{2.11}$$

Where C_m is wind heeling moment coefficient. Its value is taken as 1.22 from paragraph 4.3.2.2 of Annex 3 of SDC 6/WP.6, while ρ_A is density of air.

This pressure is also a random variable, as it depends on the significant wave height. As each value of significant wave height in the scatter diagram has an associated statistical frequency, one can compute the CDF for the significant wave height:

$$CDF(H_S) = \int_0^{H_S} P_H(h)\, dh \tag{2.12}$$

P_H is a statistical frequency of the significant wave height, available from a wave scatter table (e.g., IACS Recommendation 34). The CDF of the wind pressure is essentially a rescaling of the CDF (2.12) with the formula (2.11).

With that, the values of the mean wind pressure can be computed for a given figures of safety level, *SL* and added to

$$SL = 1 - CDF \tag{2.13}$$

The setting for the safety level for the level 1 criterion will define both the wave steepness and the wind pressure. Beyond these, there are no more random parameters involved in the level 1 criterion. Now, if the standard for level 2 is established above the safety level for the level 1 criterion, the criteria always will be consistent between the levels.

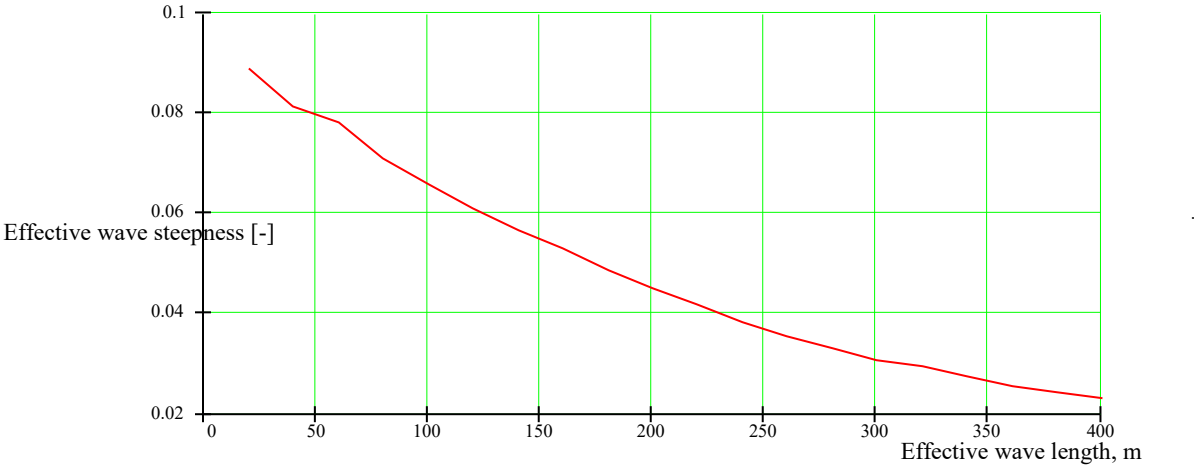

Figure 2.10. Steepness of Effective Wave for Safety Level of 1 %

Table 2.1. Safety Level and Wave Steepness

Safety level	0.005	0.01	0.015	0.02	0.025	0.03	0.035	0.04	0.045	0.05
Ship Length, m	Wind Pressure. kPa									
	0.5258	0.4678	0.4338	0.4071	0.3825	0.3695	0.3566	0.3437	0.3308	0.3179
20	0.0978	0.0891	0.0834	0.0827	0.0776	0.0730	0.0711	0.0690	0.0686	0.0685
40	0.0910	0.0813	0.0772	0.0757	0.0739	0.0701	0.0695	0.0632	0.0629	0.0627
60	0.0824	0.0782	0.0697	0.0688	0.0687	0.0662	0.0643	0.0603	0.0580	0.0579
80	0.0747	0.0708	0.0642	0.0631	0.0625	0.0619	0.0601	0.0567	0.0541	0.0541
100	0.0703	0.0659	0.0617	0.0583	0.0579	0.0576	0.0551	0.0509	0.0508	0.0506
120	0.0655	0.0609	0.0573	0.0545	0.0537	0.0527	0.0485	0.0482	0.0481	0.0473
140	0.0599	0.0566	0.0515	0.0506	0.0503	0.0478	0.0459	0.0455	0.0447	0.0439
160	0.0560	0.0532	0.0487	0.0469	0.0464	0.0437	0.0433	0.0428	0.0426	0.0406
180	0.0511	0.0488	0.0456	0.0434	0.0430	0.0403	0.0400	0.0389	0.0381	0.0376
200	0.0482	0.0449	0.0429	0.0404	0.0398	0.0379	0.0376	0.0351	0.0351	0.0349
220	0.0456	0.0417	0.0400	0.0374	0.0365	0.0355	0.0355	0.0332	0.0319	0.0319
240	0.0420	0.0383	0.0374	0.0349	0.0337	0.0331	0.0327	0.0316	0.0294	0.0293
260	0.0394	0.0354	0.0350	0.0330	0.0311	0.0311	0.0310	0.0297	0.0282	0.0269
280	0.0366	0.0329	0.0323	0.0305	0.0289	0.0286	0.0285	0.0281	0.0260	0.0251
300	0.0342	0.0308	0.0303	0.0292	0.0270	0.0268	0.0263	0.0259	0.0243	0.0234
320	0.0320	0.0295	0.0283	0.0270	0.0253	0.0251	0.0248	0.0238	0.0234	0.0219
340	0.0302	0.0275	0.0266	0.0247	0.0239	0.0235	0.0235	0.0217	0.0213	0.0206
360	0.0285	0.0255	0.0251	0.0227	0.0225	0.0221	0.0217	0.0199	0.0196	0.0195
380	0.0270	0.0242	0.0232	0.0213	0.0211	0.0205	0.0203	0.0185	0.0184	0.0184
400	0.0257	0.0230	0.0220	0.0203	0.0200	0.0189	0.0187	0.0176	0.0174	0.0173

Table 2.2. Safety Level and Wave Steepness (Continued)

Safety level	0.055	0.06	0.065	0.07	0.075	0.08	0.085	0.09	0.095	0.1
Ship Length, m	Wind Pressure. kPa									
	0.3112	0.3046	0.2980	0.2914	0.2848	0.2782	0.2716	0.2650	0.2584	0.2529
20	0.0683	0.0664	0.0663	0.0662	0.0661	0.0633	0.0626	0.0620	0.0601	0.0571
40	0.0626	0.0625	0.0624	0.0619	0.0611	0.0607	0.0605	0.0604	0.0577	0.0556
60	0.0577	0.0575	0.0575	0.0572	0.0569	0.0567	0.0560	0.0559	0.0527	0.0520
80	0.0536	0.0536	0.0536	0.0535	0.0533	0.0521	0.0509	0.0509	0.0473	0.0464
100	0.0503	0.0500	0.0491	0.0490	0.0490	0.0481	0.0449	0.0446	0.0443	0.0441
120	0.0471	0.0469	0.0447	0.0444	0.0442	0.0424	0.0422	0.0418	0.0418	0.0405
140	0.0438	0.0425	0.0406	0.0406	0.0406	0.0406	0.0405	0.0394	0.0394	0.0372
160	0.0405	0.0392	0.0383	0.0372	0.0371	0.0370	0.0367	0.0366	0.0366	0.0350
180	0.0375	0.0375	0.0368	0.0347	0.0345	0.0333	0.0330	0.0330	0.0329	0.0321
200	0.0347	0.0346	0.0330	0.0328	0.0328	0.0317	0.0303	0.0303	0.0297	0.0297
220	0.0319	0.0313	0.0308	0.0308	0.0307	0.0304	0.0288	0.0285	0.0270	0.0270
240	0.0292	0.0291	0.0288	0.0288	0.0282	0.0282	0.0272	0.0255	0.0248	0.0248
260	0.0269	0.0269	0.0267	0.0264	0.0259	0.0259	0.0252	0.0244	0.0228	0.0228
280	0.0250	0.0249	0.0247	0.0246	0.0245	0.0245	0.0232	0.0225	0.0216	0.0213
300	0.0234	0.0232	0.0232	0.0226	0.0225	0.0224	0.0222	0.0200	0.0199	0.0198
320	0.0219	0.0218	0.0217	0.0209	0.0207	0.0207	0.0206	0.0186	0.0185	0.0185
340	0.0204	0.0204	0.0204	0.0203	0.0188	0.0187	0.0186	0.0175	0.0174	0.0172
360	0.0194	0.0189	0.0188	0.0188	0.0172	0.0170	0.0169	0.0165	0.0164	0.0164
380	0.0181	0.0176	0.0176	0.0175	0.0157	0.0157	0.0157	0.0156	0.0155	0.0155
400	0.0165	0.0164	0.0164	0.0163	0.0148	0.0147	0.0147	0.0145	0.0142	0.0142

2.2.5 Possible Criteria

Theoretically, the consistency between the levels can be achieved if one consider the same criterion for both levels, but interpreted the criterion deterministically for the level 1 and probabilistically for the level 2.

The second reason for the inconsistency between the levels of the pure loss vulnerability criteria is actually the oversimplification of the level 1 criteria. It is common knowledge in Naval Architecture that GM alone does not characterize stability at large heel angles. Thus, level 1 criteria should include enough information to characterize stability at large angles. At the same time it should be more conservative and less accurate than the level 2 criterion. This idea can be implemented by formulating the level 1 criterion for the GZ curve in the worst possible position of ship in a wave (not necessarily when the midship section is located at exactly at the wave crest). Next, the level 2 criteria can be defined based on the stability variation throughout a complete wave pass. The conservatism of the level 1 is then ensured by the simple fact that the worst GZ curve does not last too long.

Possible formulations for the criteria are summarized in Table 2.3.

Table 2.3. Possible formulations for vulnerability criteria of pure loss of stability

#	Level 1: worst GZ curve for the wave pass; one wave steepness, chose by the safety level and ship length	Level 2: all the GZ curves during the wave pass, wave steepness for all the cells of scatter diagram
1	Static angle under the wind pressure p=504 Pa	#1: Time during the wave pass, while the static angle is greater than the standard, should be smaller than a quarter of natural roll period
2		#2: Time during the wave pass, while the static angle is greater than the standard, should be smaller than a time to reach maximum roll angle during the wave pass
3	Static angle under the mean wind pressure corresponding to chosen safety level	#1: Time during the wave pass, while the static angle is greater than the standard, should be smaller than a quarter of natural roll period
4		#2: Time during the wave pass, while the static angle is greater than the standard, should be smaller than a time to reach maximum roll angle during the wave pass
5	Dynamic angle under the mean wind pressure corresponding to chosen safety level	#3&4: Dynamic angle developed during the wave pass under the mean wind pressure should be less than the standard value with (#4) or without (#3) taking into account surging and possible transition to surf-riding.

Indeed, the level 1 criterion becomes more complex compared to the GM based-formulation that has been in works since 2011, including those currently drafted in Annex 3 of SDC 6/ WP.6 (Peters, et al. 2011). The new level 1 proposal requires computation of the GZ curve over the wave pass; these calculations do require a specialized a computer with specialized

software. This seems to be inconsistent with the original intention (Peters et al. 2011) to limit level 1 efforts to spreadsheet-type calculations. However:

- The GZ curve in a wave can be computed with most standard ship hydrostatic software. The level 1 criterion without any simplification can still be applied using the spreadsheet if the worst-case GZ curve during a wave pass can be produced by the standard ship hydrostatic software;
- It may be possible to approximate the worst GZ curve during pass with the worst GM during the wave pass. If this will be found a possibility, the level of complexity of the proposed level 1 criterion will be on the same level as originally envisioned.

The level 1 criterion in the Annex 3 of SDC 6/WP.6 of course will remain the simplest, however, its utility may be questionable due to the lack of ability to distinguish ships vulnerable to the pure loss of stability.

2.2.6 Treatment of Weather-tight Volumes

As mentioned in subchapter 2.2.1, the idea to include weathertight volumes into consideration of vulnerability of pure loss of stability helps with inconsistency of level 2 criteria caused CR1 criterion (Peters and Belenky 2016). Again, the idea is that the submergence of the weather-tight volume does not last long. The wave will pass and stability is expected to be restored. Also an increase of the submerged volume will increase the resistance, the ship will slow down and the wave will pass even quicker.

The case study for the influence of the weather-tight volume was carried out for C11 class containership, with the parameters listed in Table 2.4 and the lines shown in Figure 2.11. A schematic model of the weather-tight volume (including containers and deckhouse) is shown in Figure 2.12, while calm-water GZ curves with and without weather-tight volume are placed in Figure 2.13. The GZ curves are computed for critical KG for IS Code.

Table 2.4. Principle Characteristics of C11 Class Container Carrier

Length BP, m	262	GM (critical IS Code),m	0.38
Breadth molded, m	40	Speed, kn	24
Draft amidships, m	11.5	Windage area , m^2	7,887
KG (critical IS Code), m	19.93	Center of pressure above deck, m	14.73

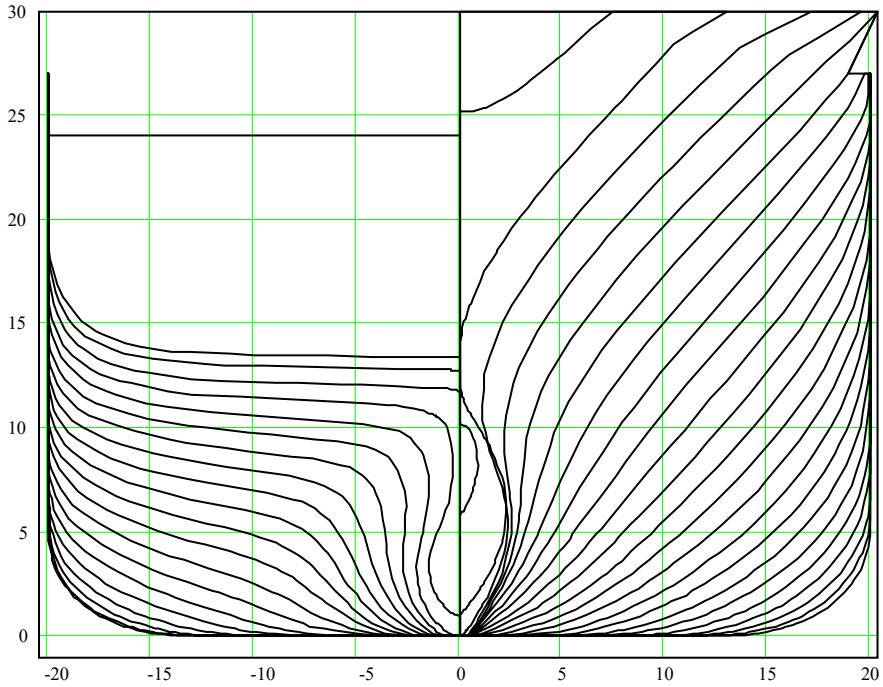

Figure 2.11. Lines of C11 Class Container Carrier

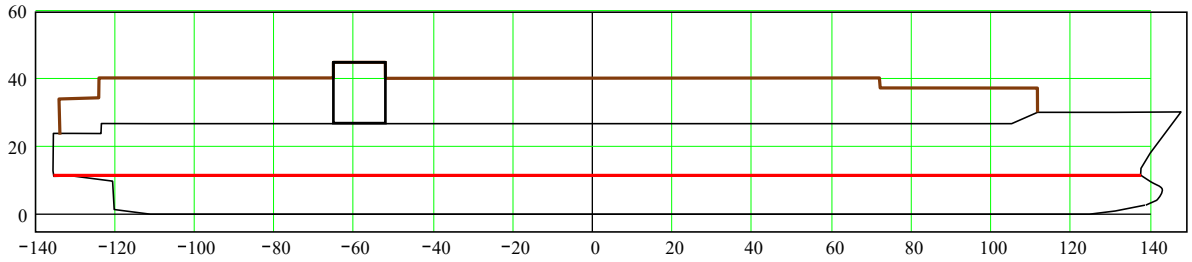

Figure 2.12. Modeling Weather-Tight Volume for C11-Class

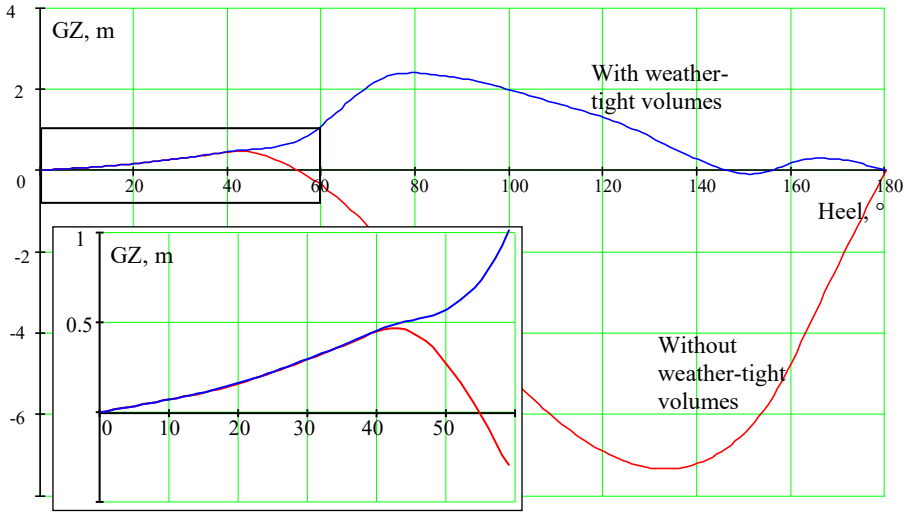

Figure 2.13. Calm-Water GZ Curve Computed for IC-Code Critical KG (Inset Contains a Zoomed-In Plot)

As expected, GZ curves coincide until about 40° and then go apart when the weather-tight volume started creating a restoring moment. Similar tendencies can be observed for the GZ curves in waves. Figure 2.14 shows 21 GZ curves computed during the pass of the wave of steepness 0.076, while the weather-tight volume was not included. Some of the GZ curves, corresponding to the near-wave-crest positions are completely negative. Inclusion of the weather-tight volume removes the complete negativity, see Figure 2.15. These near-wave-crest GZ curves keep their initial negative parts, but become positive for the larger heel angles, thanks to the volume of containers, creating the restoring moment.

Figure 2.16 shows the difference in how the weather-tight volume makes the "worst" GZ curve during the wave pass. In general, the picture is similar to calm-water GZ curve in Figure 2.14, but the divergence starts earlier, around 25 - 27°. Decrease of the wave steepness is expected to move the divergence point to large angles, as calm water is a limit case of "small wave"; see Figure 2.17.

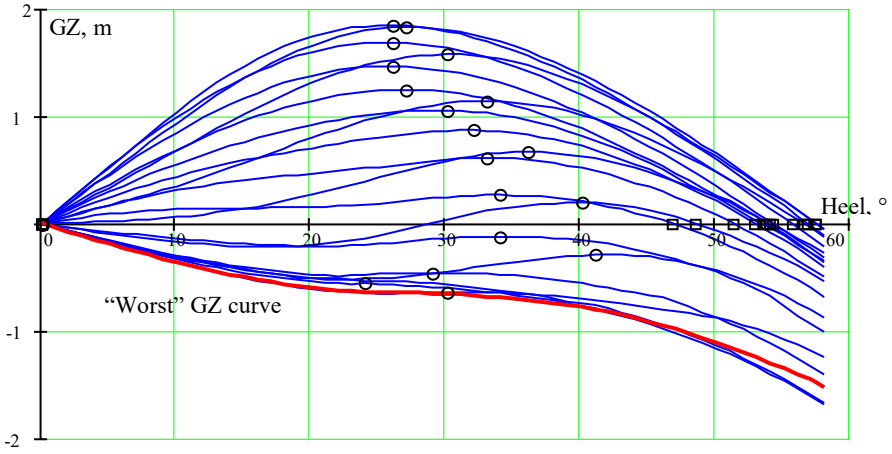

Figure 2.14. GZ Curves in Waves, Steepness 0.076, Weather-Tight Volume not Included

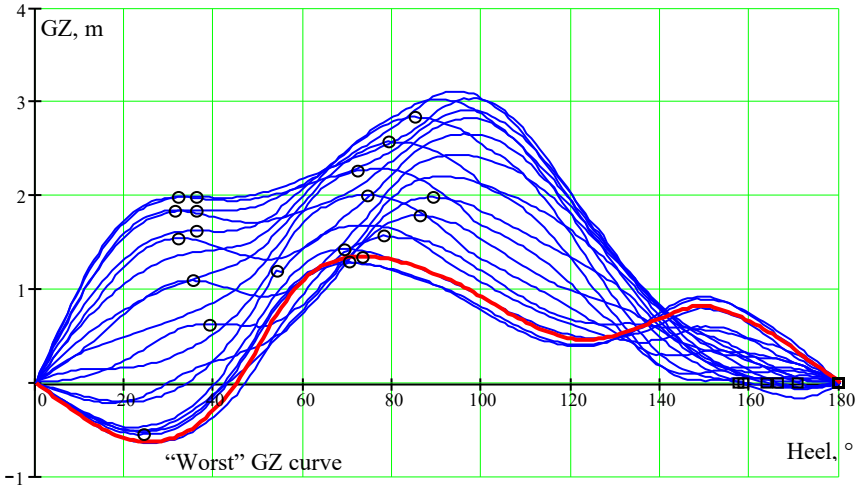

Figure 2.15. GZ Curves in Waves, Steepness 0.076, Weather-Tight Volume Included

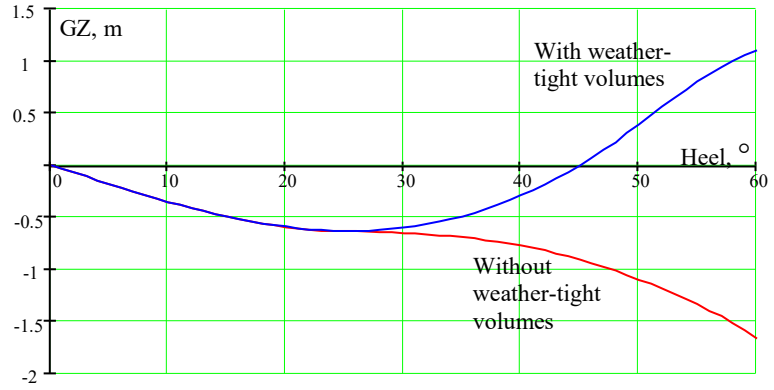

Figure 2.16. Influence of Weather-Tight Volume on "Worst" GZ Curve in Waves, Steepness 0.076

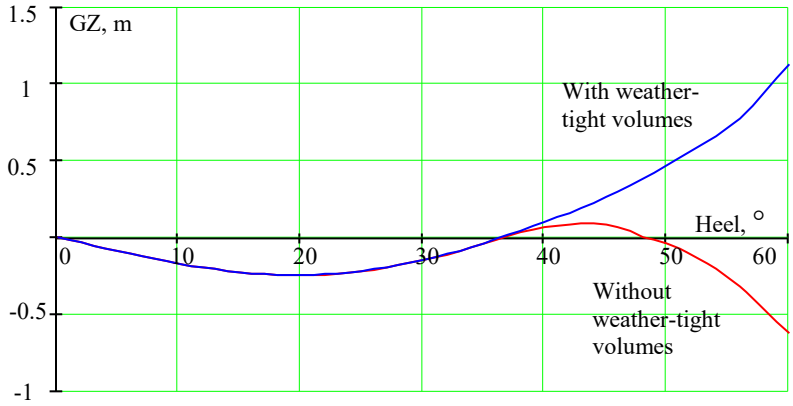

Figure 2.17. Influence of Weather-Tight Volume on "Worst" GZ Curve in Waves Steepness 0.02

Once the weather-tight volume is included in the consideration of pure loss stability, the criterion CR1 may lose its utility. As it can be seen from Figure 2.15, all angles of vanishing stability (marked by squares) are located way beyond the boundary value of 30°, even for the "worst" GZ curve (shown by the thick red line).

The "job" of the CR2 criteria is to catch those GZ curves that lead to a large roll angle. Inclusion of the weather-tight volume probably will not turn the "bad" GZ curves into the good ones, as the divergence is observed for roll angles where stability failure has already occurred.

These considerations lead to the following, albeit a bit unexpected conclusion: allowing inclusion of the weather-tight volume may be equivalent to removing the CR1 criterion. Moreover, once the CR1 criterion is removed, modeling of the weather-tight volume may actually not be necessary. However, to test this hypothesis, the C11 class container carrier will be included in the further case study in two variants: with and without weather-tight volume included.

2.2.7 Case Study

To check if the theoretical consideration of the nature of inconsistency is correct, to test the criteria, described in Table 2.3, and to check the influence of the weather-tight volumes, a case study was carried out and described in this subchapter.

As it was mentioned already the two variants of the C11 container carrier (with and without weather-tight volume) will be included in the case study. The third variant is a RoPax carrier, similar to M/S Aratere; known to suffer from a pure loss of stability accident (Maritime New Zealand, 2007). Characteristics of the sample RoPax ship can be found in Table 2.5.

The calculations are carried out as follows:

Compute currently proposed and considered in Table 2.3, level 1 criteria for IS Code KG critical (KG_{cr_ISCode})

1. Find KG critical to satisfy the level 1 criterion (KG_{cr_lvl1})
2. Compute currently proposed and considered in Table 2.3, level 2 criterion for the corresponding level 1 KG critical

Table 2.5. Principle Characteristics of RoPax Carrier

Length BP, m	140.4	GM (critical IS Code), m	0.702
Breadth molded, m	20.27	Speed, kn	19
Draft amidships, m	5.77	Windage area , m^2	2,739
KG (critical IS Code), m	9.622	Center of pressure above deck, m	9.92

One can extract important information from the difference $\Delta KG = KG_{cr\_lvl1} - KG_{cr\_ISCode}$. First, the pair of vulnerability criteria are consistent if, for $KG = KG_{cr\_lvl1}$, level 2 criterion is satisfied. The second, if KG_{cr_lvl1} corresponds to realistic loading condition, the ship is vulnerable to the pure loss of stability. The RoPax is expected to be vulnerable, while C11-class is not, despite the latter is known for significant stability variations in waves. The results of RoPax Case study are placed in Table 2.6. Safety level adopted for the level 1 criteria is 2 %. A rose background is used when a criterion is not satisfied.

Table 2.6. Results of Case Study for RoPax Carrier (GM, m or Heel Angle, and ° for Level 1 and Probability for Level 2)

Criteria		IS Code	Simplified GM	Direct calc. for GM in Waves	Static Angle Under P=504 Pa	Static Angle Under with Wind Pressure of Given Safety Level	Dynamic. Angle Under with Wind Pressure of Given Safety Level
Column		1	2	3	4	5	6
□KG, m		0	-1.33	-0.147	-0.437	-0.421	-0.692
Level 1	Simplified GM, m	-1.281	0.05	-1.134	-0.808	-0.86	-0.589
	Direct calc. for GM in waves, m	-0.097	1.23	0.05	0.377	0.325	0.596
	Static angle under P=504 Pa, deg	30.2	3.9	25.8	15.0	16.6	9.5
	Static angle under wind press. of given safety level	29.4	3.1	24.8	13.3	15.0	7.9
	Dynamic angle under wind press. of given safety level	44.3	6.3	37.6	22.8	25.0	15.0
Level 2	CR1	0	0	0	0	0	0
	CR2	0.537	$2.0\ 10^{-4}$	0.366	0.148	0.148	0.055
	#1: Time while stat. angle is large compare to quarter of roll period	0.173	0	0.083	$5.1\ 10^{-3}$	$9.2\ 10^{-3}$	$2.87\ 10^{-3}$
	#2: Time while stat. angle is large compare to time to reach it	0.022	0	0.013	$7.94\ 10^{-4}$	$1.25\ 10^{-3}$	$3.5\ 10^{-4}$
	#3: Dynamic angle without account of surging	0.271	0	0.146	0.03	0.039	$4.77\ 10^{-3}$
	#4: Dynamic angle with account of surging	0.173	0	0.142	0.047	0.059	$8.28\ 10^{-3}$

The first question to be addressed is: can any criteria detect vulnerability? To address this question, calculations for IS Code critical KG are carried out. The value of GM in IS-Code critical condition is 0.702 m. There is no information available, if such GM is unpractical for summer load line; there is a motivation to keep GM as low as possible to provide a comfortable ride for passengers. A ship, similar to considered RoPax carrier, has suffered from a stability accident that may be attributed to pure loss of stability (Maritime New Zealand, 2007). Thus, the considered RoPax ship is assumed to be vulnerable to pure loss of stability in IS Code-critical conditions.

The Table 2.6 is configured in order to test and compare the consistency of the six criteria, which are presented in four numbered columns. The base loading condition is the maximum KG

for which the criteria of the 2008 IS Code are satisfied (column 1) – termed the "limiting 2008 IS Code critical condition": all the results in this column were computed for those KG. Column 2 shows the level 1 criterion as proposed in Annex 2 IMO SDC 6/WP.6 (column 2: "simplified GM"); column 3 shows the previously proposed level 1 criteria that involved the direct calculation of GM in a longitudinalt wave; and column 4 presents the static angle criterion computed for the worst GZ curve, see #1 and 2 in Table 2.3. Column 5 contains results for the static angle computed with wind pressure, corresponding to the accepted safety level (see #3 and 4 in Table 2.3). Column 6 shows the results of application of dynamic angle criterion, described as #5 in Table 2.3. The section, marked "level 2" shows results of calculation for level 2: long-term probability.

All the level 1 criteria detect the vulnerability: GM-based criteria are below standard of 0.05 m and angle-based criteria show exceedance of 15° used as standards for both static and dynamic angle-based criteria. For the level-2, probabilistic vulnerability criteria, the standard 0.06 is used as directed in paragraph 1.3.2 of Annex 3 of SDC 6/WP.6. Then, all the level 2 criteria detect vulnerability, except the criterion #2, comparing a time during a wave pass when the static angle exceeds 15° with a time necessary to reach the angle of 15° in the worst possible condition.

The second question is the consistency between level 1 and 2. To answer this question, critical KG values are computed for all the level 1 criteria. Then, the values of level 2 criteria are computed and compared with the standard. If the criteria are consistent, no vulnerability are expected on the level 2. All the criteria are analyzed here: the consistency are expected for all the combinations of the criteria proposed in this report, except when the level-1 criterion uses the dynamic angle, while the level 2 criterion is based on a static angle. Indeed, a dynamic angle always exceeds a static angle and additional conservatism introduced with time based conditions may not be always sufficient to compensate for the difference between the level static and dynamic angle.

The critical state for the level-1 criteria (simplified GM formula) per paragraph 1.2 Annex 3 of CDC 6/WP.6, requires lowering KG by 1.33 m, as the simplified GM formula is known to be very conservative for non-wall-sided ships. Indeed, such conservatism leads to no vulnerability to pure loss of stability on the level 2, but the ship may become very stiff.

The version of the vulnerability criteria for pure loss of stability prior to the SDC-5/6 intersessional period allowed using direct calculation of GM in waves (paragraph 2.10.2.3 of Annex 1 SDC2/WP.4). Table 2.6 shows that there is a significant inconsistency with all the level 2 criteria except from #2.

This inconsistency is hardly surprising. No guaranteed consistency can be expected for GM-based criteria. GM value does not describe stability in large angles. Also the GM-based criteria use wave steepness 0.0334 (paragraph 1.2.2, Annex 3 of CDC 6/WP.6) leading to different safety levels for ships of different lengths.

One can estimate actual level of safety provided by the GM-based criteria. Using table 2.1 for the ship length of 140.4 m, one can obtain a steepness of effective waves as a function of the safety level, see Figure 2.18. Then, this steepness is used to compute GM in waves with the simplified formula from paragraph 1.2.2, Annex 3 of CDC 6/WP.6 for the IS-Code critical KG. The result is shown in Figure 2.19. Figure 2.18 shows the steepness value of 0.0334 is too small for the considered case and falls out of range. Nevertheless, the safety level of the level 1

criterion can be estimated by extrapolation, using either the closest linear interval resulting the safety level of 10.9 % or linear regression, yielding 10.3 %. Similar calculations carried out for the direct calculation of GM are presented in Figure 2.20. Safety levels are 11.0 % and 11.8 %, respectively.

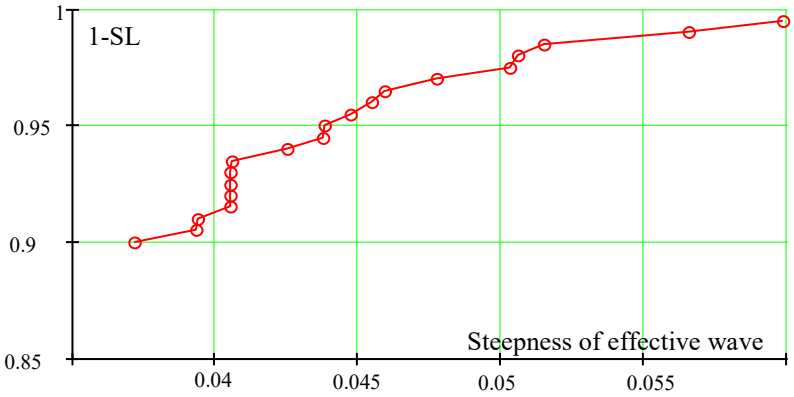

Figure 2.18. Steepness of Effective Wave as a Function of Safety Level

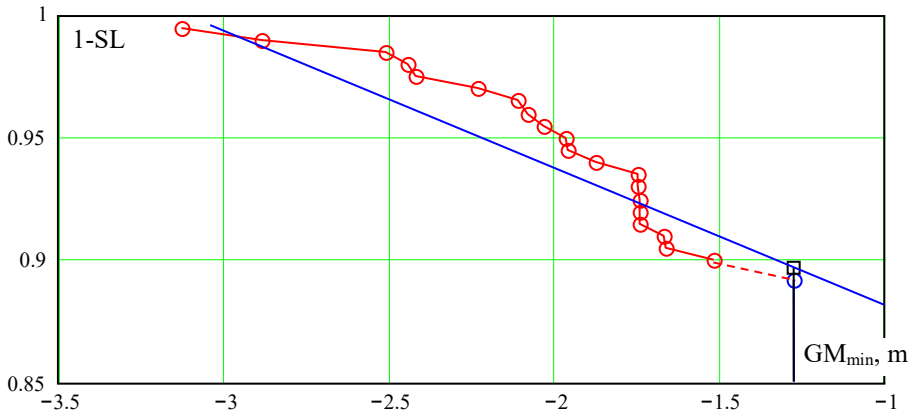

Figure 2.19. Minimum GM in Waves, Computed with Simplified Formula as a Function of Safety Level

The actual values of safety level for the level 1 vulnerability criterion is almost twice of the accepted standard of 6 % (paragraph 1.3.1, Annex 3 of CDC 6/WP.6). That explains the second reason of inconsistency.

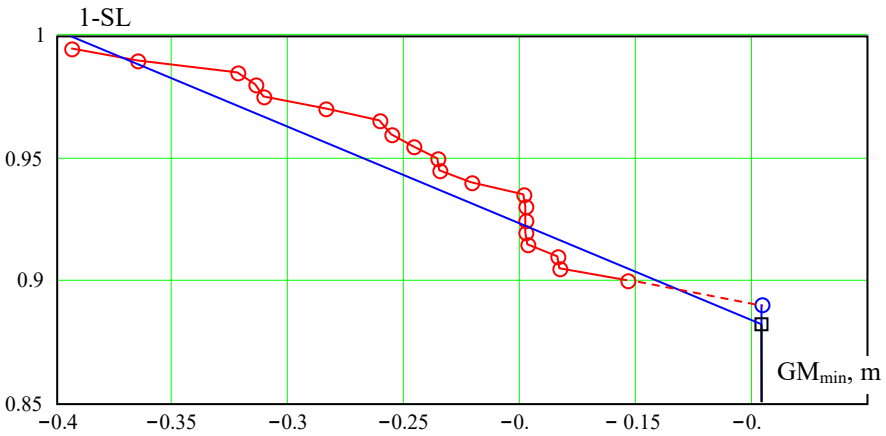

Figure 2.20. Minimum Direct GM in Waves, as a Function of Safety Level

On the other hand, as seen from the Table 2.6, all proposed level 1 criteria (columns 4, 5, and 6) are consistent with all proposed level 2 criteria. The consistency was observed even in the cases when level 1 criterion was using the static angle, while level 2 was based on the dynamic angle. The situation, however, is very close to the inconsistency: the level 2 criterion #4 is very close to the standard (0.059) for the level-1 criterion using static angle under mean wind pressure corresponding to the given safety level.

The IS Code mean wind-pressure and corresponding static angle yields quite the conservative criterion. The mean wind pressure is based on the accepted safety level of 2 % is only 407 Pa, see Table 2.1. That makes the former criterion more conservative than the latter, requiring lowering KG to 0.437 m vs 0.421 m (see Table 2.6, columns 4 and 5). The level-1 dynamic angle criterion is more conservative than both level-1 static angle criteria, despite it using smaller mean wind-pressure of 407 Pa; it requires lowering KG for 0.692 m. All the proposed level 2 criteria follow the same tendency: dynamic angle is more conservative than the static angle. This conservatism makes the dynamic angle criterion pass with significant margin: 0.0083 < 0.06 (see Table 2.6, column 6).

Table 2.7 contains results of C11 class containership; weathertight volumes were included in calculation of GZ curve in wave and the standard angle was taken equal 15° – same as for the RoPax (rose background is used when a criterion is not satisfied). The following observations can be made:

- Vulnerability for IS-Code critical KG is detected by all the criteria, except Level 2 /#2. “Old” post-panamax container ships are not known for pure loss of stability. However, their lowest operational GM is about 1 m (likely due to damage stability criteria requirements). Also, these ships are known for significant variation of stability in waves (leading to a known parametric roll accidents). Thus, the indicated vulnerability to pure loss of stability in KG-critical condition with GM = 0.38 m is, probably, not wrong, but not observable in realistic operational conditions.
- No vulnerability or inconsistency between the levels is observed for KG critical based on simplified GM criterion as defined in paragraph 1.2, Annex 3 of CDC 6/WP.6. Application of this criterion, however, would make the minimum GM = 3.693 - 0.38 =

3.3 m, excluding most of full-load conditions. Such exclusion is hardly reasonable, having in mind the absence of known accidents caused by the pure loss of stability.

- Inconsistency is observed in the previously proposed level 1 criteria that used the direct calculation of GM (column 3).
- No inconsistency is observed for any of the criteria, described in Table 2.3.

Table 2.7. Results of Case Study for C11 Container Carrier with Weather-Tight Volumes Included, with the Limit Angle 15° (GM, m or Heel Angle, ° for Level 1 and Probability for Level 2)

Criteria		IS Code	Simplified GM	Direct calc. for GM in Waves	Static Angle Under P=504 Pa	Static Angle Under with Wind Pressure of Given Safety Level	Dynamic Angle Under with Wind Pressure of Given Safety Level
Column		1	2	3	4	5	6
□KG, m		0	-3.693	-1.574	-1.457	-1.425	-1.665
Level 1	Simplified GM, m	-3.643	0.05	-2.069	-2.186	-2.218	-1.978
	Direct calc. for GM in waves, m	-1.524	2.169	0.05	-0.067	-0.099	0.141
	Static angle under P=504 Pa, deg	44.344	1.128	12.1	15	15.8	9.9
	Static angle under wind press. of given safety level	44.155	0.912	11.0	14.1	15	8.7
	Dynamic angle under wind press. of given safety level	64.873	1.655	18.1	22.1	23.2	15
Level 2	CR1	0	0	0	0	0	0
	CR2	0.849	0	0.086	0.108	0.108	0.057
	#1: Time while stat. angle is large compare to quarter of roll period	0.445	0	$1.66\ 10^{-3}$	$8.484\ 10^{-3}$	$8.69\ 10^{-3}$	$1.44\ 10^{-3}$
	#2: Time while stat. angle is large compare to time to reach it	0.011	0	0	0	0	0
	#3: Dynamic angle without account of surging	0.18	0	$1.275\ 10^{-3}$	$2.346\ 10^{-3}$	$2.38\ 10^{-3}$	$6.423\ 10^{-4}$
	#4: Dynamic angle with account of surging	0.18	0	$6.051\ 10^{-4}$	$1.107\ 10^{-3}$	$1.275\ 10^{-3}$	$2.683\ 10^{-4}$

To check the influence of the inclusion of weather-tight volumes, all the C11 calculations were repeated with water-tight volumes only. The results are summarized in Table 2.8 (rose background is used when a criterion is not satisfied). The observations are as follows:

- Both static and dynamic angles could not be computed for 2008 IS-Code critical KG.
- CR1 criterion has a non-zero value.
- All other values are similar.

It means that, for any of the criteria from Table 2.3, modeling of the weather-tight volumes is not really necessary, as vulnerability to pure loss of stability can be determined before the weather-tight volume enter water with exception of minimized stability cases.

Table 2.8. Results of Case Study for C11 Container Carrier without Weather-Tight Volumes, with the Limit Angle 15° (GM, m or Heel Angle, and ° for Level 1 and Probability for Level 2)

Criteria		IS Code	Simplified GM	Direct Calc. for GM in Waves	Static Angle Under P = 504 Pa	Static Angle Under with Wind Press. of Given Safety Level	Dynamic. Angle Under with Wind Press. of Given Safety Level
Column		1	2	3	4	5	6
□KG, m		0	-3.693	-1.578	-1.462	-1.43	-1.67
Level 1	Simplified GM, m	-3.643	0.05	-2.065	-2.18	-2.212	-1.973
	Direct calc. for GM in waves, m	-1.528	2.165	0.05	-0.065	-0.097	0.142
	Static angle under P=504 Pa, °	-	1.13	12.1	15	15.8	9.9
	Static angle under wind press. of given safety level	-	0.914	11.0	14.1	15	8.7
	Dynamic angle under wind press. of given safety level	-	1.652	18.1	22.1	23.2	15
Level 2	CR1	0.057	0.057	0.057	0.057	0.057	0.057
	CR2	0.849	0	0.086	0.108	0.108	0.057
	#1: Time while stat. angle is large compare to quarter of roll period	0.445	0	$1.66\ 10^{-3}$	$8.484\ 10^{-3}$	$8.69\ 10^{-3}$	$1.44\ 10^{-3}$
	#2: Time while stat. angle is large compare to time to reach it	0.011	0	0	0	0	0
	#3: Dynamic angle without account of surging	0.18	0	$1.275\ 10^{-3}$	$2.346\ 10^{-3}$	$2.38\ 10^{-3}$	$6.423\ 10^{-4}$
	#4: Dynamic angle with account of surging	0.18	0	$6.051\ 10^{-4}$	$1.107\ 10^{-3}$	$1.275\ 10^{-3}$	$1.248\ 10^{-4}$

Finally, the calculations for C11 were repeated for the standard angle of 25° as recommended for cargo vessels by paragraph 1.2, Annex 3 of CDC 6/WP.6. The results are

shown in Table 2.9 (a rose background is used when a criterion is not satisfied). No qualitative difference can be seen compare to results shown in Table 2.7 and Table 2.8. All the criteria described in Table 2.3 still yield consistent results.

Table 2.9. Results of Case Study for C11 Container Carrier without Weather-Tight Volumes, with the Limit Angle 25° (GM, m or Heel Angle, and ° for Level 1 and Probability for Level 2)

Criteria		IS Code	Simplified GM	Direct Calc. for GM in waves	Static Angle Under P = 504 Pa	Static Angle Under with Wind Pressure of Given Safety Level	Dynamic Angle Under with wind Pressure of Given Safety Level
Column		1	2	3	4	5	6
□KG, m		0	-3.693	-1.578	-0.993	-0.974	-1.374
Level 1	Simplified GM, m	-3.643	0.05	-2.065	-2.649	-2.669	-2.269
	Direct calc. for GM in waves, m	-1.528	2.165	0.05	-0.535	-0.554	-0.153
	Static angle under P=504 Pa, °	-	1.13	12.1	25	25.4	17.4
	Static angle under wind pressure of given safety level	-	0.914	11.0	24.7	25	16.6
	Dynamic angle under wind pressure of given safety level	-	1.652	18.1	36.9	37.5	25
Level 2	CR1	0.057	0.057	0.057	0.057	0.057	0.057
	CR2	0.849	0	0.086	0.0857	0.0857	0.0128
	#1: Time while stat. angle is large compare to quarter of roll period	0.445	0	$1.66\ 10^{-3}$	0.0023	0.0041	$1.95\ 10^{-5}$
	#2: Time while stat. angle is large compare to time to reach it	0.011	0	0	0	0	0
	#3: Dynamic angle without account of surging	0.18	0	$1.275\ 10^{-3}$	0.0013	0.0017	$5.695\ 10^{-5}$
	#4: Dynamic angle with account of surging	0.18	0	$6.051\ 10^{-4}$	0.0013	0.0013	$6.582\ 10^{-5}$

2.2.8 Choice of Alternative Criteria

To facilitate choices within the alternative vulnerability criteria, the present case study is complemented by calculations of the critical KG based on level 2 criteria for all the considered cases. The results are summarized in bullets below and in Table 2.10:

- The value of required KG change for the criterion #2 is positive. The criterion #2 fails to indicate vulnerability, where other criteria do. The result shown in Table 2.10 are consistent with Tables 2.5-2.8. If true then it can be excluded from further consideration;
- Other criteria seem to be capable of distinguishing between a containership and a RoPax, using standard angle 15° for the RoPax and 25° for a containership as recommended in paragraph 1.2, Annex 3 of CDC 6/WP.6.
- Criteria #3 and #4 have better physical backgrounds compared to criterion #1 as the natural period of roll in calm water is not really relevant for large roll angles caused by significant variation in the stability in waves.
- Based on the results in Table 2.10, criterion #4 seems to be more conservative than criterion #3; also its mathematical model is more detailed. However, in some cases (see Table 2.7), criterion #3 yielded a larger value than criterion #4. Thus, for the sake of conservatism, it makes sense to compute both of them and pick the largest value.

Table 2.10. ΔKG for Proposed Level 2 Criteria

	RoPax R_{PL2} = 15	C11 with Weather-Tight Volume R_{PL2} = 15	C11 w/o Weather-Tight Volume R_{PL2} = 15	C11 W/o Weather-Tight Volume R_{PL2} = 25
#1: Time while stat. angle is large compare to quarter of roll period	-0.2	-1.01	-1.01	-0.5
#2: Time while stat. angle is large compare to time to reach it	0.11	0.48	0.55	-
#3: Dynamic angle without account of surging	-0.352	-0.5	-0.5	-0.05
#4: Dynamic angle with account of surging	-0.41	-0.64	-0.64	-0.22

Based on the results of the calculations shown in Table 2.6 through Table 2.10, the alterative criterion is taken as the largest value between dynamic angles with and without account of surging.

2.2.9 Formulation of Alternative Criteria for Level 1

A ship is not considered vulnerable for pure loss of stability if:

$$\varphi_d \leq R_{PL2} \tag{2.14}$$

Where a dynamic angle of heel φ_d, calculated by equalizing area *a* and area *b*, as shown in Figure 2.21, R_{PL2} = 15° for passenger vessels and 25° otherwise.

The angle φ_d, is determined as a response to a dynamically applied wind heeling moment with the arm l_w, computed as:

$$l_w = K_D \cdot \frac{p_A \cdot W_A \cdot Z_A}{g \cdot m} \cdot sin(\beta) \tag{2.15}$$

Where W_A is the windage area, and Z_A represents the height of the geometric center of the windy area above the waterline (as no wind drift is assumed), *m* is mass of the ship and g is the gravity

acceleration. K_D is a coefficient accounting for a sudden gust; similar the 2008 IS Code, it is assumed:

$$K_D = 1.5$$

A wind direction is assumed at a stern quartering angle of β = 20° relative to following seas. The mean wind pressure p_A is taken from Table 2.1 by linear interpolation for the selected safety level.

The choice of safety levels determines the conservativeness of the level 1 criterion. It has to be less than a standard for the level 2 criterion. Calculations, presented in Table 2.6-Table 2.10 used 2 % for safety level.

The wave steepness for computation of the GZ curve in waves is selected from Table 2.1 by linear interpolation for selected safety level and ship length. Determination of the dynamic angle of heel is carried out with the worst GZ curve in wave computed for selected wave steepness. The worst GZ curve is determined by the largest static angle caused by the heeling moment with the arm l_w, as defined by the equation (2.3). Figure 2.21 shows the Determination of the dynamic angle for the level 1 alliterative vulnerability criteria for pure loss of stability.

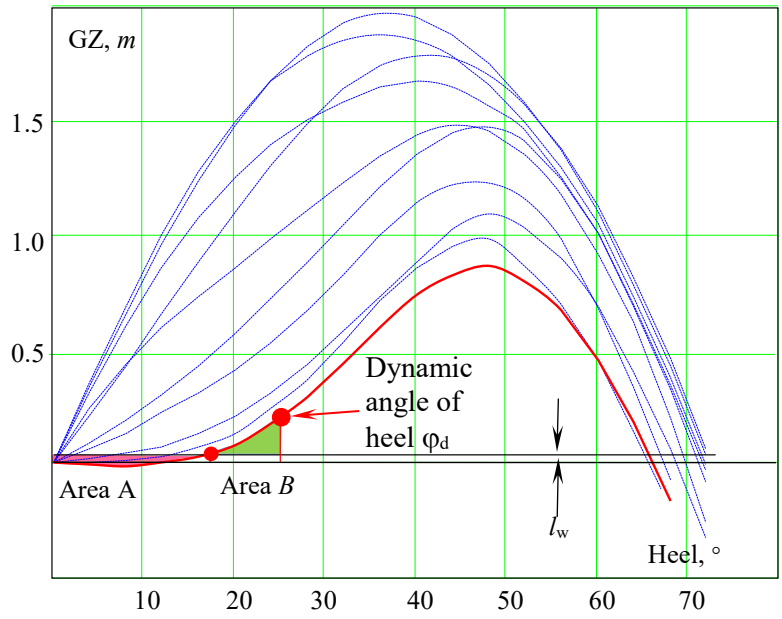

Figure 2.21. On Determination of the Dynamic Angle for the Level 1 Alliterative Vulnerability Criteria for Pure Loss of Stability

2.2.10 Formulation of Alternative Criteria for Level 2

For the pure loss of stability level 2 assessment, a ship is considered not to be vulnerable if:

$$CR \leq R_{PL0} \tag{2.16}$$

Where $R_{PL0} = 0.06$, while the criterion CR is calculated as:

$$CR = \sum_{i=1}^{N} W_i C_i \tag{2.17}$$

Where W_i is weighting factor for the considered short-term environmental condition, taken from Table 1.3.2 in Annex 3 of SDC 6/WP.6, N is a number of wave cases, while the short-term criterion C is defined as:

$$C_i = \begin{cases} 1 & \varphi_d > R_{PL2} \\ 0 & \text{otherwise} \end{cases} \tag{2.18}$$

The dynamic angle φ_d is determined for each short-term environmental condition as:

$$\varphi_d = \max(\varphi_{d1}, \varphi_{d2}) \tag{2.19}$$

Where φ_{d1} is the maximum angle determined by numerical solution of ship rolling equation, while φ_{d2} is the maximum angle determined by numerical solution of coupled rolling and surging equations. The rolling equation is formulated as follows:

$$(I_x + A_{44})\ddot{\varphi} + R_\varphi(\dot{\varphi}) + mgGZ(\varphi, x_c) = mgl_w \tag{2.20}$$

Where, I_x is the moment of inertia in roll; A_{44} are the added mass in roll, and R_ϕ is the roll damping. Quadratic or linear model for roll damping is recommended. If coefficients are not available, they can be estimated with simplified Ikeda method recommended in section 7.5 of Annex 19 of SDC5/INF.4/Add.1. The GZ curve in waves is precomputed and then is interpolated for the particular values of roll angle and position on the wave – see paragraph 3.3.2.4 of Annex 19 of SDC5/INF.4/Add.1 for the calculation of the position on wave x constant forward speed v_s , equal to the service speed is assumed:

$$x_c = (c - v_s)t \tag{2.21}$$

Where t is time and c is the wave celerity. A numerical integration is performed for the duration of one wave pass and largest encountered roll angle for that one wave pass is recorded. Initial conditions correspond to the wave trough, service speed and zero initial roll and roll rate.

To compute the angle φ_{d2}, coupled rolling and surging equations are considered in the following form:

$$\begin{cases} (m + A_{11})\ddot{\xi}_G + R_x(\dot{\xi}_g) - T_e(\dot{\xi}_g, n) = F_x(\xi_G, t) \\ (I_x + A_{44})\ddot{\varphi} + R_\varphi(\dot{\varphi}) + mgGZ(\varphi, x_c) = mgl_w \end{cases} \tag{2.22}$$

Where A_{11} is the added mass in surge; R_x is the ship resistance in calm water; T_e is the ship thrust, achieved with commanded number of propeller revolutions, n; F_x is the Froude-Krylov wave force in direction of surge. Calculation of these values is described in paragraph 4.3.3 of Annex 19 of SDC5/INF.4/Add.1. The wave characteristics (wave number and amplitude) required for computation of the Froude-Krylov wave force are the same as for the calculation of the GZ curve. The position of a ship on a wave is computed as:

$$x_c = (c - \dot{\xi}_g)t \tag{2.23}$$

To ensure conservative result, initial condition position on the wave is varied, while initial roll angle and rate are taken as zeros, the initial forward speed corresponds to the service speed (21 initial positions, uniformly distributed over ship length, are considered sufficient). Numerical integration of the equation of motion (2.8) is repeated for each initial position on the wave and the largest absolute value of roll angle is taken as the φ_{d2} value.

Grim effective wave concept is used to represent each short-term environmental condition with a single regular wave, as recommended in section 3.2.2 of Annex 19 of SDC5/INF.4/Add.1.

2.2.11 Sample Calculations for Alternative Criteria

Limited sample calculations were carried out for three ships in realistic loading conditions. The objective is to see if the results of the application of alternative vulnerability criteria contradict existing operation experience. The results are placed in Table 2.11.

None of the tested ships are known for the stability accident that can be attributed to the pure loss of stability. Also LNG carriers and bulk carriers generally are not known for significant variations of stability in following waves. The fast container carrier featured two screws and a cruiser stern, from which only a moderate stability variation could be expected.

Table 2.11. Results of Sample Calculation

Value	LNG Carrier	Bulk Carrier	Fast Container Carrier
Length, BP, m	257	145	274.3
Breadth, m	41.68	23.03	32.16
Loading condition	SLL	SLL	SLL
Draft, m	12.00	10.80	10.57
Volumetric displacement, m^3	100,400	29,510	50,700
KG, m	15.93	9.01	13.51
GM, m	2.55	0.73	0.21
Long. windage area projection, m^2	5874	979	5253
Altitude of center of windage area, m	11.63	5.56	9.85
Service speed, kn	21	15	33
Level 1 criterion, $\Box_d$, deg	0.24	0.2	7.7
Level 2 criterion, *CR*	0	0	0.00011

The results in Table 2.11 generally meet these expectations: none of the tested ship was found vulnerable to the pure of stability. The containership has shown appreciable values for the both levels criteria, which does not contradict to expected moderate stability variation.

When completing the consideration of the assessment of the pure loss of stability, it can be stated that developed alternative vulnerability criteria, while consistent are not overly conservative. That said that their further testing and evaluation could be recommended in the course of trial application of the second generation of IMO intact stability criteria.

2.3 Issues Related to Vulnerability Criteria for Parametric Rolling

2.3.1 Sources of Possible Inconsistencies

Consistency between level 1 and level 2 vulnerability criteria for parametric roll was identified as an outstanding issue at the 5th session of SDC and was included in the terms of references of the intersessional correspondence group (paragraph 3.3.6 of SDC 6/5). The inconsistency manifests itself, when a loading condition is identified as “non-vulnerable” by the level 1 assessment and is found to be vulnerable by the level 2 assessment.

The level 1 vulnerability criterion, formulated in section 2.2 of Annex 3 of SDC6/WP.6 is intended to detect conditions when parametric resonance becomes possible using the simplest mathematical model available – the Mathieu equation with damping. The level 2 vulnerability criterion is described in section 2.2 of Annex 3 of SDC6/WP.6 and contains two checks based on different mathematical models. The check 1 is also based on the Mathieu equation with damping, computed for the range of encounter frequencies. The check 2 is focused on magnitude of parametric roll. The latter is computed by numerical integration of a nonlinear roll equation with periodical variation of GZ curve.

In principle, a combination of a linear Mathieu equation for the level 1 criterion and a nonlinear equation with periodic stiffness for the level 2 criterion should yield consistent criteria. The reason is that a linear equation is sufficient for determination of a range of frequencies where parametric resonance is possible, while stiffness nonlinearity is "responsible" for the magnitude (because of nonlinearity instantaneous natural frequency changes, taking the dynamical system from the conditions parametric resonance). Conservatism of the level 1 criterion is meant to be ensured by an indication of vulnerability for any condition where parametric roll is possible, including those with small magnitude.

Nevertheless, inconsistencies between the levels were encountered during sample calculations, which lead to the requirement to address this problem in paragraph 3.3.6 of SDC 6/5.

The solution, chosen by the correspondence group, is to use a simplified formula (Paragraph 2.2.2 of Annex 3 SDC 6/5) for calculation of the variation of GM in the waves exclusively. The formula is known to overestimate the variation, providing additional conservatism for the level 1 criterion. This additional conservatism seems not to produce too many false positive cases, also level 2 criterion is not known for excessive conservatism. As a result, vulnerability criteria for parametric roll were felt to be ready to trial use, see SDC 6/5/6. Thus, the objective of this section is to summarize a discussion on theoretical reasons for inconsistency between the levels of the parametric-roll vulnerability criteria

2.3.2 Inconsistencies Related to Roll Damping

The level 1 vulnerability criterion for parametric roll as formulated in paragraph 2.2.1 of Annex 3 SDC 6/ WP.6 is based on a condition of instability of the Mathieu equation with damping;

$$\ddot{\varphi} + 2\delta\dot{\varphi} + \omega_m^2\left(1 + h\cos(\omega_e t)\right)\cdot\varphi = 0 \tag{2.24}$$

Where φ is a roll angle, δ is damping coefficient, h is a magnitude of parametric excitation, ω_m is a natural frequency, while ω_e is the frequency of encounter.

More precisely, the criterion is based on an amplification factor of an approximate solution, see Peters, et al (2011) equation (16), reproduced here for the sake of convenience:

$$\varphi(t) = \frac{\sqrt{2}}{2}\varphi_0 e^{-\delta t}\left(e^{-\frac{h}{4}\omega_m t}\sin\left(\omega_m t + \frac{\pi}{4}\right) - e^{\frac{h}{4}\omega_m t}\sin\left(\omega_m t - \frac{\pi}{4}\right)\right) \tag{2.25}$$

Where φ_0 is initial roll angle.

There are two terms inside the parenthesis; one has an exponential function with negative argument – this term decays fast, thus is inconsequential for stability of the solution:

$$\varphi(t) = -\frac{\sqrt{2}}{2}\varphi_0 e^{\left(\frac{h}{4}\omega_m - \delta\right)t}\sin\left(\omega_m t - \frac{\pi}{4}\right) \tag{2.26}$$

It is obvious from equation (2.26) that the term $\left(\frac{h}{4}\omega_m - \delta\right)$ defines whether the solution will decay (if the expression in parenthesis is negative) or will grow, i.e. becomes unstable (if the expression in parenthesis is positive). Having in mind that (see Peters, et al 2011 for details)

$$h = \frac{\Delta GM}{GM} \tag{2.27}$$

Where ΔGM is a variation of the GM value during a wave pass; GM is taken with free surface correction according to paragraph 2.2.1 of Annex 3 SDC 6/ WP.6. As a result, the criterion is formulated as

$$\frac{\Delta GM}{GM} \leq 4\mu \tag{2.28}$$

Where $\mu = \delta/\omega_m$ is roll damping, expressed in terms of critical damping (critical damping does not allow oscillatory solution and $\delta_{cr} = \omega_m$).

The standard for the level 1 criterion assumes damping μ= 0.0425 plus influence of bilge keels (except for the case of the sharp bilge, when the damping is assumed around 0.4675 = 1.87/4). If the roll damping is smaller used for the level 2 is less than assumed in the level 1, the parametric roll vulnerability may be inconsistent between the levels, see example in Figure 2.22.

The example for the C11-class containership in Figure 2.22 shows that the roll damping, calculated with the simplified Ikeda method for speeds below 13 kn, is actually smaller than assumed in the level 1 criterion with account of the bilge keels. However, large variations of GM in waves, typical for the C11 class, "masks" possible inconsistency. At the same time, it may become an issue for a ship with a smaller variation of stability in waves.

The decision made by the SDC5/6 correspondence group was to use this simplified formula for GM variation exclusively (Item 2 in Annex 4 SDC6/INF.3). As a result, the level 1 criterion becomes more conservative; for example for C11 class containership (principle characteristics are given in Table 2.4) for KG = 19 m and calm water GM = 1.375 m, the magnitude of GM variation based on simplified formula is ΔGM = 2.04 m, while direct calculation yields ΔGM = 1.57 m; the values of the criteria were 1.485 and 0.888, respectively.

This conservatism may compensate for possible inconsistency between the levels of parametric roll vulnerability criteria.

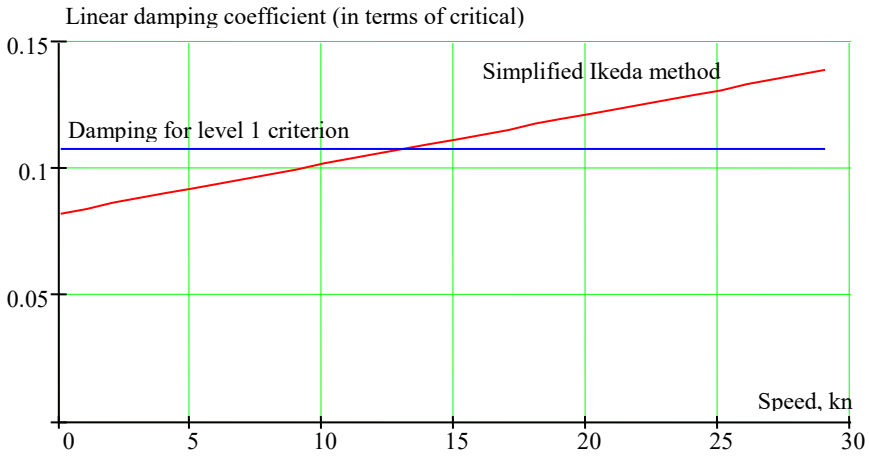

Figure 2.22. Comparison of Damping Estimates between Level 1 and Level 2 Check 2 for C11-Class Containership

2.3.3 Inconsistencies Related to Approximation of GM

The Mathieu equation is the simplest model of parametric resonance thus, it is a very logical choice for mathematical basis of a simple criterion of likelihood of parametric roll. Besides the level 1 criterion, it is used in guidance by ABS (ABS, 2019) and ITTC (ITTC, 2017). The Mathieu equation has a cosine or sine function to model periodic change of stiffness.

For variation of ship stability, using a sine or cosine function is an approximation, as shown by Spyrou, et al (2008). According to the Spyrou, et al (2008), there are two aspect. First, the minimum of the *GM* usually does not occur when the wave crest is located exactly amidship. The minimum of stability in general and GM, in particular, occurs when the wave crest is located aft of the midship. In particular, for the considered example with C11-class containership (See Table 2.4), the minimum GM occurs with the wave crest was located about 18.3 m aft of the midship, see Figure 2.23.

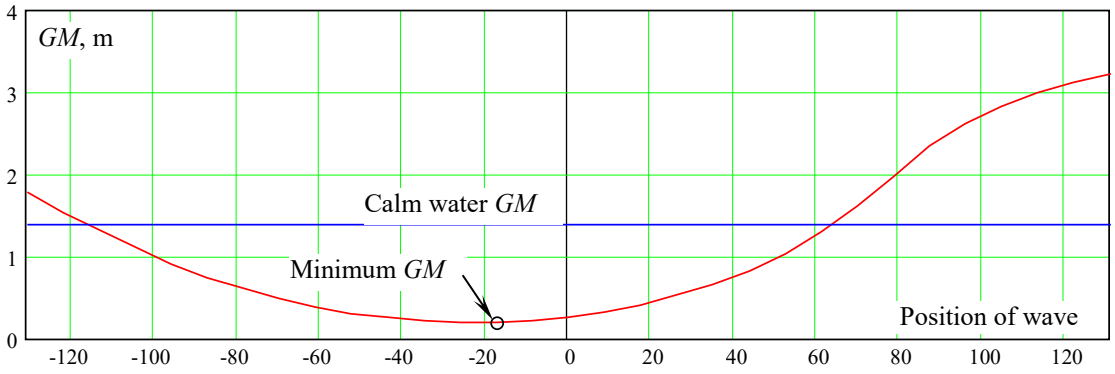

Figure 2.23. GM Value as Wave Crest Position for C11-Class Containership, KG = 19 m

The second aspect of aspect of approximation is the shape of a GM in a wave as a function of the wave-crest position compared to the sine or cosine functions. Following Spyrou et al. (2008), Figure 2.24 shows actual GM in wave form against the shifted cosine/sine approximation. The curve is extended to visualize the periodicity.

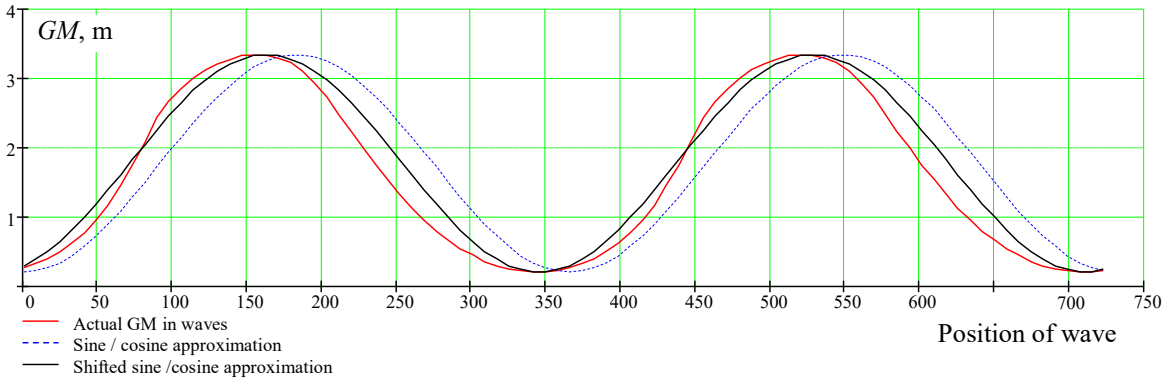

Figure 2.24. Actual GM Value Compare to Cosine or Sine Approximation for C11-class Containership, KG = 19 m

One can see clearly from Figure 2.24 that the actual GM function is quite different for a sine or cosine function. It is not symmetric relative to the mean. In the considered example, the mean value of the GM was 1.63 m while the half-distance between maxima and minima of the GM value was:

$$GM_m = \frac{GM_{max}+GM_{min}}{2} = 1.76\,m$$

Note that both these values are not close to calm water conditions, GM = 1.375 m. The actual GM is also asymmetric relative to its own maximum.

These imperfections, in principle, can lead to inconsistency between the levels, as the Mathieu equation is NOT a linearized version of roll equation of motion with actual GZ curve as stiffness that is used for the second check assessment in the level 2 criterion:

$$\begin{gathered}(\mathrm{I_x} + \mathrm{A_{44}})\ddot{\varphi} + \mathrm{R_\phi}(\dot{\varphi}) + \mathrm{mgGZ}(\varphi, \mathrm{x}) = 0 \\ \text{Linearinzation} \Downarrow \\ (\mathrm{I_x} + \mathrm{A_{44}})\ddot{\varphi} + B_{44}\dot{\varphi} + \mathrm{mg}GM(\mathrm{x})\varphi = 0\end{gathered} \tag{2.29}$$

Where a B_{44} liner-roll damping coefficient and $GM(x)$ actually show periodic functions describe the GM variation in waves.

Using actual $GM(x)$ for the level 1 criterion, it is possible (it can be computed), but hardly practical, as it defeats the purpose of the level 1 criterion as a simple and easy-to-use scanning tool.

3. VULNERABILITY CRITERIA FOR DEAD SHIP CONDITION

3.1 General Description and Implementation

The assumed situation (scenario) for a dead ship condition, which is when a ship loses its propulsion and drifts along in beam seas under the action of wind and waves, is consistent with severe wind and rolling criterion contained in the 2008 IS Code.

The level 1 vulnerability criterion is the same as the severe wind and rolling criterion with the exception that the roll period table is extended from 20 to 30 s. The level 2 criterion is a probabilistic criterion in which wind and waves are considered stochastic processes. In the level 2 vulnerability criterion, the vulnerability is associated with a probability of exceedance of a heel angle of 50° or the downflooding angle, whichever is less, during the exposure time of 1 hr.

The event of exceedance is modeled with a Poisson flow of events and the time before (or the time between) the event occurs has an exponential distribution. The parameter for this distribution is calculated assuming a normal distribution of roll angles and rates. The mean value of roll is computed as a static heel-angle under the steady component of wind. The variance of roll angles and rate is computed through the solution of the roll equation, linearized at the static angle. Roll damping is also linearized. The linearization of the roll equation allows the application of a frequency domain approach. The result (i.e. the probability of exceedance in 1 hr) is weight-averaged through a given wave scatter diagram for which purpose IACS recommendation 34 is used as a default.

The steps in making the computations are as follows:

- For each cell of the scatter diagram:
    - Calculate the mean wind speed velocity and the static angle of heel;
    - Set the wind and wave spectra;
    - Calculate the effective angle of wave slope;
    - Calculate the amount of roll damping;
    - Calculate the variances of roll and roll rate under the combined action of irregular waves and gusty wind;
    - Calculate the upcrossing rate of a heel angle of 50° or the downflooding angle, whichever is less, which is a parameter of exponential distribution of time before the exceedance event; and
    - Calculate the probability of at least one exceedance of a heel angle of 50° or the downflooding angle during 1 hr on the either side of a ship.
- Find the weight-average of the probability of exceedance for all non-zero cells over the scatter diagram.

The calculations were implemented in a form of MathCAD worksheets that provide a self-documented prototype for testing and benchmarking with commercial software.

3.2 Effective Wave-slope angle Function

The level 2 vulnerability criterion for the dead-ship condition uses a representation of roll motion in beam seas with a single degree-of-freedom second-order ordinary differential equation, while the wave excitation is modeled with a stochastic process of the effective angle of the wave slope.

If a ship is small in comparison with a wave (i.e. the ratio of the wavelength to the ship's beam is large), the waterline across the ship beam does not differ much from a straight line, thus the wave heeling moment can be computed with just the equivalent angle of the wave slope. However, if the ship beam is comparable with wave's length, the wave surface curvature over the beam is substantial, making wave heeling calculation inaccurate. The concept of effective wave-slope angle was introduced to account for the inaccuracies when the ship beam is comparable with the wave's length. Essentially, it is a coefficient that alters the approximate wave-slope angle to match the actual wave-heeling moment.

The working version of the Explanatory Notes offers a "standard" for computing an effective wave slope as a function of a wave frequency (see paragraph 3.6.3 in Annex 4 of SDC 4/5/1 Add.3). In this simplified method, the shape of the ship's cross-sections (i.e. the actual stations) were substituted by a rectangle of the corresponding breadth and the draft modified to maintain the same cross-sectional area. The application of this method lead to somewhat unexpected results (see Figure 4.2 in Annex 4 of SDC 4/5/1 Add. 3) An augmented version of that figure is in Figure 3.1, where the region of low wave's length to beam ratio expanded.

One could expect as the wave becomes very short, the wave heeling moment should be small and the effective wave slope coefficient should trend to zero. However, the behavior of the function in Figure 3.1 is quite different, since it shows a peak when the wave's length is slightly less than the ship breadth. This feature may be an artefact of the simplified method recommended by working version Explanatory Notes in paragraph 3.6.3 of Annex 4 of SDC 4/5/1Add.3.

3.2.1 Barge Study: Formulation of the Problem

The "standard" method, described in paragraph 3.6.3 in Annex 4 of SDC 4/5/1Add.3, uses an approximation of the actual ship station with rectangle. Thus, a logical deduction is that it must yield exact results of a prismatic, parallelepiped-shaped barge (i.e. the block coefficient, C_B = 1.00). The numerical integration of undisturbed wave-pressures should produce the effective wave-slope angle identical to the "standard" method up to the numerical accuracy of their respective methods.

In principle, a closed-form solution can be written for the barge. However, such a solution could not be applicable to any other shape, so a numerical solution is preferable because it compares with the results of the "standard" method for a realistic ship hull forms. Such a comparison will be very useful to evaluate the "standard" method and formulate a recommendation about its applicability and utility. The characteristics of the barge used in the study are in Figure 3.1. Table 3.1 show the characteristics of the prismatic barge.

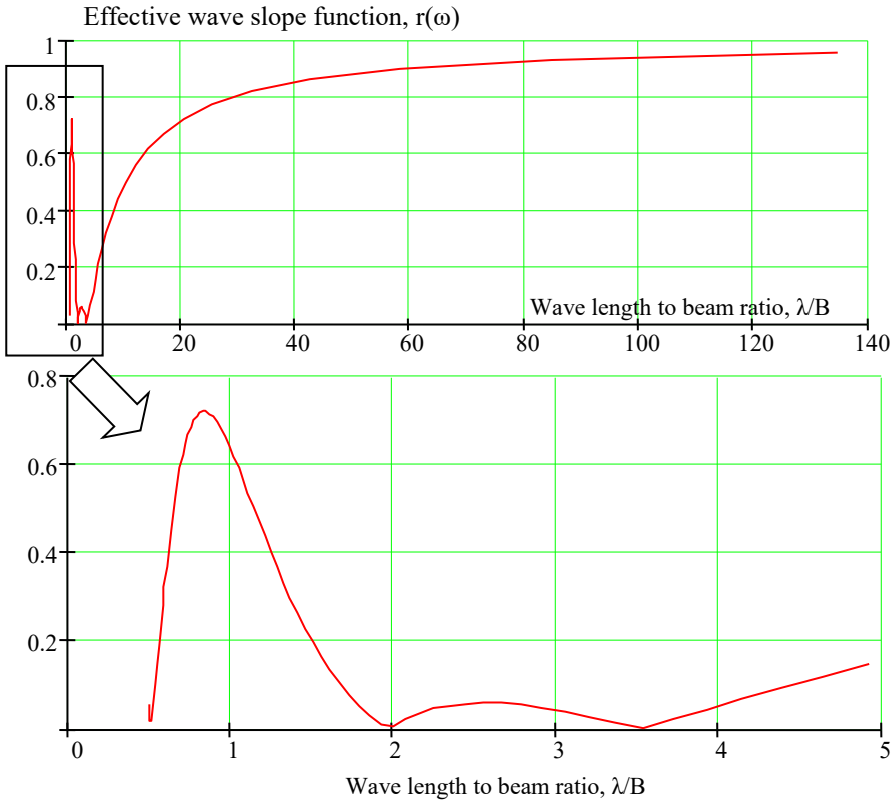

Figure 3.1. Effective Wave Slope Function Computed for C11 Class Containership, Draft 11.50 m KG = 18.92 m.

Table 3.1. Characteristics of the Prismatic Barge

Length, BP, m	100.00
Beam, m	20.00
Draft amidships, m	5.00
Depth amidships, m	10.00
Trim, °	0.0
KG, m	7.00
Displacement, t	10.000.

3.2.2 Undisturbed Wave Pressure in Time Domain

Following the classic assumptions of Strip Theory (Newman, 1977), a ship in beam-plane regular-waves, is considered. The coordinate system for this assessment is accepted as shown in Figure 3.2. Note that the submerged portion of the ship is described with negative z-coordinates. The *x*-axes points forward, the *y*-axes is positive on the starboard side and located at the current waterline.

A pressure in an undisturbed wave field is

$$p(x,y,z,t) = \rho g A_w \exp(k_w z)\cos(k_w y - \omega t) \tag{3.1}$$

Where ρ is the water density, g is the gravitational acceleration, A_w is the wave amplitude, k_w is the wave number (spatial frequency), ω is the temporal frequency, and t is time. As the wave is assumed as a plane, the pressure does not depend on the coordinate x.

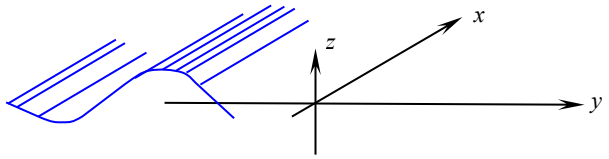

Figure 3.2. Coordinate System for Time Domain Wave Pressure

A portion of the wave force acting on a station is expressed as an integral along a line s, representing a station. The ship is assumed symmetric relative to the center plane:

$$d\vec{F}(t) = \int_s p\left(y(s), z(s), t\right)\vec{n}(s)ds + \int_s p\left(-y(s), z(s), t\right)\vec{n}(s)ds \tag{3.2}$$

Where $\vec{n}(s)$ is an outer normal vector expressed as:

$$\vec{n} \cdot ds = n \cdot dy - \vec{j} \cdot az\ ; \tag{3.3}$$

The line s is considered to be discretized with a series of points, (y_j, z_j) j=1,..,N_i , where N_i is a number of points used to discretize the i-th station, while i = 1,…Ns, where Ns is a number of stations (see Figure 3.3). The y-projection of the vector $d\vec{F}(t)$ can expressed as a sum of integrals computed over the N_i-1 linear segments, representing the line s.

$$dF_y(t) = \sum_{j=1}^{N_i-1}\left[-\int_{z_j}^{z_{j+1}} p\left(y(z), z, t\right)dz + \int_{z_j}^{z_{j+1}} p\left(-y(z), z, t\right)dz\right]\Delta z_j \tag{3.4}$$

Where:

$$\Delta z_j = z_{j+1} - z_j\ . \tag{3.5}$$

Assuming that the segments are sufficiently small, the integrals in equation (3.4) can be substituted by a pressure value in the center of each segment (y_{jCj}, z_{Cj}):

$$y_{Cj} = 0.5(y_{j+1} + y_j)\ \ ;\ \ z_{Cj} = 0.5(z_{j+1} + z_j) \tag{3.6}$$

Resulting in:

$$dF_y(t) = \sum_{j=1}^{N_i-1}\left[-p\left(y_{Cj}(z_{Cj}), z_{Cj}, t\right) + p\left(-y_{Cj}(z_{Cj}), z_{Cj}, t\right)\right]\Delta z_j \tag{3.7}$$

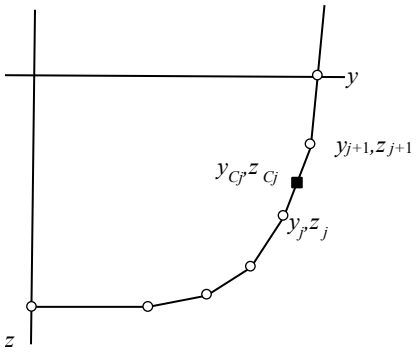

Figure 3.3. Representation of a Station

To be considered sufficiently small for most of ships, the length line segments can be taken about 0.02*B*, 0.04*B* long for the most ships

The *z*-projection of the vector $d\vec{F}(t)$ is derived in a way similar to the y-projection:

$$dF_z(t) = \sum_{j=1}^{N_i-1} \left[p\left(y_{Cj}(z_{Cj}), z_{Cj}, t\right) - p\left(-y_{Cj}(z_{Cj}), z_{Cj}, t\right) \right] \Delta y_j \tag{3.8}$$

Where:

$$\Delta y_j = y_{j+1} - y_j . \tag{3.9}$$

Having both the y and z projections of $d\vec{F}(t)$ allows a moment to be considered relative to the ship's center of gravity, located at a point (0, z_g):

$$\begin{aligned} dM_x(t) = \sum_{j=1}^{N_i-1} \Bigg(& -\int_{z_j}^{z_{j+1}} p\left(y(z), z, t\right)(z_g - z)dz + \int_{y_j}^{y_{j+1}} p\left(y(z), z, t\right) y dy \\ & + \int_{z_j}^{z_{j+1}} p\left(-y(z), z, t\right)(z_g - z)dz + \int_{y_j}^{y_{j+1}} p\left(-y(z), z, t\right) y dy \Bigg) \end{aligned} \tag{3.10}$$

The equation for the moment, dM_x(t), given in equation (3.10) may be simplified by substituting the pressure integrals with the pressure at the centers of each segments (see equation (3.6) above):

$$\begin{aligned} dM_x(t) = \sum_{j=1}^{N_i-1} \Bigg(& \left(p\left(y_{Cj}(z_{Cj}), z_{Cj}, t\right) - p\left(-y_{Cj}(z_{Cj}), z_{Cj}, t\right) \right) \int_{z_j}^{z_{j+1}} (z - z_g)dz + \\ & + \left(p\left(y_{Cj}(z_{Cj}), z_{Cj}, t\right) - p\left(-y_{Cj}(z_{Cj}), z_{Cj}, t\right) \right) \int_{y_j}^{y_{j+1}} y dy \Bigg) \end{aligned} \tag{3.11}$$

The remaining integrals can be evaluated in closed form:

$$
\begin{aligned}
&dM_x(t) = \\
&\sum_{j=1}^{N_i-1}\Big(\Big(p\left(y_{Cj}(z_{Cj}),z_{Cj},t\right)-p\left(-y_{Cj}(z_{Cj}),z_{Cj},t\right)\Big) \\
&\qquad\cdot\left(\frac{(z_{j+1}^2-z_j^2)}{2}-z_g(z_{j+1}-z_j)\right) \\
&\qquad+\Big(p\left(y_{Cj}(z_{Cj}),z_{Cj},t\right)-p\left(-y_{Cj}(z_{Cj}),z_{Cj},t\right)\Big)\frac{1}{2}\left(z_{j+1}^2-z_j^2\right)\Big) \\
&=\sum_{j=1}^{N_i-1}\Big(\Big(p\left(y_{Cj}(z_{Cj}),z_{Cj},t\right)-p\left(-y_{Cj}(z_{Cj}),z_{Cj},t\right)\Big) \\
&\qquad\cdot\left(\frac{1}{2}(z_{j+1}-z_j)(z_{j+1}+z_j)-z_g(z_{j+1}-z_j)\right) \\
&\qquad+\Big(p\left(y_{Cj}(z_{Cj}),z_{Cj},t\right)-p\left(-y_{Cj}(z_{Cj}),z_{Cj},t\right)\Big) \\
&\qquad\cdot\left(\frac{1}{2}(y_{j+1}-y_j)(y_{j+1}+y_j)\right)\Big) \\
&=\sum_{j=1}^{N_i-1}\Big(p\left(y_{Cj}(z_{Cj}),z_{Cj},t\right)-p\left(-y_{Cj}(z_{Cj}),z_{Cj},t\right)\Big) \\
&\qquad\cdot\left(\Delta z_j(z_{Cj}-z_g)+y_{Cj}\Delta y_j\right)
\end{aligned}
\tag{3.12}
$$

The integration, along the ship length, of the sectional moments of wave forces caused by an undisturbed wave felid pressure makes a complete Froude-Krylov wave excitation moment:

$$
M_x(t)=\sum_{i=1}^{N_S} dM_{xi}(t)\Delta x_i \qquad \Delta x_i = x_{j+1}-x_j \tag{3.13}
$$

3.2.3 Amplitude of Wave Moment

Calculations of roll response for level 2 vulnerability criteria are carried out using a Response Amplitude Operator (RAO). Thus, to use pressure integration for the effective wave-slope angle-function, the amplitude of the wave excitation moment must be expressed. To achieve this, the equation for pressure in an undisturbed wave field (3.1) is substituted into (3.12), the cosine function is expanded and trigonometric identities are applied:

$$
\begin{aligned}
dM_x(t) &= \rho g A_w \sum_{j=1}^{N_i-1}\exp(k_w z_{Cj})\Big(\cos(k_w y_{Cj}(z_{Cj})-\omega t)- \\
&\qquad\cos(-k_w y_{Cj}(z_{Cj})-\omega t)\Big)\cdot\left(\Delta z_j(z_{Cj}-z_g)+y_{Cj}\Delta y_j\right) \\
&= \rho g A_w \sum_{j=1}^{N_i-1}\exp(k_w z_{Cj})\Big(\cos(k_w y_{Cj}(z_{Cj}))\cos\omega t \\
&\qquad+\sin(k_w y_{Cj}(z_{Cj}))\sin\omega t-\cos(k_w y_{Cj}(z_{Cj}))\cos\omega t \\
&\qquad+\sin(k_w y_{Cj}(z_{Cj}))\sin\omega t\Big)\cdot\left(\Delta z_j(z_{Cj}-z_g)+y_{Cj}\Delta y_j\right)
\end{aligned}
$$

$$= \quad 2\rho g A_w \sin\omega t \sum_{j=1}^{N_i-1} \exp(k_w z_{Cj}) \sin(k_w y_{Cj}(z_{Cj})) \left(\Delta z_j (z_{Cj} - z_g) + y_{Cj} \Delta y_j \right) \tag{3.14}$$

$$= \quad dA_{Mx} \sin\omega t$$

Where the amplitude of the wave moment for a given section (i.e. the sectional amplitude) is expressed as:

$$dA_{Mx} = 2\rho g A_w \sum_{j=1}^{N_i-1} \exp(k_w z_{Cj}) \sin(k_w y_{Cj}(z_{Cj})) \left(\Delta z_j (z_{Cj} - z_g) + y_{Cj} \Delta y_j \right) \tag{3.15}$$

By integrating along the ship length (i.e. taking into account (3.13)), the amplitude for the entire hull is:

$$A_{Mx} = 2\rho g A_w \sum_{i=1}^{N_S} \sum_{j=1}^{N_i-1} \exp(k_w z_{Cj}) \sin(k_w y_{Cj}(z_{Cj})) \left(\Delta z_j (z_{Cj} - z_g) + y_{Cj} \Delta y_j \right) \Delta x_i \tag{3.16}$$

The expression for amplitude (3.16) was verified by computing the wave moment, M_x, with equation (3.13) and checking if the observed amplitude, A_{Mx}, coincides with a number obtained from equation (3.16). Figure 3.4 shows this comparison for the wave frequency $\omega = 0.6$ 1/s and a wave height, H_w, of 2 m (i.e. wave amplitude, $A_w = 1$ m).

The amplitude of the wave moment (3.16) is a function of the wave number, k_w. The wave number is related to the wave frequency by way of the dispersion relationship for linear waves in deep water:

$$k_w = \frac{\omega^2}{g} \quad , \tag{3.17}$$

The amplitude (3.16) can be presented as a function of wave frequency: $A_{Mx}(\omega)$. Finally, the effective wave slope function, $r(\omega)$, based on numerical pressure integration can be presented as:

$$r(\omega) = \frac{A_{Mx}(\omega)}{\Delta \cdot GM \cdot \alpha_0(\omega)} , \tag{3.18}$$

Where GM is the upright GM value (m), Δ is the weight of displacement (t), α_0 is the amplitude of the angle of wave slope at the centerline (radians).

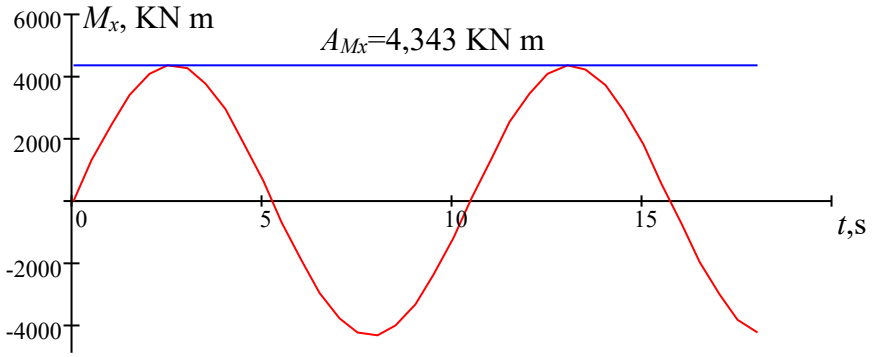

Figure 3.4. Verification of Amplitude of Wave Moment (ω = 0.6 1/s, A_w = 1 m)

The equation (3.18) provides a baseline true value for the effective wave slope function because it is computed with a minimum of assumptions of the hull geometry: the ship was assumed to be symmetric and long enough for the strip theory to be applicable. To emphasize that no additional approximations of ship geometry are needed, this method is further referred as "direct" pressure integration

3.2.3 Comparison of Direct Pressure Integration with "Standard" Method for the Barge

Figure 3.5 and Figure 3.6 show a comparison between the "standard" and direct pressure integration methods. As the "standard" method is based on a rectangular station approximation, the comparison with the results of computations for the barge (see Table 3.1) are expected to be nearly the same. Figure 3.5 shows the effective wave-slope angles function computed with the two different methods as well as with the Large Amplitude Motions Program (LAMP) as a function of wave frequency. While Figure 3.6 shows these quantities as a function of the ratio between wave's length and the ship beam, similar to Figure 3.1 and Figure 4.2 in Annex 4 of SDC 4/5/1Add. 3.

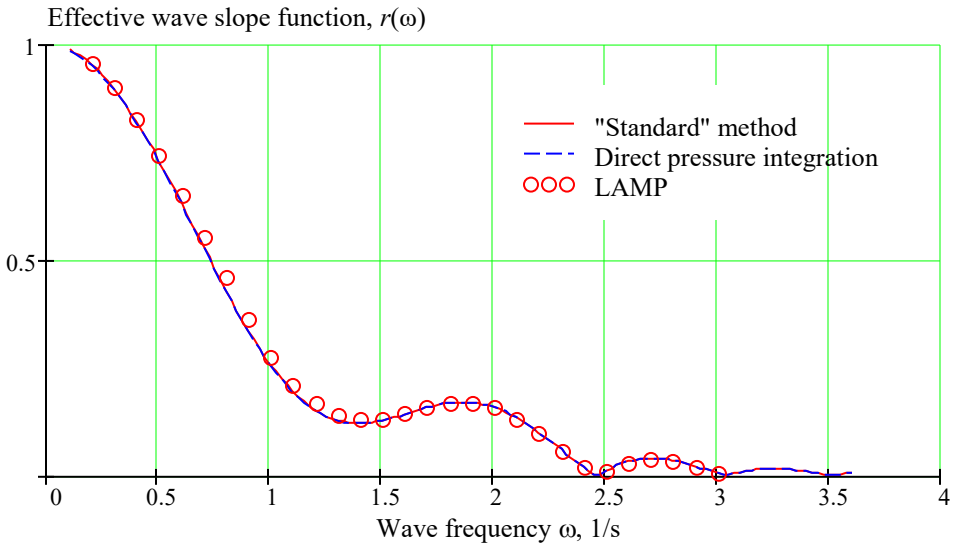

Figure 3.5. Comparison of Different Methods of Calculation of Effective Wave Slope Function, r(ω), for a Prismatic Barge as a Function of Wave Frequency, ω

The comparison between results of calculations on the direct pressure integration and the standard method on the barge show identical results in Figure 3.5 and Figure 3.6, confirming that the standard method is correct within its assumptions.

Figure 3.5 and Figure 3.6 also show a comparison with the results of the computations with outcomes of the Large Amplitude Motion Program (LAMP), see Shin, *et al* (2003). LAMP is a three-dimensional (3D) potential flow code that does not use strip theory. In other words, fluid flow is computed in 3D space rather than using the assumption that 3D flow can be represented by a series of 2D flows. Hence, a comparison of other calculation methods with a LAMP computation allows an evaluation to be made on how important 3D effects are.

While the LAMP results on the prismatic barge theoretically must be identical to the previous two methods, the zoomed-in portion of Figure 3.6 shows a small difference. The maximum difference found was 0.034, which can be attributed to numerical, most probably caused by how LAMP models the ends of the barge (in LAMP, the centers of the first and last layers of panels are not permitted to be at the first and the last stations).

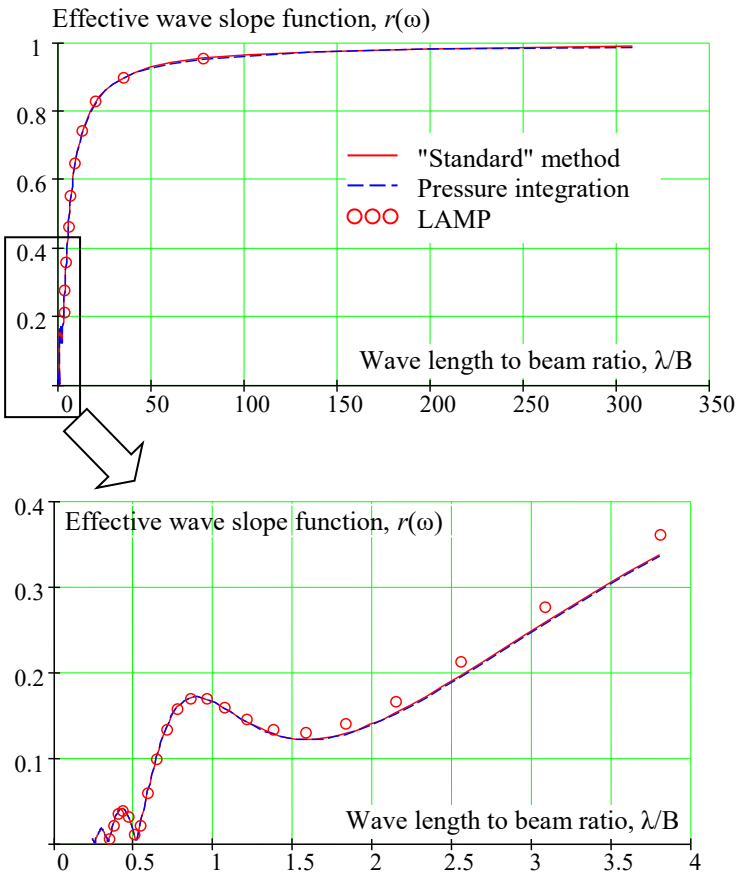

Figure 3.6. Comparison of Different Methods of Calculation of Effective Wave Slope Function, r(ω), for a Prismatic Barge as a Function of the Ratio Between Wave's length and Ship Beam, *λ/B*

3.2.4 Barge Study: Conclusions

The following conclusion can be made because of the prismatic barge study:

- Comparisons of direct pressure integration and the standard method yielded identical results, thus the "standard" method is correct within its assumptions.
- Direct pressure integration and LAMP produced very close results; that is additional verification of the direct pressure integration. The favorable comparison also creates a background to use LAMP for further assessment of 3D effects.

3.2.5 Comparison of Direct Pressure Integration with "Standard" Method for the C11

Figure 3.7 and Figure 3.8 show comparison of an effective wave-slope function for C11 class container carrier computed with three different methods: "standard" method, direct pressure integration, and LAMP. The purpose of this comparison is to understand how strong the effect of approximation of the station with the rectangles can be.

The difference between LAMP calculations and direct pressure integration seems not to be significant. Thus, it points out how the effect of 3D flow may be not so significant for

computation of roll exaction in beam seas. This conclusion is consistent with a multi-decade practice of application of the strip theory.

The difference between the direct pressure integration and "standard" method seems to be significant. The difference is especially large in the frequency range 0.4 1/s and upwards, corresponding to the wave period of 15 s and smaller. The difference somewhat decreases for the lower frequencies. However, the "standard" method remain non-conservative through the entire range of frequencies, including the possible resonance periods 20-25 s (0.25-0.3 1/s). As it can be seen from Figure 3.8, the non-conservative tendency of the "standard" method is retained for long waves as well.

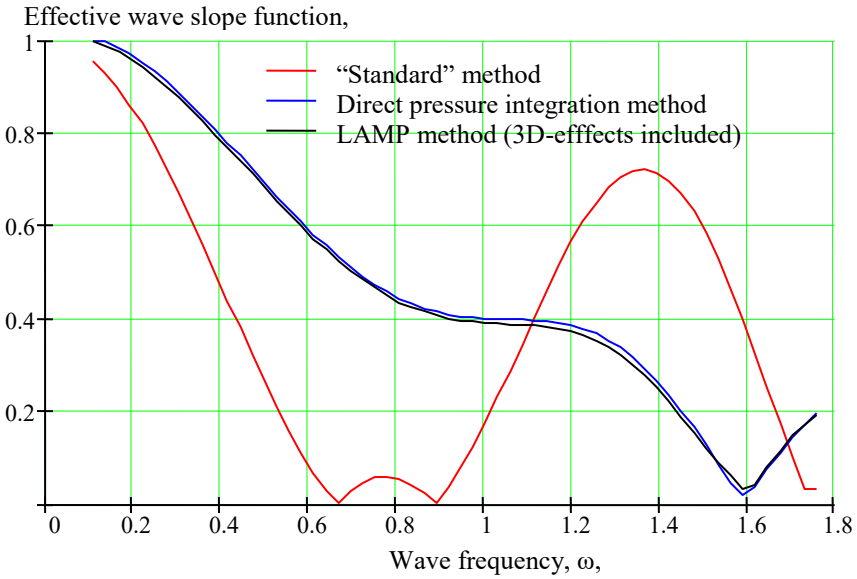

Figure 3.7. Comparison of Different Methods of Calculation of Effective Wave Slope for the C11 Class Container Carrier as Function of Wave Frequency (Draft 11.50 m KG = 18.92 m)

The other observation is related with the high frequency/low wave length to beam ratio behavior. All methods shows the tendency to increase of effective wave slope, while short waves (fraction of the ship beam) should not excite a significant roll motion. As the understanding of this effect may be important for the correct regulatory application, it deserved the separate study.

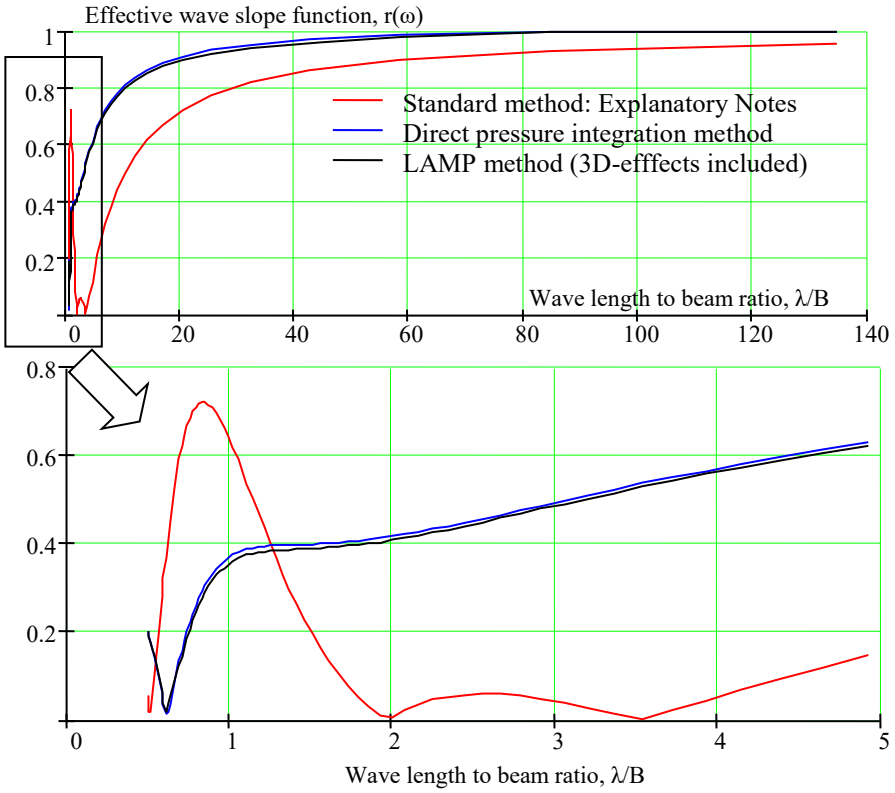

Figure 3.8. Comparison of Different Methods of Calculation of Effective Wave Slope for the C11 Class Container Carrier as Function of the Ratio Between Wave length and Ship Beam (Draft 11.50 m KG = 18.92 m)

3.2.6 Effective Wave Slope Function in High Frequency Range

The effective wave slope functions computed for the barge (Figure 3.6) show a zero value at the λ/B=0.5, i.e. when exactly two waves fit across the ship beam. The reason is obvious; the pressures generated by such wave compensate each other and produce no moment relative to the center of gravity. Can it be a key for the unexpected behavior of the effective wave slope in high frequencies?

Consider contributions to the wave moment separately from the bottom and the sides. Equation (3.16) easily separates into two components; since the index of the point on the edge is known, say Ne_i:

$$A_{Bx} = 2\rho g A_w \sum_{i=1}^{N_S} \sum_{j=1}^{Ne_i-1} \exp(k_w z_{Cj}) \sin(k_w y_{Cj}(z_{Cj})) \left(\Delta z_j (z_{Cj} - z_g) + y_{Cj} \Delta y_j \right) \Delta x_i \qquad (3.19)$$

$$A_{Sx} = 2\rho g A_w \sum_{i=1}^{N_S} \sum_{j=Ne_i}^{N_i-1} \exp(k_w z_{Cj}) \sin(k_w y_{Cj}(z_{Cj})) \left(\Delta z_j (z_{Cj} - z_g) + y_{Cj} \Delta y_j \right) \Delta x_i \qquad (3.20)$$

Figure 3.9 shows both bottom and side components of the amplitude of the wave moment along with its resultant value. The calculations were done for a wave of a constant steepness equal to 0.01.

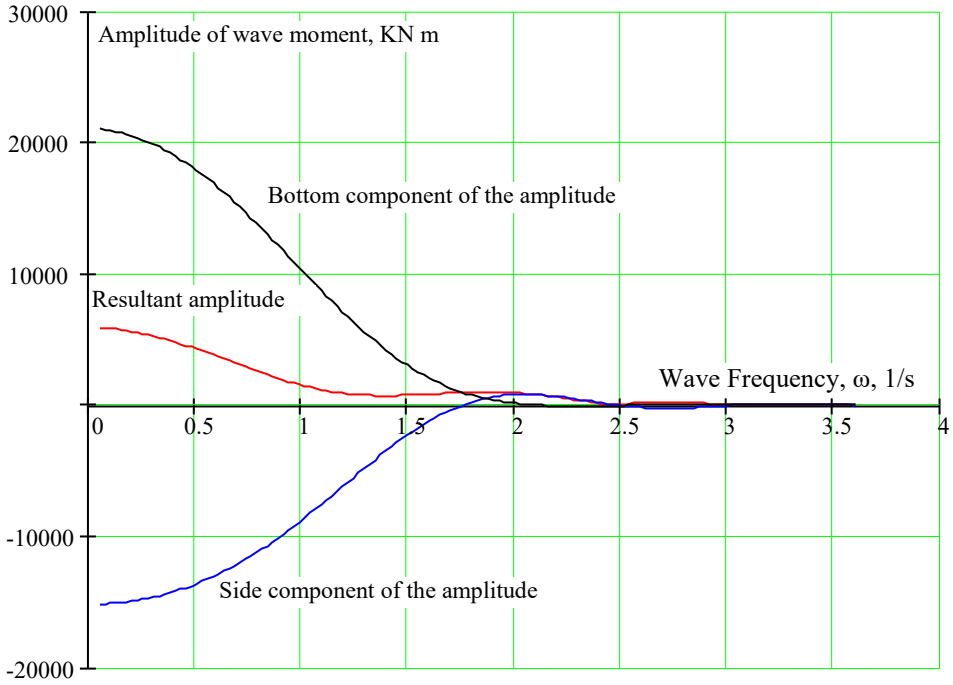

Figure 3.9. Bottom and Side Components of the Amplitude of Wave Moment as Functions of Wave Frequency, Computed for the Barge, Wave Steepness 0.01

Figure 3.9 shows that the side and the bottom components of the amplitude of the wave moment are of different signs. However, the side component becomes positive around 1.77 1/s or the wave's length to beam ratio of 1.0, see Figure 3.10. This transition to positivity is a reason why a local maximum appears on the resultant amplitude curve near the frequency of 2.0 1/s (also seen in Figure 3.5). Then the side component becomes negative again; its evolution against the wave's length to beam ratio, described as decaying oscillations, once the wave's length becomes comparable with the ship breadth.

The bottom component of the amplitude shows different behavior; it becomes negative between 0.4-0.7λ/B and then approaches zero, as the wave amplitude decreases to keep the steepness constant. This different behavior of the amplitude components and their opposite signs forms the "lobes" on the amplitude plot (see the zoomed portion of Figure 3.10Figure 3.9). These "lobes" also show themselves in effective wave slope plots (see the zoomed portion of Figure 3.6) and explain its "unexpected" behavior in high frequencies.

This effect may increase for the case of high KG values. The bottom component is not dependent on KG, as the lever is measured horizontally from the center of a segment to the centerline. The side component is sensitive to the KG; since the lever is measured vertically from the center of a segment to the position of the center of gravity, see Figure 3.11.

The effect of KG increase is shown in Figure 3.12 and Figure 3.13. The value of KG for the barge (see Table 3.1) was increased from 7.000 m to 8.405 m making the GM drop from 1.560 m to low 0.150 m. That change made the side component of the wave moment amplitude to grow in absolute value from 200 kN m to almost 400 kN m at the wave length to beam ratio of 0.43 (compare values in Figure 3.9 and Figure 3.12).

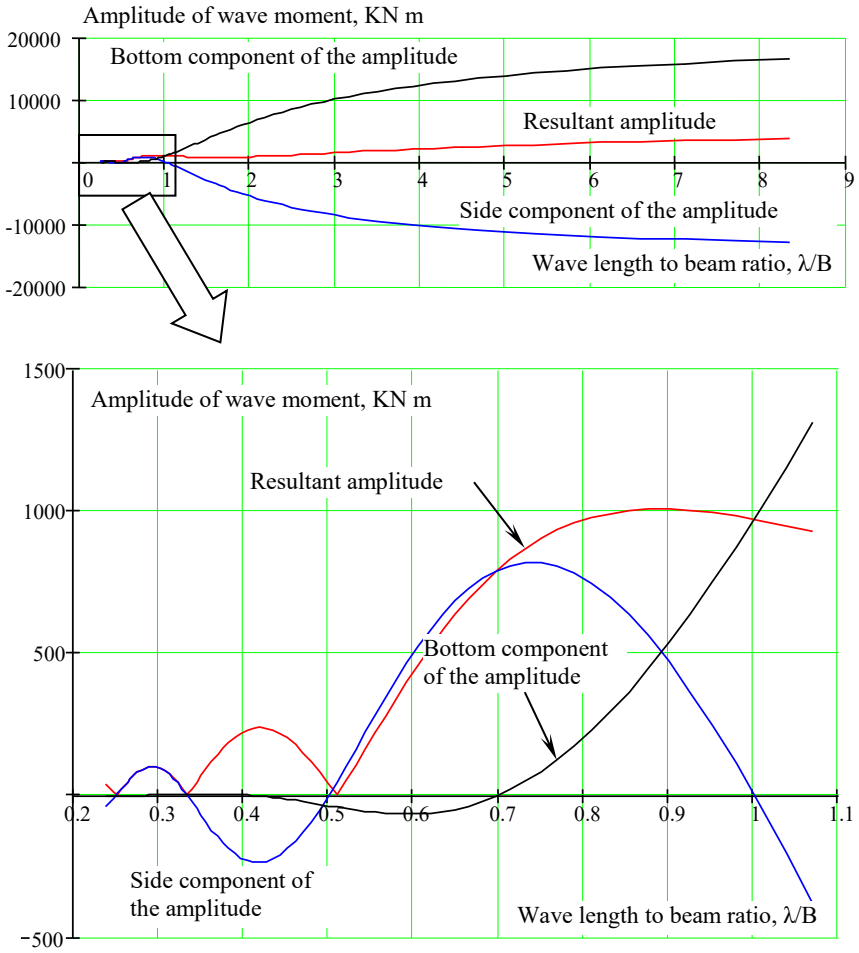

Figure 3.10. Bottom and Side Components of the Amplitude of Wave Moment, as Functions of Wave's length to Beam Ratio, Computed for the Barge, Wave Steepness 0.01

The increased contribution from the segments on the side increases the value of the effective wave slope dramatically for the low wave length to ship beam ratios, making it well above the unity. In addition, the effect of wave's length being comparable to ship breadth (finiteness of wave length) extends to longer waves. Compare Figure 3.12 and Figure 3.6, one can still see the reduction of the excitation produced by a wave of 100 ship beams for GM = 0.15 m (Figure 3.12), but the effective wave slope function is close to 1 for GM = 1.56 m (Figure 3.6).

Figure 3.13 shows the effect of high KG on effective wave slope in the low ratios of wave lengths to ship beam (high frequency) for C11-class container carrier. The KG was equal to 20.17 making GM = 0.15 m. Calculations used the "standard" method and direct pressure integration.

The effect of high KG manifests itself for the C11-class in a way, similar to the barge. The effective wave slope function take a shape of "lobes" for short waves and exceeds the unity. The influence of the finite wave length is extended to longer waves (compare Figure 3.14 and Figure 3.8). However, this aspect of the high KG effect is not as strong as for the barge.

Comparing the "standard" method with direct pressure integration, one may notice that the "standard" method seems to exaggerate the high KG effect, while remaining non-conservative for long waves.

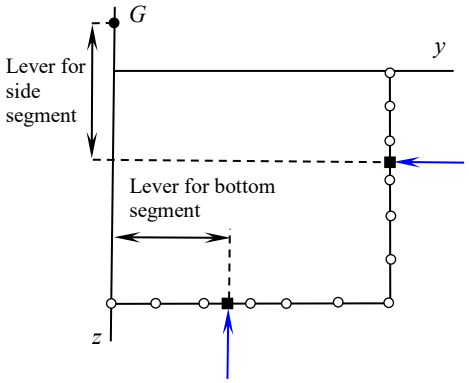

Figure 3.11. Lever for a Moment Created by Pressure on Bottom and Side Segments

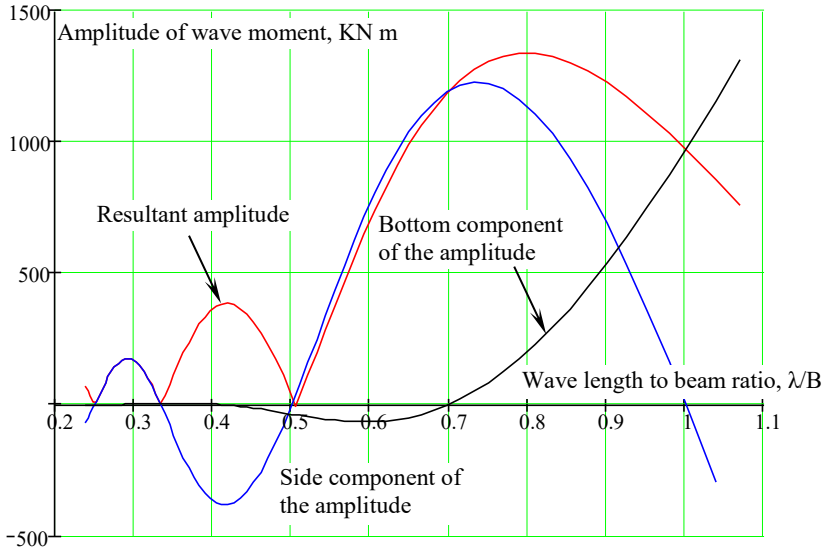

Figure 3.12. Bottom and Side Components of the Amplitude of Wave Moment, as Functions of Wave Length to Beam Ratio, Computed for the Barge with High KG = 8.405 m, GM = 0.15 m, Wave Steepness 0.01

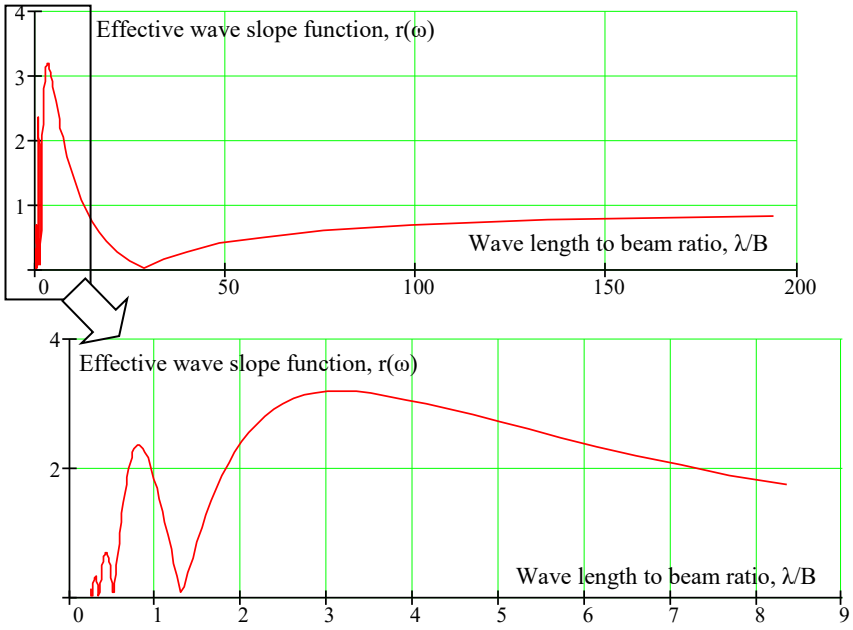

Figure 3.13. Effective Wave Slope Angle, as a Function of Wave Length to Beam Ratio, Computed for the Barge with KG = 8.405 m, GM = 0.15 m, Wave Steepness 0.01

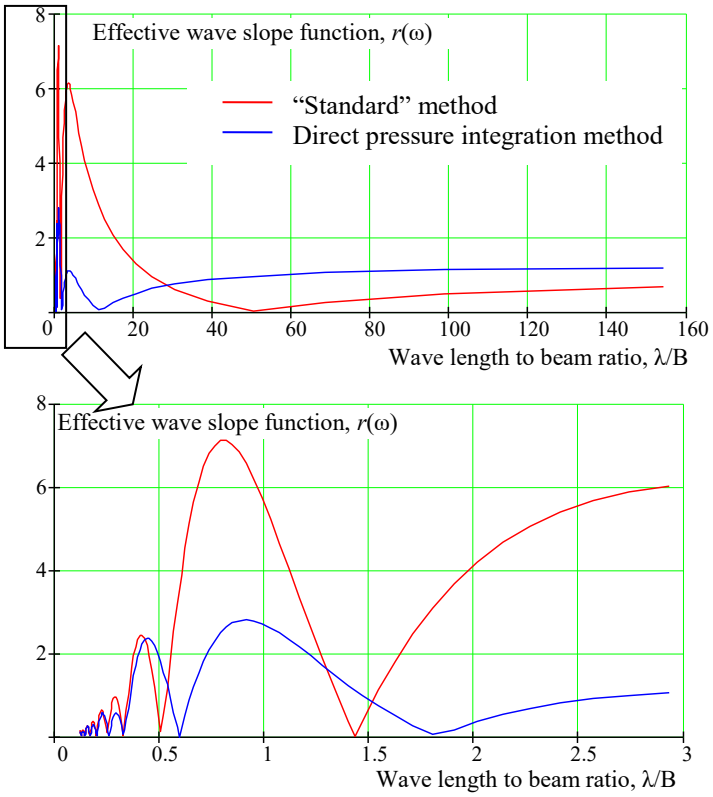

Figure 3.14. Effective Wave Slope Angle, as a Function of Wave Length to Beam Ratio, Computed for C11 with GM = 0.15 m, Wave Steepness 0.01

3.2.7 Summary and Conclusions of Effective Wave Slope Function Calculation

The effective wave slope function is a tool to account for a finite of the wave compared to the size of a ship. The necessity for this tool rises form an assumption made in linear beam seas roll theory, where a ship is assumed to be infinitely small compared to a wave.

An approximate method, referred as "standard" is described in paragraph 3.6.3 in Annex 4 of SDC 4/5/1Add.3, where the actual ship stations were substituted by the rectangles of the same draft and beam. The example given in Figure 4.2 of the cited documents has shown some unexpected behavior of the effective wave slope function in short waves, where a little wave forces may be expected, yet the function shows a peak.

The described study took place to understand the behavior of the effective wave-slope function. The study concluded that:

- The effective wave-slope angle-function may experience a large value in short waves, caused by a change of the sign of wave pressure contribution from the ship's sides. High KG value increases this effect.
- The effective wave-slope angle-function can be computed with direct-pressure integration that does not require any additional approximations of ship geometry.
- The "standard" method of calculation of the effective wave-slope angle-function is not necessarily conservative for the long waves but may artificially increase the value of the function in short waves.
- Based on these conclusions, the direct pressure integration method may be recommended for computer implementation of the second level vulnerability criteria for dead ship condition.

3.3 Calculation of Variances of Roll Motions

3.3.1 General

The level 2 vulnerability assessment for dead ship condition requires calculation of variances of roll angles and rats under action of irregular beam seas and gusty wind. Per the working version of explanatory notes Annex 4 of SDC 4/5/1Add.3, paragraph 3.4.2.7, these calculations are to be performed in a frequency domain, i.e. by integrating the spectra of roll angles. The spectrum of roll motion is calculated in accordance with formulae 3.4.2.7-2, its relevant equations are repeated below for the sake of convenience:

$$S(\omega) = H_{rel}^2(\omega) \cdot S_{\alpha\alpha,c}(\omega) + H^2(\omega) \cdot \frac{S_{\delta Mwind}(\omega)}{(W \cdot \overline{GM})^2} \tag{3.21}$$

Where ω is a frequency, $S_{\alpha\alpha,c}(\omega)$ is a spectrum of wave excitation, $S_{\delta Mwind}(\omega)$ is a spectrum of heeling moment caused by gusty wind, W is weight displacement of a ship and $\overline{GM}$ which is the GM value in calm water. $H(\omega)$ a $H_{rel}(\omega)$ are the response amplitude operator (RAOs) for roll motions described by the following equations

$$H_{rel}^2(\omega) = \frac{\omega^4 + (2 \cdot \mu_e \cdot \omega)^2}{(\omega_{0,e}^2(\varphi_S) - \omega^2)^2 + (2 \cdot \mu_e \cdot \omega)^2} \tag{3.22}$$

$$H^2(\omega) = \frac{\omega_0^4}{(\omega_{0,e}^2(\varphi_S) - \omega^2)^2 + (2 \cdot \mu_e \cdot \omega)^2} \tag{3.23}$$

Where μ_e is equivalently linearized roll damping coefficient and $\omega_{0,e}(\varphi_S)$ is natural roll frequency, corresponding to the instantaneous GM-value computed at static angle φ_S.

RAO describes the physical properties of a dynamic system oscillating under the action of random excitation. In this paradigm, using different RAOs for the same dynamic system for different excitations seem to be inconsistent. Why are the physical properties of a ship under the action of irregular waves and gusty winds described by different RAOs and what are the consequences?

3.3.2 Roll motion in relative coordinates

The structure of equation (3.46) and used index "rel" indicates that relative roll motion RAO described roll response on waves. Consider the derivation and principle assumptions in the basis of the relative roll motion model.

The main idea of the relative-roll motion-model is to express equations of motion in terms of relative angle between the water surface and the calm water waterline. Indeed, if the wave is very long, its curvature can be neglected over the ship beam. Assuming the waterline being flat, it makes it so that the restoring action is proportional (and for a large angle – a function of) the relative roll angle ϕ_r, which is defined as:

$$\phi_r(t) = \phi(t) - \alpha(t) \tag{3.24}$$

Where $\alpha(t)$ is the instantaneous wave slope angle.

This concept, allegedly coming from W. Froude, was meant to allow the inclusion of nonlinearity using calm waters to compute the forces. Per Newton's second law, the inertial action can be expressed through the sum of all moment acting on the body:

$$I_X \ddot{\quad} \quad + M_D + M_R \tag{3.25}$$

Where I_X is the moment of inertia in a vacuum. The other symbols stands for: M_I – which is a moment of hydrodynamic forces proportional to acceleration. It reflects the inertia of a wave, when involved in the motions of a ship:

$$M_I = -A_{44}(\ddot{\quad} \quad \ddot{\quad} \quad \ddot{\quad} \tag{3.26}$$

Where A_{44} is a coefficient of added inertia. This moment is assumed proportional to additional accelerations caused by the body motions.

M_D - is a moment of damping forces. It expresses the dissipation caused by waves and eddies made by the body as well as the energy loss due to friction.

$$M_D = -B_{44}(\dot{\quad} \quad \dot{\quad} \tag{3.27}$$

Where B_{44} is a dimensional damping coefficient. The moment of damping forces is assumed proportional to additional velocity caused by the motion of the body.

M_R - is a moment of hydrodynamic forces caused by waves as well as the hydrostatic moments caused by changing the submerged volume.

$$M_D = -W \cdot GZ(\phi - \alpha) = -W \cdot GZ(\phi_r) \tag{3.28}$$

The moment is assumed as a function of motion displacement additional to the wave. i.e. relative motion to the wave.

Substitution of equation (3.50-52) into the Newton's second law (3.49), the following equation of roll motion can be written:

$$(I_X + A_{44})\ddot{\quad} \quad \dot{\quad} \quad Z(\phi_r) = -I_X\ddot{\quad} \tag{3.29}$$

Expressing equation (3.53) in terms of angular acceleration one can obtain a nonlinear ordinary differential equation in "standard" form:

$$\ddot{\quad} \quad \dot{\quad} \quad (\phi_r) = -a_X\ddot{\quad} \tag{3.30}$$

Where:

$\mu_r = \dfrac{B_{44}}{2(I_X + A_{44})}$ - Linear damping coefficient for relative motions.

$\omega_0^2 = \dfrac{W \cdot GM}{I_X + A_{44}}$ - Square of natural roll frequency

$f_r(\phi_r) = \dfrac{1}{GM} GZ(\phi_r)$ - roll restoring function, normalized by GM

$a_X = -\dfrac{I_X}{I_X + A_{44}}$ - Wave excitation coefficient

Linear relative roll damping coefficient μ_r can be further considered as a result of equivalent linearization as described in paragraph 3.4.1.7 of Annex 4 of SDC 4/5/1 Add.3:

$$\mu_r = \mu_e \tag{3.31}$$

Linearizing the roll restoring around the heel angle under the steady wind φ_S, as shown in Figure 3.4 of Annex 4 of SDC 4/5/1 Add.3, and taking into account that

$$\ddot{\quad} \quad \alpha \tag{3.32}$$

The roll equation becomes:

$$\ddot{\quad} \quad \dot{\quad} \quad \dot{\quad} \quad \omega_{0,e}\,\rho_S \quad \omega^2\alpha \tag{3.33}$$

The equation (3.33) is linear ordinary differential equation that allows the RAO-based solution, which can be expressed as:

$$H_{rel}^2(\omega) = \frac{}{(\omega_{0,e}^2(\varphi_S \quad} \cdot \quad \frac{a_X^2\omega^4}{(2 \cdot \mu_e \cdot \omega)^2} \tag{3.34}$$

The equation (3.34) is different from the RAO in (3.21). It lacks the term $(2\mu_e\omega)^2$ and has a coefficient "a_X" that (3.21) does not have. That means the derivation of the relative roll in Annex 4 of SDC 4/5/1 Add.3 differs from the above equation.

3.4.3 Roll motion in relative coordinates: alternative derivation

Consider a linear equation of roll motions:

$$(I_X + A_{44})\ddot{\phi} + B_{44}\dot{\phi} + M \cdot \phi = W \cdot GM \cdot \alpha \tag{3.35}$$

It formally introduces a new variable expressed by equation (3.48); after simplification, one will get:

$$(I_X + A_{44})\ddot{\phi}_r + B_{44}\dot{\phi}_r + M \cdot \phi_r = -(I_X + A_{44}) \cdot \ddot{\phi} \tag{3.36}$$

Rewiring (3.35) in terms of angular acceleration, then taking into account that

$$\dot{\phi} = \sin \omega t, \quad \ddot{\phi} = \alpha_0 \cos \omega t \tag{3.37}$$

The (3.36) becomes:

$$\ddot{\phi}_r + 2\mu_e \dot{\phi}_r + \omega_0^2 \phi_r = \alpha(\omega^2 + 2\mu_e \omega) \tag{3.38}$$

Consider equation (3.38) as linearized at the heel angle under the steady wind φ_S,

$$\ddot{\phi}_r + 2\mu_e \dot{\phi}_r + \omega_0^2(\varphi_S) \cdot \phi_r = \alpha_0(\omega^2 \cos \omega t + 2\mu_e \omega \sin \omega t) \tag{3.39}$$

The RAO of (3.39) coincides with (3.21). Thus, the relative roll motion model used for the level 2 vulnerability criteria is obtained from a linear roll motion just by variable substitution (3.24), thus it inherits all assumptions of the linear roll equation (3.35).

3.3.4 Roll Motion in Relative vs. Absolute Coordinates

Figure 3.15 shows the difference between RAO of roll motions in relative and absolute coordinates. While the resonance peaks are almost the same, the asymptotic behavior is quite different. The relative RAO tends to zero, when the frequency goes to zero, but goes to a constant when the frequency tends to infinity. The RAO in absolute coordinate has exactly opposite behavior.

A consequence that may be important for the problem at hand is that relative RAO has sensitivity to excitation in high frequency area, where the effective wave slope function may take large values in the case when *KG* is high. That may lead to a large value of the variance of the relative roll motions, while the absolute roll motion variance remains realistic.

In addition, formula (3.45) is essentially a sum of spectra. However, these spectra represent different values of the absolute roll angle and relative roll angle, and therefore cannot add into the equation.

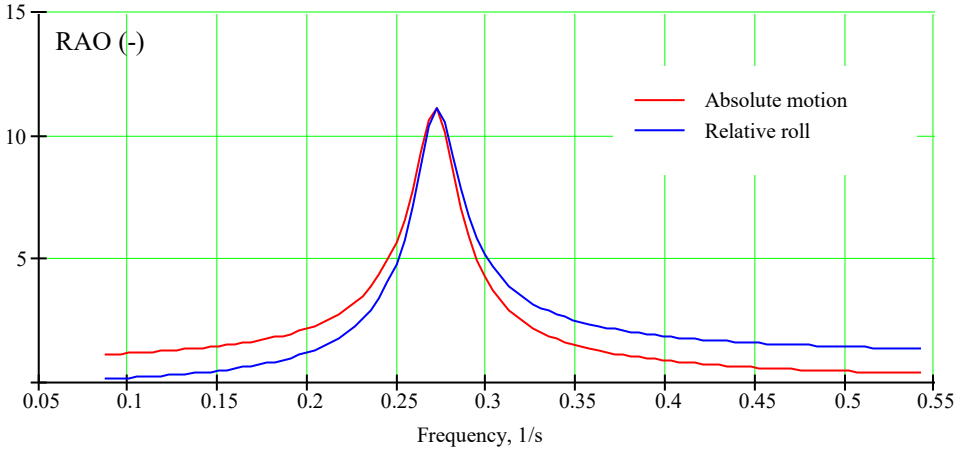

Figure 3.15. Absolute and Relative Roll Motion RAO for C11

3.3.5 Summary and conclusions on calculation of roll variance

The calculation of the variance of roll motion under the action of irregular beam seas and gusty winds is necessary for the level 2 vulnerability assessment in dead ship conditions. Per paragraph 3.4.2.7 of Annex 4 of SDC 4/5/1 Add.3, these calculations are to be performed in the frequency domain, i.e. by integrating the spectra of roll angles and motions. However, spectrum of roll response on waves is computed in relative coordinates (roll angle is measured relative to wave slope); while the response spectrum of wind gust are computed in absolute coordinates (roll angle is measured relative to the horizon).

As the spectra of different values cannot be added to the formulae 3.4.2.7-2 in the Annex 4 of SDC 4/5/1Add.3 it is considered mathematically inconsistent.

3.4 Case Study for the C11-Class Container Ship

3.4.1 General

The objective of the study is to examine the implementation of dead ship condition vulnerability criteria level 2 as described in a working version of explanatory notes in Annex 4 of SDC 4/5/1 Add.3. This shows that supporting the draft amendments to part B of the 2008 IS Code with regard to vulnerability criteria of Levels 1 and 2 for the dead-ship condition failure mode contained in document SDC 3/WP.5 Annex 1.

Examination of methods, proposed for use with the level-2 vulnerability criteria for dead ship condition indicated that the “standard” method for effective wave-slope function and the relative roll-motion models might be of concern regarding inaccuracy and inconsistency. However, both these methods may have alternatives. Instead of the “standard” method for effective wave slope, direct pressure integration may be used. The RAO of roll in absolute coordinates (roll angle is measured relative to the horizon) may be used instead of RAO in relative coordinates (roll angle is measured relative to the local wave slope). The focus of this study is to see how the application of these methods affects the results.

3.4.2 Evaluation of the Excitation

To evaluate the influence of the different methods for calculation of the effective wave-slope function, consider intermediate results for roll excitation from irregular waves and gusty wind. As many sea states need to be considered while computing the level 2 criterion (see the Annex 4 of SDC 4/5/1 Add.3, Table 3.1), this study will be focused on significant wave height of H_s, of 9.5 m, because it represents severe, but still observable weather situation. The mean zero-crossing periods, $T_z = 10.5$ s is chosen as a most probable value (159.9 per 100,000 occurrences for $H_s = 9.5$ m). To see how longer or shorter wave period may affect the excitation, smallest and largest observed values of the mean zero-crossing periods are also included in the study.

The spectra of the actual and effective wave slope are plotted in Figure 3.16 through Figure 3.18, computed for the most probable (10.5 s), as well as the smallest (6.5 s) and largest (18.5 s) observed values of the mean zero-crossing periods, T_z.

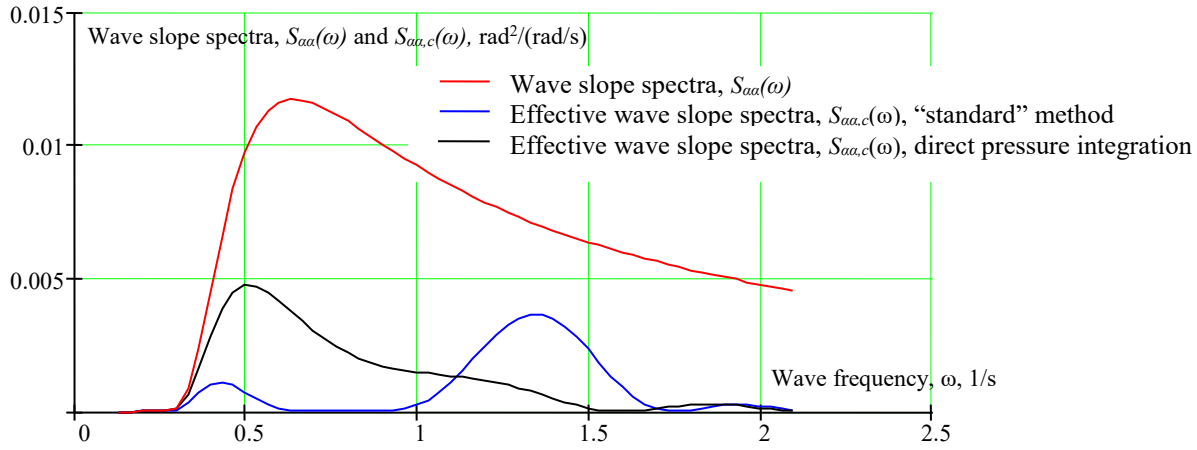

Figure 3.16. Spectra of Actual and Effective Wave Slope, $H_s = 9.5$ m; $T_z = 10.5$ s

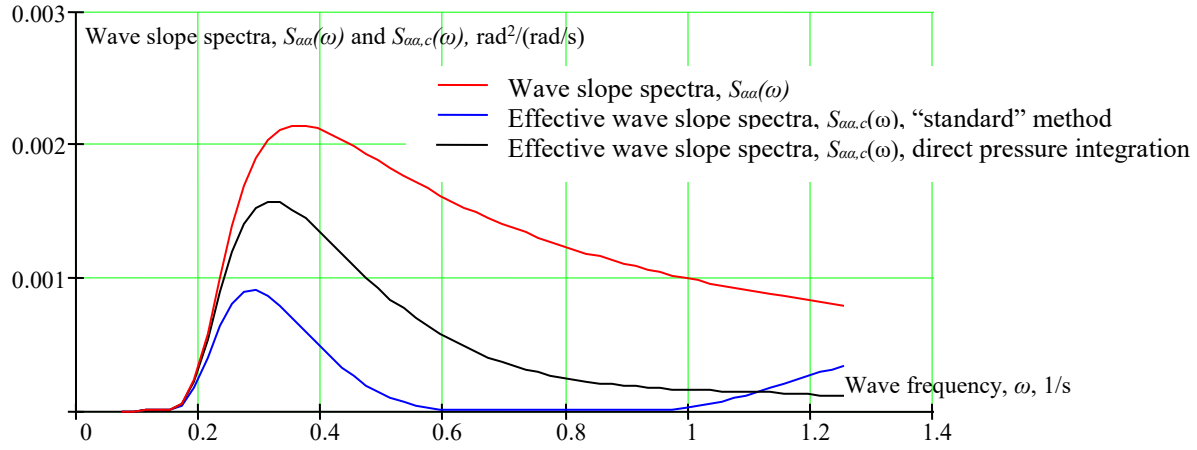

Figure 3.17. Spectra of Actual and Effective Wave Slope, $H_s = 9.5$ m; $T_z = 18.5$ s

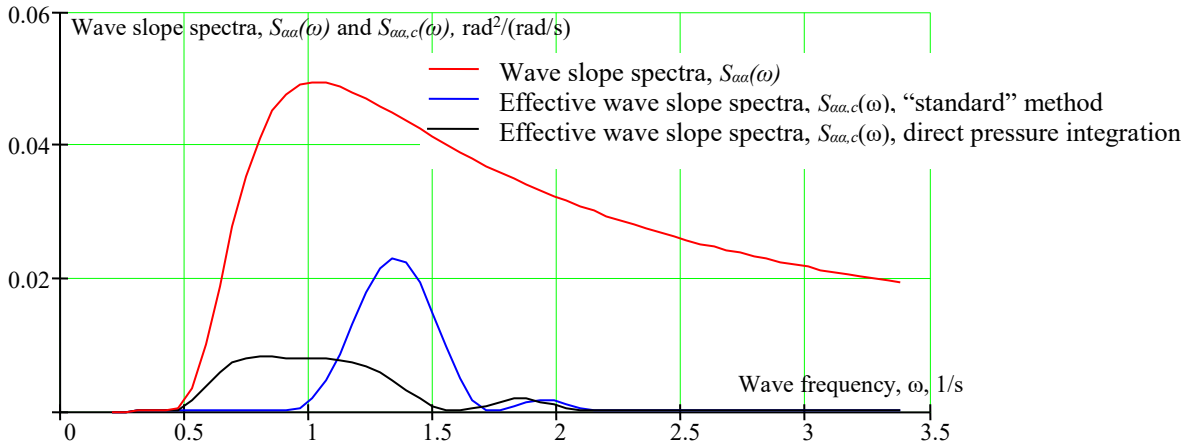

Figure 3.18. Spectra of Actual and Effective Wave Slope, H_s = 9.5 m; T_z = 6.5 s

Figure 3.19 through Figure 3.21 show the spectra of wave excitation, $S_{Mwaves}(\omega)$, and wind excitation, $S_{\delta Mwind,tot}(\omega)$. $S_{Mwaves}(\omega)$ is computed using the "standard" method and the direct pressure integration method for the effective wave slope function, $r(\omega)$. The same three environmental conditions are examined: H_s = 9.5 m, and T_z = 10.5 s, 18.5 s, and 6.5 s.

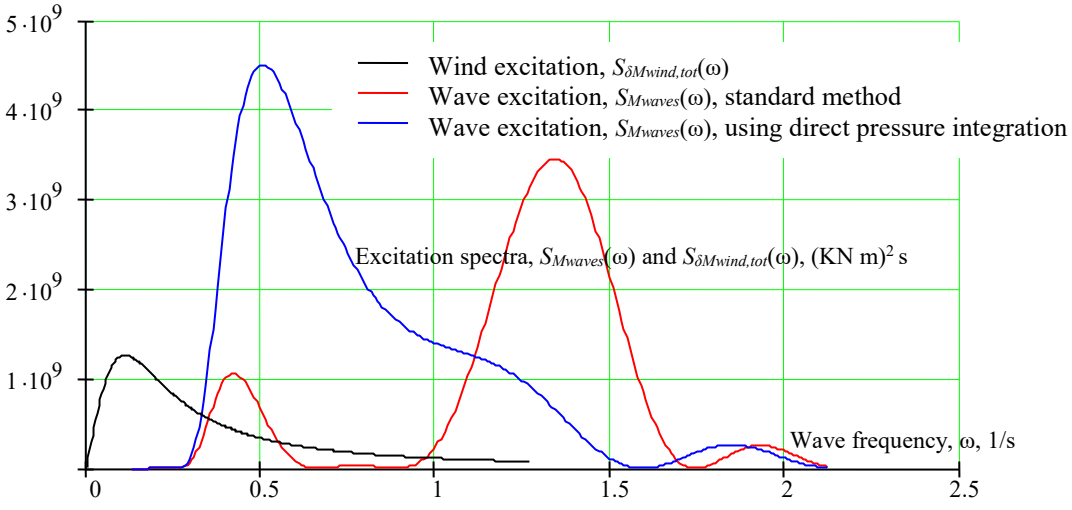

Figure 3.19. Spectra of Wave and Wind Excitation, H_s = 9.5 m; T_z = 10.5 s (Most Probable)

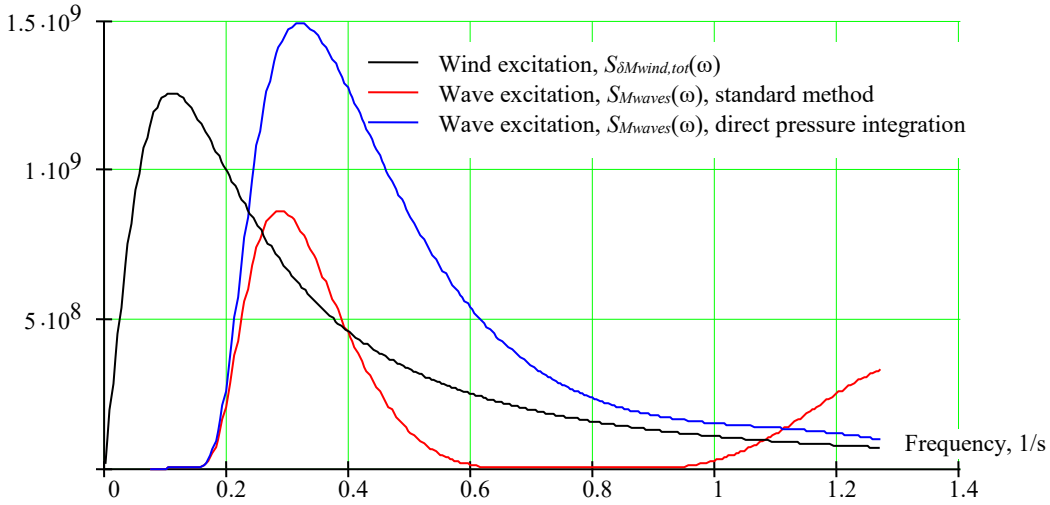

Figure 3.20. Spectra of Wave and Wind Excitation, H_S = 9.5 m; T_Z = 6.5 s

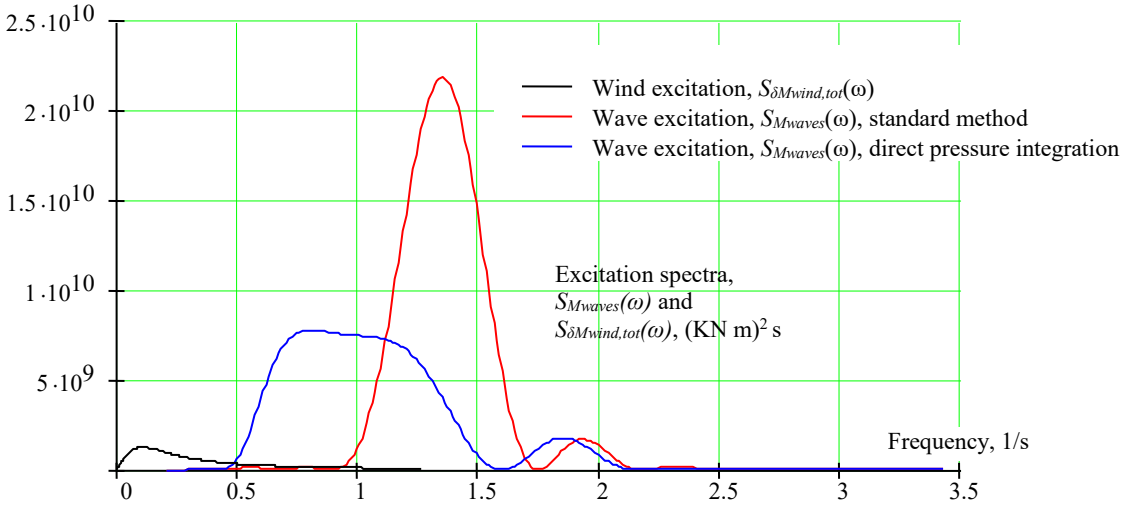

Figure 3.21. Spectra of Wave and Wind Excitation, H_S = 9.5 m; T_Z = 6.5 s

Application of different methods for calculation of the effective wave-slope function lead to very different shapes of effective wave slope and wave excitation spectra. The peak around 1.35 1/s observed at the effective wave slope function computed with "standard" method (See Figure 3.8) is carried through further, causing peaks on all the spectra. This peak is a result of pour approximation of increase wave excitation in high frequencies due to the influence of side pressures. In the case of C11, the side pressure effect was insufficient to cause a peak around 1.35 1/s. However, it lead to forming an inflection point on the plot of the effective wave slope function computed with direct pressure integration (See Figure 3.8). This inflection point also carried through the effective wave slope and roll excitation spectra, see Figure 3.16 and Figure 3.19. All the presented spectra, except those shown in Figure 3.17 and Figure 3.20 (where

frequency range is not extended high enough) indicated more energy in high frequencies and less energy in lower frequencies if the standard method was used for effective wave slope function.

3.4.3 Evaluation of Roll Response

The application of roll motions in relative coordinates is another area of concern. Figure 3.22 shows three spectra: the roll response to wind gusts and the roll responses to wave excitation in absolute and relative coordinates. Indeed, direct comparison of the absolute and relative roll response is not possible; however, putting these graphs on the same plot still may reveal frequency ranges of relatively high energy. The effective wave slope function was computed with direct pressure integration for the spectra in Figure 3.22.

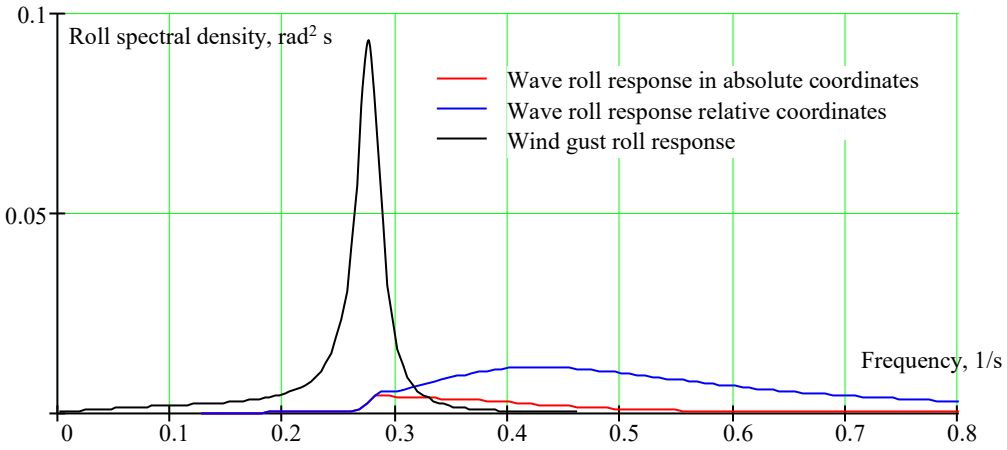

Figure 3.22. Roll Response Spectra in a Sea State H_s = 9.5m; T_z = 10.5s

Significant portions of energy in Figure 3.22 comes from wind gusts, because the mean zero-crossing period of waves is too short for the considered loading case of C11 with natural roll period of 23 s (roll period corresponding to GM value at the steady wind heeling angle 22.7 s). Figure 3.23 shows the roll spectra for longer-wave mean zero-crossing period, where the wind component is no longer dominant in the roll response.

The difference between spectra roll motion in relative and absolute coordinates is also dependent on the sea state. Referring to Figure 3.15, one could expect more energy in high-frequency range for the relative roll motion spectra. This seems to be the case for both sea states shown in Figure 3.22 and Figure 3.23. This effect, however, appears stronger for shorter mean zero-crossing periods in Figure 3.22. As the period becomes longer (Figure 3.23) the difference in energy distribution between the absolute and relative roll-motion decreases, as there is less energy in the high frequency range for longer waves.

To understand how high-frequency sensitivity of effective wave-slope functions can interact with the relative or absolute roll-motion model consider the roll spectra. Figure 3.24 shows two roll spectra, based on roll RAO in absolute coordinates, computed for different effective wave slope functions: “standard” and direct pressure. Figure 3.25 is similar to the previous one, but is based off the roll RAO in relative coordinates.

When comparing these two figures, the shift of energy towards the higher frequency is evident. It is also clear that the “standard” method for effective wave slope function in

combination with relative roll RAO leads to the largest shift towards high frequencies. The area under the spectra, i.e. variance seems to be smaller for the "standard" method, which is consistent with the previous observations.

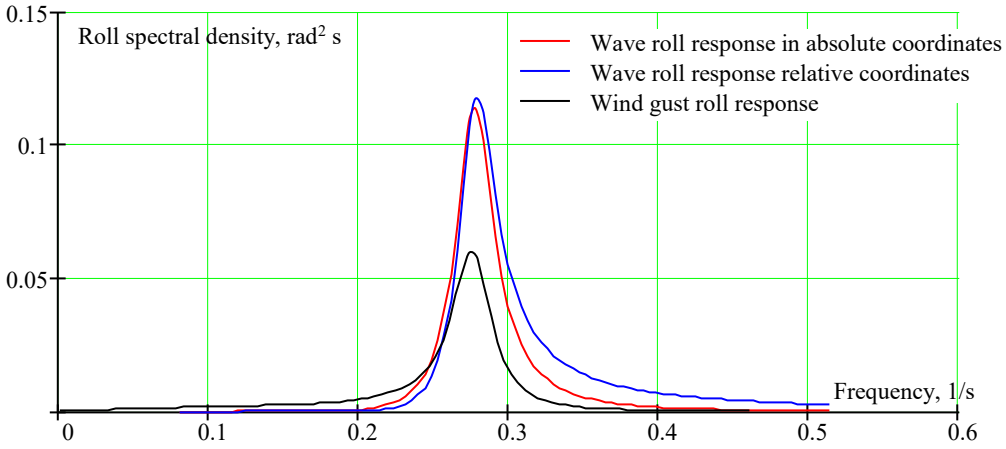

Figure 3.23. Roll Response Spectra in Sea State H_s = 9.5m; T_z = 16.5s

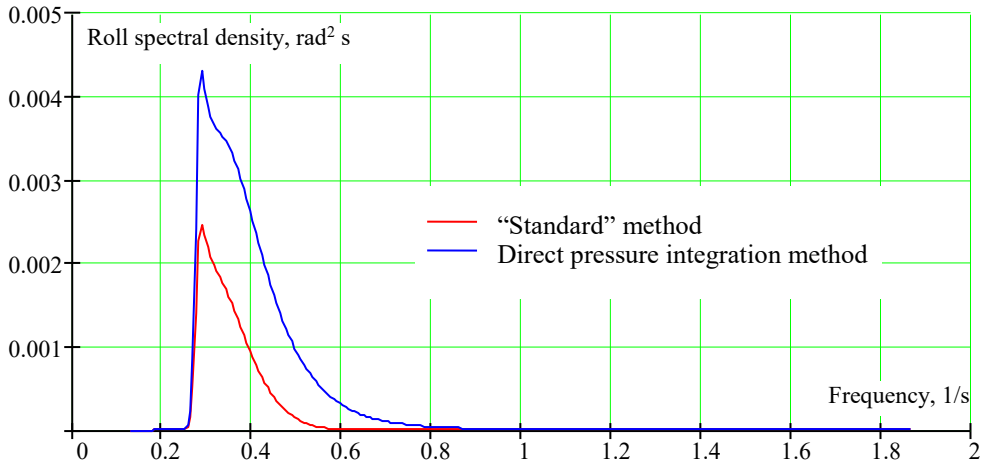

Figure 3.24. Complete Roll Response (Wind and Waves) Spectra for H_s = 9.5 m; T_z = 10.5s. Wave Roll Response in is Absolute Coordinates

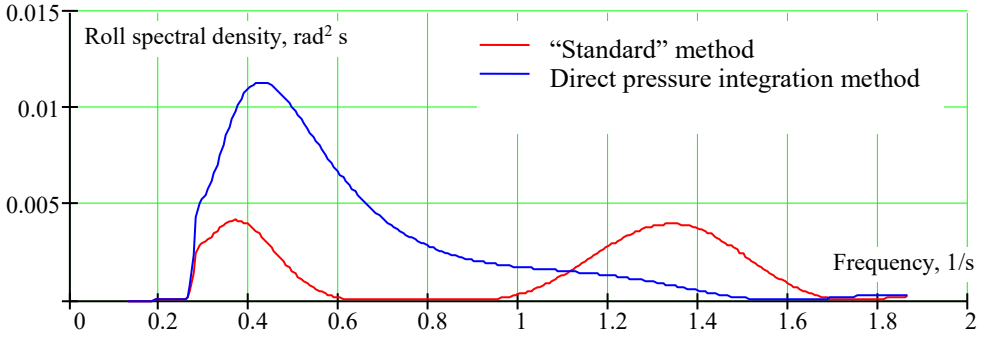

Figure 3.25. Complete Roll Response (Wind and Waves) Spectra for H_s = 9.5m; T_z = 10.5 s. Wave Roll Response is in Relative Coordinates

The level two vulnerability criterion is based on upcrossing probability, thus, the variance of the roll rate is also needed to evaluate the criterion. An artificial sensitivity of roll response to high frequency, introduced by a combination of "standard" method for effective wave slope and relative coordinates for roll response, may feel stronger on the roll-rate spectra. The differentiation of spectra involves multiplication by the square of the frequency.

Figure 3.26 shows three spectra: roll rate response to wind gusts, the roll-rate response to wave excitation in absolute and relative coordinates. An effective wave slope was computed with direct pressure integration. One can see a dramatic difference for a spectrum of roll-rate response to waves caused by the application of relative coordinates.

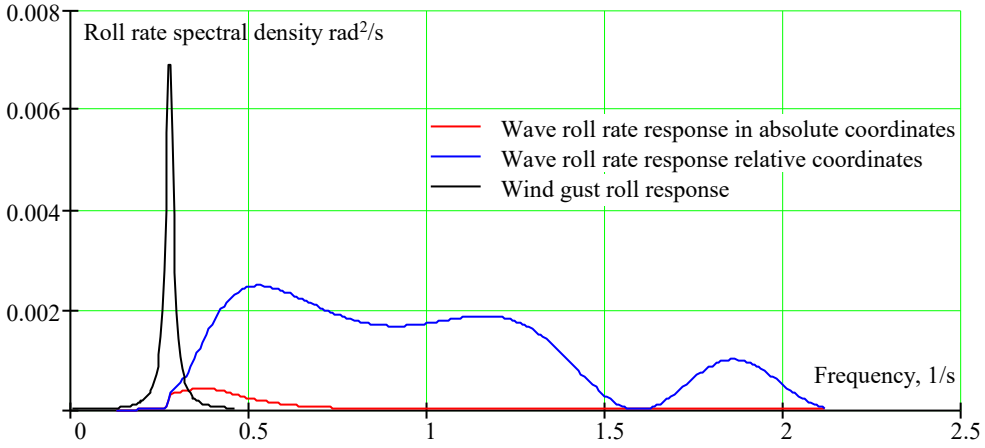

Figure 3.26. Roll Rate Response Spectra in Sea State H_s = 9.5m; T_z = 10.5s

Figure 3.27 shows the difference between the complete roll-rate spectra in absolute coordinates (includes both wind and wave responses) made by a method of calculation of the effective wave slope function. As the spectrum in absolute coordinates do not have a significant high-frequency sensitivity, the "standard" method for effective wave-slope function provides smaller values, which is consistent with the previous observations. Most of the energy is distributed near natural roll frequency (0.27 1/s), as one would expect for a resonance phenomenon.

Figure 3.28 shows the effect made by the application of relative coordinates. The energy distribution shifted significantly in the high-frequency range. The graphs do not contain the expected resonance peak around the natural frequency (0.27 1/s). The "standard" method of effective wave slope produced a peak in around 1.35 1/s, which seems to be the result of the amplification of the effective wave-slope peak (see Figure 3.8) by the RAO in relative coordinates.

The combination of the relative coordinates and the "standard" method for effective wave-slope function leads to the non-physical distribution of energy in a roll angle spectrum (Figure 3.25) and especially in the spectrum of roll rates (Figure 3.28). The values of standard deviation of roll angle and rates for some considered cases are in Table 3.2 for easy numerical comparisons.

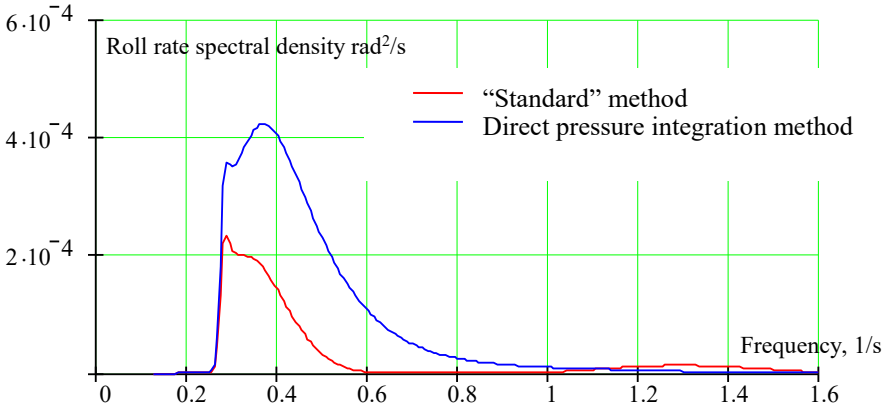

Figure 3.27. Complete Roll Rate Response (Wind and Waves) Spectra for H_s = 9.5m; T_z = 10.5 s. Wave Roll Response is in Absolute Coordinates

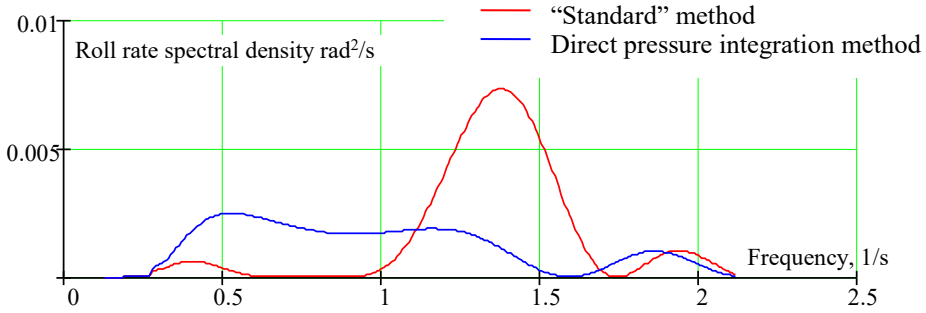

Figure 3.28. Complete Roll Rate Response (Wind and Waves) Spectra for H_s = 9.5m; T_z = 10.5 s. Wave Roll Response is in Relative Coordinates

Table 3.2. Standard Deviations for the Selected Cases

Effective Wave Slope Function	RAO Coordinates	Excitation Excitation	Standard deviation		Figure No.
			Roll, °	Rates °/s	
"Standard"	Absolute	Wind	3.56	0.966	-
	Absolute	Wave	1.014	0.372	-
	Relative	Wave	2.868	3.204	-
	Absolute	Combined	3.702	1.035	3.23, 3.26
	Relative	Combined	4.572	3.346	3.24, 3.27
Direct pressure integration	Absolute	Wind	3.56	0.966	3.21,3.25
	Absolute	Wave	1.578	0.626	3.21, 3.25
	Relative	Wave	4.07	2.803	3.21, 3.25
	Absolute	Combined	3.894	1.151	3.23, 3.26
	Relative	Combined	5.407	2.964	3.24, 3.27

3.4.4 Integral Convergence

Standard deviations of roll σ_ϕ and roll rate $\sigma_{\dot{}}$ formally expressed through integrals with infinite upper limits (see also equation 3.4.2.7-2 in Annex 4 of SDC 4/5/1 Add.3):

$$\sigma_\phi = \sqrt{\int_0^\infty S_\phi(\omega)\, d\omega} \qquad \sigma_{\dot{}} \qquad \sqrt{\int_0^\infty S_\phi(\omega)\, \omega^2\, d\omega} \tag{3.40}$$

Where $S_\phi(\omega)$ is a spectral density of roll angles.

Formula (3.40) as well as equation 3.4.2.7-2 in Annex 4 of SDC 4/5/1 Add.3 can be evaluated numerically if the integral converges. This converges can be achieved if

$$\lim_{\omega\to\infty} S_\phi(\omega) = 0 \;\; ; \;\; \lim_{\omega\to\infty} (S_\phi(\omega)\cdot\omega^2) = 0 \tag{3.41}$$

The effective wave slope function must tend towards zero with high frequencies, based on physical consideration, as a wave with a high frequency is essentially calm water. Both the direct pressure integration method and "standard" method exhibit this behavior, see Figure 3.29.

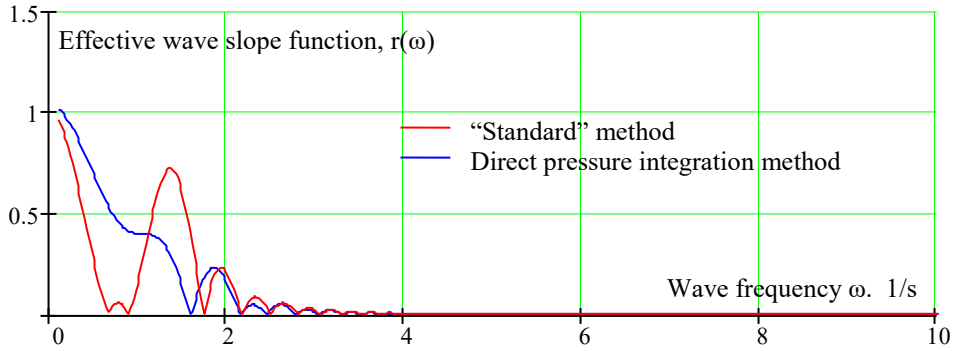

Figure 3.29. Limit of Effective Wave Slope Function (C11 Class Containership)

Note that without effective wave slope the standard deviation for roll rate in relative cannot be computed, as the spectral limit is not zero:

$$\lim_{\omega\to\infty}(S_{\phi}(\omega)\cdot\omega^2) =$$
$$= \lim_{\omega\to\infty}\left(\frac{\omega^4 - (2\cdot\mu_{\cdot}\cdot\omega)^2}{(\omega_{0,e}^2(\varphi_{S\cdot}} \frac{}{(2\cdot\mu_e\cdot\omega)^2}\left(\frac{\omega^2}{g}\right)^2 \right.$$
$$\left. \times \frac{H_S^2}{4\pi}\left(\frac{2\pi}{T_Z}\right)\omega^{-5}\exp\left(-\frac{1}{\pi}\left(\frac{2\pi}{T_Z}\right)\omega^{-4}\right)\cdot\omega^2 \right)$$
$$= \lim_{\omega\to\infty}\left(\frac{\omega^{10}}{\omega^9}\right) = \lim_{\omega\to\infty}(\omega) \neq 0 \qquad (3.42)$$

Where H_S is significant wave height and T_Z is mean zero-crossing period of waves, g is gravity acceleration. That is why the high-frequency behavior of effective wave-slope function is important for convergence of standard deviation of roll rate in relative coordinates. All other cases (standard deviation of roll rates in absolute coordinates, standard deviation of roll angles) do converge even without effective wave slope function.

3.4.5 Limits of the Integration

To ensure the integration domain covers all the non-zero values of the spectral density of roll angles and rates, numerical integration was performed separately on wind and wave exited rolls and rates.

For wave-excited roll-angles and -rates lower $\omega_{w\text{-}low}$ upper $\omega_{w\text{-}up}$ limits were taken as:

$$\omega_{w-low} = 0.3\omega_m \;;\; \omega_{w-up} = 5\max(\omega_m, \omega_0) \qquad (3.43)$$

Where ω_m is modal frequency of wave spectrum and ω_0 is the natural frequency of roll in calm waters.

For wind-gust exited-roll motions and rates, lower $\omega_{a\text{-}low}$ upper $\omega_{a\text{-}up}$ limits were taken as:

$$\omega_{a-low} = 0.001,\ 1/s \;;\; \omega_{a-up} = \min(\omega(S_v < 0.01), 5\omega_0) \qquad (3.44)$$

Where $\omega(S_v<0.01)$ is a frequency where wind gust spectral density fells below 0.01 m^2/s.

3.4.6 Value of the Criteria

Table 3.3 shows the results for the criterial value C computed as described in paragraph 3.4.2 Annex 4 of SDC 4/5/1 Add.3 and paragraph 2.13.3 of Annex 1 of SDC 3/WP.5. The tendencies, described in the previous subsection remain the "standard" method for effective wave-slope function seems to provide a less conservative result compared to the direct pressure integration. The application of relative coordinates for the roll response on waves produces larger values, compared to absolute coordinates.

Table 3.3. Value of the Criteria

Effective Wave Slope Function	RAO Coordinates for Wave Roll Response	C-Value
"Standard"	Absolute	8.149E-11
	Relative	2.214E-8
Direct Pressure Integration	Absolute	4.034E-9
	Relative	1.451E-6

Note that the result is also provided in the example in section 4 of the Annex 4 of SDC 4/5/1 Add.3: C=1.286E-9, which is different from the comparable number from Table 3.3 (C = 2.214E-8). What could be the reason for this difference?

Verification took place on a MathCAD worksheet that was used for calculating the criteria by using the reimplementation of certain elements and comparisons with the original implementations. Those elements included computations of the standard deviation of roll and roll rates, rate, and short-term probabilities of exceedance of "dangerous" angles. The verification of the roll damping is described in section 7.

Table 4.1 of Annex 4 of SDC 4/5/1 Add.3 provides intermediate results – values $W_i C_{Si}$, weighted short-term probability. Consider one of the values from that table; e.g. corresponding to significant wave height of 12.5 m and mean zero-crossing period 12.5 s. Table 4.1 of Annex 4 of SDC 4/5/1 Add.3 has:

$$W_i C_{Si} = 5.21 \cdot 10^{-15}$$

The statistical weight for the sea state comes from the scatter diagram (see Table 3.1 Annex 4 of SDC 4/5/1 Add.3)

$$W_i = 1.1 \cdot 10^{-4}$$

The short-term probability of exceedance of a dangerous angle during 1 hr:

$$C_{Si} = 4.736\ 10^{=11}$$

The exceedance rate is computed as (referring to formula 3.4.2.7-1 of Annex 4 of SDC 4/5/1 Add.3)

$$\lambda_{EA} = -\frac{\ln(1 - C_{Si})}{T_{\exp}} = 1.316\ 10^{=14}\ , 1/s \qquad T_{\exp} = 3600\ s$$

Where $T_{\exp}$ is the accepted exposure time. As expected, the above crossing rate value is smaller than the one computed in the present case study:

$$\lambda_{EA1} = 3.207\ 10^{=12}\ , 1/s$$

To provide the "best guess" on the origin of the difference consider λ_{EA} as defined by the formula 3.4.2.7-1 of Annex 4 of SDC 4/5/1 Add.3 as a function of the upper limit of the integration, see Figure 3.30. Assuming that all the differences between the EN example and the current case-study calculation came from a different upper-limit integration, one can determine the "hypothetical" upper limit for the EN. Consider this example:

$$\omega_{EN-up} = 0.42\ ,1/s$$

Assume that the upper limits of the integration is the same for computing the standard deviation of the roll and roll rates. Figure 3.3.31 shows these upper limits on the plots of roll spectral density of roll (Figure 3.3.31a) and roll rates (Figure 3.3.31b). The reason for the difference between the EN example and the current calculation may be that the EN calculation did not include any secondary peaks of spectral densities. As it was shown in the subsection 3.2 and 3.3, a combination of the "standard" method for an effective wave-slope function and relative coordinates for wave-induces roll motions may cause an unexpected behavior of spectral density in high frequencies. As this behavior is not confirmed by existing practical experience, it could be characterized as "a numerical artefact" and be removed from the EN calculation.

Such a removal, essentially, may have a similar effect to using absolute coordinates and direct-pressure integration for effective wave-slope function. An argument for this possibility is that the value of the long-term criteria computed in absolute coordinates with the direct-pressure integration (4.034E-9, see table 3.3) is the closest to the EN value (1.286E-9); also see a similar comparison on the crossing rates in Figure 3.30.

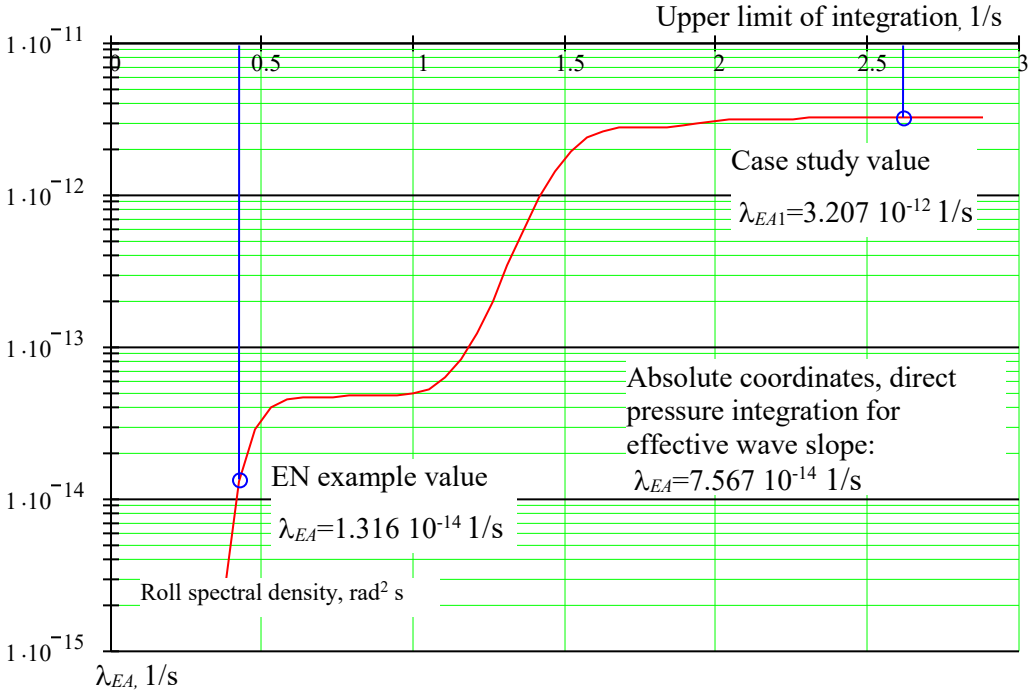

Figure 3.30. λ_{EA} as a Function of the Upper Limit of Integration H_s = 12.5 m; T_z = 12.5 s.

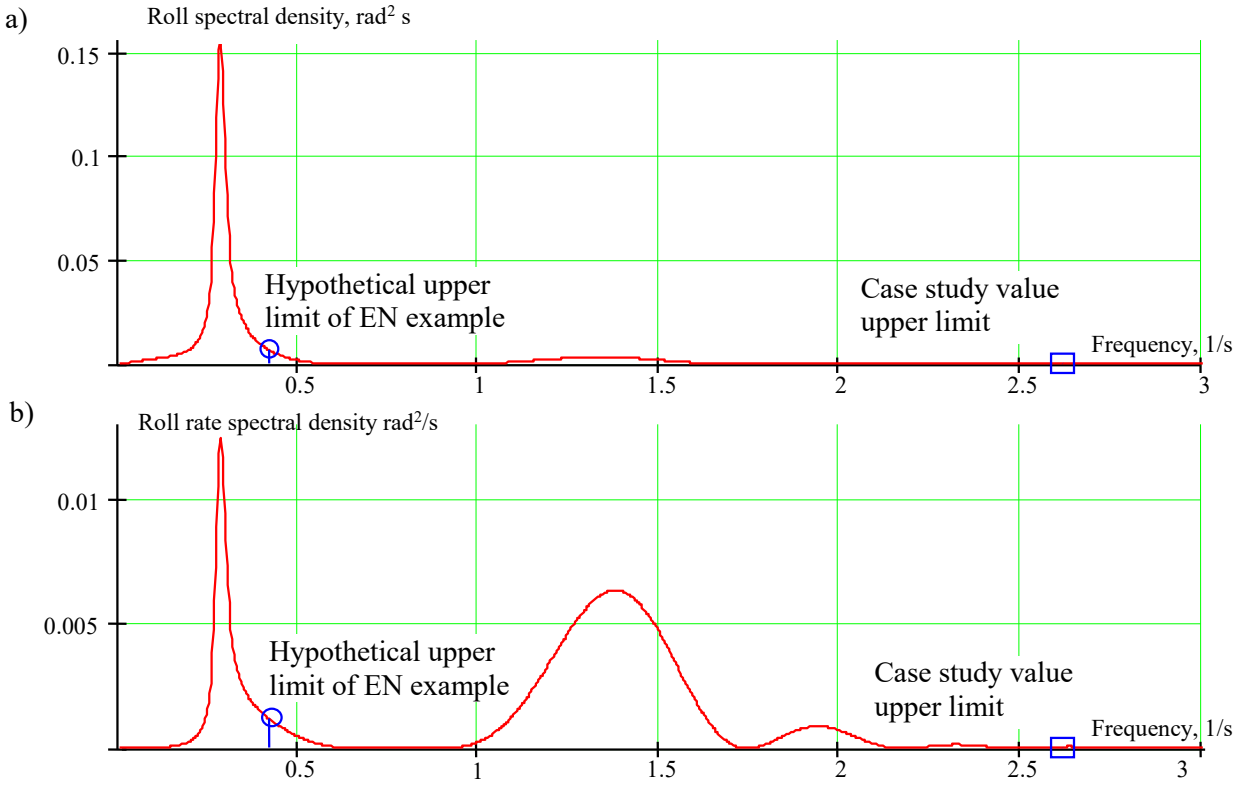

Figure 3.3.31. Spectral Densities of Roll (a) and Roll Rates (b) in Relative Coordinates, Using "Standard" Effective Wave Function for H_s = 12.5 m; T_z = 12.5 s with Upper Limits of Integration Shown

Another indirect argument is a proposal to limit the application of the "standard" method for an effective wave slope by a frequency corresponding to "wavelength to ship-breadth ratio of 0.5" (Annex 13 of SDC4/INF.4/Add.2). For the considered case, it corresponds to the wave's length equal to 20 m and wave frequency 1.756 1/s. As seen in Figure 3.3.31, it will not remove the second peak. However, a limitation of wavelength to ship breadth ration of two (wave's length 80 m and wave frequency 0.878 1/s) will remove this "unusual" high frequency-behavior.

On the other hand, the example first appeared in Annex 19 of SDC 3/INF.10, where the numbers are the same as in the latest version in Annex 4 of SDC 4/5/1 Add.3. So the mistake in either calculations cannot be excluded, thus the benchmarking with the exchange of the intermediate results can be recommended.

Note that sum all the elements of Table 4.1 of Annex 4 of SDC 4/5/1 Add.3 yields 1.3216E-9 rather than 1.286E-9 indicated on the page 22 of Annex 4 SDC 4/5/1 Add.3.

All the numbers for the level 2 criteria are small and should be judged as not vulnerable in a dead-ship condition for the considered loading-conditions.

3.4.7 Summary and Conclusions

The objective of the study was to examine what is the effect of inaccuracies caused by application of "standard" method for effective wave-slope function and using relative

coordinates (roll angle measured relative to wave slope) for roll response to irregular waves. The comparison took place in order to get the direct-pressure integration method for an effective wave-slope function and consistent presentation of roll response in absolute coordinates (roll angle measured relative to the horizon) for roll responses to waves and wind.

This comparison concluded that:

- The "Standard" method provides less conservative results compared to direct pressure integration.
- The application of relative coordinates for wave-roll responses leads to larger values of the criteria, however, it is caused by artificial sensitivity of roll-rate spectrum to high frequencies, leading to physically unrealistic distributions of energy in the spectra.

These conclusions, however, are limited by a single case study described here; further consideration of this matter will be carried out in the next subsection where sample calculations are described.

3.5 Sample Calculations

3.5.1 Input and Output of Sample Calculations

Sample calculations were carried out with the purpose to test the process of vulnerability assessments in dead-ship condition. Another objective is to carry out comparisons for different calculation options formulated in the previous subsections, but using a wider set of data.

There were five ships used for sample calculations with 5 - 6 loading conditions each, totaling 27 cases. Main input data are in Table 3.4.

Table 3.4. Input Data for Sample Calculations

Ship Type	Loading Case Identifier	Length, bp, m	Beam, *B*, m	Depth, *D*, m	Draft, *d*, m	Displaced Volume, Molded, m^3	*KG*, m	*GM*, m
Container ship	Benchmark	262.00	40.00	24.45	11.50	67,500	18.92	1.40
	SLL				12.70	77,540	19.92	0.30
	PL1				12.29	74,660	17.54	2.84
	PL2-KG1				10.70	61,150	20.01	0.43
	PL2-KG2				10.70	61,150	17.50	2.94
	LL1				8.29	43,910	16.00	5.77
RoPax Ferry	SLL	137.00	20.25	12.78	5.77	9,737	8.71	1.59
	PL1				5.54	9,262	8.67	1.73
	PL2				5.40	8,891	8.79	1.70
	LL1				4.91	7,833	8.94	1.80
	LL2				4.47	6,882	9.27	1.83
Cruise Ship, Location 1	Load 1	242.30	36.00	26.00	8.70	54,090	17.37	1.65
	Load 2				8.40	51,760	17.39	1.93
	Load 3				8.40	51,760	17.94	1.38
	Load 4				7.90	48,290	17.16	2.64
	Load 5				7.90	48,290	15.53	4.27
Bulk Carrier	SLL	145.00	22.85	15.00	10.80	29,510	9.02	0.70
	PL1				8.45	22,455	8.34	1.16
	Pl2				8.37	22,219	7.46	2.00
	LL1				4.25	10,507	6.44	5.36
	LL2				6.69	17,340	5.08	4.65
LNG Carrier	SLL	257.00	41.60	24.00	12.00	100,381	15.94	2.41
	PL1				11.33	94,034	15.94	2.76
	PL2				9.95	81,504	15.89	3.80
	LL1				5.60	42,756	11.86	16.28
	LL2				7.28	57,289	12.74	10.64

To evaluate the possible inconsistency between IS code and vulnerability criteria on dead ship conditions, the stability of each sample vessel in each loading condition was checked in accordance with paragraph 2.2 and 2.3 of 2000 IS Code. All cases met the requirements of paragraph 2.2 of the 2008 IS Code. Results for the paragraph 2.3 are in Table 3.5 along with the results of Level-1 vulnerability assessment in dead-ship condition.

Table 3.5. IS Code and Level 1 Results

Ship Type	Loading Case Identifier	Draft, d, m	Period of Roll, T, s	B/d	KG/d-1	2008 IS Code, A/2.3 Weather Criterion					Level 1	
						Static Angle, φ0°	Roll angle, φ1, °	Area "a", m rad	Area "b", m rad	IS Code, A/2.3 b>a?	Roll Angle, φ1, °	Area "a", m rad
Container ship	Benchmark	11.50	23.0	3.48	0.65	5.5	15.5	0.071	0.390	Y	13.4	0.056
	SLL	12.70	48.3	3.15	0.57	15.8	16.9	0.034	0.075	Y	12.7	0.023
	PL1	12.29	15.9	3.25	0.43	2.1	17.7	0.153	0.903	Y	17.7	0.153
	PL2-KG1	10.70	42.2	3.74	0.87	14.4	15.9	0.045	0.042	N	12.0	0.031
	PL2-KG2	10.70	16.2	3.74	0.64	2.6	16.7	0.148	0.907	Y	16.7	0.148
	LL1	8.29	12.4	4.83	0.93	2.0	20.3	0.393	1.477	Y	20.3	0.393
RoPax Ferry	SLL	5.77	12.7	3.52	0.51	6.5	19.8	0.129	0.394	Y	19.8	0.129
	PL1	5.54	12.3	3.66	0.56	6.4	20.5	0.147	0.405	Y	20.5	0.147
	PL2	5.40	12.5	3.75	0.63	6.8	20.5	0.148	0.370	Y	20.5	0.148
	LL1	4.91	12.4	4.13	0.82	7.6	21.1	0.168	0.298	Y	21.1	0.168
	LL2	4.47	12.5	4.53	1.07	8.6	21.6	0.186	0.198	Y	21.6	0.186
Cruise Ship	Load 1	8.70	20.4	4.14	1.00	9.0	17.7	0.129	0.269	Y	16.7	0.118
	Load 2	8.40	19.0	4.29	1.07	8.3	18.4	0.153	0.273	Y	18.0	0.147
	Load 3	8.40	22.5	4.29	1.14	11.2	18.3	0.127	0.097	N	16.1	0.105
	Load 4	7.90	16.6	4.56	1.17	6.7	20.2	0.226	0.369	Y	20.2	0.226
	Load 5	7.90	13.0	4.56	0.97	4.2	22.8	0.407	0.936	Y	22.8	0.407
Bulk Carrier	SLL	10.80	19.8	2.13	-0.16	1.5	15.9	0.031	0.238	Y	15.2	0.029
	PL1	8.45	16.0	2.73	-0.01	1.6	17.9	0.066	0.659	Y	17.9	0.066
	Pl2	8.37	12.2	2.75	-0.11	0.9	20.6	0.142	0.942	Y	20.6	0.142
	LL1	4.25	8.7	5.42	0.51	1.0	25.8	0.580	1.712	Y	25.8	0.580
	LL2	6.69	8.3	3.44	-0.24	0.6	19.9	0.295	1.907	Y	19.9	0.295
LNG Carrier	SLL	12.00	18.4	3.47	0.33	1.2	16.2	0.109	1.099	Y	16.0	0.107
	PL1	11.33	17.4	3.68	0.41	1.2	17.0	0.136	1.199	Y	17.0	0.136
	PL2	9.95	15.3	4.19	0.60	1.0	19.5	0.244	1.433	Y	19.5	0.244
	LL1	5.60	9.0	7.44	1.12	0.5	30.0	2.017	3.843	Y	30.0	2.017
	LL2	7.28	10.1	5.73	0.75	0.6	26.2	1.138	3.063	Y	26.2	1.138

Table 3.6 contains the results of level 2 vulnerability assessments in dead-ship conditions. Following the Case Study in the Subsection 3.4, calculations were done for two methods of calculation of effective wave-slope functions ("standard" method and direct pressure integration) and for the wave-excited roll-motion in relative and absolute coordinates, totaling four options.

Table 3.6. Results of Level 2 Assessment

Ship Type	Loading Case Identifier	Draft, *d*, m	Period of Roll, *T*, s	*B/d*	*KG/d*-1	Long-Term Probability Index, *C*			
						Relative		Absolute	
						Standard	Direct	Standard	Direct
Container ship	Benchmark	11.50	23.0	3.48	0.65	2.214E-8	1.451E-6	8.149E-11	4.034E-9
	SLL	12.70	48.3	3.15	0.57	0.042	0.011	0.011	0.011
	PL1	12.29	15.9	3.25	0.43	3.514E-7	3.514E-7	7.452E-9	1.747E-7
	PL2-KG1	10.70	42.2	3.74	0.87	0.058	5.885E-3	4.922E-3	4.925E-3
	PL2-KG2	10.70	16.2	3.74	0.64	3.997E-7	1.494E-5	8.509E-9	1.554E-7
	LL1	8.29	12.4	4.83	0.93	1.772E-4	9.077E-4	2.693E-5	1.17E-4
RoPax Ferry	SLL	5.77	12.7	3.52	0.51	1.659E-3	3.204E-3	5.018E-4	7.301E-4
	PL1	5.54	12.3	3.66	0.56	2.64E-3	4.658E-3	9.336E-4	1.287E-3
	PL2	5.40	12.5	3.75	0.63	3.186E-3	5.421E-3	1.072E-3	1.446E-3
	LL1	4.91	12.4	4.13	0.82	7.525E-3	0.011	3.024E-3	3.663E-3
	LL2	4.47	12.5	4.53	1.07	0.018	0.022	7.509E-3	8.475E-3
Cruise Ship	Load 1	8.70	20.4	4.14	1.00	2.555E-4	3.531E-4	4.051E-5	4.224E-5
	Load 2	8.40	19.0	4.29	1.07	3.811E-4	5.425E-4	3.267E-5	4.189E-5
	Load 3	8.40	22.5	4.29	1.14	3.988E-3	3.537E-3	8.158E-4	8.502E-4
	Load 4	7.90	16.6	4.56	1.17	3.954E-4	6.516E-4	3.245E-5	4.911E-5
	Load 5	7.90	13.0	4.56	0.97	8.868E-5	2.155E-4	5.059E-6	1.178E-5
Bulk Carrier2	SLL	10.80	19.8	2.13	-0.16	3.36E-9	7.353E-8	2.796E-11	1.827E-10
	PL1	8.45	16.0	2.73	-0.01	7.842E-10	9.257E-9	3.06E-12	1.727E-11
	Pl2	8.37	12.2	2.75	-0.11	9.206E-6	2.937E-5	1.073E-6	2.54E-6
	LL1	4.25	8.7	5.42	0.51	1.607E-3	2.257E-3	7.388E-4	1.201E-3
	LL2	6.69	8.3	3.44	-0.24	1.884E-4	3.375E-4	1.754E-4	2.734E-4
LNG Carrier	SLL	12.00	18.4	3.47	0.33	4.714E-7	1.209E-6	1.181E-7	2.736E-7
	PL1	11.33	17.4	3.68	0.41	5.959E-6	1.362E-5	1.904E-6	4.06E-6
	PL2	9.95	15.3	4.19	0.60	3.877E-4	6.995E-4	1.772E-4	3.142E-4
	LL1	5.60	9.0	7.44	1.12	0.171	0.189	0.172	0.19
	LL2	7.28	10.1	5.73	0.75	0.072	0.085	0.068	0.08

3.5.2 Observation of the Result of Sample Calculations

Both Table 3.5 and Table 3.6 contain columns with data on applicability of the weather criterion. As formulated in paragraph 2.3.5 of the 2008 IS Code with the table and formulae of the weather criterion in paragraph 2.3.4 of the 2008 IS code, which are only applicable when:

- The *B/d* is smaller than 3.5
- The (*KG/d*-1) is between -0.3 and 0.5
- The roll period *T* is smaller than 20 s

If a ship at a considered loading-condition does not satisfy these limitations, the weather criteria are not applicable, but the vulnerability criteria for dead-ship condition are expected to work. These cases are highlighted with yellow in Table 3.5 and Table 3.6. Indeed, most of the cases included in the sample calculation are intended for the application of a vulnerability assessment; five cases where weather criterion is applicable are included for comparison.

One case (container ship, loading PL2-KG1, is highlighted with light red and green colors in Table 3.5 and Table 3.6) does not satisfy the weather criterion: the "b" area (0.042 m rad) is smaller than the "a" area (0.045 m rad). However, in this case B/d=3.74, (KG/d-1)=0.87>0.5 and T = 42.2 s > 20 s, thus, the weather criterion is not applicable. The level 1 vulnerability criterion does not indicate the vulnerability as the area "a" is decreased to 0.031 rad m and falls below the area "b" that remains 0.042 m rad, see Table 3.5.

Look further into this case for level 2 assessment. The largest C-value is given by the combination of "standard" method for effective wave slope function and roll response to wave computed in relative coordinates. This value is 0.058, with the standard of 0.06, (see paragraph 4.3.1 of Annex 3 of SDC 6/WP.6) the case is considered not vulnerable to stability failure in dead ship condition. However, it is very close to the standard – almost falling into an inconsistency between the levels. If the standard remained as 0.04 (paragraph 2.13.3.1 of Annex 1 of SDC 3/WP.5), this case would show an inconsistency between the levels if the "standard" wave-slope function is combined with the roll response computed in relative coordinates for the level 2 assessment.

Does the vulnerability criterion C = 0.058 indicate danger for this particular loading case? Probably not, but it can be attributed to non-physical behavior of the "standard" wave-slope function combined with wave-roll responses computed in relative coordinates. The changing any of these options drops the value about an order of magnitude to 0.0049 - 0.0058, which is far from the standard.

Also, consider the loading case SLL for the same ship. The GM value in this case is 0.3 m vs. 0.43 m in the PL2-KG1 case - see Table 3.4. The expectation would be that the SLL case is worse than PL2-KG1 from the stability perspective. However, the level 2 vulnerability criterion, computed with "standard" wave slope function and wave roll response in relative coordinates indicate vice versa: the C-value decreases from 0.058 to 0.042. Simultaneously, the C-values computed with any other option indicate the expected trend – increase the C-value from 0.0049-0.0058 to 0.011, which indicates the drop of GM from 0.43 m to 0.3 m increases stability hazard.

Note that there is no indication of vulnerability on the level 1 for the containership SLL case. If the standard remained as 0.04 (paragraph 2.13.3.1 of Annex 1 of SDC 3/WP.5), this case would show an inconsistency when the "standard" wave-slope function is combined with roll response that was computed in relative coordinates for the level 2 assessment as well. No options show the inconsistency in this case.

The third case, worthy of a detailed examination is the cruise ship with the loading case - "Loading 3". The weather criterion is not satisfied, however, it is not applicable. The level 1 vulnerability criterion indicated a possible vulnerability, but the level 2 assessment shows none. In principle, this result is acceptable, as the level 2 assessment is meant to be less conservative, compared to the level 1 assessment. The problem is that the C-values are rather low for all the options (about an order of magnitude below the standard), while one could expect values to be quite closer to the standard if level 1 indicated a vulnerability.

Compare this result with container ship SLL case. The static angle is 15.8°, so the weather criterion is very close to being violated in its applicable part (the requirement for static angle is always applicable), and the *C*-value for the level 2 (for three options) is close to the standard. One could expect similar behaviors with a cruise ship Load 3 case, but it was not observed. Based on this argument, there seems to be enough of a reason to suspect inconsistency within this case.

Finally load cases LL1 and LL2 of the liquid natural gas (LNG) carrier shows vulnerability for very high GM values, shown in light orange in Table 3.6. Formally, these cases are inconsistent since the level 1 criterion does not indicate any vulnerability. However, the reason for such behavior is clear – large motions are very likely a result of resonance motions that were generated by large GM values. These two cases are the subject of concerns for excessive accelerations and should be excluded from considerations for dead-ship conditions based on their GM values.

3.6 Alternative Formulation for the Level 2 Criteria

No inconsistencies between the levels (except of a couple near-misses) were spotted in the sample calculations, described in the subsection 3.6. Nevertheless, the consistency between level 1 and level 2 vulnerability assessment was identified as an outstanding issue at the 5th session of SDC; the corresponding action item was included in the terms of references of the intersessional correspondence group (paragraph 3.3.7 of SDC 6/5).

One possible source between the levels is the difference in a mathematical model describing stability failure in a dead-ship condition. The idea is to develop a formulation that would be a “half-way” between the currently proposed level 2 criterion as described in the section 4.2 of Annex 3 SDC 6/WP.6 and the level 1 or weather criterion. This alternative formulation may be used as a “tool of study”, in which the same mathematical model is used as the weather criterion, but is formulated in a probabilistic way. Such a formulation may be helpful to better identify sources of inconsistency, so they can be addressed and studied separately.

Annex 15 of SDC 4/INF.4/Add.4 and Annex 1 of SDC 5/ INF.4, as well as Peters & Belenky (2019) contain formulations of an alternative level 2 criterion, which uses the same general scheme of application of the weather criterion. However, it also uses the input parameters that are given a probabilistic interpretation - see Figure 3.32. Two parameters are given probabilistic interpretations:

- The heeling moment caused by wind speed related to significant wave height
- The back roll angle is taken from roll-motion calculation in irregular waves

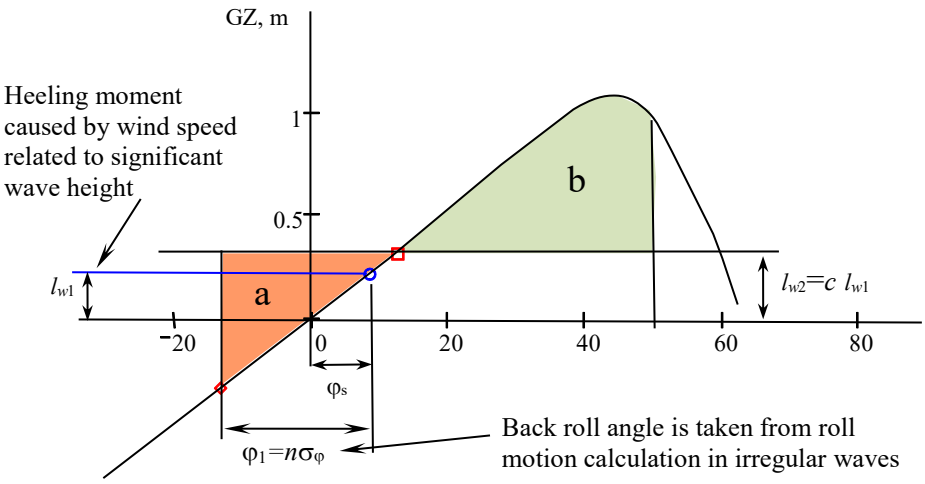

Figure 3.32. On the Formulation of the Alternative Level 2 Vulnerability Criterion

The alternative formulation is considered for the value CSi in the paragraph 4.3.2 if Annex 3 of SDC.6/WP.6:

$$\begin{aligned} C_{Si} &= 0 \quad \text{if } a \le b \quad \text{and} \quad \varphi_s \le 16 \text{ or } \varphi_s \le 0.8\,\varphi_d \\ C_{Si} &= 1 \quad \text{otherwise} \end{aligned} \tag{3.45}$$

Where a and b are as defined similar to paragraph 2.3 of the 2008 IS Code and illustrated in Figure 3.32, φ_d is the angle of the deck immersion. The other parameters defined as:

$$l_{w1} = \frac{P \cdot A \cdot Z}{g \cdot m} \tag{3.46}$$

Where A is the projected lateral-area of the portion of the ship and deck cargo above the waterline, Z is the vertical distance from the center of A to the center of underwater lateral area or approximately to a point at one half of the mean draft. The unit, m, is the mass of the ship and g is the gravity acceleration, P if the pressure computed as:

$$P = \frac{\rho_A U_{Wm}^2}{2} \cdot C_m \tag{3.47}$$

Where C_m is wind heeling moment coefficient. Its value is taken as 1.22 from paragraph 4.3.2.2 of Annex 3 of SDC 6/WP.6, while ρ_A is the density of air. The mean wind speed U_{Wm} is taken from paragraph 4.3.2.2 of Annex 3 of SDC 6/WP.6

$$U_{Wm} = \left(\frac{H_S}{0.06717}\right)^{2/3} \tag{3.48}$$

Where H_S is the significant wave-height corresponding to the considered cell of the scatter table. The angle of roll, φ_1, is calculated as a factor, n, of the standard deviation of absolute roll motion, σ_φ:

$$\sigma_\varphi = \left(\int_0^\infty (S_{ae}(\omega) + S_{mw}(\omega)) H^2(\omega) d\omega\right)^{1/2} \tag{3.49}$$

Where $H(\omega)$ is RAO of roll motion in absolute coordinates:

$$H^2(\omega) = \frac{\omega_{0S}^4}{\left(\omega_{0S}^2+\omega^2\right)^2+\left(2\delta_{\varphi e}\cdot\omega\right)^2} \tag{3.50}$$

Where ω_{0S} is a modified-roll natural frequency computed at the heel angle caused by the steady wind at the considered cell of the scatter table, ω is the circular frequency; $\delta_{\varphi e}$ is the equivalent linear roll-damping, computed with any accepted or prescribed linearization method.

The spectral density of roll excitation $S_{\alpha e}(\omega)$, caused by irregular waves, is computed as:

$$S_{\alpha e}(\omega) = r^2(\omega)S_\alpha(\omega) = r^2(\omega)\frac{\omega^2}{g}S_z(\omega) \tag{3.51}$$

Where $r(\omega)$ is effective wave-slope function, computed with direct pressure integration as described in the subsection 3.2, $S_\alpha(\omega)$ is spectral density of the angles if wave-slope, $S_z(\omega)$ is the spectral density of wave elevations

$$S_z(\omega) = \frac{4\pi^3 H_S^2}{T_Z^4}\omega^{-5}\exp\left(\frac{16\pi^3}{T_Z^4}\omega^{-4}\right) \tag{3.52}$$

Where T_Z is the mean zero-crossing period corresponding to the considered cell of the scatter table.

The spectral density of roll excitation $S_{\alpha e}(\omega)$, caused by gusty wind, is computed as:

$$S_{mw}(\omega) = (\rho_A C_m U_{Wm} A \cdot Z)\cdot S_v(\omega) \tag{3.53}$$

Where $S_v(\omega)$ is the spectral density of wind velocities caused by random gusts:

$$S_v(\omega) = 4K\frac{U_{Wm}^2}{\omega}\cdot\frac{X_D^3((\omega))}{\left(1+X_D^2(\omega)\right)^{4/3}} \tag{3.54}$$

Where:

$$X_D(\omega) = \frac{600\cdot\omega}{\pi\cdot U_{Wm}};\quad K=0.003 \tag{3.55}$$

The sample calculations for the alternative criterion for the ships, described in Table 3.4, are summarized in Table 3.7. Yellow color highlighted cases where the weather criterion is not applicable; highlights with green, orange, and light red colors are used in the same meaning as in tables 3.5 and 3.6 as shown here for easy reference.

One can see that all the sample ships are indicated as non-vulnerable for stability failure in dead ship condition, using the standard of 0.06 as set in the section 4.3 of Annex 3 of SDC 6/WP.6. At the same time, the largest values of the criteria are obtained for the case where the criteria from IS Code 2008 as shown were close:

- Container ship, SLL: small GM
- Container ship, PL2-KG1: small GM and areas *a* and *b* are close
- RolPax ferry LL1 and LL2: areas *a* and *b* are close
- Cruise ship Load 3: vulnerability indicated on level 1
- LNG carrier LL1 and LL2: very large GM, possible high acceleration

The alterative criterion produces smaller numbers, so the standard for the alterative criterion may need to be different. In general, its behavior seems to be similar to the C-value, computed in absolute coordinates and with direct pressure integration for the effective wave

slope function. It is not surprising as the mathematical models, used for description of ship motions, were similar.

Table 3.7. Results of Level 2 Assessments with Alternative Criterion

Ship Type	Loading Case Identifier	draft, *d*, m	Period of roll, *T*, s	*B/d*	*KG/d*-1	Alternative C-value
Container ship	Benchmark	11.50	23.0	3.48	0.65	0
	SLL	12.70	48.3	3.15	0.57	0.011
	PL1	12.29	15.9	3.25	0.43	0
	PL2-KG1	10.70	42.2	3.74	0.87	4.914E-3
	PL2-KG2	10.70	16.2	3.74	0.64	0
	LL1	8.29	12.4	4.83	0.93	0
RoPax Ferry	SLL	5.77	12.7	3.52	0.51	2.58E-4
	PL1	5.54	12.3	3.66	0.56	5.73E-4
	PL2	5.40	12.5	3.75	0.63	7E-4
	LL1	4.91	12.4	4.13	0.82	2.346E-3
	LL2	4.47	12.5	4.53	1.07	7.516E-3
Cruise Ship	Load 1	8.70	20.4	4.14	1.00	7.9E-5
	Load 2	8.40	19.0	4.29	1.07	1.14E-4
	Load 3	8.40	22.5	4.29	1.14	2.066E-3
	Load 4	7.90	16.6	4.56	1.17	1.08E-4
	Load 5	7.90	13.0	4.56	0.97	0
Bulk Carrier2	SLL	10.80	19.8	2.13	-0.16	0
	PL1	8.45	16.0	2.73	-0.01	0
	PI2	8.37	12.2	2.75	-0.11	0
	LL1	4.25	8.7	5.42	0.51	1E-6
	LL2	6.69	8.3	3.44	-0.24	1E-6
LNG Carrier	SLL	12.00	18.4	3.47	0.33	0
	PL1	11.33	17.4	3.68	0.41	0
	PL2	9.95	15.3	4.19	0.60	5E-6
	LL1	5.60	9.0	7.44	1.12	0.014
	LL2	7.28	10.1	5.73	0.75	4.978E-3

3.7 Consistency between the Levels

3.7.1 Probabilistic Study: Formulation of the Problem

Consider the consistency between the level 1 and level 2 criteria, apart from the applicability and general regulatory issues. As the level 1 vulnerability criterion is the weather criterion with an extended table for the roll period, the consistency problem essentially focuses on the probabilistic interpretation of the weather criterion. The problem attracted the attention of naval architects long ago (e.g. Dudziak & Buczkowski, 1978) abridged versions are available in Belenky & Sevatsianov (2007).

The author touched this problem in an attempt to assess probability capsizing of a series of ships in KG-critical condition based on the criteria to be included in the 2008 IS Code (Belenky, 1995). With some surprise at the time, the value of the capsizing probability had shown significant variation. This outcome meant that compliance with the weather criterion does not necessarily mean that a probability of stability failure will fall within a certain range.

Consider the Weather Criterion as used as the Level 1 criterion, it has the following characteristics:

- Use of a deterministic model for the wind gust as 1.5 times the mean wind speed.
- Use of a semi-empirical method to determine the rollback angle.
- Definition of failure as a physical possibility of exceedance of an unacceptable level resulting from a single wind gust.

The Weather Criterion was developed based on ships with loading conditions with certain characteristics ($B/d < 3.5$ and $-0.3 < (KG/d - 1) < 0.5$ and $T < 20$s). When the loading condition is beyond those ranges, the 2008 IS Code permits model tests to be used to assess wind heeling and the rollback angle. Otherwise, for Level 1 vulnerability criteria, the Weather Criterion model is extended up to $T < 30$ s.

On the other hand, the Level 2 vulnerability criteria developed using a probabilistic model for the wind gust based on the spectrum of wind velocity in which the roll-back angle is assessed from ship motion calculations, and stability failure is defined as a probability of exceeding an unacceptable level within one hour's duration. Because the Level 2 model is expected to be more advanced/detailed than the Level 1/Weather Criterion model, some degree of inconsistency can be expected. However, partly because the Weather Criterion is mandatory, there is no information about a stability accident involving the dead ship condition to assist with setting the standard for the Level 2.

To address these challenges, three objectives can be established:

- Ensure that the calculation methods used for the vulnerability criteria Level 2 are robust and are used within their applicability range.
- Choose the standard to ensure the integrity of the 2008 IS Code and consistency between the Levels 1 and 2 vulnerability criteria.
- Accept a certain probability of inconsistency and treat this probability as a safety level to be used to set the standard.

How can the consistency between the Weather Criterion and the Level 2 vulnerability criteria be assessed?

Consider a ship in a critical condition on the Weather Criterion, such that any increase of the *KG* will mean the criterion is not satisfied. This critical condition means that either area *a* exactly equals area *b*, or the angle of heel under steady action of wind exactly equals its limit value (16° or 80 % of deck edge immersion, whichever is less).

The Level 2 vulnerability criterion is formulated probabilistically. The result of the calculation for Level 2 is a probability of at least one exceedance of the prescribed roll angle within an hour. The Level 2 vulnerability criterion can be applied to loading conditions of several ships where the Weather Criterion is fully applicable and are in a critical condition. If the Weather Criterion and Level 2 vulnerability criterion are consistent, then the calculated probabilities should be the same.

However, because of using different mathematical models for ship rolling under wind and wave action, those probabilities cannot be the same. Variations of these probabilistic values assess the inherent level of inconsistency between Levels 1 and 2.

3.7.2 Probabilistic Study: Calculation Procedure

The first step in this procedure is to ensure that B/d <3.5, which can be achieved by selecting a draft. A ship where no operational draft corresponds to the condition B/d <3.5 should be excluded from the sample.

The initial KG value is computed as:

$$KG_0 = BM + KB - GM_{min} \tag{3.56}$$

Here, the lowest GM_{min} = 0.15 m is taken from the requirements in the paragraph 2.2.4 of part A of the 2008 IS code.

Using the accepted draft, KG_0 and assuming zero trim, the *GZ* curve can be calculated. However, this does not guarantee that this KG_0 is realistic, as it may not satisfy the other requirements of the 2008 IS code, part A/2.2. Nevertheless, there is sufficient information to compute the maximum KG based on the requirements of the 2008 IS code, A/2.2. This maximum *KG* is referred to as KG_1.

There are limiting values of the *KG* based on the draft that derived from satisfying the inequality -0.3 < (*KG*/*d* - 1) < 0.5:

$$KG_2 = 1.5d \qquad KG_3 = 0.7d \tag{3.57}$$

Finally, there is the roll period condition T < 20 s. Having in mind that the roll period is computed as described in paragraph A/2.3.4, 2008 IS Code:

$$T = \frac{2 \cdot C \cdot B}{\sqrt{GM}} \tag{3.58}$$

Where *B* is the molded breadth and *C* is computed as:

$$C = 0.373 + 0.023\frac{B}{d} - 0.043\frac{L_{WL}}{100} \tag{3.59}$$

Where L_{WL} is the waterline length of the ship (m).

Thus, the *KG* meeting the requirement T = 20 s computes as:

$$KG_4 = BM + KB - \frac{C^2 B^2}{100} \tag{3.60}$$

The KG value for further computation can be chosen as:

$$KG = \min(KG_1, KG_2, KG_4) \tag{3.61}$$

However if the chosen KG is less than KG_3, the ship should be excluded from the sample as the applicability ranges of the Weather Criterion cannot be achieved. The result of this formula this also has to be checked for practicality – if such a KG value can be actually obtained for the ship.

Because the KG-value is defined by the conditions of applicability of the Weather Criterion, it can achieve the critical condition of the Weather Criterion. Those critical conditions are frequently achieved by artificially increasing the windage area and height of its center until either area a exactly equals area b, or the angle of heel under steady action of wind exactly equals 16° or 80 % of deck edge immersion, whichever is less.

The choice of the draft, KG value and the windage characteristics together - with the assumption of zero trim - defines all the input data needed for the calculation of the Level 2 vulnerability criteria. The calculation flow follows the description provided in Annex 4 of SDC 4/5/1 with the exception of two elements:

Instead of using the "standard" methodology for the estimation of the effective wave-slope, a direct pressure integration method is used, as described in Annex 10 of SDC 4/INF.4

Instead of using the relative response amplitude operator (RAO), H_{rel}, the absolute RAO, H, is used in the formula 3.3.2.7-2 from Annex 4 of SDC 4/5/1.

The Level 2 vulnerability criteria value, C, is computed as described in paragraph 2.13.3.2.1 of the Annex 1 of IMO document SDC 3/WP.5. Each criterion value, C, represents one point in a further statistical assessment. In addition, the alternative criterion value CA is computed as described in Annex 15 of SDC4 /INF.4/Add.2 with the factor at the standard deviation taken as $n = 3$.

3.7.3 Probabilistic Study: Sample Ships and Results

The total volume of samples is 74 cases, based on 32 ships. Each case represents a loading condition of a ship where the weather criterion is completely applicable. Geometric parameters of the considered cases are given in Table 3.8.

Characteristics of static stability for the cases considered are available from Table 3.9. The parameters included are: the vertical center of gravity KG, estimated period of roll T, metacentric height GM, angle of maximum of the GZ curve (φ_{max}), maximum value of the GZ curve (GZ_{max}), and the angle of vanishing stability φ_v.

Table 3.8. Principal Characteristics of Sample

#	Case description	*LBP*, m	*d*, m	LBP/B	*D*/*d*	B/d	C_B	C_M	C_W
1	C4-class Cargo Ship L1	158.8	9.75	6.9	1.3	2.3	0.59	0.986	0.72
2	C4-class Cargo Ship L2	158.8	8.65	6.9	1.5	2.6	0.58	0.984	0.69
3	C4-class Cargo Ship L3	158.8	7.84	6.9	1.7	2.9	0.57	0.983	0.68
4	Fast Container Ship L1	274.3	10.57	8.5	1.8	3.0	0.54	0.920	0.67
5	Fast Container Ship L2	274.3	9.75	8.5	2.0	3.3	0.53	0.914	0.65
6	Fast Container Ship L3	274.3	9.19	8.5	2.1	3.5	0.52	0.909	0.65
7	RoPax L1	140.4	5.80	6.9	1.4	3.5	0.59	0.925	0.80
8	RoPax L2	140.4	6.30	6.9	1.3	3.2	0.61	0.931	0.82
9	Handysize Bulkcarrier L1	148.9	10.80	6.5	1.4	2.1	0.80	0.990	0.87
10	Handysize Bulkcarrier L2	148.9	7.98	6.5	1.8	2.9	0.77	0.986	0.85
11	Handysize Bulkcarrier L3	148.9	8.37	6.5	1.8	2.8	0.77	0.989	0.85
12	LNG Carrier L1	257.0	12.00	6.2	2.0	3.5	0.78	0.981	0.83
13	LNG Carrier L2	257.0	13.00	6.2	1.8	3.2	0.79	0.983	0.83
14	LNG Carrier L3	257.0	14.00	6.2	1.7	3.0	0.80	0.984	0.84
15	C11-class Container Ship L1	262.0	12.70	6.6	1.9	3.1	0.58	0.963	0.80
16	C11-class Container Ship L2	262.0	12.29	6.6	1.9	3.3	0.58	0.962	0.80
17	C11-class Container Ship (bench.)	262.0	11.50	6.6	2.1	3.5	0.56	0.959	0.77
18	Passenger Ship L1	248.3	10.30	6.9	2.5	3.5	0.72	0.983	0.87
19	Passenger Ship L2	248.3	11.00	6.9	2.4	3.3	0.74	0.984	0.88
20	Cargo Ship L1	121.9	7.00	7.0	1.9	2.5	0.70	0.985	0.79
21	Cargo Ship L2	121.9	8.00	7.0	1.7	2.2	0.71	0.987	0.81
22	Cargo Ship L3	121.9	6.00	7.0	2.2	2.9	0.69	0.983	0.76
23	Bulk carrier L1	280.0	13.50	6.0	1.8	3.5	0.80	0.996	0.87
24	Bulk carrier L2	280.0	14.25	6.0	1.7	3.3	0.80	0.996	0.88
25	Bulk carrier L3	280.0	15.00	6.0	1.6	3.1	0.81	0.996	0.88
26	Old Panamax Container Ship L1	283.2	12.12	8.8	1.5	2.7	0.64	0.949	0.83
27	Old Panamax Container Ship L2	283.2	14.00	8.8	1.3	2.3	0.67	0.956	0.87
28	Old Panamax Container Ship L3	283.2	11.00	8.8	1.7	2.9	0.62	0.944	0.79
29	Old Panamax Container Ship L4	283.2	9.50	8.8	2.0	3.4	0.60	0.935	0.75
30	Large Container Ship L1	330.0	15.13	7.2	1.9	3.0	0.65	0.980	0.84
31	Large Container Ship L2	330.0	14.00	7.2	2.0	3.3	0.64	0.978	0.83
32	Large Container Ship L3	330.0	16.50	7.2	1.7	2.8	0.67	0.981	0.87
33	VLCC L1	320.0	21.08	5.5	1.5	2.8	0.80	0.998	0.88
34	VLCC L2	320.0	16.57	5.5	1.9	3.5	0.78	0.997	0.85
35	VLCC L3	320.0	23.00	5.5	1.3	2.5	0.81	0.998	0.89
36	Large Container Ship L1	326.9	13.15	7.2	1.9	3.5	0.58	0.901	0.77
37	Large Container Ship L2	326.9	15.00	7.2	1.6	3.0	0.61	0.913	0.82

Table 3.8 Principal Characteristics of Sample (continued)

#	Case description	*LBP*, m	*d*, m	LBP/B	D/d	B/d	C_B	C_M	C_W
38	Very Large Container Ship L1	376.0	16.49	6.5	2.3	3.5	0.61	0.950	0.80
39	Very Large Container Ship L2	376.0	18.00	6.5	2.1	3.2	0.63	0.952	0.82
40	Container Ship L1	198.4	10.43	6.7	2.0	2.9	0.60	0.980	0.78
41	Container Ship L2	198.4	8.60	6.7	2.4	3.5	0.57	0.975	0.72
42	Container Ship L3	198.4	12.50	6.7	1.7	2.4	0.64	0.983	0.84
43	ITTC A1 Containership L1	150.0	10.79	5.5	1.3	2.5	0.70	0.967	0.87
44	ITTC A1 Containership L2	150.0	8.00	5.5	1.7	3.4	0.66	0.956	0.77
45	ITTC A1 Containership L3	150.0	9.00	5.5	1.5	3.0	0.67	0.961	0.80
46	Ro-Ro Ship L1	138.4	6.91	5.7	2.6	3.5	0.67	0.990	0.86
47	Cargo Ship L1	206.4	10.00	6.9	1.7	3.0	0.56	0.980	0.67
48	Mid-size Container Ship L1	228.2	10.43	7.7	2.0	2.9	0.60	0.980	0.78
49	Small Cargo Ship L1	79.6	3.94	5.9	2.2	3.5	0.69	0.983	0.77
50	Small Cargo Ship L2	79.6	5.29	5.9	1.6	2.6	0.71	0.987	0.81
51	Mid-size Cargo Ship L1	170.7	9.56	6.7	1.5	2.7	0.58	0.982	0.69
52	Mid-size Cargo Ship L2	170.7	7.24	6.7	2.0	3.5	0.55	0.976	0.64
53	Pod Propelled Containership L1	293.0	10.00	9.8	2.6	3.0	0.52	0.944	0.78
54	Pod Propelled Containership L2	293.0	12.00	9.8	2.1	2.5	0.57	0.953	0.86
55	4000 TEU Container Ship L1	267.5	12.00	8.3	1.8	2.7	0.70	0.966	0.86
56	4000 TEU Container Ship L2	267.5	10.00	8.3	2.1	3.2	0.68	0.959	0.82
57	C10-class Container Ship L1	260.8	12.00	6.6	1.6	3.3	0.57	0.974	0.78
58	C10-class Container Ship L2	260.8	14.00	6.6	1.4	2.8	0.61	0.978	0.84
59	C9-class Container Ship L1	240.7	13.00	7.5	1.5	2.5	0.62	0.952	0.79
60	C9-class Container Ship L2	240.7	10.00	7.5	2.0	3.2	0.58	0.938	0.72
61	C9-class Container Ship L3	240.7	11.50	7.5	1.7	2.8	0.60	0.946	0.76
62	Middle-size Container Ship L1	189.7	9.00	8.0	1.6	2.6	0.75	0.992	0.82
63	Middle-size Container Ship L2	189.7	7.50	8.0	1.9	3.2	0.73	0.991	0.80
64	Intermediate-size Container Ship L1	205.7	10.00	7.1	1.6	2.9	0.61	0.972	0.72
65	Intermediate-size Container Ship L2	205.7	9.00	7.1	1.8	3.2	0.60	0.969	0.70
66	Small-size freighter L1	85.1	5.35	6.4	1.3	2.5	0.73	0.990	0.85
67	Small-size freighter L2	85.1	4.28	6.4	1.7	3.1	0.71	0.987	0.81
68	Mid-size freighter L1	98.7	5.74	6.2	1.7	2.8	0.71	0.987	0.81
69	Mid-size freighter L2	98.7	4.57	6.2	2.1	3.5	0.69	0.984	0.77
70	C2-class Cargo Ship L1	91.8	5.74	5.7	1.7	2.8	0.57	0.980	0.68
71	C2-class Cargo Ship L2	91.8	4.57	5.7	2.1	3.5	0.54	0.975	0.64
72	C3-class Cargo Ship L1	126.5	6.80	6.2	2.1	3.0	0.54	0.975	0.64
73	3000 TEU Container Ship L1	228.2	8.60	7.7	2.4	3.5	0.57	0.975	0.72
74	3000 TEU Container Ship L2	228.2	12.50	7.7	1.7	2.4	0.64	0.983	0.84

Table 3.9. Stability Characteristics of Sample

#	Case description	*KG*/*d* - 1	*T*, s	*GM*, m	φ_{max}, deg	GZ_{max}, m	φ_v, deg
1	C4-class Cargo Ship L1	-0.12	16.2	1.02	26	0.42	56
2	C4-class Cargo Ship L2	-0.05	16.0	1.09	26	0.44	57
3	C4-class Cargo Ship L3	0.03	15.9	1.15	26	0.45	58
4	Fast Container Ship L1	0.19	20.0	1.09	46	1.35	78
5	Fast Container Ship L2	0.29	20.0	1.13	46	1.38	79
6	Fast Container Ship L3	0.38	20.0	1.16	46	1.40	79
7	RoPax L1	0.50	12.7	1.58	73	2.00	129
8	RoPax L2	0.50	20.0	0.61	72	1.07	108
9	Handysize Bulkcarrier L1	-0.16	20.0	0.68	42	0.67	69
10	Handysize Bulkcarrier L2	0.10	20.0	0.75	42	0.70	70
11	Handysize Bulkcarrier L3	0.04	20.0	0.74	42	0.71	71
12	LNG Carrier L1	0.36	20.0	2.04	38	2.11	63
13	LNG Carrier L2	0.23	20.0	1.96	38	2.07	63
14	LNG Carrier L3	0.13	20.0	1.90	38	2.03	62
15	C11-class Container Ship L1	0.46	20.0	1.77	42	1.34	65
16	C11-class Container Ship L2	0.50	19.0	2.00	42	1.38	65
17	C11-class Container Ship (bench.)	0.50	15.6	3.06	44	2.23	76
18	Passenger Ship L1	0.50	16.1	2.39	36	1.40	74
19	Passenger Ship L2	0.45	20.0	1.51	32	0.91	66
20	Cargo Ship L1	-0.06	20.0	0.43	56	1.23	110
21	Cargo Ship L2	-0.15	20.0	0.42	56	1.21	110
22	Cargo Ship L3	0.09	20.0	0.45	56	1.25	111
23	Bulkcarrier L1	0.16	15.1	4.31	26	1.63	59
24	Bulkcarrier L2	0.09	14.9	4.31	26	1.63	59
25	Bulkcarrier L3	0.02	14.7	4.31	26	1.63	59
26	Old Panamax Container Ship L1	0.14	20.0	1.01	41	1.24	68
27	Old Panamax Container Ship L2	0.01	20.0	0.96	41	1.20	67
28	Old Panamax Container Ship L3	0.24	20.0	1.05	41	1.26	68
29	Old Panamax Container Ship L4	0.43	20.0	1.12	42	1.31	69
30	Large Container Ship L1	0.31	20.0	1.88	41	1.89	65
31	Large Container Ship L2	0.43	20.0	1.95	41	1.93	66
32	Large Container Ship L3	0.20	20.0	1.81	41	1.84	65
33	VLCC L1	-0.01	20.0	3.00	28	1.54	53
34	VLCC L2	0.29	20.0	3.36	29	1.71	55
35	VLCC L3	-0.09	20.0	2.90	28	1.49	52
36	Large Container Ship L1	0.50	17.9	2.53	34	1.68	54
37	Large Container Ship L2	0.35	20.0	1.90	34	1.33	50

Table 3.9 Stability Characteristics of Sample (continued)

#	Case description	*KG*/*d* - 1	*T*, s	*GM*, m	φ_{max}, deg	GZ_{max}, m	φ_v, deg
38	Very Large Container Ship L1	0.46	20.0	2.82	49	3.15	78
39	Very Large Container Ship L2	0.33	20.0	2.69	49	3.05	77
40	Container Ship L1	0.20	20.0	1.11	51	1.88	89
41	Container Ship L2	0.41	20.0	1.20	51	1.95	90
42	Container Ship L3	0.04	20.0	1.04	51	1.83	88
43	ITTC A1 Containership L1	0.02	20.0	0.99	34	0.88	55
44	ITTC A1 Containership L2	0.32	20.0	1.11	34	0.94	56
45	ITTC A1 Containership L3	0.17	20.0	1.06	34	0.91	56
46	Ro-Ro Ship L1	0.50	12.9	2.18	31	0.85	72
47	Cargo Ship L1	0.06	18.2	1.33	26	0.55	57
48	Mid-size Container Ship L1	0.21	20.0	1.03	51	1.82	88
49	Small Cargo Ship L1	0.35	20.0	0.32	43	0.63	74
50	Small Cargo Ship L2	-0.01	20.0	0.29	43	0.61	73
51	Mid-size Cargo Ship L1	-0.04	17.2	1.13	26	0.47	57
52	Mid-size Cargo Ship L2	0.25	18.1	1.13	26	0.46	57
53	Pod Propelled Containership L1	0.43	20.0	0.90	66	1.72	100
54	Pod Propelled Containership L2	0.21	20.0	0.83	66	1.66	99
55	4000 TEU Container Ship L1	0.12	20.0	1.06	40	1.24	66
56	4000 TEU Container Ship L2	0.35	20.0	1.15	40	1.29	67
57	C10-class Container Ship L1	0.44	20.0	1.76	40	1.66	64
58	C10-class Container Ship L2	0.26	20.0	1.65	40	1.59	63
59	C9-class Container Ship L1	0.02	20.0	1.11	48	1.67	80
60	C9-class Container Ship L2	0.28	20.0	1.23	48	1.76	81
61	C9-class Container Ship L3	0.13	20.0	1.16	48	1.71	81
62	Middle-size Container Ship L1	-0.01	20.0	0.70	40	1.02	68
63	Middle-size Container Ship L2	0.20	20.0	0.75	40	1.05	69
64	Intermediate-size Container Ship L1	0.10	20.0	1.03	38	0.98	66
65	Intermediate-size Container Ship L2	0.21	20.0	1.08	38	1.01	66
66	Small-size freighter L1	-0.01	20.0	0.28	34	0.42	54
67	Small-size freighter L2	0.23	20.0	0.30	34	0.43	54
68	Mid-size freighter L1	0.07	20.0	0.40	39	0.66	66
69	Mid-size freighter L2	0.37	20.0	0.43	39	0.68	66
70	C2-class Cargo Ship L1	0.03	17.4	0.53	26	0.24	55
71	C2-class Cargo Ship L2	0.28	18.1	0.54	26	0.24	55
72	C3-class Cargo Ship L1	0.08	20.0	0.63	33	0.37	87
73	3000 TEU Container Ship L1	0.42	20.0	1.12	51	1.88	89
74	3000 TEU Container Ship L2	0.05	20.0	0.97	51	1.77	87

As seen in Table 3.8 and Table 3.9, the Weather Criterion is completely applicable to all the considered cases. However, vulnerability criterion Level 2 includes calculations of the standard deviation of roll angles. These calculations use linearization of the GZ curve at the static heel angle. Thus, moderate motions and cases limit applicability of the level 2 calculations where the roll motions are too large then need to be excluded from further consideration.

Calculations of the Level 2 criterion *C* value as well as alterative *CA* value (Subsection 3.6), involves weight averaging over the wave scatter table. As the scatter table is a long-term average, moderate sea states have more statistical weight compared to high sea states, despite the fact that high sea states are the most dangerous. High sea states also represent conditions where large roll motions are likely. To account for these arguments properly, the criterion of applicability of the linear roll motion calculations should involve averaging over the high sea states rather than over all seas states in the wave scatter diagram.

The definition of a high sea state in this context is related to the wind pressure used in the weather criterion. As described in paragraph A/2.3.4, 2008 IS Code, the wind pressure is equal to P = 504 Pa. The formula (3.48) relates the significant wave height to the mean wind speed:

$$U = 6.05178\sqrt[3]{H_S^2} \tag{3.62}$$

Thus, mean wind pressure can be also related to significant wave height, H_S:

$$P = 3.02189 \cdot \rho_A \cdot \sqrt[3]{H_S^2} \tag{3.63}$$

Where ρ_A = 1.222 kg/m^3 is air density. The significant wave height corresponding to the wind pressure used in the weather criterion is:

$$H_S = 0.11297\sqrt[4]{\left(\frac{P}{\rho_A}\right)^3} = 10.34\,m \tag{3.64}$$

The wind pressures exceeding P = 504 Pa correspond to rows 11 through 17 (HS of 10.5m through 16.5 m) of the scatter table in IACS Recommendation 34. Thus, all sea states identified in these lines are assumed as "high sea states" for the purpose of this analysis.

Weight-averaged static angle φ_{SW}, corresponding to high sea states is computed as:

$$\varphi_{SW} = \frac{\sum_{i=h}^{NHs}\sum_{j=1}^{NTz} W_{i,j}\varphi_S(Hs_i, Tz_j)}{\sum_{i=h}^{NHs}\sum_{j=1}^{NTz} W_{i,j}} \tag{3.65}$$

Where $\varphi_S(Hs_i,Tz_j)$ is a static heel angle computed as described in the section 4.3 of Annex 3 of SDC.6/WP.6 for each significant wave height H_S and a zero-crossing mean period Tz.; W_{ij} is the weight of the sea state defined by the rows i and column j of the standard scatter table of IACS Recommendation 34. The unit, h, is the initial index for significant wave height corresponding to high seas states, h = 11, NHs and NT_Z and the number of rows and columns in scatter table, respectively.

The Weight-averaged standard deviation σ_{RW}, which corresponds to high sea states, is computed as:

$$\sigma_{RW} = \frac{\sum_{i=h}^{NHs}\sum_{j=1}^{NTz} W_{i,j}\sigma_R(Hs_i, Tz_j)}{\sum_{i=h}^{NHs}\sum_{j=1}^{NTz} W_{i,j}} \tag{3.66}$$

Where $\sigma_R(Hs_i, Tz_j)$ is a standard deviation computed with equation (3.49). The criterion of applicability is proposed in the following form:

$$\varphi_{SW} + k \cdot \sigma_{RW} < \varphi_{\max} \tag{3.67}$$

Where k is a factor, defining how strictly the assumption of linearity is supported, φ_{max} is the angle of maximum of GZ curve, available from Table 3.9. Each value of k corresponds to a percentage of time when linearity is approximately satisfied:

$$Pt = Q_N(k) \tag{3.68}$$

Where Q_N is the k-quantile of standard normal distribution (k = 1 corresponds to 84 %, k = 1.25 corresponds to 90 %, and k = 1.5 corresponds to 93 %).

The criterion value C and alternative criterion value CA are placed into Table 3.10 along with the values of static angle σ_{SW} and roll standard deviation σ_{RW}, which are weight-averaged over the high sea states.

3.7.4 Probabilistic Study: Limitations of Linear Calculations

Prior to further processing, the assumption of linear roll motion calculations must be supported by excluding the cases where roll motion is too large to for the linear assumption to be valid. The exclusion is carried out with the criterion formulated in paragraph 4.8 and illustrated in Figure 3.33 for the factor k = 1.0. Cases, where the applicability criterion takes negative values, are not included in further processing, leaving 70 out of 74 cases

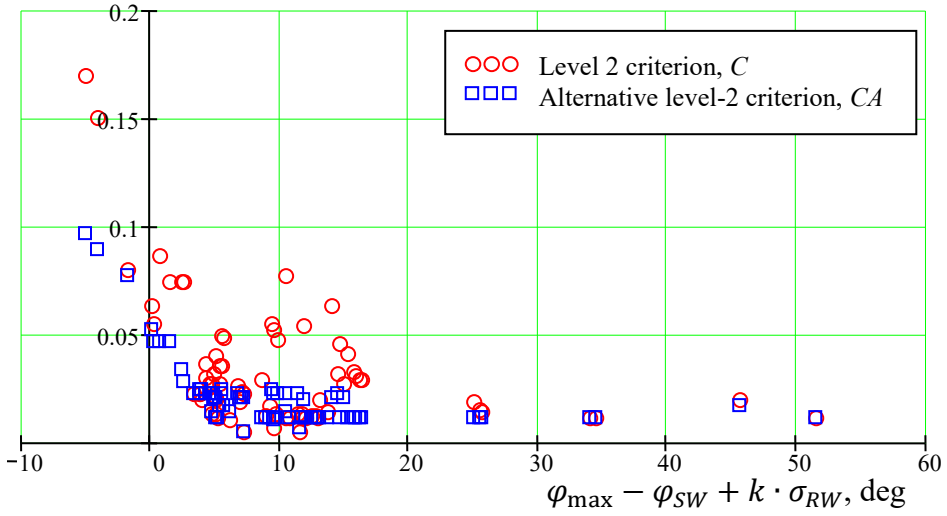

Figure 3.33. Application of Linear Roll Assumption

Table 3.10. Results of Calculation

#	Case description	φ_{SW}, deg	σ_{SW}, deg	C	CA
1	C4-class Cargo Ship L1	10	9	0.0188	0.0204
2	C4-class Cargo Ship L2	11	10	0.0203	0.0204
3	C4-class Cargo Ship L3	11	10	0.0216	0.0231
4	Fast Container Ship L1	20	16	0.0478	0.0231
5	Fast Container Ship L2	20	16	0.0527	0.0231
6	Fast Container Ship L3	20	17	0.0553	0.0241
7	RoPax L1	15	13	0.0201	0.0172
8	RoPax L2	12	9	0.0112	0.0112
9	Handysize Bulkcarrier L1	20	10	0.0123	0.0112
10	Handysize Bulkcarrier L2	20	10	0.0122	0.0112
11	Handysize Bulkcarrier L3	20	10	0.0118	0.0112
12	LNG Carrier L1	20	14	0.0368	0.0231
13	LNG Carrier L2	20	13	0.0315	0.0206
14	LNG Carrier L3	20	13	0.0269	0.0167
15	C11-class Container Ship L1	21	10	0.0115	0.0112
16	C11-class Container Ship L2	21	10	0.0118	0.0141
17	C11-class Container Ship (bench.)	21	11	0.0138	0.0231
18	Passenger Ship L1	18	9	0.0067	0.0108
19	Passenger Ship L2	17	8	0.0047	0.0049
20	Cargo Ship L1	19	11	0.0157	0.0112
21	Cargo Ship L2	19	12	0.0189	0.0112
22	Cargo Ship L3	19	11	0.0140	0.0112
23	Bulkcarrier L1	10	12	0.0305	0.0231
24	Bulkcarrier L2	10	11	0.0276	0.0230
25	Bulkcarrier L3	10	11	0.0272	0.0227
26	Old Panamax Container Ship L1	20	16	0.0357	0.0170
27	Old Panamax Container Ship L2	17	16	0.0289	0.0112
28	Old Panamax Container Ship L3	20	16	0.0406	0.0206
29	Old Panamax Container Ship L4	20	17	0.0498	0.0231
30	Large Container Ship L1	20	14	0.0239	0.0206
31	Large Container Ship L2	20	14	0.0260	0.0231
32	Large Container Ship L3	20	14	0.0226	0.0206
33	VLCC L1	14	10	0.0134	0.0141
34	VLCC L2	14	11	0.0201	0.0241
35	VLCC L3	14	9	0.0119	0.0115
36	Large Container Ship L1	19	10	0.0133	0.0206
37	Large Container Ship L2	18	10	0.0109	0.0141

Table 3.10. Results of Calculation (Continued)

#	Case Description	φSW, °	σSW, °	C	CA
38	Very Large Container Ship L1	20	14	0.0318	0.0231
39	Very Large Container Ship L2	20	14	0.0271	0.0206
40	Container Ship L1	20	15	0.0327	0.0112
41	Container Ship L2	20	16	0.0458	0.0112
42	Container Ship L3	20	15	0.0314	0.0112
43	ITTC A1 Containership L1	11	17	0.0489	0.0170
44	ITTC A1 Containership L2	19	20	0.1701	0.0964
45	ITTC A1 Containership L3	18	20	0.1501	0.0895
46	Ro-Ro Ship L1	11	9	0.0053	0.0065
47	Cargo Ship L1	12	14	0.0547	0.0469
48	Mid-size Container Ship L1	20	15	0.0294	0.0112
49	Small Cargo Ship L1	19	10	0.0140	0.0112
50	Small Cargo Ship L2	19	11	0.0202	0.0112
51	Mid-size Cargo Ship L1	11	15	0.0631	0.0521
52	Mid-size Cargo Ship L2	12	16	0.0800	0.0769
53	Pod Propelled Containership L1	21	12	0.0114	0.0112
54	Pod Propelled Containership L2	20	11	0.0113	0.0112
55	4000 TEU Container Ship L1	20	18	0.0749	0.0285
56	4000 TEU Container Ship L2	20	18	0.0746	0.0339
57	C10-class Container Ship L1	20	14	0.0353	0.0243
58	C10-class Container Ship L2	16	12	0.0130	0.0112
59	C9-class Container Ship L1	20	16	0.0546	0.0202
60	C9-class Container Ship L2	20	18	0.0774	0.0231
61	C9-class Container Ship L3	18	16	0.0632	0.0205
62	Middle-size Container Ship L1	19	9	0.0113	0.0112
63	Middle-size Container Ship L2	19	9	0.0112	0.0112
64	Intermediate-size Container Ship L1	20	17	0.0742	0.0469
65	Intermediate-size Container Ship L2	20	18	0.0863	0.0469
66	Small-size freighter L1	15	10	0.0128	0.0112
67	Small-size freighter L2	19	10	0.0204	0.0112
68	Mid-size freighter L1	19	11	0.0175	0.0112
69	Mid-size freighter L2	19	10	0.0131	0.0112
70	C2-class Cargo Ship L1	12	10	0.0229	0.0231
71	C2-class Cargo Ship L2	13	10	0.0226	0.0231
72	C3-class Cargo Ship L1	18	11	0.0231	0.0241
73	3000 TEU Container Ship L1	20	16	0.0410	0.0112
74	3000 TEU Container Ship L2	20	15	0.0289	0.0112

3.7.5 Probabilistic Study: Correction for Ship Length Distribution

The distribution of length (which is related to the size of ship) of the available ship sample is not necessarily the same as that of the world fleet. To make the present calculations representative of the world fleet, the criterion values are weighted to reproduce a distribution of ship lengths of the world fleet covered by IMO instruments. Figure 3.34 shows distributions (in a form of histograms) of lengths (*LBP*) of the sample ships (bars) and the world fleet covered by IMO instruments (solid bars). The latter distribution is based on data obtained from the USCG Marine Information for Safety and Law Enforcement (MISLE) system (some of this information is publically available through the USCG Maritime Information Exchange: https://cgmix.uscg.mil).

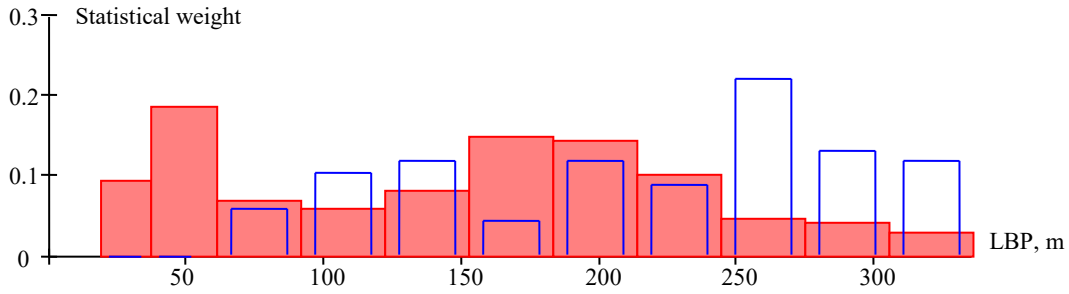

Figure 3.34. Distribution of Ship Lengths in the Sample (Transparent Bars) and in the World Fleet Covered by IMO Instruments (Solid Bars)

A correction for the ship length distribution is carried out with the following weighting function:

$$W(L) = Kn\frac{W_F(L)}{W_S(L)} \tag{3.69}$$

Where W_F is the statistical weights the fleet covered by IMO instruments (Figure 3.34, solid bars); W_S is the statistical weight of the presented sample, Kn is the normalizing coefficient.

3.7.6 Probabilistic Study: Distribution of Criteria Values

The histogram for the criterion values C is in Figure 3.35, while the histogram for alternative criterion values CA is in Figure 3.36 Solid bars are used for the original data, taken from Table 3.10, after the inapplicable cases were removed as described in paragraph 3.7.4. The transparent bars are used for the corrected data, weighted for ship length, as described in paragraph 3.7.5.

The most prominent feature of the histogram in Figure 3.36 is the bar around the criterion value $CA = 0.011$, which includes 26 cases. These are the cases where the static angle was the limiting value rather than the ratio of area b to area a. These cases are not random and will be processed separately for the distribution fit.

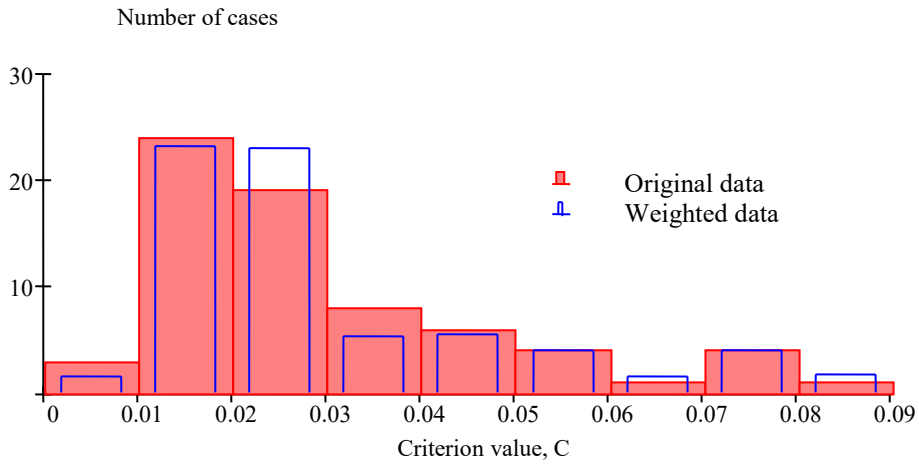

Figure 3.35. Distribution of the Criterion Value C Based on Original (Solid Bars) and Weighted Data (Transparent Bars)

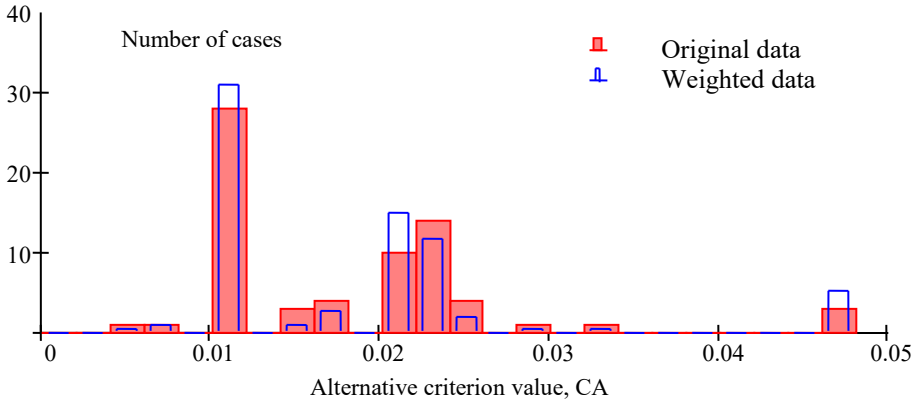

Figure 3.36. Distribution of the Alternative Criterion Value CA Based on Original (Solid Bars) and Weighted Data (Transparent Bars)

3.7.7 Probabilistic Study: Estimates of Mean and Standard Deviation

The mean values of both criteria are estimated as:

$$\hat{E}_C = \sum_{i=1}^{n} W_{Li} C_i \;\; ; \;\; \hat{E}_{CA} = \sum_{i=1}^{n} W_{Li} CA_i \tag{3.70}$$

The standard deviations for both criteria are estimated as:

$$\hat{\sigma}_C = \sqrt{\sum_{i=1}^{n} W_{Li} \left(C_i - \hat{E}_C \right)^2} \;\; ; \;\; \hat{\sigma}_{CA} = \sqrt{\sum_{i=1}^{n} W_{Li} \left(CA_i - \hat{E}_{CA} \right)^2} \tag{3.71}$$

The numerical values for the mean and standard deviation estimates are in Table 3.11 together with their respective confidence intervals computed for a 95 % confidence level, see the Appendix for the description of the computation of confidence interval.

Table 3.11. Estimates of Mean Values and Standard Deviations of the Criterion Values

	Mean value estimate			Estimate of standard deviation		
	Value	Upper Boundary	Lower Boundary	Value	Upper Boundary	Lower Boundary
Criterion, *C*	0.029	0.034	0.025	0.02	0.025	0.017
Alternative criterion, *CA*	0.024	0.027	0.021	0.00967	0.0132	0.00762

The data presented in Table 3.11 shows that the standard deviation estimate of the alternative criterion *CA* is significantly smaller than that of *C* (about twice as small), which indicates that the alternative criterion is "less random," and therefore less prone to inconsistency.

3.7.7 Probabilistic Study: Fitting the Distribution

To set the standard corresponding to the acceptable probability of inconsistency, a theoretical distribution is fitted to the data. The asymmetric character of the distribution is in Figure 3.35. Once the deterministic values of *CA* at 0.011 are removed from the histogram in Figure 3.36 , the distribution may be characterized as asymmetric as well.

A lognormal distribution is used to fit to the data. Its probability density function is expressed as:

$$PDF(x) = \frac{1}{x \cdot s\sqrt{2\pi}} \cdot \exp\left(-\frac{\left(\ln(x) - \mu\right)^2}{2s^2} \right) \tag{3.72}$$

Where symbols μ and *s* stand for location and scale parameters of the lognormal distribution, respectively. Theses parameters can be estimated through the mean value and standard deviation:

$$\hat{\mu}_C = \ln\left(\hat{E}_C \sqrt{1 + \frac{\hat{\sigma}_C^2}{\hat{E}_C^2}} \right); \quad \hat{\mu}_{CA} = \ln\left(\hat{E}_{CA} \sqrt{1 + \frac{\hat{\sigma}_{CA}^2}{\hat{E}_{CA}^2}} \right) \tag{3.73}$$

$$\hat{s}_C = \sqrt{\ln\left(1 + \frac{\hat{\sigma}_C^2}{\hat{E}_C^2} \right)}; \qquad \hat{s}_{CA} = \sqrt{\ln\left(1 + \frac{\hat{\sigma}_{CA}^2}{\hat{E}_{CA}^2} \right)} \tag{3.74}$$

Where $\hat{\mu}_C$ and $\hat{s}_C$ are the location and scale parameters estimated for the criterion value *C* and $\hat{\mu}_{CA}$ and $\hat{s}_{CA}$ are the location and scale parameters estimated for the alternative criterion value *CA*.

Q-Q plots visually evaluate how satisfactory the fit is, where points represent the data, and the line represents the fitted theoretical distribution. If the fit is ideal, the points appear on the line. Figure 3.37 shows the Q-Q plot for the criterion value *C*, while the Q-Q plot for the alternative criterion *CA* is in Figure 3.38.

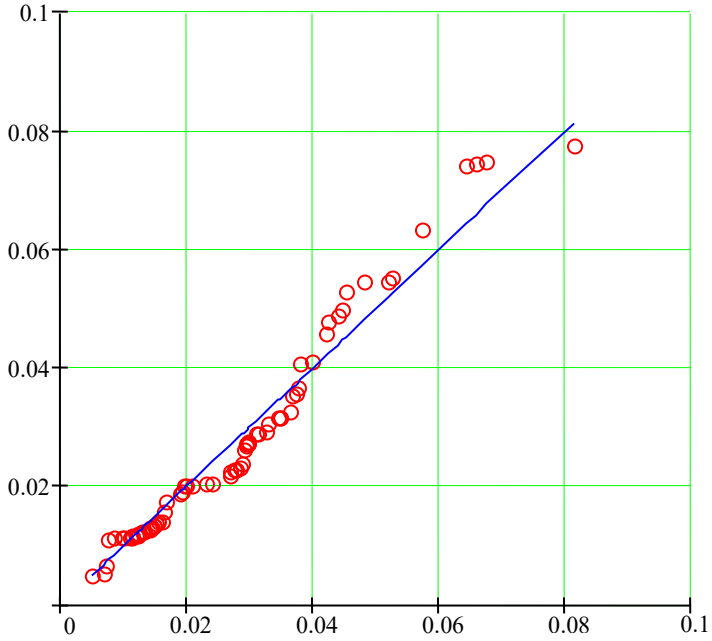

Figure 3.37. Q-Q Plot for the Criterion Value C

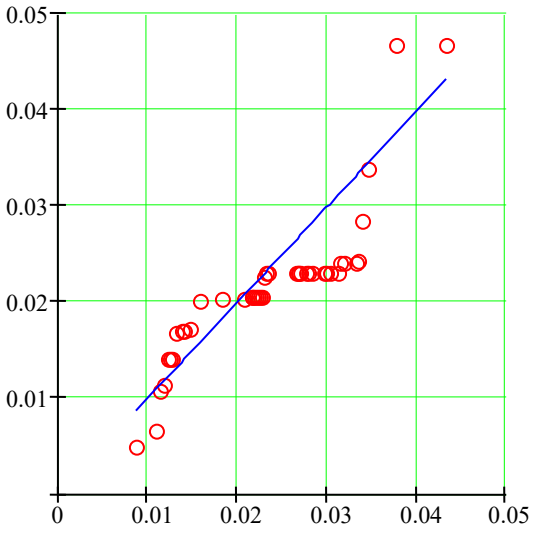

Figure 3.38. Q-Q Plot for the Alternative Criterion Value CA

The criterion value *C* in Figure 3.37 shows a better fit when compared to the alterative criterion *CA* in Figure 3.38. This outcome is partially explained by understanding that the number of points included for the alternative criterion was reduced from 70 to 44 after the deterministic values were removed as described in paragraph 3.7.6.

3.7.8 Probabilistic Study: Possible Standard Values

Given the probability of inconsistency P_C, a possible standard for the criterion C is computed as:

$$St = \exp\left(Q_N(P_C, \hat{E}_C, \hat{\sigma}_C)\right) \tag{3.75}$$

Where Q_N is a normal quintile corresponding to P_C

A possible standard for the alternative criterion CA is computed taking into account that some cases yield a deterministic value:

$$St_A = W_R \exp\left(Q_N(P_C, \hat{E}_{CA}, \hat{\sigma}_{CA})\right) + W_D St_D \tag{3.76}$$

Where $W_R = 44/70 = 0.567$ is the weight of the random values of CA, $W_D = 26/70 = 0.433$ is the weight of deterministic values of CA, $St_D = 0.011$ is the deterministic value of CA corresponding to the cases in which the static angle is the limiting factor.

Possible standards have been computed for a number of probabilities of inconsistency, see Table 3.12 through Table 3.16, computed for different factor *k,* the confidence probability was 95 %, and the description of computation of the confidence interval is given in the Appendix.

Increase of factor *k* makes the application of assumption of roll motion linearity stricter; as a result, less data points are available, which increases the confidence interval. On the other hand, the available data points became more consistent – this decreases the confidence interval. The choice of the factor *k* can be solved based on optimization strategy, whatever gives the smallest confidence interval. Figure 3.39 shows how the inconsistency (expressed through standard deviation of the criterion value) changes with the increase of *k*-factor. As the change is substantial and almost monotonic, the *k*-factor can be used as a parameter to control the inconsistency. The bars presented for each *k*-factor show the boundaries of the confidence interval.

Table 3.12. Possible Standards for the Level 2 Vulnerability Criterion (Factor k = 0.0)

Accepted Probability of Inconsistency	Standard for Level 2 Vulnerability Criterion				Standard for Alternative Level 2 Vulnerability Criterion			
	Standard	Lower Boundary	Upper Boundary	Relative Uncertainty	Standard	Lower Boundary	Upper Boundary	Relative Uncertainty
1E-10	1.0000	0.7963	1.0000	-	0.6786	0.2789	3.0142	4.0307
0.0050	0.1758	0.1303	0.2724	0.8080	0.0777	0.0610	0.1107	0.6399
0.0100	0.1476	0.1108	0.2197	0.7378	0.0677	0.0539	0.0925	0.5706
0.0200	0.1218	0.0928	0.1742	0.6676	0.0584	0.0471	0.0773	0.5175
0.0300	0.1079	0.0830	0.1503	0.6243	0.0532	0.0433	0.0691	0.4845
0.0400	0.0985	0.0762	0.1346	0.5923	0.0497	0.0407	0.0635	0.4601
0.0500	0.0914	0.0712	0.1230	0.5666	0.0470	0.0387	0.0593	0.4404
0.0600	0.0858	0.0671	0.1139	0.5450	0.0448	0.0370	0.0560	0.4238
0.0700	0.0812	0.0637	0.1065	0.5262	0.0430	0.0357	0.0533	0.4094
0.1000	0.0708	0.0562	0.0902	0.4807	0.0388	0.0326	0.0471	0.3746

Table 3.13. Possible Standards for the Level 2 Vulnerability Criterion (factor k = 1.0)

Accepted Probability of Inconsistency	Standard for Level 2 Vulnerability Criterion				Standard for Alternative Level 2 Vulnerability Criterion			
	Standard	Lower Boundary	Upper Boundary	Relative Uncertainty	Standard	Lower Boundary	Upper Boundary	Relative Uncertainty
1E-10	1.000	0.5828	1.000	N/A	0.1347	0.0791	0.3871	2.2861
0.0050	0.1184	0.0990	0.1496	0.4275	0.0380	0.0313	0.0513	0.5241
0.0100	0.1016	0.0850	0.1254	0.3974	0.0352	0.0294	0.0461	0.4750
0.0200	0.0859	0.0720	0.1049	0.3828	0.0324	0.0274	0.0411	0.4230
0.0300	0.0773	0.0649	0.0937	0.3736	0.0307	0.0263	0.0383	0.3909
0.0400	0.0713	0.0599	0.0861	0.3667	0.0295	0.0254	0.0363	0.3673
0.0500	0.0669	0.0562	0.0803	0.3611	0.0286	0.0248	0.0347	0.3483
0.0600	0.0633	0.0532	0.0757	0.3564	0.0278	0.0242	0.0335	0.3325
0.0700	0.0603	0.0507	0.0719	0.3523	0.0272	0.0238	0.0324	0.3187
0.1000	0.0535	0.0450	0.0633	0.3421	0.0257	0.0227	0.0300	0.2855

Table 3.14. Possible Standards for the Level 2 Vulnerability Criterion (Factor k = 1.15)

Accepted Probability of Inconsistency	Standard for Level 2 Vulnerability Criterion				Standard for Alternative Level 2 Vulnerability Criterion			
	Standard	Lower Boundary	Upper Boundary	Relative Uncertainty	Standard	Lower Boundary	Upper Boundary	Relative Uncertainty
1E-10	0.7404	0.3705	1.0000	-	0.0384	0.0337	0.0474	0.3575
0.0050	0.0913	0.0753	0.1171	0.4571	0.0217	0.0200	0.0237	0.1682
0.0100	0.0796	0.0659	0.0998	0.4258	0.0209	0.0194	0.0228	0.1602
0.0200	0.0684	0.0570	0.0846	0.4039	0.0202	0.0188	0.0218	0.1515
0.0300	0.0622	0.0520	0.0762	0.3901	0.0197	0.0184	0.0212	0.1461
0.0400	0.0579	0.0485	0.0704	0.3797	0.0194	0.0181	0.0208	0.1421
0.0500	0.0546	0.0458	0.0661	0.3714	0.0191	0.0179	0.0205	0.1388
0.0600	0.0519	0.0436	0.0626	0.3643	0.0189	0.0177	0.0202	0.1361
0.0700	0.0497	0.0418	0.0596	0.3581	0.0187	0.0175	0.0200	0.1337
0.1000	0.0447	0.0377	0.0530	0.3429	0.0182	0.0171	0.0194	0.1279

Figure 3.40 through Figure 3.47 show the influence of the *k*-factor on the possible standard for different values of the probability of inconsistency. The results, shown in each figure, assume a different probability of inconsistency from which possible standard values are determined. Figure 3.40 assumes an extremely low probability (10^{-10} – practically zero) and the subsequent figures assume increasing probabilities of inconsistency (In Figure 3.47, the probability of inconsistency is 0.07)

Table 3.15. Possible Standards for the Level 2 Vulnerability Criterion (Factor k = 1.25)

Accepted Probability of Inconsistency	**Standard for Level 2 Vulnerability Criterion**				**Standard for Alternative Level 2 Vulnerability Criterion**			
	Standard	**Lower Boundary**	**Upper Boundary**	**Relative Uncertainty**	**Standard**	**Lower Boundary**	**Upper Boundary**	**Relative Uncertainty**
1E-10	0.7404	0.3683	1.000	-	0.0384	0.0337	0.0474	0.3575
0.0050	0.0913	0.0752	0.1176	0.4647	0.0217	0.0200	0.0237	0.1682
0.0100	0.0796	0.0658	0.1002	0.4321	0.0209	0.0194	0.0228	0.1602
0.0200	0.0684	0.0569	0.0849	0.4091	0.0202	0.0188	0.0218	0.1515
0.0300	0.0622	0.0519	0.0764	0.3946	0.0197	0.0184	0.0212	0.1461
0.0400	0.0579	0.0484	0.0706	0.3838	0.0194	0.0181	0.0208	0.1421
0.0500	0.0546	0.0457	0.0662	0.3751	0.0191	0.0179	0.0205	0.1388
0.0600	0.0519	0.0436	0.0627	0.3677	0.0189	0.0177	0.0202	0.1361
0.0700	0.0497	0.0418	0.0597	0.3612	0.0187	0.0175	0.0200	0.1337
0.1000	0.0447	0.0377	0.0531	0.3454	0.0182	0.0171	0.0194	0.1279

Table 3.16. Possible Standards for the Level 2 Vulnerability Criterion (factor k=1.25)

Accepted Probability of Inconsistency	Standard for Level 2 Vulnerability Criterion				Standard for Alternative Level 2 Vulnerability Criterion			
	Standard	Lower Boundary	Upper Boundary	Relative Uncertainty	Standard	Lower Boundary	Upper Boundary	Relative Uncertainty
1E-10	0.9085	0.3640	4.0879	4.0990	0.0374	0.0322	0.0474	0.4064
0.0050	0.0926	0.0733	0.1281	0.5915	0.0200	0.0186	0.0217	0.1578
0.0100	0.0797	0.0630	0.1067	0.5478	0.0193	0.0180	0.0208	0.1496
0.0200	0.0676	0.0534	0.0891	0.5278	0.0185	0.0173	0.0199	0.1408
0.0300	0.0609	0.0481	0.0795	0.5153	0.0181	0.0169	0.0194	0.1353
0.0400	0.0563	0.0444	0.0729	0.5060	0.0177	0.0167	0.0190	0.1313
0.0500	0.0528	0.0417	0.0680	0.4984	0.0175	0.0164	0.0187	0.1280
0.0600	0.0500	0.0394	0.0641	0.4920	0.0173	0.0163	0.0184	0.1253
0.0700	0.0477	0.0376	0.0608	0.4865	0.0171	0.0161	0.0182	0.1229
0.1000	0.0424	0.0334	0.0535	0.4729	0.0167	0.0157	0.0177	0.1171

Figure 3.40 through Figure 3.47 show that the possible standard value also decreases with the increase of the *k*-factor as the inconsistency decreases. However, the decrease of inconsistency by the increase of the *k*-factor has an added difficulty, as the application of the criteria may be limited. The limitation of applicability, however may not be too restrictive as it applies for the rather artificial condition where the weather criterion is at one of its limits, but still applicable. Table 3.17 shows data for the cases that are excluded for the *k*-factor 1.0 (shaded) and 1.2 (the whole table).

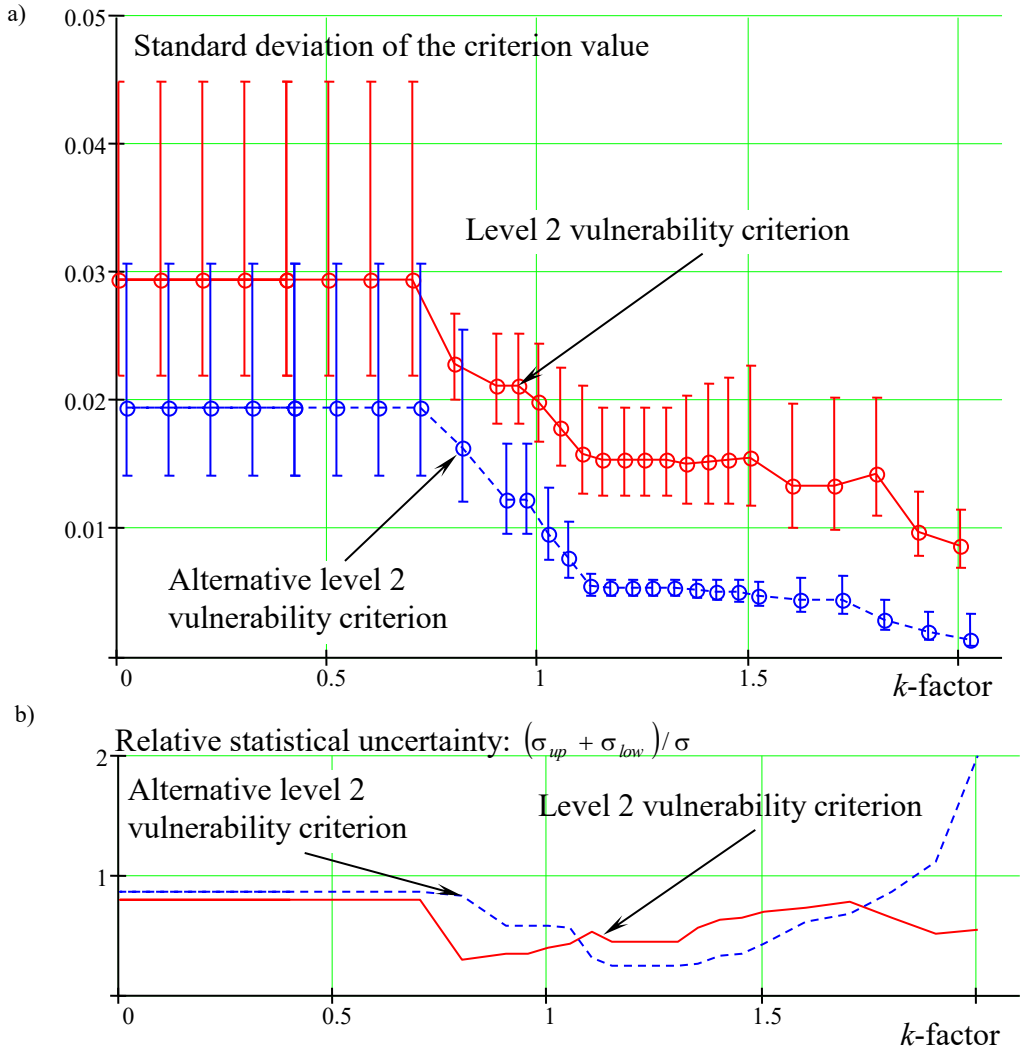

Figure 3.39. Inconsistency vs. *k*-Factor: a) Standard Deviation of Criterion Value; b) Relative Statistical Uncertainty of the Standard Deviation Estimate

Table 3.17. Excluded Cases the k-Factor 1.0 (Shaded) and 1.2 (the Whole Table)

#	Case description	φ_{max}, deg	φ_{SW}, deg	σ_{SW}, deg	C	CA
44	ITTC A1 Containership L2	34	19	20	0.1701	0.0964
45	ITTC A1 Containership L3	34	18	20	0.1501	0.0895
47	Cargo Ship L1	26	12	14	0.0547	0.0469
51	Mid-size Cargo Ship L1	26	11	15	0.0631	0.0521
52	Mid-size Cargo Ship L2	26	12	16	0.0800	0.0769
55	4000 TEU Conatiner Ship L1	40	20	18	0.0749	0.0285
56	4000 TEU Conatiner Ship L2	40	20	18	0.0746	0.0339
64	Intermediate-size Container Ship L1	38	20	17	0.0742	0.0469
65	Intermediate-size Container Ship L2	38	20	18	0.0863	0.0469

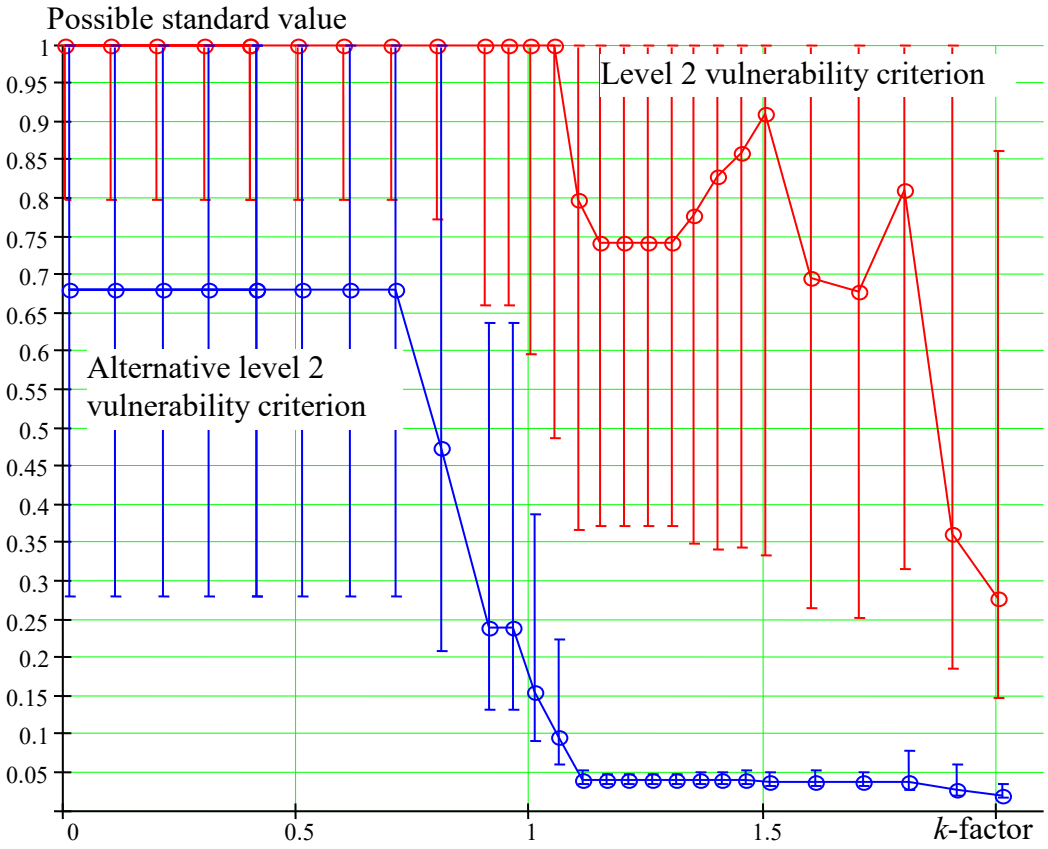

Figure 3.40. Possible Standard vs. *k*-Factor: No Inconsistency Accepted (Probability 10^{-10})

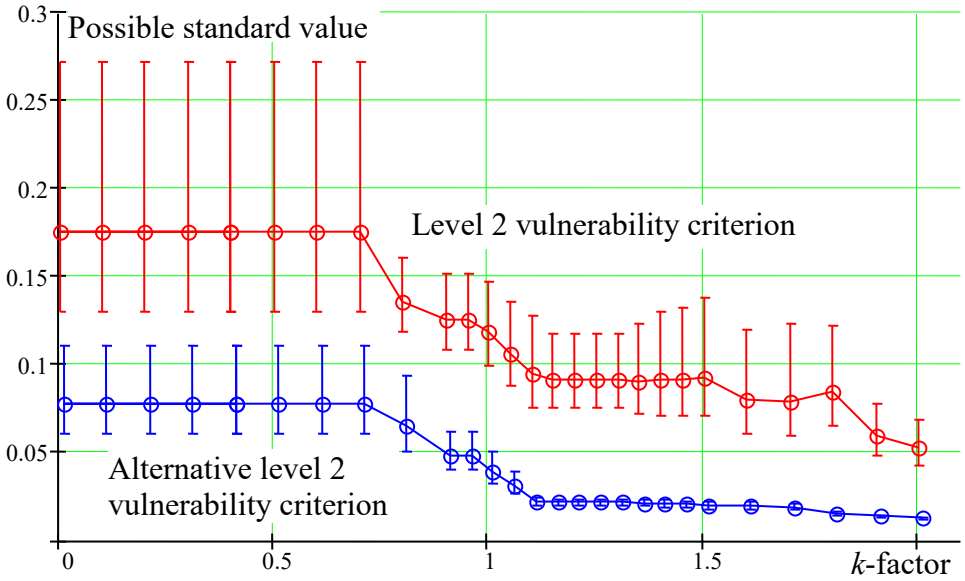

Figure 3.41. Possible Standard vs. *k*-Factor: Probability of inconsistency 0.005

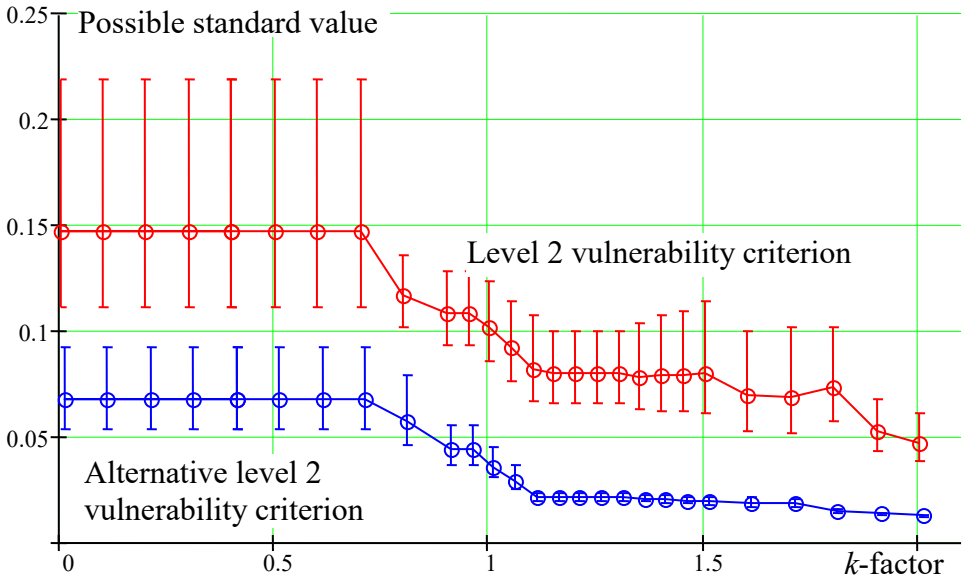

Figure 3.42. Possible standard vs. *k*-Factor: Probability of Inconsistency 0.01

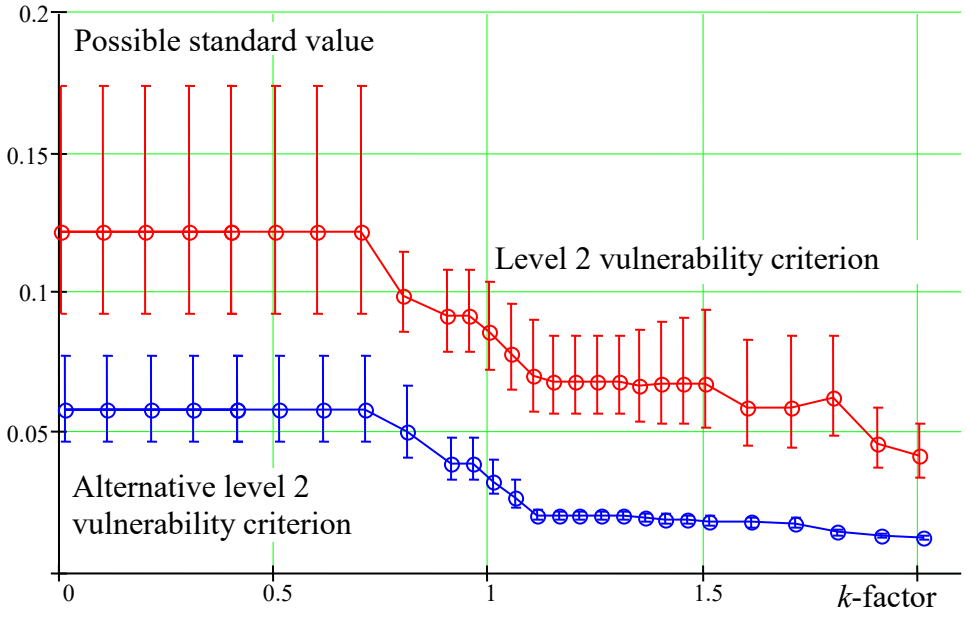

Figure 3.43. Possible Standard vs. *k*-factor: Probability of Inconsistency 0.02

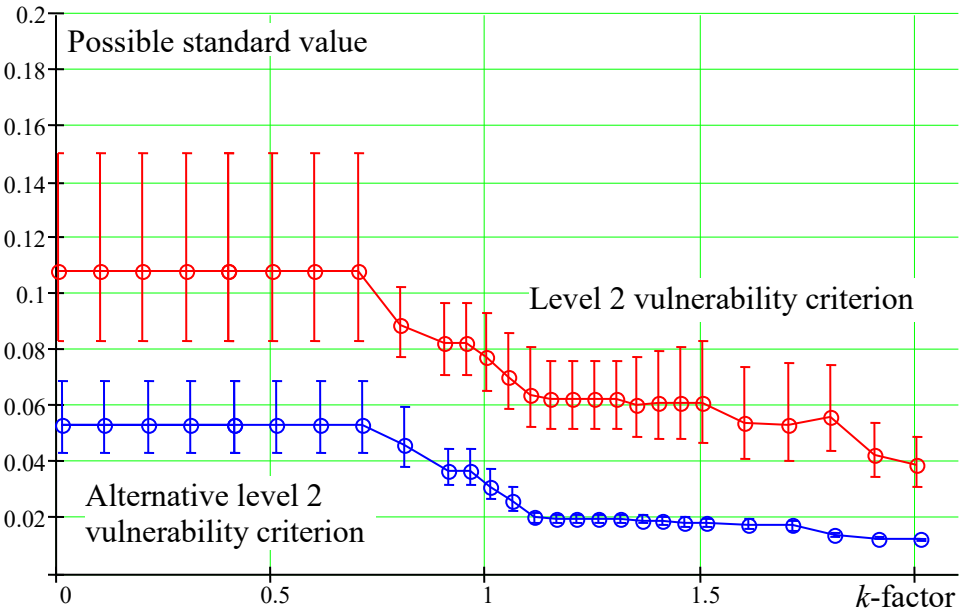

Figure 3.44. Possible Standard vs. *k*-Factor: Probability of Inconsistency 0.03

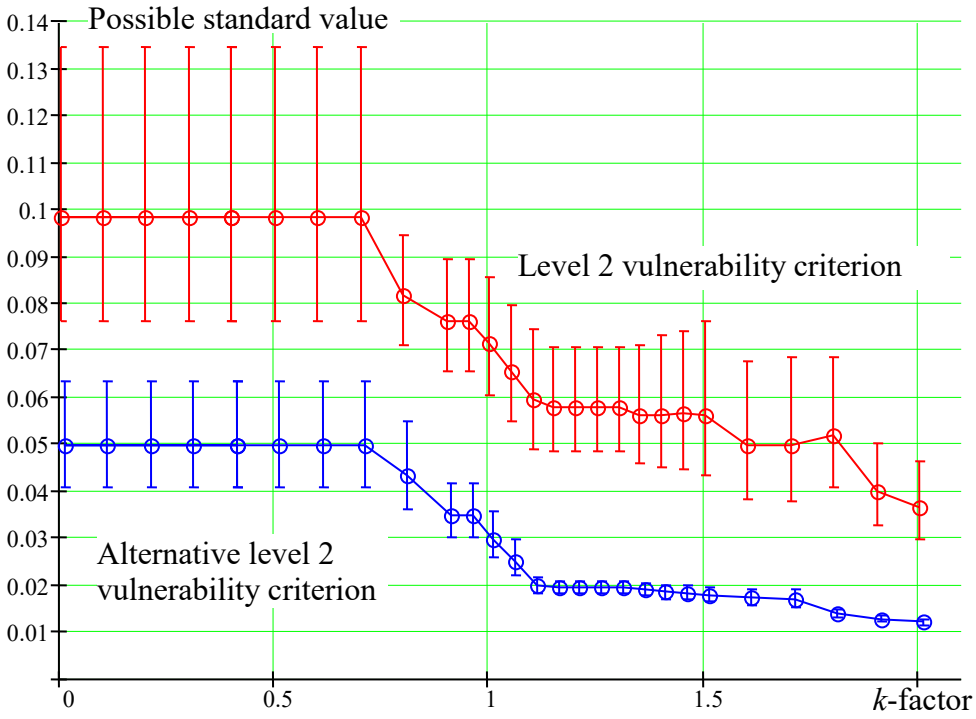

Figure 3.45. Possible Standard vs. *k*-Factor: Probability of Inconsistency 0.04

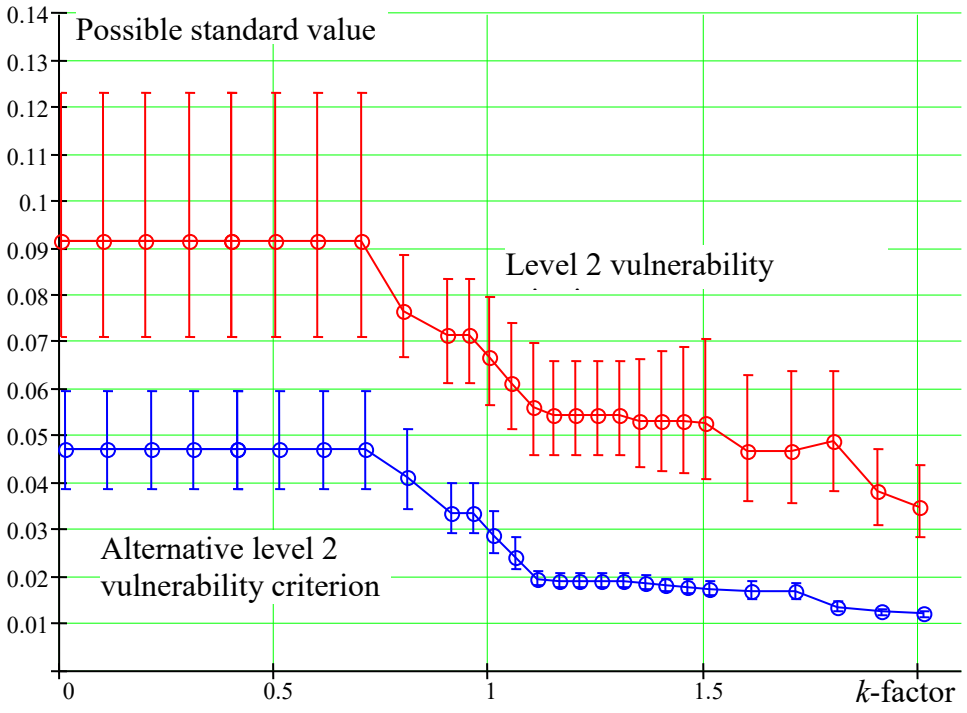

Figure 3.46. Possible Standard vs. *k*-Factor: Probability of Inconsistency 0.05

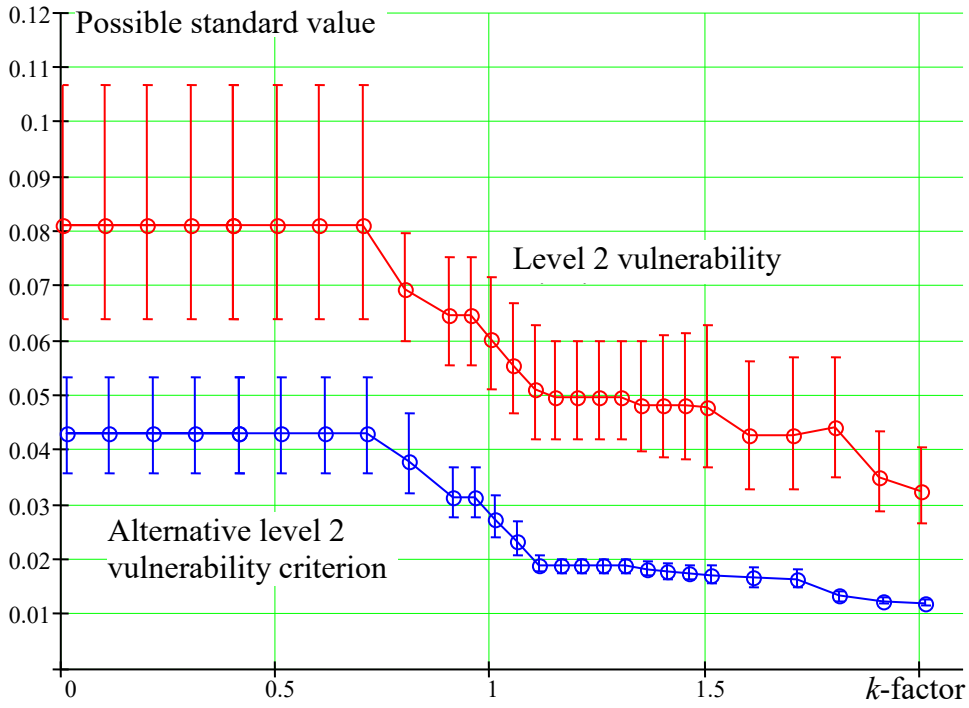

Figure 3.47. Possible Standard vs. *k*-Factor: Probability of Inconsistency 0.07

The containerships in Table 3.17 show a very large weight averaged static angle, most probably caused by the typically large windage area of containerships. The cargo ships were excluded most probably because their angle of maximum GZ was too close to the limiting value. Despite this, the limitations imposed by the *k*-factor are not likely to be too severe and it still makes sense to keep *k*-factor as small as practicable.

Figure 3.40 through Figure 3.47 reveal the optimal value of the k-factor as 1.15. A decrease in inconsistency after that value seems to be not too significant (see Figure 3.39) and changes in possible standards (see Figure 3.40 through Figure 3.47) are not dramatic. Possible standards are in Table 3.14, depending on the accepted probability of inconsistency.

This study is based on statistics and the proposed standard values are based on estimates. Thus, the possible standard values bear some statistical uncertainty that is expressed in the form of a 95 % confidence interval. The boundary of confidence intervals can be used in two ways: 1.) the upper boundary can be used as a standard – then there is only a 2.5 % probability that the actual standard should be set higher, but the drawback of that approach is that the standard may be set too high. 2) The actual estimate becomes a standard, but the width of the confidence interval is used as a consideration for choosing other values.

If no inconsistency is acceptable, only the alternative vulnerability level 2 criterion can be considered (see Figure 3.40). If the *k*-factor is set to 1.15, the standard may be accepted at the level 0.05 (compared to the standard from paragraph 4.3.1 of Annex 3 SDC 6/WP.5 which is 0.06). The statistical uncertainty is small for the alternative level 2 criterion at *k*-factor 1.15, shown in Figure 3.40, so the question discussed in previous paragraph does not apply.

If one sets the inconsistency probability to 0.05 (a frequently used level of significance), the standard for the original level 2 formulated criteria should be accepted as 0.067 or 0.055 with or without explicit account for statistical uncertainty, respectively. If the alterative level 2 criterion is used, the standard can be set to 0.02. The *k*-factor has to be set to 1.15 for both criteria (see Figure 3.46).

If the preference is to maximize applicability and keep the *k*-factor to zero, the use of the original level 2 criterion will require too large a value for the standard (0.11 with and 0.08 without explicit account of statistical uncertainty) even for a significant probability of inconsistency of 0.07 (see Figure 3.47). As seen from Figure 3.40 and Figure 3.41, even the alterative criterion will require large values for the standard. By maximizing applicability (*k*-factor equals 0), the standard for the alternative level 2 criterion can be set 0.06 with an account of statistical uncertainty if 0.05 is accepted as the probability of inconsistency (see Figure 3.46). Without an explicit account for statistical uncertainty of the standard, the standard value of 0.06 can be achieved with 0.02 probability of inconsistency (see Figure 3.43). Other combinations can be seen form Figure 3.42 and Figure 3.44 and from Table 3.12.

To choose the level 2 vulnerability criterion and standard based on the probabilistic rationale developed because of this study, one should answer the following questions:

- Is an inconsistency between the level 2 criterion and the Weather criterion (or between the level 1 and 2 of the vulnerability criteria for dead-ship condition) acceptable, taking into account paragraph 3.2.2.3.7 of the Explanatory Notes to the 2008 IS Code, recalling the explanation that certain imperfections should be expected even from the mandatory criteria?
- Is reduction of the applicability of the level 2 criteria with the application of the *k*-factor an acceptable way to control possible inconsistency?
- Should the statistical uncertainty of a possible standard be taken into account explicitly, by using the upper boundary of the confidence interval at the expense of increasing the standard?

The results of this study were submitted to SDC4/5 intersessional intact stability correspondence group and included as Annexes 7 and 12 of SDC5/INF.4. However, there were no working groups on intact stability at SDC 5, so these questions were not raised and discussed. The decision was made by SDC5/6 intersessional intact stability correspondence group to keep the vulnerability criteria for dead ship condition, as they were originally proposed (i.e. All the problems related to “standard” wave slope function and relative motion formula) and set the standard to 0.06.

According to this study, if the standard is set to 0.06, while using the upper limit of the confidence interval for standard, 7 % of inconsistency can be anticipated and the *k*-factor would be equal 1.15 (excluding 9 ships or 12 %), see Figure 3.47.

Note that the level 2 vulnerability criteria values in Table 3.10 was computed for a consistent mathematical model of ship motions, i.e. using pressure integration for the wave-slope function and the formula for standard deviation of roll angles used absolute coordinates. As seen from Table 3.6, the use of the “standard” method for wave-slope function and computing the standard deviation of roll angles in relative coordinates may increase the inconsistency between the levels. Thus, the probability of inconsistency 7 % should be taken as a low boundary estimate.

3.7.9 Probabilistic Study: Summary

The objective of the probabilistic study was to find out if it is possible to achieve consistency between the levels for vulnerability criteria of a dead-ship condition. Both of the level 2 vulnerability criteria, original and alternative version, were included in the study. It was found that:

- A choice of a standard can keep probability of inconsistency between the levels below a certain value, if the applicability of the both original and alternative level 2 criteria is limited
- Lower probability of inconsistency can be achieved by accepting a less conservative standard and limiting its applicability of the criterion
- If no inconsistency between the levels is acceptable, the alterative criterion can be used; a choice of standard is specifically done to exclude inconsistency, however the applicability of the criterion will be limited
- If the limitation of applicability is not acceptable, a choice can be made between the conservatism of a standard and the probability of inconsistency

In general, this study can be considered as an example of an approach to the development of a regulation using imperfect criteria, continuing the topic raised and developed by N. Sevastianov (1963, 1978, 1982). The English version is also available (Sevastianov, 1994, Chapter 1 of Belenky and Sevastianov, 2007). The Explanatory Notes to the 2008 IS Code recognizes an uncertain nature of criteria with the statistical elements and explains a rational approach to set a standard (see paragraph 3.2.2.3.7, Explanatory Notes to the 2008 IS Code). More in-depth information on the subject is available from (Kobylinski and Kastner, 2003).

A criterion that contains any statistical estimate is subject to statistical uncertainty, because a value, estimated on a finite sample size, is a random number. As a result, a safe ship could be categorized as "dangerous, while a ship that suffered from stability failure could be evaluated as "safe", e.g. see Figure 17 from the Explanatory Notes to the 2008 IS Code, MSC.1/ Circ 1281.

The dead ship condition is the only mode of failure included in the second-generation intact-stability criteria that also is covered in Part A of the 2008 IS Code. The severe wind and rolling criterion (weather criterion), described in the section 2.3 of the 2008 IS Code has a loading condition limitation for the use of the formulas and tables for calculation of the roll back angle in the paragraph 2.3.5. These limitations are described in the paragraphs 2.3.5 and include the breadth to draft ratio, KG to draft ratio and natural roll period.

To address these applicability limitations, MSC Circular 1200 (MSC.1/Circ.1200) describes an alternative way to obtain the roll-back angle through the performance of model tests. However, the assessment of the weather criterion is unchanged. The level 1 vulnerability criterion uses the extended roll period table from MSC.1/Circ.1200, so the limitation for two other parameters remain to be addressed at the level 2 assessment, which is a probabilistic long-term criterion based on an averaged upcrossing rate. As the level 2 assessment does not provide the roll back angle outside the applicability range of the weather criterion, the level 2 assessment is essentially an alternative outside of the current stability regulatory framework. It does not mean, however, that alternative criteria should not be sought and examined; the original (with direct pressure integration and absolute coordinates) and alterative level 2 vulnerability criteria are recommended for the trial application of the second generation of IMO intact stability criteria.

4. VULNERABILITY CRITERIA FOR EXCESSIVE ACCELERATIONS

4.1 General Description and Implementation

4.1.1 General

The assumed situation (scenario) essentially modeled after the accident with Chicago Express (BSU, 2009). The accident occurs at about 02:45 in the morning local time on 24 September 2008, 25 nm south of Hong Kong. The accident accompanied with 44° roll resulting in one fatality, one serious injury and four minor injuries. At about 00:18 in the morning local time of 15 September 2009, while at the sea off of Hong Kong a German container ship, Guayas, suffered from another accident of a similar scenario, resulting in the fatal injury of a crew member on the bridge (BSU, 2011).It is assumed that a group of large waves approaches a ship from her side at a speed of 2 - 4 kn. The periods of these waves are close to the natural period of the roll of the ship, resulting in synchronous resonant response. The hazard is lateral acceleration developing as a result of fast reaching large roll angles, which in turn is exacerbated by a significant height where crew can be located.

4.1.2 Level 1 Vulnerability Criterion

Level 1 criterion is a value of transversal acceleration acting at location, furthest from the center of gravity, where crew may be present. The description of the criteria in section 5.2 of Annex 3 of SDC 6/WP.6, defines the location in terms of a distance from roll, pitch, and yaw axes; clarification may be needed on where these axes are assumed relative to the center of gravity. Calculation of the criteria include the following elements:

- Natural roll period; computation is meant to be standard for the entire second generation IMO intact stability criteria
- Effective wave slope is computed with an approximate formula in paragraph 5.2.1 of Annex 3 of SDC 6/WP.6; no explanation is given on assumptions in paragraph 2.2.2.3 of Annex 5 of SDC 4/5/1/Add.4; a brief description and references needed to be added in the explanatory notes
- Wave steepness is taken from the extended table of steepness for vulnerability assessment in dead ship conditions, Fig.2.1 in Annex 4 of SDC 4/5/1/Add.3
- Non-dimensional logarithm decrement of roll decay is computed with an approximate formula, originally developed for level 1 vulnerability assessment of parametric roll, see paragraph 2.11.2 Annex 2 SDC 2/WP2
- Coefficient of simultaneous action of yaw and pitch motions; while it seems to be meaningful, no description of its origin is given in the Explanatory Notes, while such description seems to be necessary
- Characteristic roll amplitude; its derivation and assumptions is given in explanatory notes

4.1.3 Level 2 Vulnerability Criterion

Level 2 criterion is a long-term averaged probabilistic index, computed as described in section 5.2 of Annex 3 of SDC 6/WP.6. The index is an exponent portion of the upcrossing rate over the level of standard. Normally the rate of upcrossing of a given level a by a zero-mean normal stochastic process $\underline{x}(t)$ expressed as:

$$\lambda = \frac{1}{2\pi}\frac{\sigma_d}{\sigma_x}\exp\left(-\frac{a^2}{2\sigma_x^2}\right) \tag{4.1}$$

Where σ_x is standard deviation of of the process x, σ_d is the standard deviation of the derivative of the precess x. Apparently, the developers of the criteria chose to drop the ratio of the standard deviations $\sigma_d/(2\pi\ \sigma_x)$, see paragraph 5.3.2.1 Annex 3 SDC 6/WP.6.

Dropping the term $\sigma_d/(2\pi\ \sigma_x)$ may have the following justification. The process is the lateral accelerations at a location. Temporal derivative of an acceleration does not have immediate physical meaning. Another possible reason may be related with convergence of the integral involving ITTC spectrum, paragraph 2.1.4 of the explanatory notes in Annex 5 of SDC 4/5/1/Add.4.

The convergence issue is driven by the fact that the formula for the spectrum contains the division by the wave frequency power 5. The roll motions are excited by wave slope, so multiplication by the square of the wave number contains power four of the frequency. In order to get spectrum of acceleration, the response spectrum has to be differentiated twice which brings the power of frequency in numerator to eight. The square of RAO increases the power of denominator to nine. So the integral over the acceleration spectrum formally converges, as the power of the frequency in it the integrand's numerator is less than in its denominator. This convergence, however, is slow; it is a good idea to set a rule for the upper limit of integration.

An attempt to compute standard deviation of the derivative of the acceleration increases the power of numerator to 10. It exceeds the power of the denominator, and the integral cannot be computed and does not converge. However, if the effective wave slope function is applied, the integral converges as the effective wave slope function eventually forces the integrand to zero for high frequencies, given issues considered in the subsection 3.2 of this report are successfully resolved by applying direct pressure integration.

Exclusion of the term $\sigma_d/(2\pi\ \sigma_x)$, leaves the only standard deviation (a term "root-mean-square is used in the working version of explanatory notes paragraph 3.1.5 of Annex 5 SDC 4/5/1/Add.4). These calculations involve the following elements:

- The influence of energy spread (short-crestedness) may be accounted by a formula in the paragraph 3.1.6 of Annex 5 SDC 4/5/1/Add.4; however, to simplify the calculations, a constant coefficient of 0.75 is introduced for account for the reduction due to wave energy spread.
- Limits of the frequency integration are established in paragraph 3.1.6 of Annex 5 SDC 4/5/1/Add.4; setting the integration limits are important for a consistent application of the criteria.
- Two methods are proposed for computing equivalent roll damping: equivalent stochastic linearization and simply calculation of the equivalent roll damping at a 15° roll angle, 3.1.8 of Annex 5 SDC 4/5/1/Add.4; Simplified Ikeda method is meant to use as a source of data on roll damping, per paragraph 3.1.9 of Annex 5 SDC 4/5/1/Add.4.
- No effective wave slope function is used. Amplitudes of the Froude-Krylov component of wave excitation are computed by direct pressure integration, see paragraph 3.1.0 of Annex 5 SDC 4/5/1/Add.4. The implementation is very similar to the one described in subsection 3.2 of this report.

The results of sample calculations are described in the next subsection.

4.2 Sample Calculations

4.2.1 Input and Output of Sample Calculations

Sample calculations were carried out with the purpose to test the process of vulnerability assessment in dead ship condition. Another objective is to carry out a comparison for different calculation option formulated in the previous subsections, but using wider set of data.

There were 5 ships used for sample calculation with 5-6 loading conditions each, a total of 31 cases. Main input data are placed in Table 4.1. The following acronyms and symbols and abbreviations are used in the table:

- "EA" means "excessive acceleration";
- "FP" means "forward perpendicular";
- "BL" means "baseline".
- h – height of the location above the baseline

Some intermediate values and results of vulnerability assessment are placed in Table 4.2. The right column indicates whether the criterion value the standard (R_{EA1}) selected by the SDC5/6 intersessional intact stability corresponding group, as reported on page 136 of SDC 6/INF.3 and confirmed by the experts group at SDC 6 as reported in paragraph 5.2.1 in Annex 3 of SDC 6/WP.6, which is 4.64 m/s^2. Loading conditions where the standard value is exceeded are highlighted in light red.

Results for level 2 vulnerability assessment are placed in Table 4.3. Three options for linearization roll damping are used. Two options (equivalent stochastic linearization and the (15°-option) described in the working version of explanatory notes for excessive acceleration, see paragraph 3.1.8 of Annex 5 SDC 4/5/1/Add.4. The third option is the linearization method originally prosed for the level 2 vulnerability assessment in a dead ship condition and parametric roll, see Appendix 2 SDC 4/5/1/Add.1.

Values of C that are greater than R_{EA2} = 0.00039 (as per paragraph 5.3.1 in Annex 3 of SDC 6/WP.6) are shown in bold type-face and highlighted in light red color. The GM values, corresponding to these load cases also are highlighted by light red color in Table 4.1.

Table 4.1. Input Data for Sample Calculations

Ship Type	Loading case Identifier	Length, bp, m	Beam, *B*, m	Depth, *D*, m	draft, *d*, m	Displaced Volume, molded, m^3	*KG*, m	*GM*, m	Location for EA assessment	
									from FP, m	From BL, m
Container ship	Benchmark	262.00	40.00	24.45	11.50	67,500	18.92	1.40	181.0	40.0
	SLL				12.70	77,540	19.92	0.30	181.0	40.0
	PL1				12.29	74,660	17.54	2.84	181.0	40.0
	PL2-KG1				10.70	61,150	20.01	0.43	181.0	40.0
	PL2-KG2				10.70	61,150	17.50	2.94	181.0	40.0
	LL1				8.29	43,910	16.00	5.77	181.0	40.0
RoPax Ferry	SLL	137.00	20.25	12.78	5.77	9,737	8.71	1.59	20.5	31.0
	PL1				5.54	9,262	8.67	1.73	20.5	31.0
	PL2				5.40	8,891	8.79	1.70	20.5	31.0
	LL1				4.91	7,833	8.94	1.80	20.5	31.0
	LL2				4.47	6,882	9.27	1.83	20.5	31.0
Cruise Ship, Location 1	Load 1	242.30	36.00	26.00	8.70	54,090	17.37	1.65	51.0	50.0
	Load 2				8.40	51,760	17.39	1.93	51.0	50.0
	Load 3				8.40	51,760	17.94	1.38	51.0	50.0
	Load 4				7.90	48,290	17.16	2.64	51.0	50.0
	Load 5				7.90	48,290	15.53	4.27	51.0	50.0
Cruise Ship, Location 2	Load 1	242.30	36.00	26.00	8.70	54,090	17.37	1.65	220.0	60.0
	Load 2				8.40	51,760	17.39	1.93	220.0	60.0
	Load 3				8.40	51,760	17.94	1.38	220.0	60.0
	Load 4				7.90	48,290	17.16	2.64	220.0	60.0
	Load 5				7.90	48,290	15.53	4.27	220.0	60.0
Bulk Carrier	SLL	145.00	22.85	15.00	10.80	29,510	9.02	0.70	120.0	32.0
	PL1				8.45	22,455	8.34	1.16	120.0	32.0
	Pl2				8.37	22,219	7.46	2.00	120.0	32.0
	LL1				4.25	10,507	6.44	5.36	120.0	32.0
	LL2				6.69	17,340	5.08	4.65	120.0	32.0
LNG Carrier	SLL	257.00	41.60	24.00	12.00	100,381	15.94	2.41	221.0	46.5
	PL1				11.33	94,034	15.94	2.76	221.0	46.5
	PL2				9.95	81,504	15.89	3.80	221.0	46.5
	LL1				5.60	42,756	11.86	16.28	221.0	46.5
	LL2				7.28	57,289	12.74	10.64	221.0	46.5

Table 4.2. Derived Characteristics and Excessive Acceleration, Level 1, Vulnerability Criteria Results

Ship Type	Loading case Identifier	draft, *d*, m	Period of roll, *T*, s	*GM*/*B*, %	(*h*-*d*)/*B*, %	wave slope coefficient *r*	amplitude of roll, φ, °	criterion value, m/s^2	>4.64. m/s^2
Container ship	Benchmark	11.50	23.0	5.7%	71.3%	0.93	7.7	1.54	
	SLL	12.70	48.3	1.2%	68.3%	0.98	6.1	1.09	
	PL1	12.29	15.9	11.6%	69.3%	0.85	11.8	2.74	
	PL2-KG1	10.70	42.2	1.8%	73.3%	0.98	6.3	1.13	
	PL2-KG2	10.70	16.2	12.0%	73.3%	0.88	12.4	2.85	
	LL1	8.29	12.4	23.6%	79.3%	0.86	19.4	5.43	Y
RoPax Ferry	SLL	5.77	12.7	12.4%	125%	0.88	12.2	3.71	
	PL1	5.54	12.3	13.5%	126%	0.88	12.9	4.03	
	PL2	5.40	12.5	13.3%	126%	0.89	12.9	3.99	
	LL1	4.91	12.4	14.1%	129%	0.90	13.9	4.29	
	LL2	4.47	12.5	14.3%	131%	0.91	14.7	4.47	
Cruise Ship, Location 1	Load 1	8.70	20.4	6.3%	115%	0.89	6.2	1.53	
	Load 2	8.40	19.0	7.4%	116%	0.88	6.8	1.75	
	Load 3	8.40	22.5	5.3%	116%	0.91	5.5	1.30	
	Load 4	7.90	16.6	10.2%	117%	0.87	8.1	2.27	
	Load 5	7.90	13.0	16.4%	117%	0.81	10.6	3.64	
Cruise Ship, Location 2	Load 1	8.70	20.4	6.3%	143%	0.89	6.2	1.59	
	Load 2	8.40	19.0	7.4%	143%	0.88	6.8	1.84	
	Load 3	8.40	22.5	5.3%	143%	0.91	5.5	1.34	
	Load 4	7.90	16.6	10.2%	145%	0.87	8.1	2.42	
	Load 5	7.90	13.0	16.4%	145%	0.81	10.6	3.99	
Bulk Carrier	SLL	10.80	19.8	4.7%	92.8%	0.89	7.4	1.60	
	PL1	8.45	16.0	7.7%	103%	0.87	9.8	2.33	
	Pl2	8.37	12.2	13.3%	103%	0.81	13.1	3.81	
	LL1	4.25	8.7	35.7%	121%	0.80	18.0	7.43	Y
	LL2	6.69	8.3	31.0%	111%	0.71	16.4	7.31	Y
LNG Carrier	SLL	12.00	18.4	10.0%	82.9%	0.84	9.6	2.33	
	PL1	11.33	17.4	11.5%	84.5%	0.84	10.3	2.58	
	PL2	9.95	15.3	15.8%	87.9%	0.82	12.0	3.25	
	LL1	5.60	9.0	67.8%	98.3%	0.73	19.6	9.51	Y
	LL2	7.28	10.1	44.3%	94.3%	0.74	18.0	7.49	Y

Table 4.3. Excessive Acceleration, Level 2, Vulnerability Criteria Results

Ship Type	Loading case Identifier	draft, *d*, m	Long-term probability index, *C*		
			option 1 results using statistical linearization of damping	option 2 results using fixed roll amplitude (15°) for damping	option 3 results using equivalent linearization for damping
Container ship	Benchmark	11.50	2.5E-26	2.1E-32	1.7E-26
	SLL	12.70	0.0E+00	0.0E+00	0.0E+00
	PL1	12.29	1.7E-10	2.0E-09	1.4E-10
	PL2-KG1	10.70	0.0E+00	0.0E+00	0.0E+00
	PL2-KG2	10.70	4.7E-11	5.1E-10	3.9E-11
	LL1	8.29	9.3E-07	5.7E-06	8.3E-07
RoPax Ferry	SLL	5.77	1.6E-05	7.9E-05	1.4E-05
	PL1	5.54	3.3E-05	1.5E-04	3.0E-05
	PL2	5.40	2.0E-05	9.3E-05	1.8E-05
	LL1	4.91	1.4E-05	6.6E-05	1.3E-05
	LL2	4.47	5.5E-06	2.6E-05	4.8E-06
Cruise Ship, Location 1	Load 1	8.70	3.6E-20	6.1E-27	2.6E-20
	Load 2	8.40	4.9E-17	5.1E-21	3.7E-17
	Load 3	8.40	1.1E-27	9.0E-44	7.1E-28
	Load 4	7.90	6.7E-12	9.4E-13	5.4E-12
	Load 5	7.90	9.9E-07	1.2E-06	8.8E-07
Cruise Ship, Location 2	Load 1	8.70	8.3E-19	7.9E-25	6.1E-19
	Load 2	8.40	1.0E-15	3.2E-19	7.8E-16
	Load 3	8.40	4.7E-26	1.3E-40	3.1E-26
	Load 4	7.90	7.9E-11	1.2E-11	6.6E-11
	Load 5	7.90	5.2E-06	4.5E-06	4.7E-06
Bulk Carrier	SLL	10.80	1.1E-14	3.5E-14	8.9E-15
	PL1	8.45	5.1E-10	5.1E-09	4.3E-10
	Pl2	8.37	8.1E-06	4.3E-05	7.3E-06
	LL1	4.25	**1.4E-03**	**2.5E-03**	**1.3E-03**
	LL2	6.69	**1.8E-03**	**2.3E-03**	**1.7E-03**
LNG Carrier	SLL	12.00	2.8E-08	2.7E-07	2.9E-08
	PL1	11.33	3.2E-07	2.8E-06	3.2E-07
	PL2	9.95	1.1E-05	6.4E-05	1.1E-05
	LL1	5.60	**3.5E-02**	**4.7E-02**	**3.5E-02**
	LL2	7.28	**1.4E-02**	**2.3E-02**	**1.4E-02**

4.2.2 Observation of the Results of Sample Calculations

The results of the sample calculations presented in Table 4.2 and Table 4.3 appear to be physically correct five cases of vulnerability on level 1 and four cases of vulnerability on level 2 are observed for light loads and large values of *GM*. There are three "near-misses" in level 1 calculations where the criterion value is close to or exceeds 4 m/s^2. These cases are highlighted in yellow in Table 4.2. One of them (Cruise Ship, Location 2, LL2) corresponds to large GM value 4.26 m (highlighted with yellow in Table 4.1). It is also understandable that high GM values do not always lead to excessive accelerations, as other factors such as location, roll damping, etc. also have a contribution.

No inconsistency between the between the levels 1 and 2 was observed. A container ship in LL1 condition was found to be vulnerable on the level 1, but no vulnerability was indicated at level 2. Large accelerations for the condition LL1 and LL2 for LNG carrier was suspected during a sample calculation for vulnerability in dead-ship condition, see Table 3.6 in the previous section of this report.

Table 4.3 presents the results of the level 2 calculations with three different options for damping linearization. Three options were used because damping is important for the resonance phenomenon that is believed to be responsible for the excessive acceleration failure mode. Correlation was estimated between the values of these criteria computed with different options. The correlation estimates are placed in Table 4.4.

Table 4.4. Correlation Analysis of Level 1 and Level 2 Criteria

	Level 1 Criterion Value, m/s^2	Level 2 Criterion, Option 1	Level 2 Criterion, Option 2	Level 2 Criterion, Option 3
Level 1 criterion value, m/s^2		0.667	0.679	0.665
Level 2 criterion, option 1			0.997	1.00
Level 2 criterion, option 2				0.997

The correlation coefficients in Table 4.4 were estimated as:

$$\hat{r}_{xy} = \frac{\sum_{i=1}^{N}(x_i - \hat{E}_x)(y_i - \hat{E}_y)}{(N-1)\hat{\sigma}_x\hat{\sigma}_y} \tag{4.2}$$

where *N* is a number ouf points, estimate of stanard deviataion $\hat{\sigma}_x$ and mean values $\hat{E}_x$ are computed as:

$$\hat{\sigma}_x = \sqrt{\frac{\sum_{i=1}^{N}(x_i - \hat{E}_x)^2}{(N-1)}} \tag{4.3}$$

$$\hat{E}_x = \frac{1}{N}\sum_{i=1}^{N} x_i \tag{4.4}$$

Correlation is very high between the level 2 criteria values computed with different options as well as being between the level 1 and the level 2 criteria.

It is practical to have one method of damping linearization for all of the 2nd generation intact stability criteria. Large correlation between the values of level 2 criteria indicate that it does not matter what damping linearization method will be chosen for the excessive acceleration failure mode. The correlation is also large between the level 1 and level 2 criteria – it is an indicator of consistency between the levels of the vulnerability criteria for excessive accelerations.

5. SPECIFICATIONS AND EXAMPLE FOR DIRECT STABILITY ASSESSMENT

5.1 General Considerations

5.1.1 Executive Overview

The capabilities for calculations of ship motions in waves made a significant leap forward since the time of development of the weather criterion. What is most relevant for stability regulations are those capabilities that are no longer limited by linear assumptions, so large roll angles and even capsize situations in a realistic wave can be predicted with calculations.

A dramatic increase of computing speed led to the development of computational fluid dynamics (CFD), where a computer solves the most fundamental equations on the motions of fluids, expressing the conservation of mass and momentum. A 3D field of fluid velocities for each time instant is the result of these calculations. Velocities and hydrodynamic pressures are related through the Bernoulli equation; thus, pressures on a submerged portion of a ship hull surface becomes available. Integration of these pressures over instantaneous wetted surface yields total hydrodynamic force and moment generated by the interaction of the ship and the water. Known forces and moments enable solutions to equations of motion regarding a solid body in space, resulting in the new positions of a ship, and this allows the process to loop further into future movements. The CFD model of ship motions show the details of what is going on, including the rotating propeller, the moving rudders, the wake, breaking waves, and bubbles.

The fluid domain around the ship needs to be discretized into very small cells – grid nodes where fluid velocities are computed. To get a realistic description of the fluid flow around the hull one may need hundreds of millions of the nodes. Even with the modern computation parallelization technology, these calculations can produce minutes or tens of minutes of a time series, which is not sufficient to get any statistical estimates. It does not mean that CFD has no role to play in direct stability assessment, but that its possible application will need to be revisited later.

To bring the computational cost to a more practical level, one needs to introduce assumptions by simplifying the mathematical model. The first candidate for simplification is viscosity, because water has a relatively small viscosity compared to other fluids. Also, far from the body, water behaves almost as an inviscid fluid. Mechanically, viscosity is an ability of the fluid to transfer motion across the flow. Without viscosity, parallel layers of fluid do not interact: it means no turbulence! Also a vortex cannot take place in inviscid fluid, but if it was introduced there, it will exist forever, as its energy will not dissipate. So if the location of vortexes is known, the flow can be modeled without viscosity. The location of the vortexes can be taken from short CFD calculations or from a model test. The numerical solution still requires a 3D grid, but with a fewer number of nodes to be sufficient. This method is applied frequently when there are vortexes forces (i.e. the lifting forces) are dominant – is known as the “lifting surface” approach.

Vortexes are not as important for the wave forces when the wave forces are dominant in problems of dynamic stability. Thus, one more simplification seems to be logical - to present lifting forces as a polynomial approximation and assume that the fluid does not rotate. This assumption allows the application of potential theory. That means, the fluid velocity becomes a potential field – enough to compute a scalar value of a potential at each point of space and each instant of time and fluid velocities that can be obtained trivially as partial derivation of the

potential at this point and at this instant. An easier method already exists: computing one number instead of three. However, the biggest saving of computational costs comes from the fact that in order to find a potential anywhere in the fluid domain, it needs to be enough to compute it at the boundaries. These boundaries exist on the submerged portion of the hull surface and the free surface itself (the boundary between air and water). It means that, the problem becomes 2D, essentially, instead of a space that has to be solved just on the several 3D surfaces. This problem, frequently, is referred as a "boundary-valued problem". These boundaries are discretized with panels (panel method), or just a set of lines (strip theory).

A potential flow solver inherently produces hydrostatic, Froude-Krylov, wave diffraction and radiation forces and moments. The lifting forces and their moments related with thrust, resistance, rudder action, vortex damping, as well as maneuvering forces all need to be computed (or measured) outside of the solver and brought in as polynomial approximations. That is why simulation codes based on the potential solver are frequently called a "hybrid". These lifting forces may be actually computed with short-time CFD simulations - *e.g.* a roll decay or a turn. As these CFD calculations are short, their computation cost may be reasonable and available for most consulting companies, including towing tanks and classification societies.

In depth and up-to-date state-of-the-art reviews are available from Reed and Beck (2016).

5.1.2 Maturity of Ship Motion Simulation and Possible Scheme of Regulatory Application

Two numerical codes were used in the APL "China" parametric roll post-accident study FREDYN and LAMP (France *et al*., 2003). Both codes have demonstrated quite the satisfactory performance in terms of agreement with the model test. The first publications of the theoretical background of these codes occur about 10 years before these codes were applied (de Kat and Paulling, 1989; Lin and Yu, 1990). At the turn of the century, these codes were considered mature enough to be used for practical analysis of dynamic stability.

During the first decade of 21st century, these hybrid codes have seen regular use for assessments of large motions and loads, *e.g.* (Shin *et al.*, 2003). There are several known applications of these codes exclusively for a dynamic stability assessment for practical purposes (not including applications for research purposes):

- Related to the APL China accident (France, et al, 2003)
- The ABS Guide on Parametric Roll for Containerships (ABS, 2004, 2008)
- CRNAV works (*e.g.* Perrault, 2015; Ypma, and Harmsen, 2012)

This experience made up a bulk of the background of the current draft specification regarding the direct stability analysis in Annex 1 of SDC 4/WP. However, there are two issues worth mentioning.

The successful application of advanced numerical code requires expert users, whom are not usually found at a shipyard or a naval architecture firm. They are at classifaction societies and towing tanks who have these capabilities. However, these capabilities need to be continuously supported to be dependable. Recent German submissions on direct-stability assessments were developed, allegedly, using code ROLLS (Söding, 1982), which is essentially an tool, based on ordinary differential equations (ODE). While recognizing that using the previous-generation's tools and while advanced codes already gain sufficient maturity, they may seem suboptimal, they are, in fact, still acceptable for the time being, given the currently available resources.

A numerical simulation of maneuvering in waves is less mature than other aspects of numerical simulation of a ship motion in waves, see the description of recent progress in Reed and Beck (2016). That is why ODE-based solution like OU BROACH (Hashimoto *et al.,* 2011) should be used for direct stability assessments in broaching-to failure mode.

The maturity of the codes is not the main obstacle for the practical deployment of direct stability assessment – it is the absence of universally accepted procedures of application within those codes. The development, testing, and validation of these procedures is expensive. Since stability is a statutory requirement, these procedures will develop if the application of a direct assessment will be recommended for all required by IMO instruments. However, the IMO instrument cannot include recommendations or requirements for which procedures are not available. To break this circular argument, the following steps make sense:

- Currently available experience is formulated as a Guidance in a form of MSC Circular. Most of the content is already available in Annex 1 of SDC 4/WP.4. It creates an initial motivation.
- Most organizations, possessing the capability to perform a direct stability assessment are members of IACS and ITTC. Direct stability assessment is potentially a fee-based service performed by the members of these organizations where the detailed procedures may be developed and tested by those organizations per the request of their members. IMO may monitor the progress and update references to the procedures.
- Administrations of the member states create a list of organizations with the recognized capabilities to carry out direct stability assessments. These take place once the appropriate procedures are developed by ITTC and IACS and then recommended by the IMO.

5.2 Specifications and Example for Direct Stability Assessment: Parametric Roll

5.2.1 General Requirements

As stated in paragraph 1.1.2 of Annex 1 of SDC 6/WP.6, objective of the described sample is direct-stability assessment of parametric roll.

To the satisfaction of paragraph 3.1.1 Annex 1 of SDC 6/WP.6, ship motions were evaluated with time-domain numerical simulations using Large-Amplitude Motion Program (LAMP), a general description is available from Shin, et al. (2003).

Direct stability assessment was performed for a C11-class container carrier. The principle characteristics are in Table 2.3, the lines are shown in Figure 2.11. The value of KG equals to 18.96 m, corresponding to calm-water GM value of 1.4 m. The hull is modeled with panels as shown in Figure 5.1. The hull model consists of several surfaces shown in different colors. During the simulation, each surface is re-splined separately to get a representation of the instantaneously submerged portion of hull. Also, in LAMP, different surfaces can be used differently for the calculation of forces. In particular, Froude-Krylov and hydrostatic forces are computed on all the surfaces, while diffraction and radiation forces are only on the main hull (shown in red) and stern (shown in green).

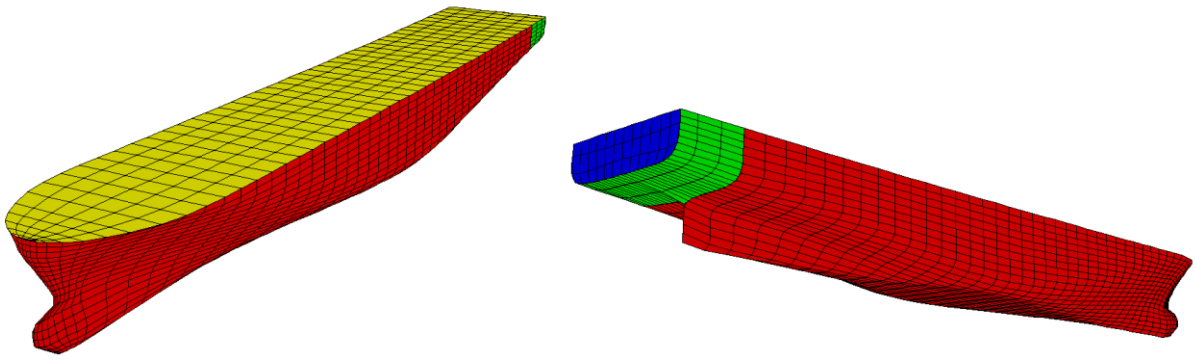

Figure 5.1 Panel Model for C11 Hull Geometry: Main Hull (Red), Stern (Green), Transom (Blue), Deck (Yellow)

5.2.2 Wave Model

Following the requirements of section 3.2.1 of Annex 1 of SDC 6/WP.6, waves are modeled with Lonuett-Higgins model, which is, *de-facto*, the industry standard. A random wave elevation z_w is at the location at x and time instant t is modeled as a sum of cosine function components, i.e. as a Fourier series

$$z_w(t,x) = \sum_{i=1}^{N} r_{wi} cos(k_{wi}x - \omega_{wi}t + \varphi_{wi}) \quad (5.1)$$

Where r_w is an amplitude of the i[th] component, while ω_{wi}, k_{wi}, and φ_{wi} are circular frequency, wave number, and a phase shift respectively; N is total number of components. The phase ship is taken as a set of independent random number distributed uniformly in range $\varphi_{wi} \in [0; 2\pi)$.

The wave number is expressed through circular frequency via dispersion relationship for small waves:

$$k_{wi} = \frac{\omega_{wi}^2}{g} \quad (5.2)$$

Where g = 9.81 m/s^2 gravity acceleration.

The amplitude of a cosine component is computed using a spectral value $S(\omega_{wi})$ at its frequency:

$$r_{wi} = 2\sqrt{S(\omega_{wi})} \quad (5.3)$$

The spectral value $S(\omega_{wi})$ is computed through the spectral dencity:

$$S_w(\omega_{wi}) = \int_{\omega_{wi}-\Delta\omega}^{\omega_{wi}+\Delta\omega} s_w(\omega)\, d\omega \approx s_w(\omega_{wi})\Delta\omega \quad (5.4)$$

Where $\Delta\omega$ is a frequency increment of discretization. Bretschneider/Peirson-Moscowitz formula was used to approximate spectral density $s_w(\omega)$, see Figure 5.2.

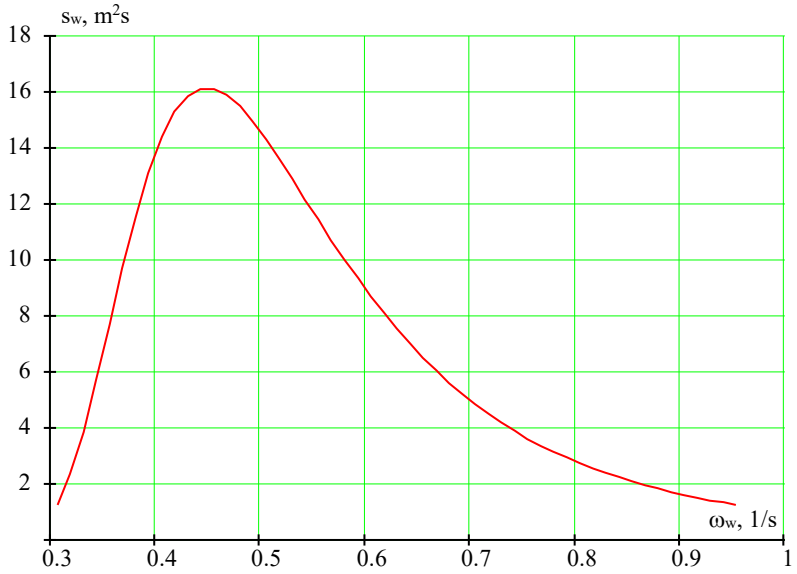

Figure 5.2 Spectral Density: Significant Wave Height 9 m, Modal Period 14 s

Longuett-Higgins model (5.1) is hydrodynamically adequate within the theory of small amplitude waves: linear dispersion relationship (5.2) is explicitly included in the model. The equation (5.1) satisfies the boundary condition on a free surface for the Laplace equation, see section 6 of Newman (1977), satisfying the requirements of paragraph 3.2.1.2 of Annex 1 of SDC 6/WP.6 as well. Hydrodynamic adequacy of the model (5.1) allows consistency by way of the calculation of pressures caused by wave pass in the fluid domain. The integration of pressures produces wave forces; these are consistent with the linear-wave model to the satisfaction of the requirements in paragraph 3.2.1.1. of Annex 1 of SDC 6/WP.6.

To check the absence of the self-repetition effect, as required of paragraph 3.2.1.2 of Annex 1 of SDC 6/WP.6, autocovariance function $R_w(\tau)$ is computed as:

$$R_w(\tau) = \int_0^\infty s_w(\omega)\cos(\omega\tau)d\omega \approx \sum_{i=1}^{N} S_{wi}\cos(\omega_{wi}\tau) \tag{5.4}$$

Where τ is time lag. Autocorrelation function $r_w(\tau)$ is normalized by the variance or $R_w(\tau = 0)$:

$$r_w(\tau) = \frac{R_w(\tau)}{R_w(0)} \tag{5.5}$$

The autocorrelation function computed using equation (5.4) and discretization with 210 frequencies for 30 minutes of the target-record length is in Figure 5.3. No increases of the autocorrelation function are observed, thus, no self-repetition effect should be expected.

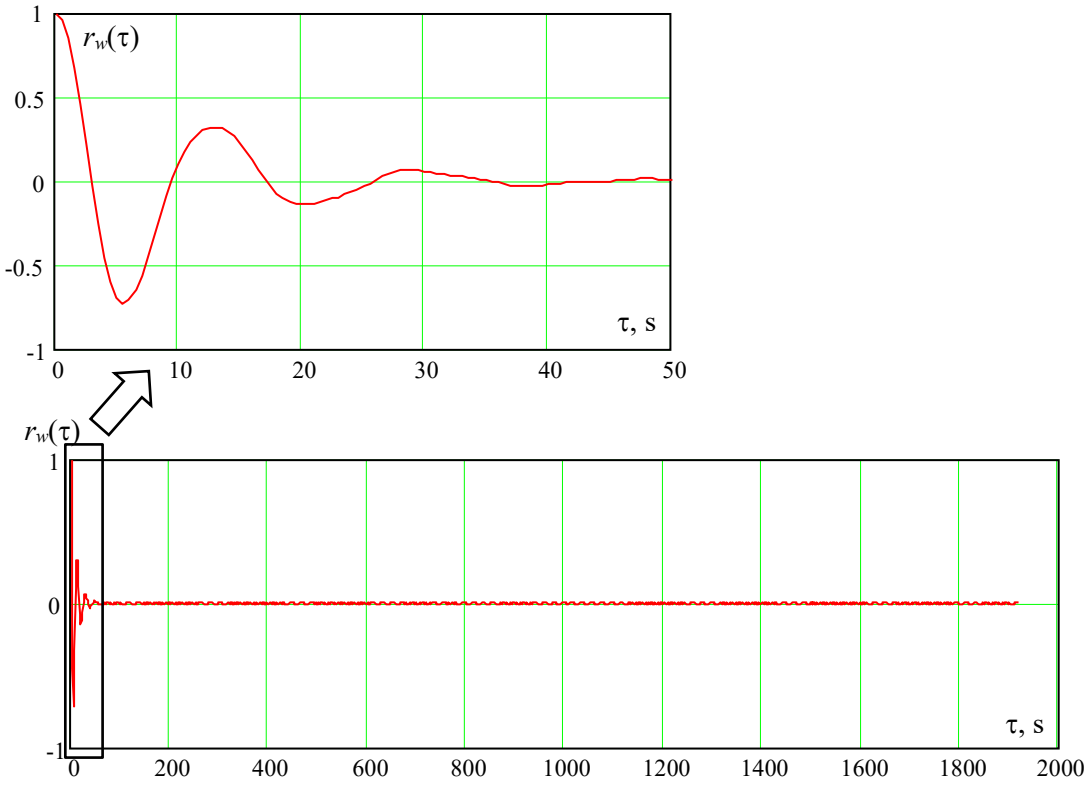

Figure 5.3. Autocorrelation Function, 210 Frequencies

The described check for the self-repetition effect was performed for a fixed point. If a ship is moving in head or oblique waves, she will encounter more waves compared to the fixed point, so the actual check of the self-repetition effect is done for each speed and heading combination, using encounter frequencyω_{ei}, instead of the true frequency:

$$\omega_{ei} = \omega_{wi} + k_{wi} v_s \tag{5.7}$$

The autocovariance and autocorrelation function are computed as follows:

$$R_{we}(\tau) = \sum_{i=1}^{N} S_{wi} \cos(\omega_{ei}\tau) \; ; \; r_{we}(\tau) = \frac{R_{we}(\tau)}{R_{we}(0)} \tag{5.8}$$

Figure 5.4 shows the autocorrelation function, computed for forward speed 20 kn in head seas (heading 180°). The presence of the self-repeating effect is obvious as the autocorrelation function grows.

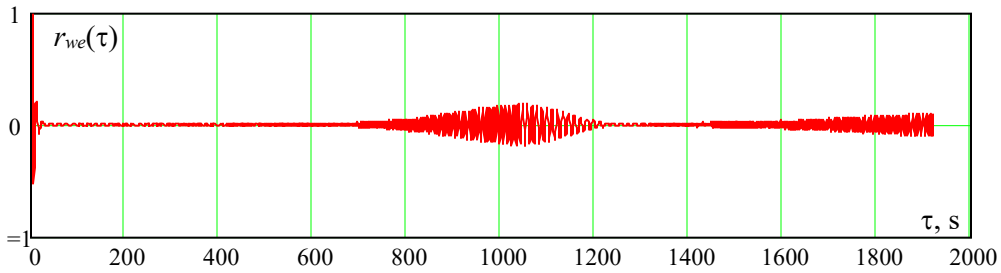

Figure 5.4. Autocorrelation Function, 210 Frequencies, Head Seas, 20 kn

It is visually clear from Figure 5.4 that the self-repetition effect manifested itself somewhere after 650 s. However, for massive computations (such as full probabilistic assessments), the search for the self-repetition effect needs to be done automatically. Use a peak-based envelope of the autocorrelation function, see Figure 5.5.

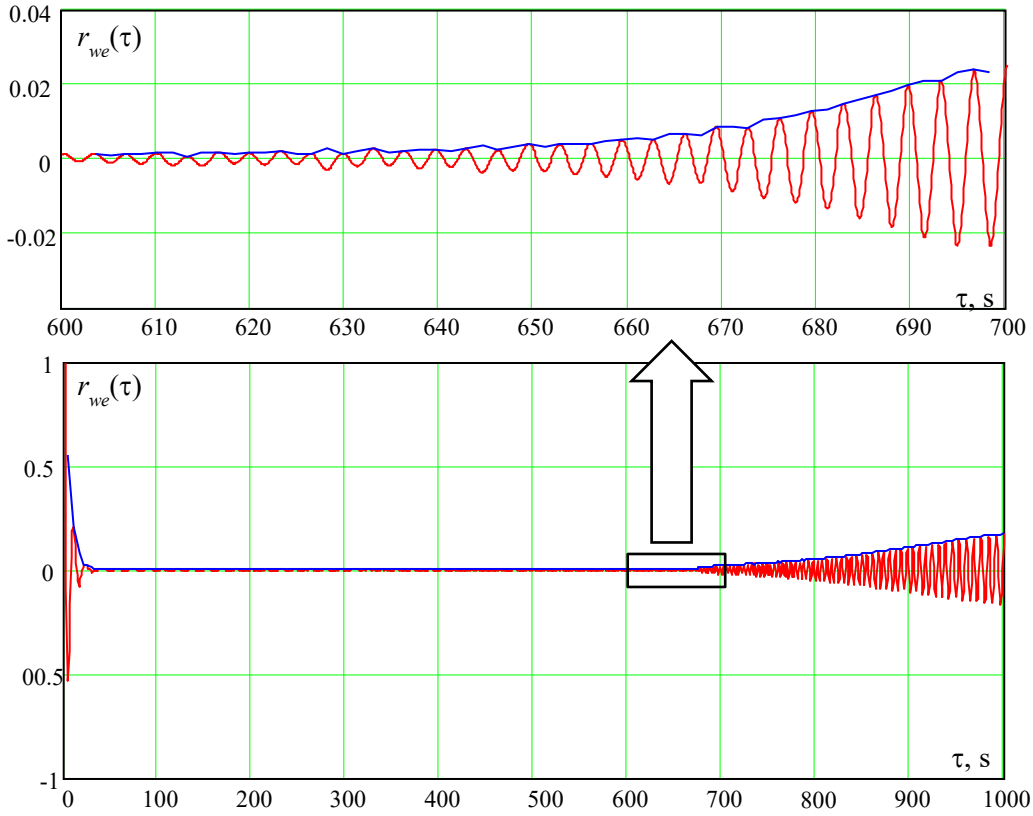

Figure 5.5. Use of Envelope to Detect Inception of the Self-Repeating Effect

A natural criterion for a time of inception of the self-repeating effect is when the envelope starts to increase. However, implementation of this criterion may encounter a problem as a small amplitude oscillation which may be observed on the envelope, but it can be seen clearly in the zoomed-in portion of the autocorrelation plot in Figure 5.5. Averaging every three values seems to remediate this problem, see Figure 5.6.

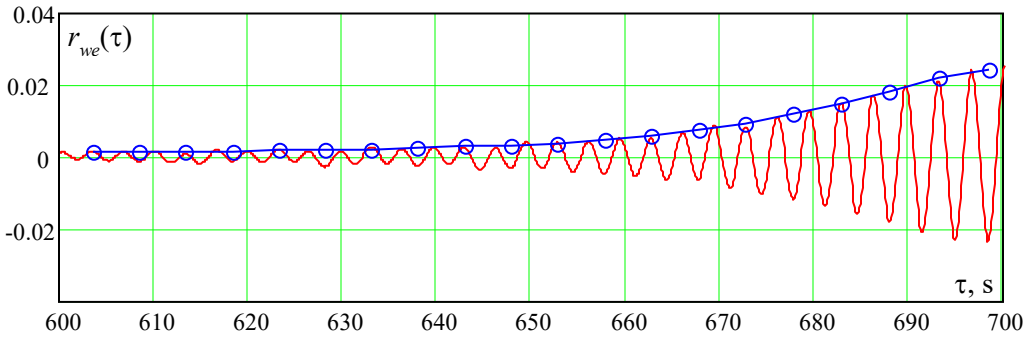

Figure 5.6. On the Detection of Inception of the Self-Repeating Effect

To prevent the criterion of self-repetition to be too sensitive, a threshold of 0.005 is introduced. The search for an increase in the averaged envelope starts only when it exceeds the threshold.

The times where the self-repeating effect caused detection are in Table 5.1. For the initial frequency discretization with 210 frequencies and for these combinations of speed and heading, the wave model (5.1) is only statistically valid for the time durations in the Table 5.1. To increase the time duration of validity of a model in head and oblique seas, the number of frequencies needs to increase to 560. This provides 30 minutes of validity for all the combinations of speeds and headings, see Table 5.2.

Table 5.1. Time of Self-Repeating Effect for 210 Frequencies for the Modal Period of 14 s

	Speed, kn			
Heading, °	5	10	15	20
105	1752	1570	1427	1307
120	1579	1318	1131	988.9
135	1465	1159	962.8	824.6
150	1379	1060	861.3	727.8
165	1335	1005	808.6	677.5
180	1318	988.9	791.1	659.3

Table 5.2. Time of Self-Repeating Effect for 560 Frequencies for the Modal Period of 14 s

	Speed, kn			
Heading, °	5	10	15	20
105	1920	1920	1920	1920
120	1920	1920	1920	1920
135	1920	1920	1920	1920
150	1920	1920	1920	1920
165	1920	1920	1920	1847
180	1920	1920	1920	1802

5.2.3 Roll Damping

Section 3.2.2 of Annex 1 of SDC 6/WP.6 contains the requirements for modeling roll damping. In fulfillment of paragraph 3.2.2.2.1, roll decay test results, available from France, *et al.* (2003), are used. At the same time, LAMP internally computes the wave component of roll damping. Also, LAMP allows for computing roll damping contributions from wing-like lifting appendages (rudders, fins, etc.) and plate-like lifting appendages (bilge keels, etc.). Combining these models with roll decay test data allows reasonable (hopefully) numerical simulations outside of the range of test parameters. Figure 5.7 shows a schematic view of modelled appendages: bilge keels and a rudder.

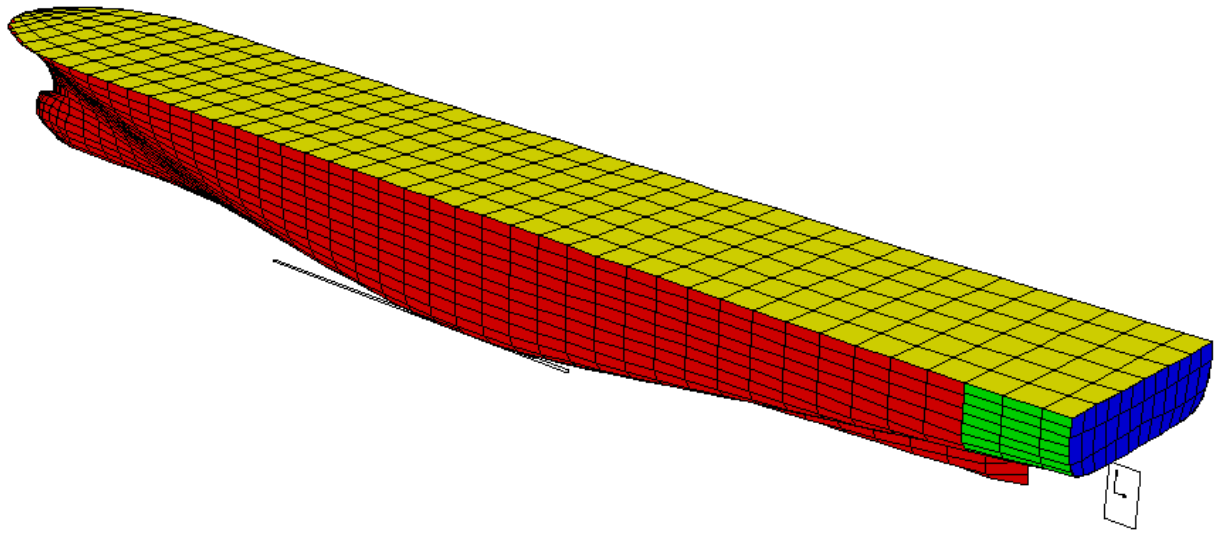

Figure 5.7. Scheme of Appendages Modeled in LAMP

The wave component of roll damping moments as well as forces generated by the appendages present are both in the LAMP simulation and the roll decay test. To avoid double counting of these components LAMP roll damping input is calibrated to match the roll decay test. The calibration technique is described in France *et al.* (2003): essentially, a roll decay test is repeated in LAMP and tries to match the experimental results.

Numerical results of the calibration are given in Table 5.3 and plotted in Figure 5.8. Linear damping coefficients are presented as fractions of critical. Quadratic coefficients for testing and simulation results are given in terms of cancelation, while LAMP input is dimensional.

$$m_{d\varphi}(\dot{\varphi}) = \omega_{\varphi 0}\mu\dot{\varphi} + \delta_2\dot{\varphi}|\dot{\varphi}| \tag{5.9}$$

Where $m_{d\varphi}(\dot{\varphi})$ is roll damping, expressed in terms of acceleration.

Table 5.3. Results of Calibration of Roll Damping

Speed, kn	Natural Frequency, $\omega_{\varphi 0}$, 1/s	Test Results		LAMP Input		Simulation Results	
		Linear μ (–)	Quadratic δ2, 1/s	Linear μ (-)	Quadratic, kg m2	Linear μ (–)	Quadratic δ2, 1/s
5	0.2148	0.01415	0.1863	0.0060	2.9e+09	0.01409	0.185
10	0.2139	0.01968	0.2980	0.0014	6.2e+09	0.01985	0.300
15	0.2131	0.04444	0.2218	0.0170	4.4e+09	0.04451	0.2228

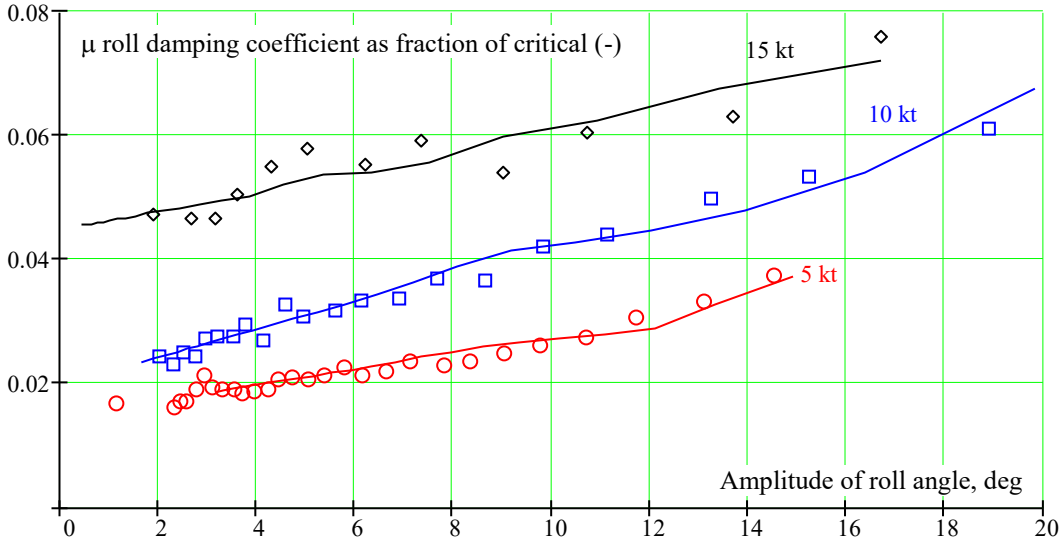

Figure 5.8. Roll Decay Test for Three Speeds (Points – Taken from France et al. 2003) and Computed with LAMP (Solid Lines)

5.2.4 Mathematical Modeling of Forces and Moments

Following requirement in paragraph 3.3.1 of Annex 1 of SDC 6/WP.6, numerical simulations were carried out with 3 degrees-of-freedom (DoF): heave, roll, and pitch. Forward speed was assumed constant and the LAMP-2 solver was used - see Shin et al. (2003) for details.

LAMP-2 computes Froude-Krylov and hydrostatic forces using body-exact formulation with the panel method (Shin et al. 2003) in satisfaction of paragraph 3.2.3.1 of Annex 1 of SDC 6/WP.6.

Radiation and diffraction forces are calculated with Rankine singularities on hull and free surfaces with a damping beach conditions (Shin et al. 2003). Radiation and diffraction calculations are body-linear, as the perturbation potential is solved over mean wetted-hull surface satisfying the requirements of paragraph 3.2.3.2 of Annex 1 of SDC 6/WP.6.

5.2.5 Qualitative Validation of Software for Simulation of Ship Motions: Backbone Curve

Qualitative validation requirements are summarized in Table 4.2 of Annex 1 of SDC 6/WP.6. Demonstration of consistency between calculated roll backbone curve and GZ curve in calm water is required for a software where hydrostatic and Froude-Krylov are calculated with

body exact formulation. The roll backbone curve is a dependency of the roll frequency in calm water on initial roll amplitude.

Numerical calculation of the backbone curve is straight-forward for a single-DoF undamped dynamical system: it requires a series of simulations starting from different initial roll angle. However, to serve the purpose of qualitative validation, the roll backbone curve of a potential-flow code should be computed in the same configuration (i.e. 3-DoF with all the forces, including roll damping) that is used for direct stability assessment. Figure 5.9 shows calculations of the backbone curve made with three different formulations representing successive steps from an undamped single-DoF dynamical system towards actual formulation.

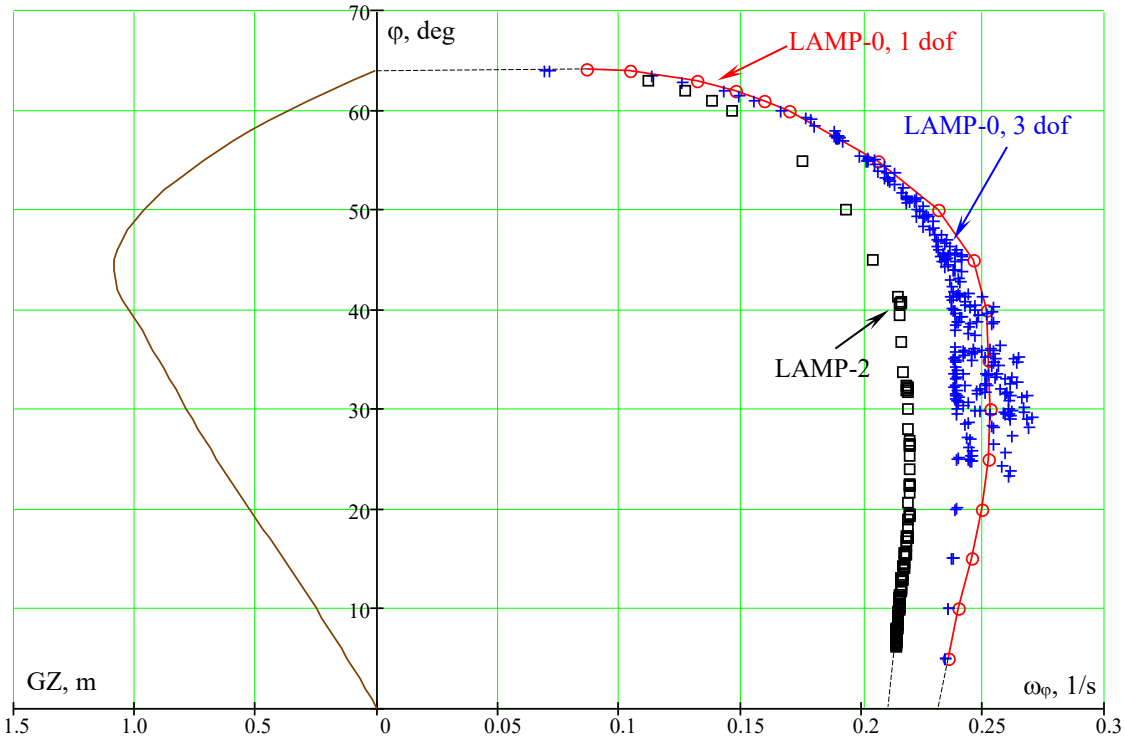

Figure 5.9. Roll Backbone Curve and GZ Curve

The closest LAMP formulation to the undamped, single-DoF dynamical system is the roll-only LAMP-0 setting. LAMP-0 formulation includes hydrostatic and Froude-Krylov forces, while hydrodynamic solver is not invoked, so there is no wave damping for roll motion and it has no added mass. The backbone curve for single-DoF LAMP-0 is shown in read in Figure 5.9. It suggests an initial increase of GM as the backbone shows initial hardening. While it is difficult to see hardening in the GZ curve in Figure 5.9, but the instantaneous GM, shown in Figure 5.10, confirms initial hardening.

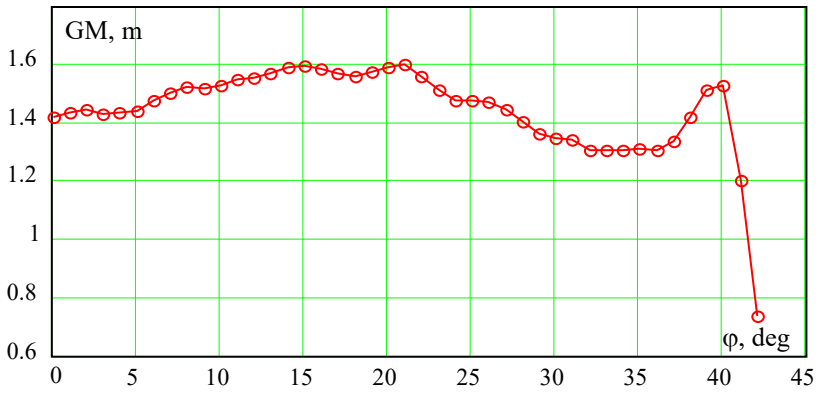

Figure 5.10. Instantaneous GM vs. Heel Angle

As expected, the backbone curve "bends" towards zero with the softening of the dynamical system around 40° of initial amplitude. An unstable equilibrium at the angle of vanishing stability slows down the dynamical system causing the period to grow. Figure 5.11 shows time history of the single-DoF roll motion – as close to the angle of vanishing stability as single-precision arithmetic's allows.

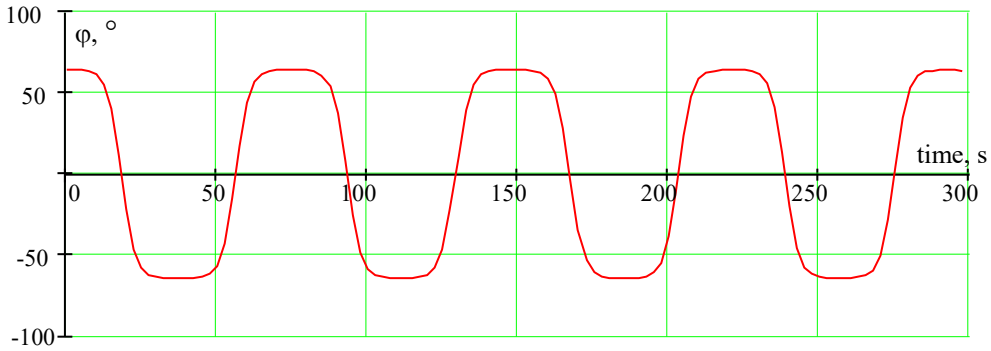

Figure 5.11. Single-DoF Roll Motion in Vicinity of Angle of Vanishing Stability

Inclusion of pitch and heave changes the physical picture as the hydrostatic coupling leads to exchange of energy between the different degrees of freedom. Figure 5.12 shows the time history of how the roll started as close to the angle of vanishing stability as possible. However, in a contrast with the single-DoF case roll motions decreases rapidly, while heave and pitch motion grow as shown in Figure 5.13. The response looks like a series of irregular beatings, which is typical for an undamped oscillator with 3-DoF. As a result, a calculation of natural frequency is performed on half-oscillation basis:

$$\omega_{\varphi}(A_i) = \frac{\pi}{t_{i+1} - t_i} \tag{5.10}$$

Where an amplitude A_i is meant to occur between zero-crossings at t_{i+1} and t_i , see Figure 5.12. The largest amplitude is the first one, A_0 as shown in Figure 5.12, so this leads to the lowest frequency on the backbone curve being computed with a quarter of an oscillation:

$$\omega_\varphi(A_0) = \frac{\pi}{2t_0} \tag{5.11}$$

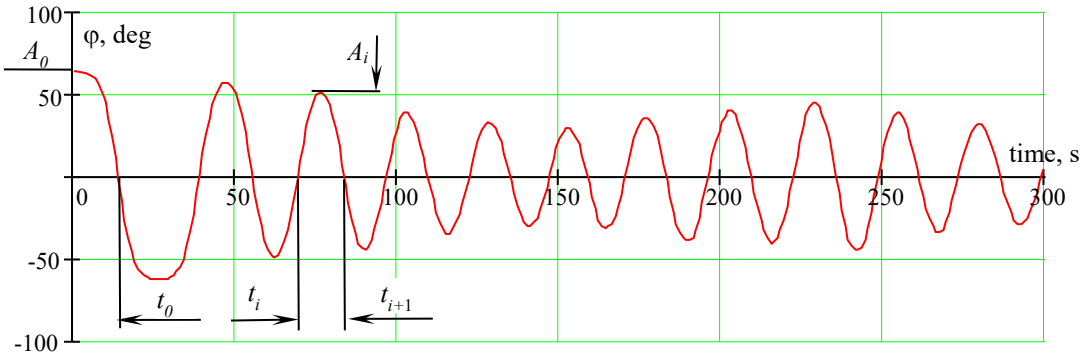

Figure 5.12. Three-DoF Roll Motion in Vicinity of Angle of Vanishing Stability

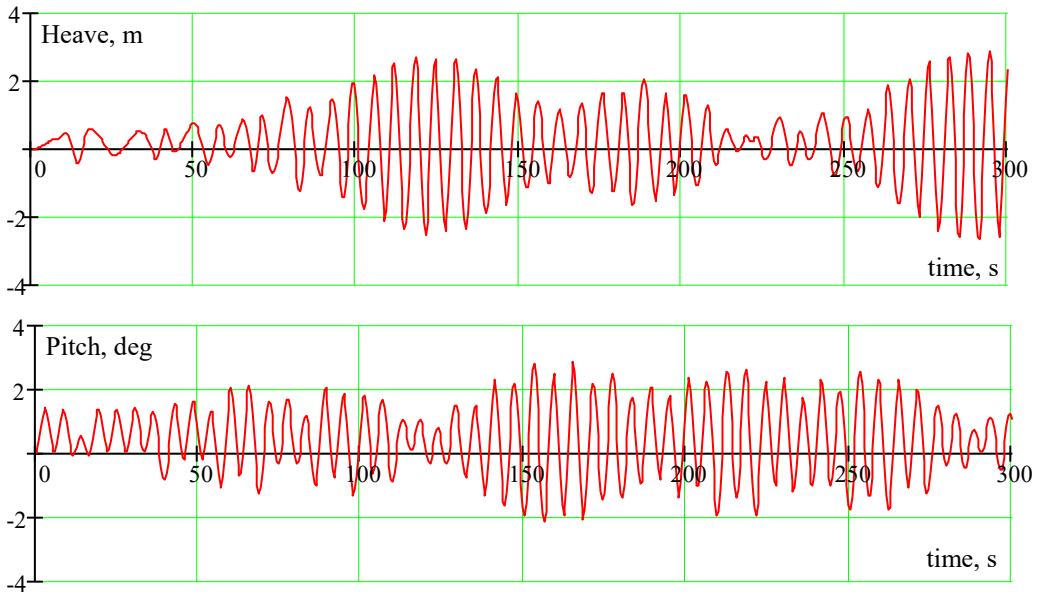

Figure 5.13. Heave and Pitch Motion for 3-dof Case

The backbone curve for 3-dof LAMP-0 settings is shown in Figure 5.9 as blue crosses. The most noticeable feature is that the results are "blurred" starting about 25°. However, after around 50°, the points seem to lay on a curve. "Blurring", evidently, is related to the nonlinear exchange of energy between different degrees of freedom.

When roll motions are relatively small, hydrostatic coupling is not sufficient for noticeable energy to transfer to heave and pitch. On the other hand, a very large roll amplitude only occurs

in the beginning of a record where roll and pitch motion are not large yet, see Figure 5.12 and Figure 5.13.

Finally, a backbone curve is calculated for 3-DoF LAMP-2 setting, that is meant to be used for a direct-stability assessment. The results are shown in Figure 5.9 as black boxes. Since damping is present in all three motions, the time histories are decaying oscillations, see Figure 5.14 and Figure 5.15. As the roll amplitude is not constant, formulae (5.10) and (5.11) are used to compute the backbone curve.

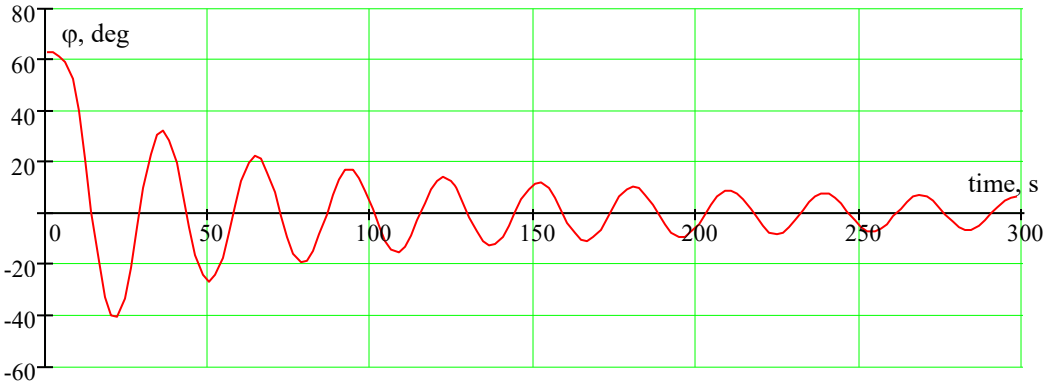

Figure 5.14. Roll Motion for 3-DoF LAMP-2 Case

The backbone curve for 3-DoF LAMP-2 setting, shown in Figure 5.9, does not have a clear "blurring" (or may be small) as the points lay on the curve. As LAMP-2 has all the damping components, pitch and heave are heavily damped motions, so they decay quickly and do not influence period of roll.

The LAMP-2 backbone curve has the same limit for large roll amplitudes as the LAMP-0 curve. This is hardly surprising as the position of unstable equilibrium is essentially hydrostatic and is not affected by radiation forces. The limits for small amplitude is different, as LAMP-0 calculations do not include added masses that are present in LAMP-2 calculations, leading to a difference in natural frequency of roll motions. There is also a small difference caused by damping itself, known from linear differential equations with constant coefficients.

In general, the topology of the backbone curve has been found to be consistent with the shape of the GZ curve, thus confirming qualitative validity of LAMP-2 (and LAMP-0 as well).

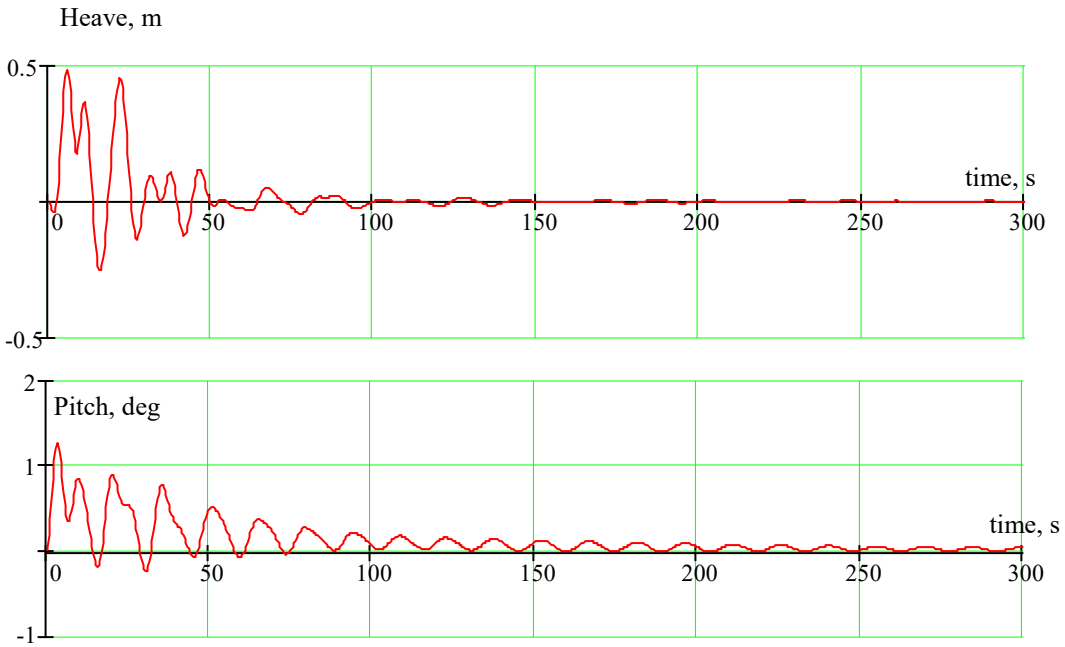

Figure 5.15. Heave and Pitch Motion for 3-DoF LAMP-2 Case

5.2.6 Qualitative Validation of Software for Simulation of Ship Motions: Response Curve

Another qualitative validation requirement from Table 4.2 of Annex 1 of SDC 6/WP.6 is a demonstration of consistency between the calculated roll backbone curve and the roll response curve. Such a demonstration is available from Shin et al, (2003). Calculations were done for a fishing vessel, and a panel model of her hull is in Figure 5.16 (without a forecastle), while the principle characteristics are given in the Table 5.4 GZ curve, which is used for the response curve calculations is in Figure 5.17.

Table 5.4. Principle Characteristics of a Vishing Vessel from (Shin et al., 2003)

Length BP, m	22
Breadth molded, m	6.62
Draft amidships, m	2.7
KG , m	2.78
Displacement, MT	197
GM ,m	0.22

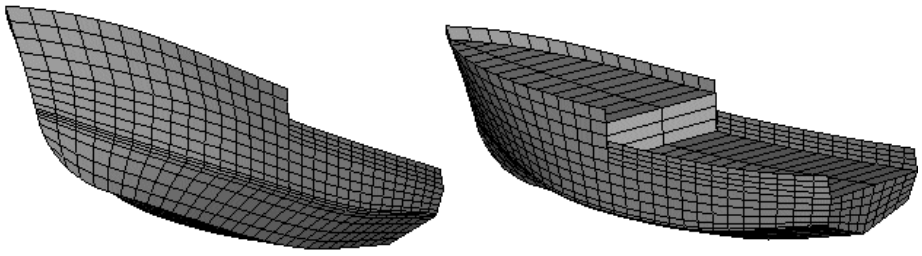

Figure 5.16. Hull Geometry of a Fishing Vessel (Shin et al., 2003)

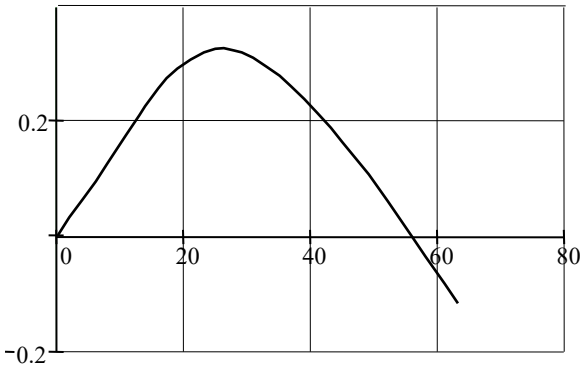

Figure 5.17. Righting Arm (GZ) Curve in Meters of the Fishing Vessel for Response Curve Calculation (Shin et al., 2003)

Calculations were carried out with LAMP-2 and consisted of a series of regular wave simulations in beam seas. After completion of initial transient a positive and negative peaks were reported. These results are in Figure 5.17 as boxes for positive peaks and negative peaks. Simulation start from high and low wave frequencies. Initial conditions for the run were assigned using the steady state response, achieved for the previous wave frequency. The backbone curve in Figure 5.18 was computed using an approximate formula.

It is clear that the roll response amplitudes computed by LAMP are located on both sides of this approximate backbone curve. Generally, they follow the topology of the response curve computed with equivalent linearization and shown as a solid curve in Figure 5.18. The softening of dynamical system is expect about 18-20° (0.3 rad) caused by the influence of the maximum of the GZ curve around 25° (see Figure 5.17). The backbone follows the expected tendency, starting to bend towards zero somewhere around 0.3 rad, see Figure 5.18a.

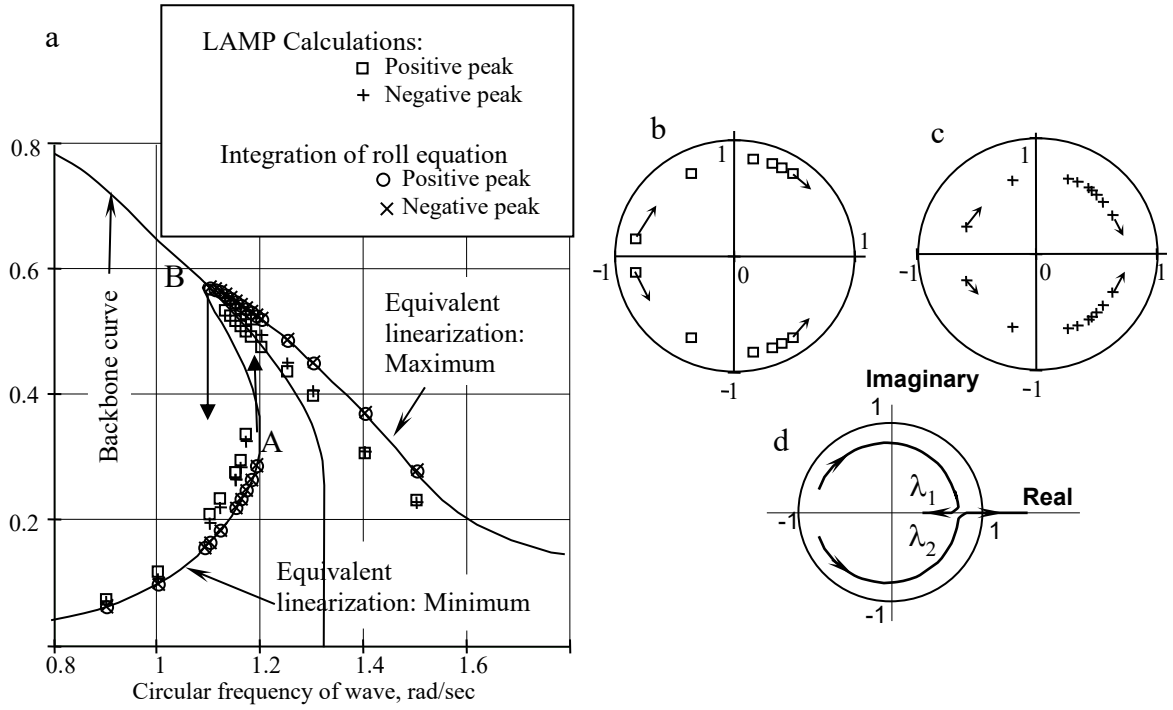

Figure 5.18. Response Curve of Roll Based on LAMP Calculation, Numerical Integration of Nonlinear Roll Equation and Equivalent Linearization (a); Eigenvalues of Jacobean Matrix for (b) LAMP Calculation, (b) Nonlinear Roll Equation (d) Theoretical Prediction; Circular Frequency Range 09-1.18 rad/s: Low Response, Wave Amplitude 0.4 m (Shin et al., 2003)

LAMP calculations were supplemented with the direct numerical integration of the approximate differential equation for rolling while using the actual GZ curve and approximate Froude-Krylov wave excitation:

$$\ddot{\varphi} + 2\delta_{\varphi}\dot{\varphi} + \omega_{\varphi 0}^2 f(\varphi) = \alpha_W \omega_{\varphi 0}^2 \sin(\omega_W t) \tag{5.12}$$

Where $\omega_{\varphi 0}$ is a natural roll frequency (for small roll angles), δ_{φ} is the roll damping coefficient (determined form roll decay LAMP simulations), α_W amplitude of wave slope, ω_W is wave frequency, while stiffness function is expressed through the GZ curve as:

$$f(\varphi) = \frac{W \cdot GZ(\varphi)}{I_x + A_{44}} \tag{5.13}$$

Where W weight displacement, I_x the transverse moment of inertia of ship mass and A_{44} is added mass in roll. Numerical integration of the ordinary differential equation (5.12) were approached in the same manner as LAMP simulations: the steady state condition of the previous frequencies are used as initial conditions for the next wave frequency. The results of numerical integration are shown in Figure 5.18a as circles for positive peaks and "X's" for the negative peaks.

As it is expected from the Nonlinear Dynamics (e.g. Thompson and Stewart, 1986), the bending of the backbone curve causes a response curve to fold, forming a range of frequencies where two stable steady state responses are possible; identified by points A and B in Figure 5.18a. The observation of the folding of the LAMP response survey demonstrate the consistency

between the backbone curve and the response curve in satisfaction of the requirement formulated in line 2 of the Table 4.2 of Annex 1 of SDC 6/WP.6.

Shin et al. (2003) provides an additional demonstration of qualitative validity of nonlinear roll modeling with LAMP. The folding of the response curve leads to appearance of two stable steady state solutions, known as a "fold bifurcation". The appearance of this bifurcation is usually indicated by an escape of the eignevalues of the perturbed solution from the unit circle in real and positive discretion as shown in Figure 5.18d (see Thompson and Stewart, 1986).

To obtain this additional indication of the possibility of fold bifurcation, Shin et al. (2003) computes the eigenvalues of a Jacobean matrix about the roll angles and rates by applying a small perturbation in a roll angle and rate to the steady state solution:

$$J = \begin{bmatrix} \frac{\varphi(t_0+T)-\varphi(t_0)}{\Delta\varphi} & \frac{\varphi(t_0+T)-\varphi(t_0)}{\Delta\dot{\varphi}} \\ \frac{\dot{\varphi}(t_0+T)-\dot{\varphi}(t_0)}{\Delta\varphi} & \frac{\dot{\varphi}(t_0+T)-\dot{\varphi}(t_0)}{\Delta\dot{\varphi}} \end{bmatrix} \tag{5.14}$$

Where $\Delta\varphi$ is a small perurbation of the steady state solution by roll angle, $\Delta\dot{\varphi}$ is a small perturbation of the steady state solution by roll rate, t_0 time instant of perturbation, T is relevant period – as in the period of regular wave excitation, $\varphi(t_0 + T)$ is the value of perturbed roll angle after a period, $\varphi(t_0)$ is the value of unperturbed roll angle, $\dot{\varphi}(t_0 + T)$ is the value of perturbed roll rate after a period, and $\dot{\varphi}(t_0)$ is the unperturbed roll rate.

Trajectories of eigenvalues of Jacobean are computed on a LAMP solution and are in Figure 5.18b, while results for ordinary differential equations are in Figure 5.18c. While accuracy of calculations (Shin *et al.* 2003) were insufficient to trace the eigenvalues all the way to escape, the observed behavior was similar to one expected from theory and shown in Figure 5.18d. This additional demonstration further confirms that LAMP reproduced nonlinear roll behavior consistent with existing knowledge. More details in the context of direct stability assessment are available from Peters *et al.* (2019).

5.2.7 Qualitative Validation of Software for Simulation of Ship Motions: Change of Stability in Waves

The third qualitative validation requirement from Table 4.2 of Annex 1 of SDC 6/WP.6 is a demonstration of capability to reproduce wave pass effect. The objective is to verify that the stability decreases when the wave crest is located near the midship sections.

Following Belenky and Weems (2008), verification of the instantaneous-stability variation in waves with numerical simulation is carried out in the following steps:

1. Set the wave length equal to ship length
2. Set a simulation run in following seas with the ship forward speed equal to the wave celerity
3. Set an initial position of a ship to have wave trough to be near the midship section. The Ship is expected to remain stationary relative to the wave, see Figure 5.19
4. Apply a constant external heeling moment
5. Record ship motions until the transition is completed and equilibrium state is achieved; extract the equilibrium heel angle
6. Repeat the procedure for different values of the external heeling moment

7. Repeat the procedure for an initial position of a ship, corresponding to a location of wave crest near the midship section

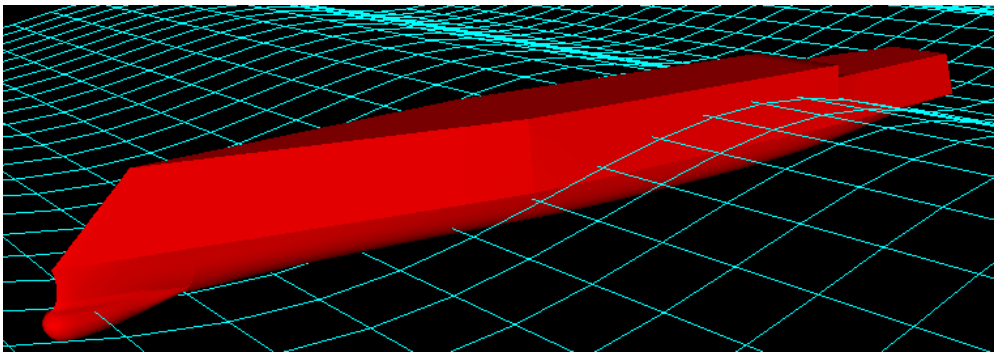

Figure 5.19. Simulation of Heading with Wave Celerity (Belenky and Weems, 2008)

Calculations were carried out for ONR tumblehome top configuration (Bishop *et al.*, 2005), principle characteristics are given in Table 5.5. External moment was implemented using an option in LAMP input; this external moment, however, it can be only applied in Earth-fixed coordinate system.

Application of the heeling moment in Earth-fixed coordinate does serve the purpose of this qualitative validation, however, some differences may be observed when comparing to the GZ curve, as it normally computed the assumed-heeling moment in a ship-fixed coordinate system. To check how large this discrepancy may be, the calculations were carried out for calm water first, see Figure 5.20.

Circles in Figure 5.20 show how the heel angle was achieved under a series of heeling moments defined in the Earth fixed coordinate system. The achieved angle is determined by averaging the last 20 % of the time history. As seen from Figure 5.20, there is some discrepancy between the GZ curve and the heeling-lever curve (heeling lever vs. achieved heel-angle). The discrepancy increases for larger values of the heeling lever. It can be explained by the influence of trim that reaches up to 0.6° for 14° of achieved heel.

Table 5.5. Principle Characteristics of a ONR Tumblehome Top Configuration

Length BP, m	154
Breadth molded, m	18
Draft amidships, m	5.5
KG , m	8.32
Displacement, MT	8675.6
GM ,m	1.5

Further calculations are carried out in waves. Wave length is equal to ship length (154 m), wave height is 6 m. Two wave positions were used for qualitative validation: the wave crest amidships and the wave trough amidships.

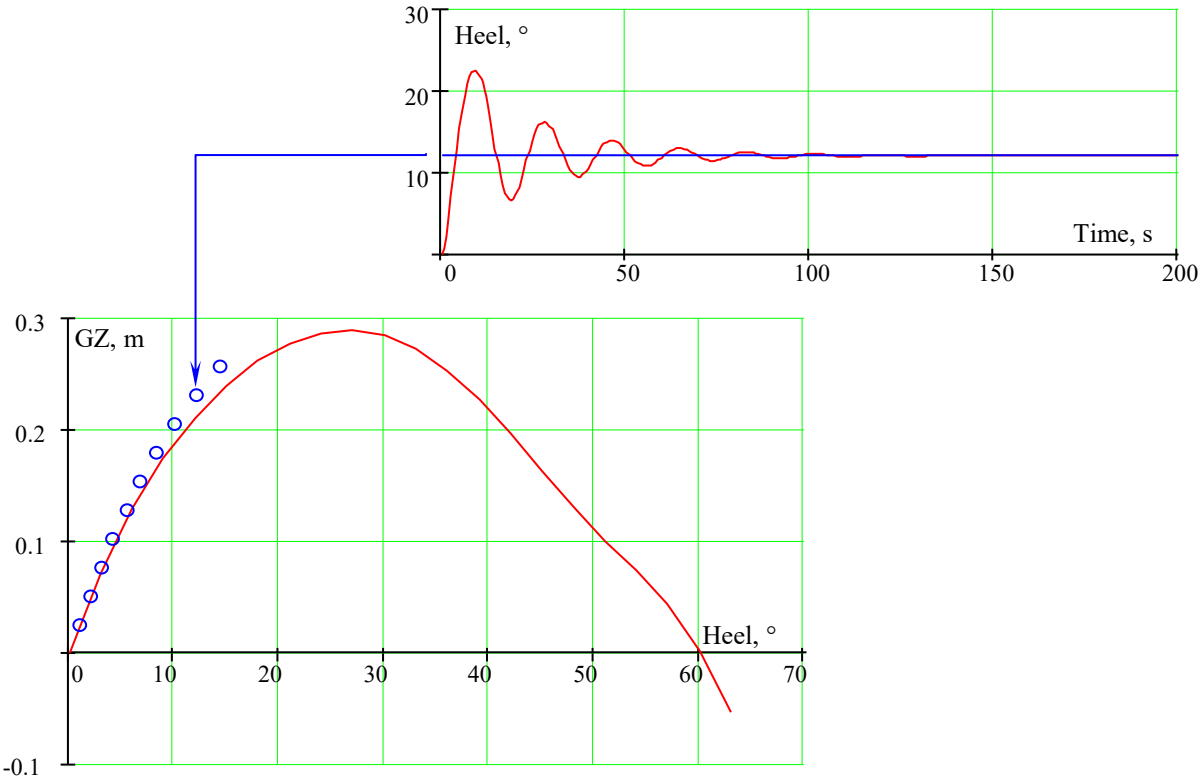

Figure 5.20. GZ Curve in Calm Water (Solid Line) and Heeling Lever Curve (Circles)

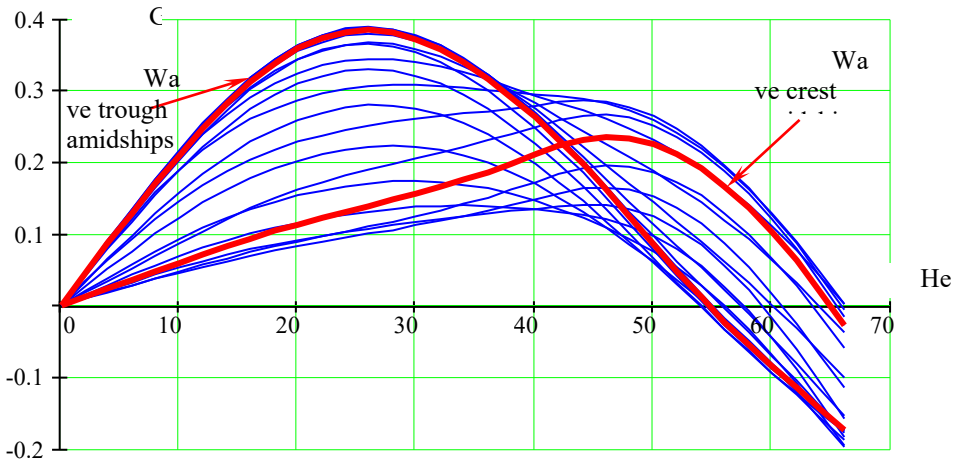

Figure 5.21. GZ Curve in Wave (Wave Length 154 m, Save Height 6 m)

Figure 5.22 and Figure 5.23 show achieved heel-angles under the external heeling moment (heeling lever curves), computed by LAMP-0 and LAMP-2, respectively for wave crest and wave trough located amidships. GZ curves that are in waves for the same wave location are also shown as a guidance along with GZ curve in calm water.

Figure 5.22 and Figure 5.23 demonstrate a change of stability in waves: achieved heel-angle under the same heeling moment is significantly larger when wave crest is located amidships, compared to when the wave through is located amidships. These figures also show that the stability on a wave trough is better when compared with calm waters, while stability on the wave crest is worse than in calm water.

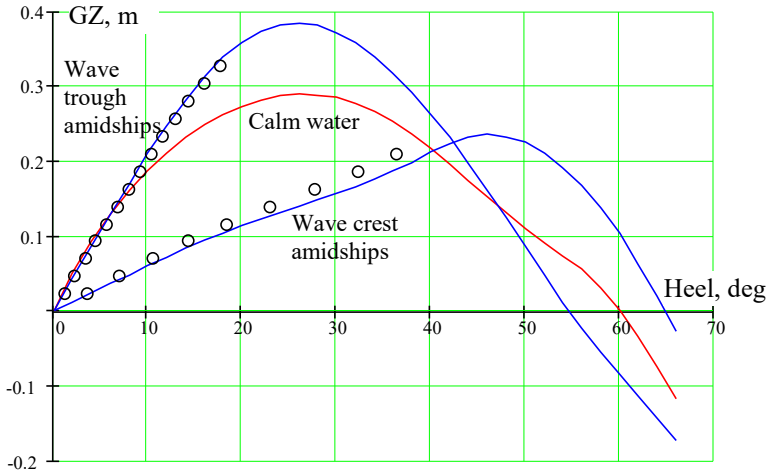

Figure 5.22. GZ Curves (Solid Lines) and Heeling Lever Curve (Circles) Computed with LAMP-0

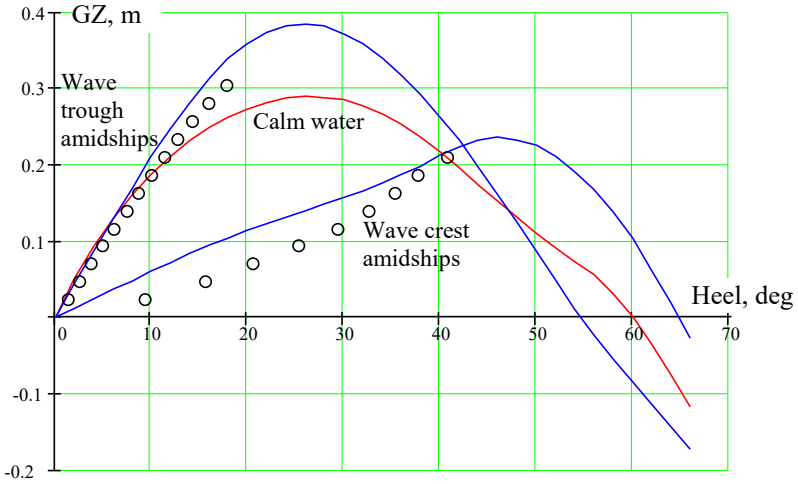

Figure 5.23. GZ Curves (Solid Lines) and Heeling Lever Curve (Circles) Computed with LAMP-2

Small discrepancies between GZ curves in wave and LAMP-0 calculations (Figure 5.22) can be explained by the application of a heeling moment in an Earth-fixed frame of reference.

This difference is larger in the case of the LAMP-2 calculation due to influences of diffraction and radiation forces that are included in LAMP-2 calculations but excluded from LAMP-0 calculations.

Note how self-consistency verifications, described in Belenky and Weems (2008), found no discrepancies. While the computation technique in the present study is similar to the cited reference, the objective of Belenky and Weems (2008) was different. The self-consistency verification was aimed on an instantaneous GZ curve, as further study went on for probabilistic characteristics of stability in irregular waves. The Calculation of the instantaneous GZ curve does NOT include balancing in heave and pitch, as it must follow d'Alembert principle and use actual instantaneous positions of a ship (Belenky et al., 2010). Spyrou et al. (2014) shows an example of use of the instantaneous GZ curve in wave to explain a sudden large single-roll angle.

While these references can be used as a demonstration of qualitative validity of LAMP for reproducing variation of stability during a wave pass, Figure 5.22 and Figure 5.23 provide sufficient information to satisfy the requirement on changes of stability in waves from Table 4.2 of Annex 1 of SDC 6/WP.6 as well.

5.2.8 Qualitative Validation of Software for Simulation of Ship Motions: Principal Parametric Resonance

The fourth qualitative validation requirement from Table 4.2 of Annex 1 of SDC 6/WP.6 is a demonstration of capability to reproduce a principal-parametric resonance. The objective is to observe increases and the stabilization of amplitudes in exact following- or head-seas when encountering a frequency that is about twice the natural roll frequency.

Figure 5.24 shows the time history of LAMP-2 simulations in exact following seas for C11-class containerships at zero forward speed. Principle dimensions are in Table 2.3 with the exception of a draft that was taken as 12.7 m, KG = 19.00 leading to GM = 1.29 m, and a natural roll frequency of 0.199 s^{-1}; the wave height was 2 m, while the wave frequency 0.42 s^{-1} (which equals the encounter frequency for zero forward speed). The entire frequency range of principle-parametric roll, computed for these conditions, is in Figure 5.25.

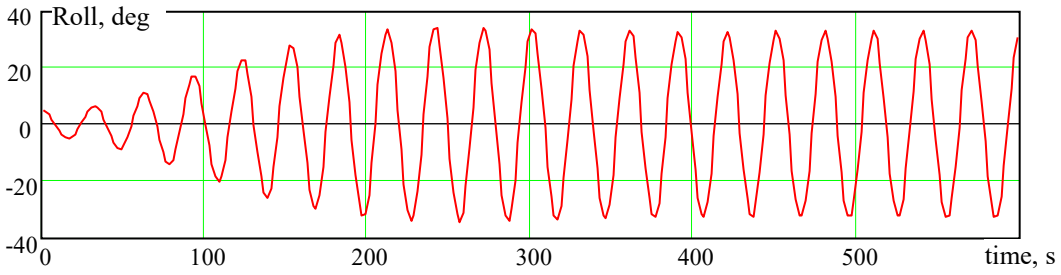

Figure 5.24. Time History of Principle Parametric Resonance Computed with LAMP-2 for C11-Class Containership with Natural Roll Period 0.199 s^{-1} and Zero Forward Speed; Wave Height 2 m, Wave Frequency 0.42 s^{-1}

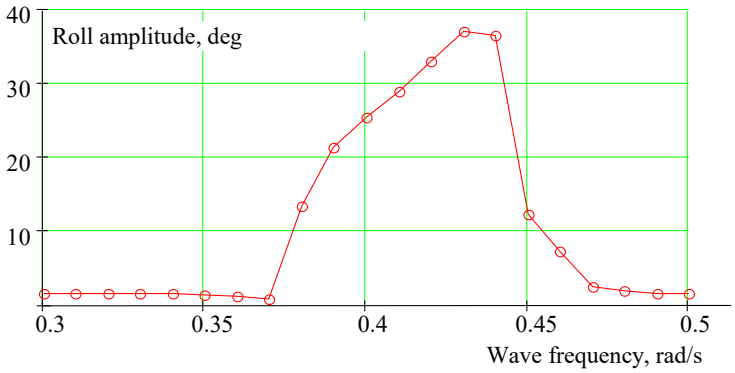

Figure 5.25. Frequency Range of Principle Parametric Resonance Computed with LAMP-2 for C11-Class Containership with Natural Roll Period 0.199 s^{-1} and Zero Forward Speed; Wave Height 2 m

There is no direct forcing in roll direction, in following seas, so parametric resonance can be the only reason of increase of roll amplitude; non-zero amplitude response is grouped around wave (encounter) frequency to roll frequency of about 2, thus it must be the principle parametric resonance. More demonstrations of principle-parametric resonance reproduction can be found in references – see Figure 30 of France et al. (2003) for a speed of 15 kn and wave heights from 1 to 4 m. Several examples are also found in Shin et al. (2004). The latter reference contains positive comparison of parametric roll-range with theoretical approximation based on the Mathieu equation – see Figure 25 of Shin et al. (2004).

Based on provided information, one can conclude that LAMP satisfies the requirements of qualitative validation for principle parametric-roll reproduction as formulated in the fourth line of Table 4.2 of Annex 1 of SDC 6/WP.6.

5.2.9 Quantitative Validation Requirements

Indicative requirements and acceptance criteria for the quantitative validation of ship-motion simulation-software for direct stability assessment are summarized in Table 4.3 of Annex 1 of SDC 6/WP.6. Lines 1, 2, and 4 are relevant for parametric roll failure mode.

Line 1 of table 4.3 of Annex 1 of SDC 6/WP.6 contains requirements for the response curve of parametric roll: the maximum (over encounter frequency) roll amplitude should not be under predicted for more than 10 % if the amplitude that is below the angle of maximum of GZ curve and 20 % otherwise. At the same time, under-prediction less than 2 % can be disregarded. A comparison of LAMP results to model test data on parametric roll is available from France et al. (2003) in Figure 28. The model test included all 6 DoF and was run for a fixed speed of 10 kn in a wave with full scale height of 8.4 m and period of 14 s. The difference between parametric roll amplitude observed in experiment and computed with LAMP-2 was within 1°. However, the comparison is only available for a single frequency, one can accept partial satisfaction of the requirements in line 1.

Line 2 of Table 4.3 of Annex 1 of SDC 6/WP.6 contains the requirements for response curve of synchronous roll. The authors of this report are not aware of published data on such a comparison.

Line 4 of Table 4.3 of Annex 1 of SDC 6/WP.6 contains requirements for variance testing for parametric roll. The objective is to demonstrate that the correct (in terms of statistics) modelling of roll response in irregular waves. The 26th ITTC specialist committee on stability in waves conducted a benchmark on numerical simulation methods for prediction of the parametric roll in in head seas (see Reed, 2011, 2019). The benchmark, however, turned inconclusive as there were not enough experimental and simulation data to estimate variance, due to practical non-ergodicity of parametric roll. Reed (2011, 2019) concluded that at least 7 to 10 records (20-30 minutes long) are needed for a conclusive variance estimate. No updated information has been published yet on comparison of model test and simulation on variance estimates. However, van Walree and de Jong (2019) reported a successful reproduction of experimental irregular parametric response using panel code PANSHIP, which gives the hope that a successful variance test will become available in the near future.

Table 4.3 does not contain any requirements for other degrees of freedom or responses. Nevertheless, it is appropriate to mention here about favorable comparisons between the model test and LAMP-2 responses are described by Shin *et al*. (2003). These responses include heave, pitch, bow acceleration, and the vertical-bending moment. Favorable comparisons between experimental and simulated pitch motion are shown in Figure 28 of France *et al*. (2003).

The lack of easily accessible data allowing quantitative validation of software for direct stability assessment can be explained by how the second-generation intact-stability criteria have not yet been published. Having this in mind, this study partially satisfies requirements of quantitative validation for direct stability assessment.

5.2.10 Direct Counting Procedure for Parametric Roll

Guidance on direct counting procedures is available from section 5.4 of Annex 1 of SDC 6/WP.6. Following requirements of paragraph 5.4.1 of Annex 1 of SDC 6/WP.6, multiple independent realizations were generated with LAMP-2. To obtain independent realizations of ship motions, independent realizations of wave elevations were used. To obtain independent realizations of wave elevation a different set of initial phases φ_{wi} were used in formula (5.1). Following recommendations of Reed (2011, 2019), 20 realizations were generated to account for practical non-ergodicity of expected parametric roll response more fully.

Sample numerical simulations were performed for a C11-class containership, of which the panel model of her hull is shown in Figure 5.1. Principle dimensions are shown in Table 2.3 with the exception of the mean draft that was taken as 11.5 m, there was no trim, KG = 18.95 leading to GM = 1.4 m. The modeling of roll damping is described in the subsection 5.2.3.

To avoid the influence of initial conditions, the wave elevations were linearly ramped from zero to their nominal value during the first 100 s of simulations. To avoid the development of parametric resonance during wave ramping, roll motions were kept at initial 5°, see Figure 5.26. This technique does not prevent immediate development of parametric roll once the ship is "released" if the conditions of development of parametric resonance are satisfied, see roll record in Figure 5.28.

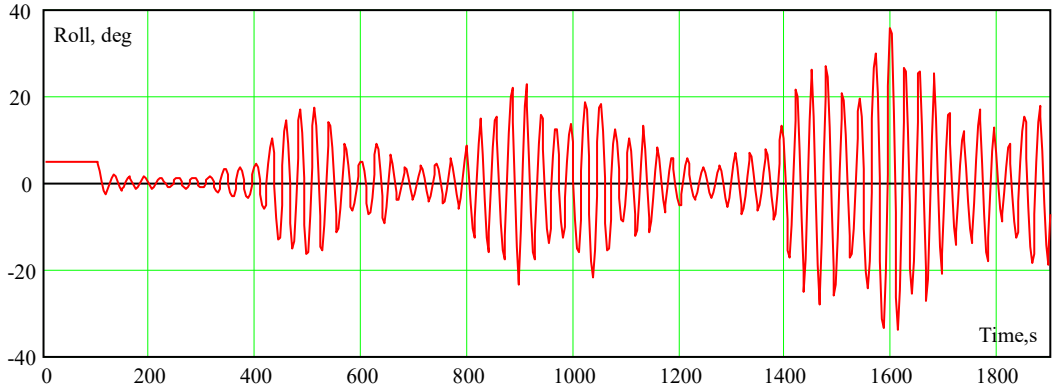

Figure 5.26. An Example of Roll Response: Record #16, Heading 1° (Almost Following), Speed 5 kn, Significant Wave Height 3.5 m, Modal Period 12 s, Mean Zero-Crossing Period 8.5 s

For each environmental condition (see the discussion on the environmental conditions in paragraph 5.2.11), simulations were carried out for five speeds from 0 to 20 kn and for wave headings from following to head seas with a 30° increment. Following seas are modeled with 1° while head seas are modeled with a 179° heading to avoid a non-conservative estimate.

Parametric resonance requires the initial disturbance to start (zero is an unstable steady state solution for parametric roll). If no initial disturbance is provided, parametric resonance will start anyway because the rounding error of the computer's arithmetic will play a roll of such disturbance. Since the rounding error is very small, development of the parametric resonance may take a long time, leading to a non-conservative estimate of failure-level exceedance rate.

Since long-crested waves are used, no roll excitation will be applied at an exact 0° heading. If parametric roll will not develop from the initial roll angle (as seen in Figure 5.26), roll motion may decay completely before the conditions of parametric resonance are encountered. Similar situations may arise if the parametric roll conditions would not occur for relatively long time. To avoid these artificial situations (as real waves are always short-crested) following seas are modeled with a 1° heading and head seas are modeled with a 179° heading.

Per the requirements of paragraph 5.4.2 of Annex 1 of SDC 6/WP.6, the counting procedure should ensure the independence of the counted stability failures event. A practical way to judge if the events related to a stochastic process are independent is to compare time between the events with a decorrelation time of the process. The decorrelation time is a duration when autocorrelation function value becomes insignificant, so two time sections of the process are considered uncorrelated. Assuming that uncorrelated values are independent (it is an assumption, as a correlation only indicates a dependence in terms of the second moment), the decorrelation time can be used as an approximate indicator of independence of the events, related to a stochastic process.

The autocovariance function (autocorrelation function is a normalized autocovariance function) of a single realization of an ensemble is estimated as:

$$\hat{R}_{\varphi}(\tau_i) = \frac{1}{N}\sum_{j=1}^{N-i}\left(\varphi_j - \hat{E}_{a\varphi}\right)\left(\varphi_{i+j} - \hat{E}_{a\varphi}\right) \tag{5.15}$$

Where N is a number of a point in the realization, τ_i is i-th time lag, while $\hat{E}_{a\varphi}$ is a mean estimate of the ensemble:

$$\hat{E}_{a\varphi} = \sum_{k=1}^{Nr} W_k \hat{E}_{\varphi k} \quad (5.16)$$

Where Nr is the number of realizations in an ensemble, and W_k is a statistical weight of k-th realization:

$$W_k = \frac{N_k}{\sum_{k=1}^{Nr} N_k} \quad (5.17)$$

$\hat{E}_{\varphi k}$ is a mean estimate of k-th realization:

$$\hat{E}_{a\varphi} = \sum_{k=1}^{Nr} W_k \hat{E}_{\varphi k} \quad (5.18)$$

Then the ensemble estimate of autocovariance function is expressed as

$$\hat{R}_{a\varphi}(\tau_i) = \sum_{k=1}^{Nr} W_k \hat{R}_{\varphi k}(\tau_i) \quad (5.19)$$

Where $\hat{R}_{\varphi k}(\tau_i)$ is the autocovariance estimate of of k-th realization. An estimate of autocorrelation function is obtained by normalizing the estimate of autocovariance function by its zero-term which is an ensemble variance estimate in this context:

$$\hat{r}_{a\varphi}(\tau_i) = \frac{\hat{R}_{a\varphi}(\tau_i)}{\hat{R}_{a\varphi}(0)} \quad (5.20)$$

Ensemble estimate of autocorrelation function is shown in Figure 5.27

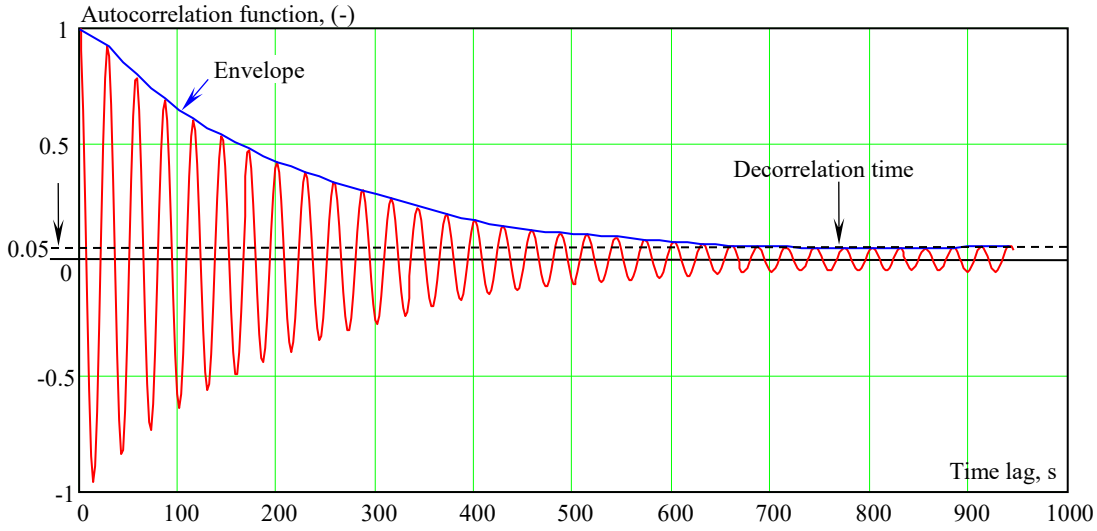

Figure 5.27. Ensemble Estimate of Autocorrelation Function. Heading 1°, Speed 5 kn, Significant Wave Height 3.5 m, Modal Period 12 s, Mean Zero-Crossing Period 8.5 s

Decorrelation time is when the autocorrelation drops below the significance level. Following industry practice, where the significance level for hypothesis testing is set to 0.05 (it means that the probability below 0.05 is considered infinitely small), the same value is used here

for decorrelation time. Since the estimate of autocorrelation function has an oscillatory character, it makes sense to use its envelope rather than the autocorrelation function itself, see Figure 5.27.

The decorrelation time was evaluated as the first intersection of the envelope with the significance level. The value for decorrelation time was determined to be 759.7 s. It is a rather large value compared to wave elevation or synchronous roll where decorrelation time is usually around 1 minute. Large autocorrelation times for parametric roll generally is expected as it is known that autocorrelation function of parametric roll does not decay for a long time, see section 7.5 of Belenky and Weems (2012).

Another aspect of the evaluation of decorrelation time for parametric roll is related with a case when the estimate of autocorrelation function does not reach the level of significance. Two subcases are possible:

- An envelope has at least one minimum, and the lowest minimum is above the significance level; this is a result of insufficient data for the estimation of autocorrelation function to the level of significance. Time lag, corresponding to the global minimum of the envelope is used as a decorrelation time.
- An envelope monotonically decreases, but does not reach the significance level; this is likely caused by insufficient length of the estimate of autocorrelation function; as it may be difficult to estimate the autocorrelation function beyond half of the record length, the conservative solution is to take the decorrelation time equal to the length of the record.

Paragraph 5.4.3 of Annex 1 of SDC 6/WP.6 contains guidance on a direct counting procedure based on estimation of the stability failure rate through averaging the time before the first failure occurs. Application of this procedure implicitly requires that each realization must contain a failure. This requirement is impractical. The valid length of roll realization depends the valid length of the wave elevation realization. The latter depends on frequency discretization. To ensure absence of a self-repeating effect, as required by the paragraph 3.2.1.2 of Annex 1 of SDC 6/WP.6, the number of frequencies may need to be increased, if longer wave records are required, see subsection 5.2.2. As the time before the first stability failure occur is random, the number of frequencies will have be set with a trial and error approach, which impractically increases computational cost.

The application of a direct counting procedure, described in paragraph 5.4.3 of Annex 1 of SDC 6/WP may be practical, if a different model of waves, is used that it is not prone for self-repeating effect. The auto regression/moving average (ARMA) wave model holds a promise (Spanos, 1983; Degtyarev et al., 2019). Recently the ARMA model becomes suitable for ship motion simulation as an algorithm for pressure calculation has become available (Degtyarev and Gankevich, 2019). However, its implementation and application still requires work (Weems et al., 2016).

Another way of a possible application of the procedure, described in paragraph 5.4.3 of Annex 1 of SDC 6/WP.6 is to implement censoring, see Meeker and Escobar, (1998). Censoring in the considered case is adding a “virtual” failure at the end of each realization that did not show a failure to take better account of the total simulation time, available for the case. Belenky and Campbell (2011) show that unless censoring is implemented, estimation of the rate of failures through averaging of time before the event, leads to significant bias.

Paragraph 5.4.4 of Annex 1 of SDC 6/WP.6 describes an alternative direct counting procedure. It is based on a number of realizations where the failure has been recorded. However, it cannot be applied if a failure has been encountered at each realization, which is possible in case of parametric roll. Also, if two or more independent failures were observed for a single realization, the described procedure may provide a biased estimate, as only one failure will be counted.

To avoid problems associated with the application of direct counting procedures described in paragraph 5.4.3 and 5.4.4 of Annex 1 of SDC 6/WP.6, a procedure based on Belenky et al. (2016a) is recommended[2]. This recommended procedure has been tested against other techniques (Belenky and Campbell, 2011), and is based on assumption of binomial distribution of the failure rate estimate (Leadbetter et al., 2011, 2019). The binomial distribution of the estimate leads to Poisson flow of failure events and exponential distribution of time before and between the failures, which is essential for the direct counting procedure. The application of the procedure is illustrated with the level of failure set to 20° instead of 40° to demonstrate how the independence of events is assured.

- Evaluate the de-correlation time T_{dc} as described in beginning of this subsection. In the considered example T_{dc} =759.7 s
- Count all upcrossings of the level ±20° and record time instant when it occurred;
- The first upcrossing after the ramp time is the first independent event. Then find an upcrossing that occurred after T_{dc} from the first upcrossing in the record; this will be the second event; continue in the same manner till the end of the record. This is a number of independent upcrossings N_{Uk} for the k-th record.
- Apply steps 2 and 3 to all records, count all the independent upcrossings $N_{aU} = \sum_{k=1}^{Nr} N_{Uk}$
- Compute the failure rate estimate as:

$$\hat{\lambda} = \frac{N_{aU}}{\Delta t \sum_{k=1}^{Nr} N_k} = \frac{N_{aU}}{T_a} \tag{5.18}$$

Where Δt is the time increment used in the simulation, while $T_a = \Delta t \sum_{k=1}^{Nr} N_k$ is the total time available in all the records

- The number of independent upcrossings N_{aU} is a random variable with binomial distribution. The binomial distribution has only one parameter – the probability that the event will occur at any particular instant of time. The this probability can be estimated as:

$$\hat{p} = \frac{N_{aU}}{\sum_{k=1}^{Nr} N_k} = \frac{N_{aU}}{N_a} \tag{5.19}$$

Where $N_a = \sum_{k=1}^{Nr} N_k$ is total time increments available in all the records.

- The variance of a variable with binomial distribution is estimated as:

$$\hat{V}_{NU} = N_a \hat{p}(1 - \hat{p}) \tag{5.20}$$

[2] Inclusion of this procedure in Annex 1 of SDC6 WP.6 was proposed by the delegation of United States to the Expert Group; however die to lack of time for technical discussion, it was not included.

- Using a normal approximation for binomial destruction, boundaries of confidence interval of failure rate estimate $\hat{\lambda}_{up,low}$ is computed as:

$$\hat{\lambda}_{up,low} = \frac{N_a U \pm Q_N\left(0.5(1+P_\beta)\right)\sqrt{\hat{V}_{NU}}}{T_a} \tag{5.21}$$

Where Q_N is quantile of standard normal distribution, P_β is the accepted confidence probability, for $P_\beta = 0.95$, $Q_N\left(0.5(1+P_\beta)\right) = 1.96$.

More details on the justification and application of this procedures are available in Belenky et al. (2008, 2016a) and Campbell and Belenky (2010).

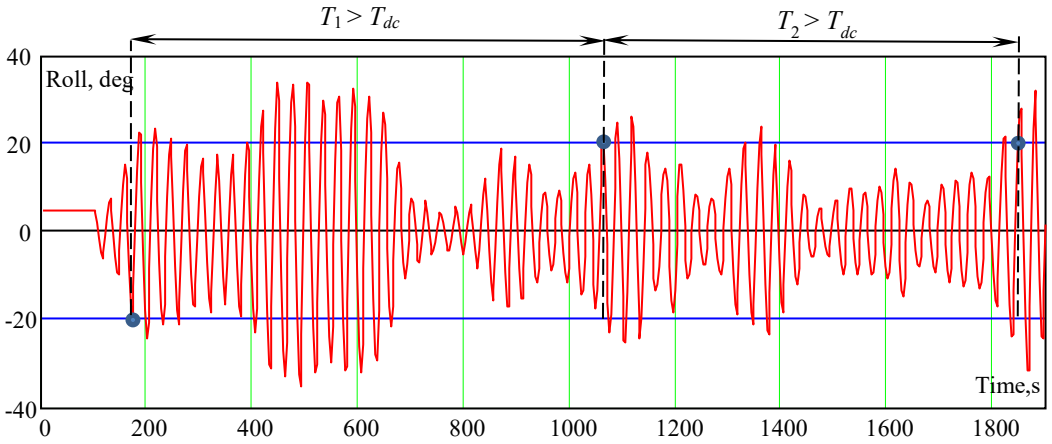

Figure 5.28. On Application of Direct Counting Procedure – Determination of Independent Upcrossings for Record #1, Heading 1° (Almost Following), Speed 5 kn, Significant Wave Height 3.5 m, Modal Period 12 s, Mean Zero-Crossing Period 8.5 s

5.2.11 Verification of Mode of Failure

Section 5.2 of Annex 1 of SDC 6/WP.6, contains guidance for verification of the mode of failure. Per paragraph 5.2.1 of the cited reference, the objective is to examine whether the failure mode has been reproduced for which the numerical method was validated.

The judging criteria for the parametric roll are detailed in paragraph 5.2.3 of Annex 1 of SDC 6/WP.6. It suggests comparison of the period of roll motion to the local encounter period of waves. The roll period is expected to be close to the natural roll period. Also it expected to be close to the twice of the local wave encounter period.

Figure 5.29 shows the zoom into time history from Figure 5.28, showing the roll motions for 5 minutes: from 400 s to 700 s. One can easily see 10 complete roll oscillations, making the observed roll period about 30 s. The details of the loading condition of the ship are in the beginning of the previous subsection, with GM = 1.4 m. The natural roll frequency, corresponding to this loading condition, may be seen in Figure 5.9 - it is about 0.21 s^{-1}. The natural roll period is $2\pi/0.21$=29.9 s – very close to the visual estimate from Figure 5.29.

Figure 5.30 shows time history wave elevation at a position of center of gravity of the ship. Thus, periods measured from Figure 5.30 are essentially encounter periods. There are 23 full oscillations in Figure 5.30 (counting by zero crossing peaks), producing an encounter period about 13 s (Actually, it is quite close to 13.9 s, reported by LAMP for this record). The ratio between an observed roll period and observed encounter wave period is about 2.3, i.e. about twice as much.

Both criteria from paragraph 5.2.3 of Annex 1 of SDC 6/WP.6 are satisfied and stability failure is positively verified as parametric roll.

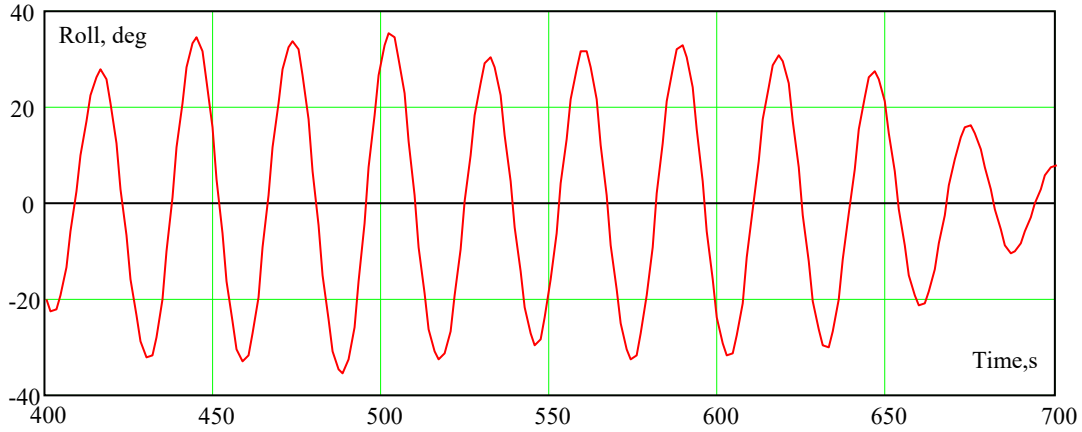

Figure 5.29. Verification of Parametric Roll: Roll Motion Zoom for Record #1, Heading 1° (Almost Following), Speed 5 kn, Significant Wave Height 3.5 m, Modal Period 12 s, Mean Zero-Crossing Period 8.5 s

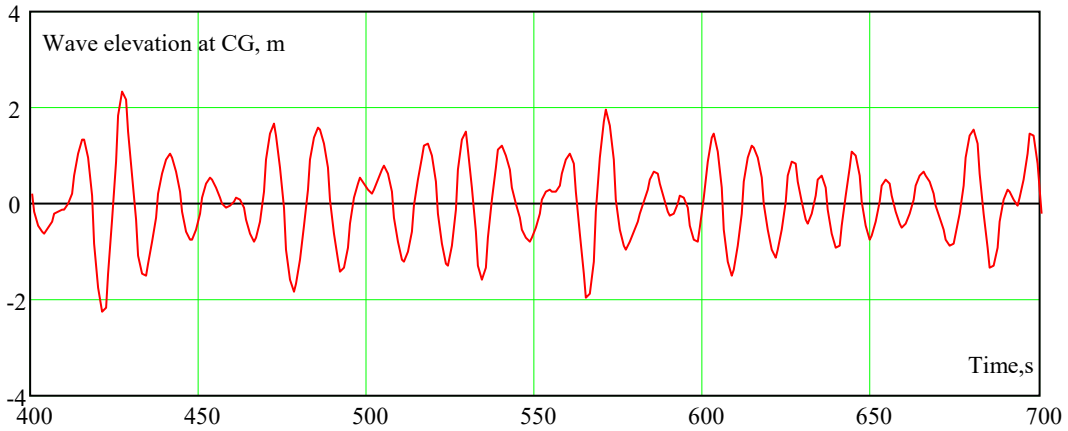

Figure 5.30. Verification of Parametric Roll: Wave Elevation at CG Zoom for Record #1, Heading 1° (Almost Following), Speed 5 kn, Significant Wave Height 3.5 m, Modal Period 12 s, Mean Zero-Crossing Period 8.5 s

5.2.12 Environmental Conditions and Full Probabilistic Assessment for Parametric Roll

The requirement to modeling of environmental and sailing conditions are provided in the section 5.3 of Annex 1 of SDC 6/WP.6. Following recommendation in paragraph 5.3.1.2, IACS Recommendation 34 was used as a source for long-term statistics for sea states.

Environmental conditions for available simulation data sets are listed in Table 5.4. Each set, except of the set #1 contains 20 records (30 minutes each) for five speeds (from 0 to 20 kn) and seven headings (1, 30, 60, 90, 120, 150 and 179°) [3], totaling 35 sailing conditions. The set # 1 covers 65 sailing conditions, as the number of headings were increased to 13 (with a 15° increment).

Sea states corresponding to each simulation data set in Table 5.6 is characterized by significant wave height *Hs*, modal period *Tm* and mean zero-crossing period Tz to facilitate use of the scatter table from IACS Recommendation 34. The mean zero-crossing period is related with a modal period that has a standard formula:

$$Tz = 0.71\,Tm \tag{5.22}$$

Table 5.4 also contains exceedance estimates and boundaries of their confidence interval, averaged for each sea state, which follow paragraph 5.3.2.3 of Annex 1 of SDC 6/WP.6:

$$\hat{\lambda}_S = \frac{1}{Ns}\sum_{i=1}^{Ns}\hat{\lambda}_i \;\; ; \quad \hat{\lambda}_S^{up,low} = \frac{1}{Ns}\sum_{i=1}^{Ns}\hat{\lambda}_i^{up,low} \tag{5.23}$$

Where *Ns* is the number of sailing conditions, values $\hat{\lambda}_i$ and $\hat{\lambda}_i^{up,low}$ are estimated with equations (5.18) and (5.20), respectively.

Table 5.6. Available Simulation Data Sets

Set	Hs, m	Tm, s	Tz, s	$\hat{\lambda}_S$	$\hat{\lambda}_S^{up}$	$\hat{\lambda}_S^{low}$
1	9.00	14.00	9.94	6.84E-04	9.04E-04	4.65E-04
2	6.50	12.00	8.52	1.81E-04	2.48E-04	1.15E-04
3	12.50	17.60	12.50	1.36E-03	1.79E-03	9.31E-04
4	3.50	12.00	8.52	1.57E-06	3.75E-06	0.00E+00
5	6.50	14.00	9.94	2.72E-04	3.62E-04	1.83E-04
6	3.50	14.00	9.94	8.64E-06	1.83E-05	9.41E-07
7	2.50	12.00	8.52	0.00E+00	0.00E+00	0.00E+00
8	6.50	17.60	12.50	1.74E-04	2.39E-04	1.09E-04
9	9.50	17.60	12.50	5.75E-04	7.56E-04	3.95E-04
10	6.50	20.23	14.36	9.99E-05	1.44E-04	5.58E-05
11	9.50	20.23	14.36	3.81E-04	5.00E-04	2.64E-04

Table 5.7 contains detailed data and results for the set #1 (see Table 5.4). Table 5.7 contains speed and heading, defining the sailing condition, and an estimate of the exceedance rate for 40° with its confidence interval. The table also contains the decorrelation time, see

[3] Modeling of following and heading seas with 1 deg and 179 deg headings, respectively, is explained in the subsection 5.2.10.

example in Figure 5.27 and total available time. The available simulation time is creased from 36,000 (20 records at 1,800 s each) to avoid a self-repeating effect (see subsection 5.2.2) or because of capsizing.

Table 5.7. Short-Term Results for Simulation Set 1

Speed, kn	Heading, °	$\hat{\lambda}_i$, s^{-1}	$\hat{\lambda}_i^{up}$, s^{-1}	$\hat{\lambda}_i^{low}$, s^{-1}	Decorrelation time, s	Available time, s
0	1	2.68E-03	1.72E-03	3.64E-03	400.4	11190
	15	3.60E-03	2.51E-03	4.69E-03	221.2	11670
	30	3.11E-03	2.30E-03	3.91E-03	249.4	18350
	45	1.79E-03	1.31E-03	2.28E-03	372.6	28980
	60	3.85E-04	1.83E-04	5.86E-04	484.5	36000
	75	0	0.00E+00	0.00E+00	686.2	36000
	90	0	0.00E+00	0.00E+00	821.4	36000
	105	0	0.00E+00	0.00E+00	518.5	36000
	120	1.92E-04	4.99E-05	3.35E-04	688.2	36000
	135	1.06E-03	7.15E-04	1.41E-03	786.2	33890
	150	2.85E-03	2.11E-03	3.58E-03	270.1	20390
	165	2.46E-03	1.70E-03	3.22E-03	373.3	16270
	179	2.95E-03	2.00E-03	3.91E-03	338.7	12520
5	1	3.85E-03	2.65E-03	5.04E-03	178.1	10400
	15	2.98E-03	1.93E-03	4.03E-03	275.8	10400
	30	3.93E-03	2.88E-03	4.98E-03	162.4	13740
	45	2.60E-03	1.96E-03	3.23E-03	187.7	24660
	60	3.02E-04	1.24E-04	4.81E-04	597.0	36000
	75	0	0.00E+00	0.00E+00	738.7	36000
	90	0	0.00E+00	0.00E+00	720.3	36000
	105	0	0.00E+00	0.00E+00	565.6	35040
	120	2.75E-05	0.00E+00	8.53E-05	439.1	31580
	135	5.91E-04	3.13E-04	8.70E-04	386.2	29300
	150	1.16E-03	7.55E-04	1.56E-03	419.6	27580
	165	1.57E-03	1.10E-03	2.05E-03	412.8	26700
	179	1.59E-03	1.11E-03	2.07E-03	392.0	26360
10	1	6.05E-04	3.26E-04	8.85E-04	725.8	29740
	15	1.17E-03	7.88E-04	1.55E-03	305.3	30760
	30	1.07E-03	6.90E-04	1.44E-03	757.9	29120
	45	1.06E-03	6.96E-04	1.42E-03	473.4	31240
	60	0	0	0	423.8	36000
	75	0	0	0	237.0	36000
	90	0	0	0	630.0	36000
	105	0	0	0	372.7	31400
	120	0	0	0	337.1	26360
	135	0	0	0	484.3	23180
	150	0	0	0	479.2	21200
	165	2.75E-05	0	9.99E-05	509.7	20100
	179	5.50E-05	0	1.58E-04	481.5	19780

Table 5.7. Short-Term Results for Simulation Set 1 (Continue)

Speed, kn	Heading, °	$\hat{\lambda}_i$, s^{-1}	$\hat{\lambda}_i^{up}$, s^{-1}	$\hat{\lambda}_i^{low}$, s^{-1}	Decorrelation time, s	Available time, s
15	1	0	0	0	122.0	36000
	15	0	0	0	809.3	36000
	30	0	0	0	25.0	36000
	45	4.48E-04	2.21E-04	6.75E-04	612.4	33480
	60	0	0	0	538.2	36000
	75	0	0	0	171.2	36000
	90	0	0	0	249.3	36000
	105	0	0	0	283.4	28540
	120	0	0	0	209.5	22620
	135	0	0	0	255.5	19260
	150	0	0	0	269.9	17230
	165	0	0	0	420.2	16170
	179	0	0	0	557.0	15820
20	1	2.47E-04	8.57E-05	4.09E-04	410.4	36000
	15	8.24E-05	0	1.76E-04	457.9	36000
	30	0	0	0	358.4	36000
	45	0	0	0	430.6	36000
	60	0	0	0	371.4	36000
	75	0	0	0	178.1	36000
	90	0	0	0	171.8	36000
	105	0	0	0	184.7	26140
	120	0	0	0	266.1	19780
	135	0	0	0	250.9	16490
	150	0	0	0	186.6	14560
	165	0	0	0	380.4	13550
	179	0	0	0	212.0	13190

"Capsizing" is defined here as exceedance of a 90° roll. To simulate true capsizing, LAMP requires special settings (to avoid inadequate calculations of diffraction and radiation forces on a mean waterline), but actual capsizing is not relevant here. Also, most of these "capsizing" events will not occur if weather-tight volumes are included (see the discussion in the subsection 2.2.6). Once 90° of roll is encountered, simulations are stopped and post-processing is carried out on the time history, preceding 90° crossing.

As it was mentioned before the data set #1 has 65 sailing conditions, while all other data sets have only 35 each, because of increasing the heading increment from 15 to 30°. To see how important it is, the computation of an average rate of exceedance and its boundaries were performed in 15° and 30° heading increments on the data from the Table 5.7. The rows containing data with 30° heading increment are highlighted in Table 5.7. The results of calculations are placed in Table 5.8. As one can see, the difference is not significant, so the 30° increment in heading seems to be adequate for the long-term assessment.

Table 5.8. Influence of the Heading Increment

Heading increment, °	$\hat{\lambda}_S$	$\hat{\lambda}_S^{up}$	$\hat{\lambda}_S^{low}$
15	6.835E-4	9.04E-4	4.651E-4
30	7.139E-4	9.445E-4	4.856E-4

With the total time of the simulation at 3,570 hours covering 415 sailing conditions, a full probabilistic assessment, as described in the section 5.3.2 of Annex 1 of SDC 6/WP.6, is attempted. Per the requirements of paragraph 5.3.2.1 the objective is to compute a long-term rate of stability failures as weighted average over all relevant sea states for the considered loading condition.

As the simulation results are not available for all the sea states in the scatter table from the IACS recommendation number 34, it attempted to "cluster" the cells of the scatter diagram around sea states from table 5.6 with the available results of simulation. The following principles are used for the clustering, trying to produce a conservative estimate:

- A cluster is rectangular; a modal period is used as representative period for irregular waves
- A modal period of close to half of a natural roll period is considered the most dangerous
- If a modal period is less than half of the natural period, the run is in the right corner of the cluster
- If a modal period is more than half of the natural period, the run is in the left corner of the cluster
- If a modal period is about one-half of the natural period, all columns are included till the next run
- A danger of parametric roll is increased with significant wave heights
    a. Lower significant wave heights are included in the cluster until the next run

A natural period is taken as 30 s (see the previous subsection), proposed clusters are shown in Table 5.9, where available sea states are highlighted with a color ranging from green to red, with the intensity corresponding to the value of exceedance rate estimate.

Table 5.9. On Clustering of Sea States

Hs	3.5	4.5	5.5	6.5	7.5	8.5	9.5	10.5	11.5	12.5	13.5	14.5	15.5	16.5	17.5	18.5
0.5	1.3	133.7	865.6	1186	634.2	186.3	36.9	5.6	0.7	0.1	0	0	0	0	0	0
1.5	0	29.3	986	4976	7738	5569.7	2375.7	703.5	160.7	30.5	5.1	0.8	0.1	0	0	0
2.5	0	2.2	197.5	2158.8	6230	7449.5	4860.4	2066	644.5	160.2	33.7	6.3	1.1	0.2	0	0
3.5	0	0.2	34.9	695.5	3226.5	5675	5099.1	2838	1114.1	337.7	84.3	18.2	3.5	0.6	0.1	0
4.5	0	0	6	196.1	1354.3	3288.5	3857.5	2685.5	1275.2	455.1	130.9	31.9	6.9	1.3	0.2	0
5.5	0	0	1	51	498.4	1602.9	2372.7	2008.3	1126	463.6	150.9	41	9.7	2.1	0.4	0.1
6.5	0	0	0.2	12.6	167	690.3	1257.9	1268.6	825.9	386.8	140.8	42.2	10.9	2.5	0.5	0.1
7.5	0	0	0	3	52.1	270.1	594.4	703.2	524.9	276.7	111.7	36.7	10.2	2.5	0.6	0.1
8.5	0	0	0	0.7	15.4	97.9	255.9	350.6	296.9	174.6	77.6	27.7	8.4	2.2	0.5	0.1
9.5	0	0	0	0.2	4.3	33.2	101.9	159.9	152.2	99.2	48.3	18.7	6.1	1.7	0.4	0.1
10.5	0	0	0	0	1.2	10.7	37.9	67.5	71.7	51.5	27.3	11.4	4	1.2	0.3	0.1
11.5	0	0	0	0	0.3	3.3	13.3	26.6	31.4	24.7	14.2	6.4	2.4	0.7	0.2	0.1
12.5	0	0	0	0	0.1	1	4.4	9.9	12.8	11	6.8	3.3	1.3	0.4	0.1	0
13.5	0	0	0	0	0	0.3	1.4	3.5	5	4.6	3.1	1.6	0.7	0.2	0.1	0
14.5	0	0	0	0	0	0.1	0.4	1.2	1.8	1.8	1.3	0.7	0.3	0.1	0	0
15.5	0	0	0	0	0	0	0.1	0.4	0.6	0.7	0.5	0.3	0.1	0.1	0	0
16.5	0	0	0	0	0	0	0	0.1	0.2	0.2	0.2	0.1	0.1	0	0	0

Values in the scatter table are summed within each cluster, producing a statistical weight for further weighted averaging. The resulting statistical weights are placed in Table 5.10. Then, the estimates for each sea state $\hat{\lambda}_{Si}$ from Table 5.6 as well as the boundaries of their confidence interval $\hat{\lambda}_{Si}^{up,low}$ are used together with weights W_i from table 5.10:

$$\hat{\lambda}_a = \sum_{i=1}^{Nr} W_i \hat{\lambda}_{Si} = 1.06 \cdot 10^{-4}\ s^{-1} \tag{5.24}$$

$$\hat{\lambda}_a^{up} = \sum_{i=1}^{Nr} W_i \hat{\lambda}_{Si}^{up} = 1.42 \cdot 10^{-4}\ s^{-1}$$
$$\hat{\lambda}_a^{low} = \sum_{i=1}^{Nr} W_i \hat{\lambda}_{Si}^{low} = 0.70 \cdot 10^{-4}\ s^{-1} \tag{5.25}$$

Where $Nr = 11$ is the number of sets/sea states, available form Table 5.6

Table 5.10. Statistical Weight of Clusters

Set	Hs, m	Tz, s	Sum of values	Statistical weight W_i
1	9.00	9.94	3165.1	3.17E-02
2	6.50	8.52	7868.3	7.87E-02
3	12.50	12.50	1117.6	1.12E-02
4	3.50	8.52	9632.1	9.63E-02
5	6.50	9.94	16677.6	1.67E-01
6	3.50	9.94	20587.7	2.06E-01
7	2.50	8.52	38344.1	3.83E-01
8	6.50	12.50	1728.1	1.73E-02
9	9.50	12.50	640.6	6.41E-03
10	6.50	14.36	149.8	1.50E-03
11	9.50	14.36	89	8.90E-04

The formula (5.24) produces the final result of the assessment. Per paragraph 5.3.2.2 of Annex 1 of SDC 6/WP the standard is $2.6 \cdot 10^{-8}\ s^{-1}$, concluding that the loading condition with GM = 1.4 has a significant problem with parametric roll as the upper boundary of the estimate is about four orders of magtintude larger than the standard $1.42 \cdot 10^{-4}\ s^{-1} > 2.6 \cdot 10^{-8}\ s^{-1}$. This result is hardly surprising, having in mind actual accident and following investigation described by France et al. (2003).

5.3 Specifications and Example for Direct Stability Assessment: Pure Loss of Stability

5.3.1 General Requirements and Considerations

General requirements for extrapolation procedures as formulated in section 5.5 Annex 1 of SDC 6/WP.6. Extrapolation procedures may be applied as alternative to direct counting procedure as stated in paragraph 5.3.1.1. Essentially, extrapolation allows extending existing numerical simulation data beyond observation. For example no exceedances of 40° was not observed over 10 hr of simulation, but there were some 30° and 35° exceedances. Extrapolation methods allow an estimate in an exceedance rate of 40°. This uses the existing data rather than run more simulations. Indeed, the extrapolation carries more statistical uncertainty than the direct counting. Assessments of extrapolation uncertainty are required by paragraph 5.5.1.3.

The objective of this section is to demonstrate the viability of the application and validation of extrapolation methods. To facilitate this objective, a reduced order mathematical model of

ship motion was used, originally intended for validation of extrapolation as required by paragraph 5.6.3 of Annex 1 of SDC 6/WP.6. It is a volume-based 3-DoF model, described in Weems et al. (2018). The model includes the body-nonlinear formulation for Froude-Krylov and hydrostatic forces, and are valid for waves longer than two breadths of a ship. Polynomials are used for all other forces. The model does not include any wind, and a sample ship has too much damping for parametric roll. Thus, observed large roll angles and capsizing are caused by pure loss of stability.

5.3.2 Theoretical Background of Peak-over-Threshold /Envelope Peak-over-Threshold (POT/EPOT)

The basic idea of the POT method is to fit a Generalized Pareto Distribution (GPD) to the observed data above a particular threshold value of the response. The mathematical background of the method is the second extreme value theorem, which states that the tail of an extreme value distribution can be approximated with a GPD above a "large enough" value (Pickands, 1975). A key feature of the POT extrapolation is that it can capture the nonlinearity of the large amplitude response, such as that caused by the changes in the restoring at large roll angles and in waves.

However, the standard POT method is only applicable to independent data points, while the roll motions of a ship are correlated because of the ship's inertia, correlated wave excitation, and "memory" in the hydrodynamic forces. The application of POT, therefore, requires an extraction of independent points from the time history, a process known as "de-clustering."

Fitting an envelope to the time history of the roll motion, as illustrated in Fig. 5.31, is a convenient way to de-cluster the data, as the peaks of the envelope of the roll response are sufficiently far from each other to provide the necessary independence. The use of an envelope to de-cluster the roll motion provides the additional letter in the acronym of the method, so POT becomes EPOT – Envelope Peaks Over Threshold.

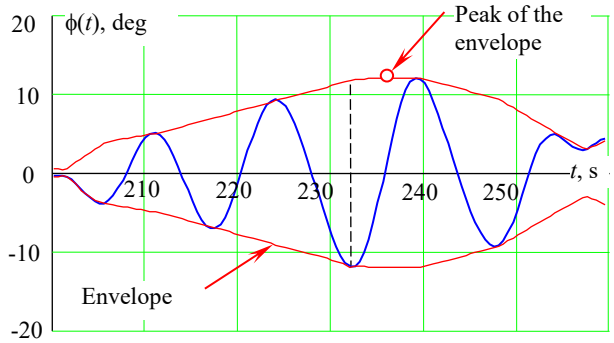

Figure 5.31. De-Clustering Using an Envelope (Belenky *et al.* 2018)

The fitting procedure for EPOT with a GPD is described in Campbell et al. (2016). This fitting includes an assessment of uncertainty, which is required by paragraph 5.5.1.3 of Annex 1 SDC 6 /WP.6. The statistical validation of the method was described by Smith and Zuzick (2015). The GPD-based EPOT method should be further improved. The upper boundary of its confidence interval is, at times, too large, making the assessment too conservative (Figure 1 of

Smith and Zuzick 2015). Also, five cases occurred for which the passing rate fell short of the required value: one roll case and four acceleration cases. These failures, however, were not that dramatic: the worst passing rate was 0.84 versus the minimally required 0.90 for 100 samples. Smith (2019) provides a justification of this requirement; paragraph 5.6.7 of Annex 1 SDC 6 /WP.6 sets the passing rate to 0.88 for 50 samples.

A way to improve the GPD-based EPOT method has become available with the determination of a relationship between the nonlinearity of roll motions and the structure of the tail of its distribution (Belenky et al. 2016b, 2019a). Including physical information into the statistical model of the tail helps to decrease the uncertainty and increase the reliability of the fitting. This approach is called a "physics-informed solution."

The first extreme value theorem (a.k.a. Fisher-Tippett-Gnedenko theorem) proves that a distribution of the largest value in a sample has a limit in the form of a Generalized Extreme Value (GEV) distribution. The second extreme value theorem (a.k.a. Pickands-Balkema-de Haan theorem) shows that the GEV distribution can be approximated by a GPD above a threshold, Coles (2001)). The tail ($y>u$) of *any* distribution can be approximated with a GPD above a sufficiently large threshold. The GPD is defined by three numbers – a shape parameter ξ, a scale parameter σ, and threshold value u – and has the following form for $y>u$:

$$\mathrm{pdf}(y) = \begin{cases} \frac{1}{\sigma}\left(1+\xi\frac{y-u}{\sigma}\right)^{-\left(1+\frac{1}{\xi}\right)} & \xi \neq 0 \\ \frac{1}{\sigma}\exp\left(-\frac{y-u}{\sigma}\right) & \xi = 0 \end{cases} \tag{5.26}$$

$$\mathrm{cdf}(y) = \begin{cases} 1-\left(1+\xi\frac{y-u}{\sigma}\right)^{-1/\xi} & \xi \neq 0 \\ 1-\exp\left(-\frac{y-u}{\sigma}\right) & \xi = 0 \end{cases} \tag{5.27}$$

The objective of the present application is to estimate a rate of exceedance $\hat{\lambda}(c)$ of a target value $c>u$ above the threshold u:

$$\hat{\lambda}(c) = \hat{\lambda}(u)\widehat{\mathrm{cdf}(c)} \tag{5.28}$$

where $\hat{\lambda}(u)$ is the rate of upcrossing of the threshold u, estimated through the direct counting procedure as described in the previous section (subsection5.2.10) of this report requirements for direct counting are formulated un section 5.4 of Annex 1 of SDC 6 /WP.6 (and paragraph 3.5.4 of the Draft consolidated Interim Guidelines).

For application of a GPD, three parameters must be found: shape ξ and scale σ and threshold u. The shape and scale parameter are estimated by the maximum likelihood method. The threshold is found from a condition of GPD applicability; Campbell et al. (2016). The scale parameter σ is positive, while the shape parameter ξ can be either positive or negative. A negative shape parameter imposes a limitation on the expressions in parenthesis of equations (5.26) and (5.27) and formally introduces a right bound to the distribution:

$$\mathrm{pdf}(y) = 0, \quad if \;\; y > u - \frac{\sigma}{\xi} \;\; \text{and} \; \xi < 0 \tag{5.29}$$

The shape parameter defines the type of tail: heavy, exponential, or light, as shown in Fig. 5.32 (No universally accepted definition of heavy and light tail exists. Other sources may use heavy/light tail in a different context). The exponential tail (ξ=0) describes, for example, the

extreme values of a normal distribution. The heavy tail ($\xi>0$) is above the exponential tail, while the light tail ($\xi<0$) is below. As the exponential tail is the smallest infinite tail, the light tail has a limit, which is its right bound. The heavy tail is unbounded.

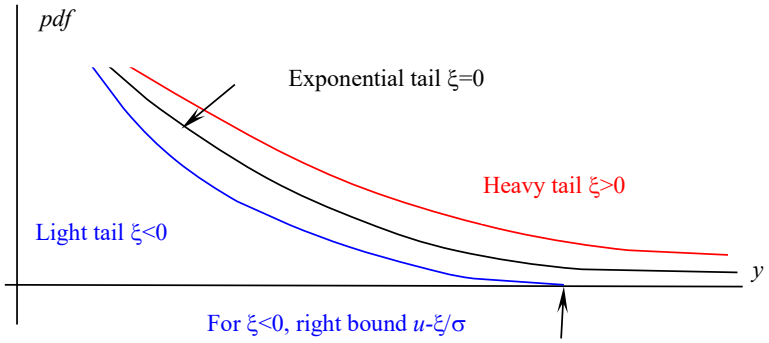

Figure 5.32. Types of Tails (Belenky *et al.* 2018)

The roll restoring arm (GZ) curves of most ships have a limited range of stability, leading to the appearance of an unstable equilibria at the angle of vanishing stability, as well a maximum value of GZ. This configuration leads to a heavy tail after the maximum of the GZ curve, which switches to a light tail in the immediate vicinity of the angle of vanishing stability. Fig. 5.33 shows such a distribution, computed for a dynamical system with piecewise linear (PWL) restoring.

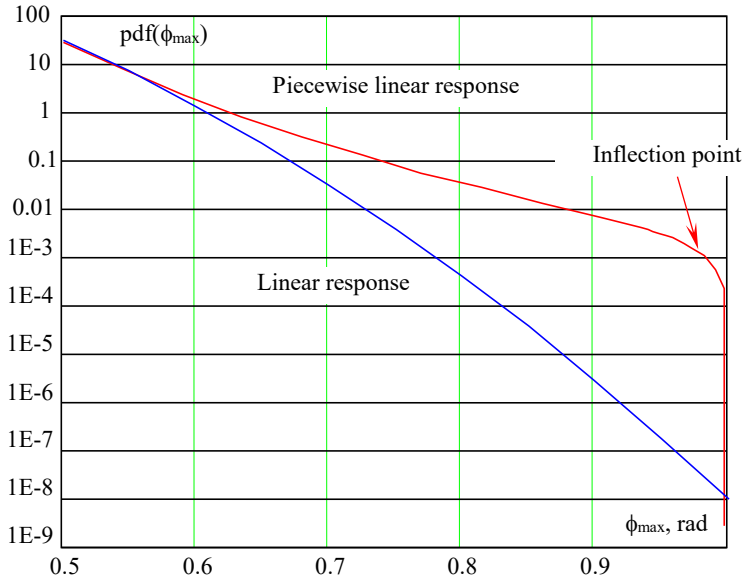

Figure 5.33. PDFs of Peaks of Linear Response and PWL Response (Belenky et al., 2016)

The piecewise linear approximation of the GZ curve allows a closed-form solution for the tail of the distribution of the peaks and instantaneous values of the roll angle (Belenky et al. 2016b, 2019a). Belenky et al. (2018) presents an argument for why the piecewise linear result

can be generalized for any dynamical system with softening stiffness, including the roll motions of many ships.

The roll angles associated with dynamic stability failures (e.g. 50 degrees per paragraph 2.3.1 of the 2008 IS Code, are usually located around and beyond the angle of the maximum of the GZ curve. Therefore, to assume a heavy tail appears appropriate for extrapolation problems associated with dynamical stability failures.

When the shape parameter ξ>0 (heavy tail) and threshold value $u = \sigma/\xi$, the GPD is equivalent to a Pareto distribution with scale $y_m = \sigma/\xi$ and shape $\alpha = 1/\xi$:

$$\mathrm{pdf}(y) = \frac{\alpha y_m^{\alpha}}{y^{\alpha+1}} \tag{5.30}$$

The conditional probability of exceedance of a target value *y* associated with dynamic stability failure is expressed as:

$$\mathrm{P}(Y > y | Y > u) = \left(\frac{u}{y}\right)^{\alpha} = \left(\frac{y}{u}\right)^{-\frac{1}{\xi}} \tag{5.31}$$

Here, the threshold *u* does not have to be the same as in the GPD case. A method for finding the threshold and estimating the shape parameter is proposed in Belenky et al. (2018), which is based on Beirlant, et al. (2004), Dupuis and Victoria-Feser (2006), and Mager (2015).

To extrapolate with equation (5.31), the threshold is found from applicability considerations so only one parameter needs to be fitted. Decreasing the number of parameters from two (in case if the GPD is used) to one decreases the statistical uncertainty. This is how the physical understanding of the process propagates into a statistical model.

5.3.3 Description of EPOT Extrapolation Procedure and Example of Application

The extrapolation procedure is demonstrating using ONR tumblehome topside configuration (Bishop, et al 2005). Principle dimensions are placed to Table 5.5. The only difference is that the KG was decreased to 7.5 m making GM=2.21 m. Example calculation were carved out for irregular waves with significant wave height 9 m and modal period of 15s. The extrapolation data sample consists from 80 half-hour records, produced with volume-based simulation tool (Weems, et al 2018). Sample record is shown in Figure 4, while a fragment of the envelope for de-clustering procedure is shown in Figure 5.34. Maximum observed angle over 40 hours of simulation was 28.1°.

The input data for fitting is designated ϕ_e and consists of *N* independent peaks extracted from the envelope of the roll time histories (Figure 5.35). The method is applied to a sample sorted in descending order – a.k.a. order statistics:

$$\mathrm{Y} = \mathrm{sort}_{\mathrm{desc}}(\phi_e) \tag{5.32}$$

The Hill estimator provides the shape parameter ξ – for the case of Pareto $\xi > 0$:

$$\hat{\xi}_k = \frac{1}{k}\sum_{i=1}^{k} \log\left(\frac{Y_i}{Y_k}\right) \tag{5.33}$$

Where the index k refers to the number of upper order statistics used in the estimation. Mager (2015) suggests the first index $k = \min(40, 0.02N)$, while the last (largest) value for the index taken as 0.2*N*.

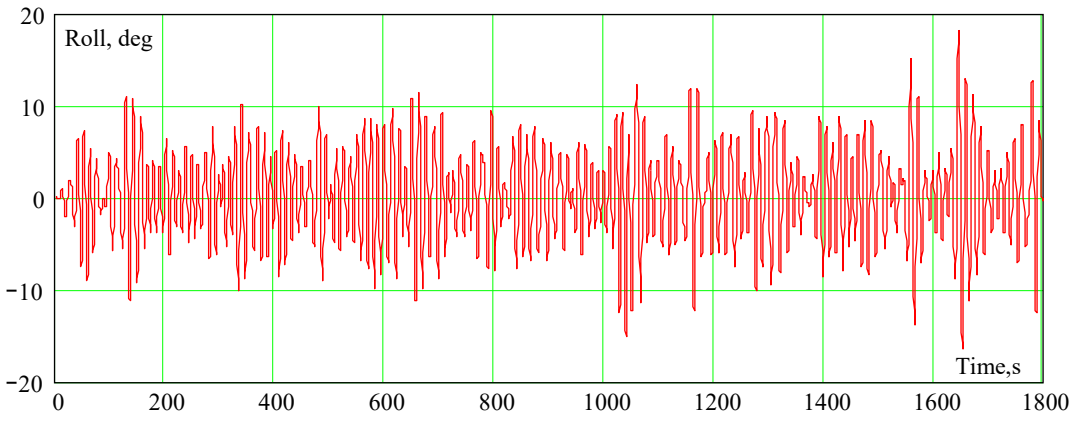

Figure 5.34. Example of Roll Record

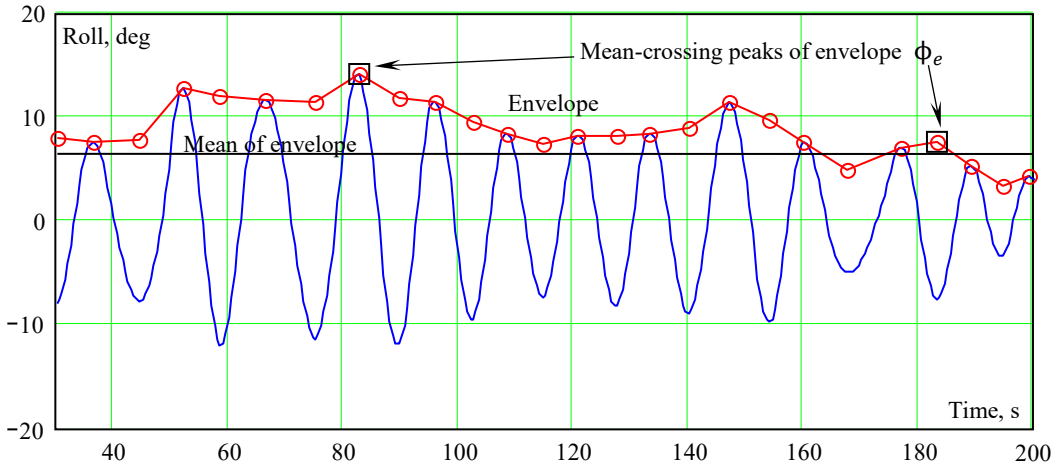

Figure 5.35. Fragment of Envelope and De-Clusterization Procedure with Mean-Crossing Peaks

The threshold u is found by an index that corresponds to a minimum of the mean squared prediction error function shown in Fig. 5.36.

$$\hat{\Gamma}(k) = \frac{1}{\hat{\xi}_k^{\,2}} \sum_{i=1}^{k} \frac{\left(\log\left(\frac{Y_{i-1}}{Y_{k-1}}\right) + \hat{\xi}_k \log\left(\frac{i}{k+1}\right)\right)^2}{\left(\sum_{j=i}^{k} j^{-2}\right)} + \frac{2}{k} \sum_{i=1}^{k} \frac{\left(\log\left(\frac{i}{k+1}\right)\right)^2}{\left(\sum_{j=i}^{k} j^{-2}\right)} - 1 \tag{5.34}$$

Once the index k corresponding to a minimum of $\hat{\Gamma}$, is found, the threshold is set as:

$$u = Y_k \tag{5.35}$$

The confidence interval for the extrapolated value is computed assuming a normal distribution for the estimate of the shape parameter $\hat{\xi}$. Its variance estimate is expressed as:

$$\widehat{Var}(\hat{\xi}) = \frac{\hat{\xi}^2}{k} \tag{5.36}$$

The boundaries of the confidence interval of the estimate are:

$$\hat{\xi}_{up,low} = \hat{\xi} \pm K_{\beta}\sqrt{\widehat{Var}(\hat{\xi})} \tag{5.37}$$

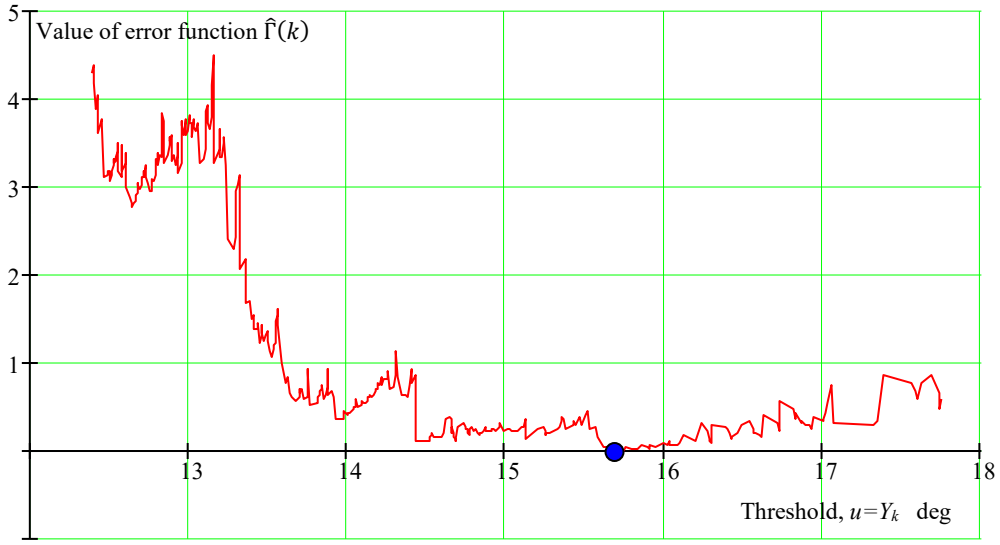

Figure 5.36. Mean Squares Prediction Error Function

Using equation (5.28) and (5.31), the extrapolated estimate of the exceedance rate of target value c can be computed as:

$$\hat{\lambda}(c) = \hat{\lambda}(u)\left(\frac{c}{u}\right)^{-1/\hat{\xi}} \tag{5.38}$$

Where $\hat{\lambda}(u)$ is the rate of upcrossing of threshold u, estimated through the direct counting procedure with its confidence interval, as described in subsection 5.2.10 of this report.

Boundaries for the extrapolated value are computed through the lower and upper boundaries of the upcrossing rate estimate $\hat{\lambda}_{low,up}(u)$ and the shape parameter estimate $\hat{\xi}_{low,up}$

$$\begin{cases} \hat{\lambda}_{low}(c) = \hat{\lambda}_{low}(u)\left(\frac{c}{u}\right)^{-1/\hat{\xi}_{low}} \\ \hat{\lambda}_{up}(c) = \hat{\lambda}_{up}(u)\left(\frac{c}{u}\right)^{-1/\hat{\xi}_{up}} \end{cases} \tag{5.39}$$

Equations (5.39) contain a product of the boundaries of two estimates. If the desired confidence probability for the entire extrapolated estimate $\hat{\lambda}(c)$ is to be $\beta = 0.95$ as recommended in 5.5.1.3 of Annex 1 of SDC 6 /WP.6 (and paragraph 3.5.4 of the Draft consolidated Interim Guidelines), then the confidence probabilities for each estimate $\hat{\lambda}(u)$ and $\hat{\xi}$ must be set as:

$$\beta_1 = \sqrt{\beta} = \sqrt{0.95} = 0.975 \tag{5.40}$$

In order to account for the difference in the confidence probability, K_β is set to 2.236 in equation (5.37) and the confidence 0.975 is used in the direct counting procedure instead of 0.95. The result of extrapolation for c=50 deg with its confidence interval is shown in Fig. 5.37.

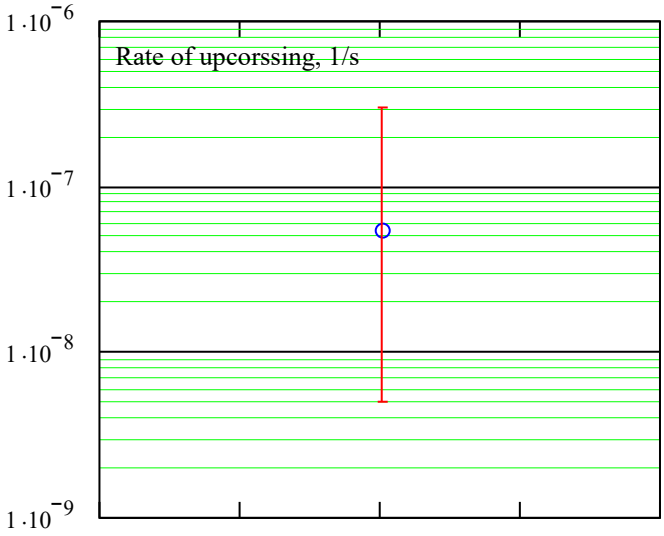

Figure 5.37. Mean Squares Prediction Error Function

5.3.4 Theoretical Background of Split-Time / Motion Perturbation Method (MPM)

Primary application area for the Split-Time / Motion Perturbation Method (MPM) is estimation of probability of capsizing. In general, the split-time method is intended for estimating the probability of complex and rare physical phenomena in which the physics of the problem changes with the extreme response, such as that caused by capsizing in dead ship conditions or pure loss of stability in stern quartering / following seas.

A capsizing of a stability-compliant ship in severe conditions cannot be observed during a simulation or set of simulations of reasonable length. So a special metric of capsizing likelihood is introduced. It is computed at the instant of upcrossing of an intermediate roll threshold a. The roll rate is perturbed until capsizing is observed (Fig. 5.38). The difference between the roll rate at upcrossing and the roll rate when capsizing is observed is the metric, as this difference indicates "the distance to trouble."

$$y_i = 1 + \dot{\phi}_{Ui} - \dot{\phi}_{Ci}\,; \quad i = 1, \ldots, N_U \tag{5.41}$$

$\dot{\phi}_{Ci}$ is the critical roll rate calculated for the i-th upcrossing, and $\dot{\phi}_{Ui}$ is the roll rate observed at the i-th upcrossing, N_U number of observed upcrossings. Computation of the metric values (5.41) over a number of upcrossings creates a sample that can be used for extrapolation up to the level 1. An estimate of a conditional probability of exceedance of the level 1 $\hat{P}(y > 1|y > a)$ is used for the estimate of capsizing rate $\hat{\lambda}_c$ as:

$$\hat{\lambda}_c = \hat{\lambda}_a \hat{P}(y > 1|y > a) \tag{5.42}$$

Where $\hat{\lambda}_a$ is an estimate of the upcrossing rate of the intermediate threshold a, evaluated using direct counting.

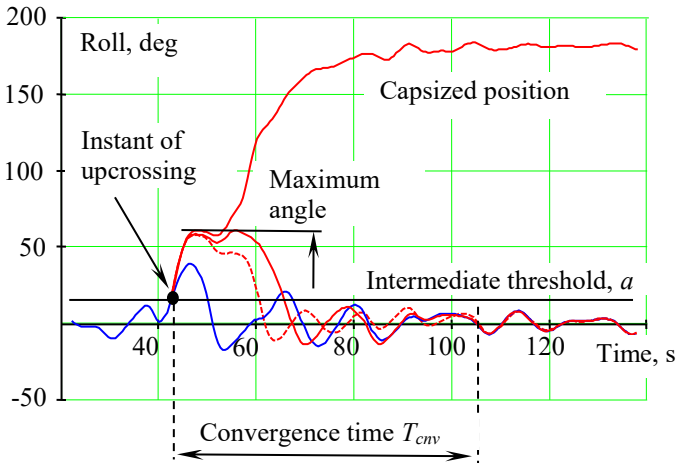

Figure 5.38. Motion Perturbation for Computing the Capsizing Metric

5.3.5 Description Split-Time/Motion Perturbation Procedure

At this time, 40 hr of simulation time history is recommended for the application of the split-time method for capsizing in dead ship conditions or caused by pure loss of stability. To avoid the self-repeating effect and achieve reasonable computational efficiency, 40 hr are presented in 80 independent records with 30 minutes duration each.

The choice of the intermediate threshold is done based on consideration of computational efficiency. If the threshold is set too high, there will be too few upcrossings available for the metric computations and additional simulation time may be required. If the threshold is set too low, there will be many upcrossings leading to dependent metric values. Thus, many of these values will be rejected during the de-clustering procedure, which will decrease computational efficiency. Based on the exiting experience for the present setup of 40 hr, 7-10 upcrossings per an independent record of 30 minutes long was found to be acceptable.

The evaluation of the metric consists from the following steps.

- Compute the time instant of upcrossing t_{Ui} and the roll rate at the instant of upcrossing $\dot{\phi}_{Ui}$ using linear interpolation between the roll angle and rate data points, respectively. Similarly compute values of heave, pitch and their derivatives at the instant of upcrossing.
- Compute perturbed solution for $\phi_0 = a$ and $\dot{\phi}_0 = \dot{\phi}_{Ui} + \Delta\dot{\phi}$, while using the values for pitch and heave, computed at the previous step, as the initial conditions for pitch and heave equations respectively. If capsizing is not observed, the perturbed solution converges with the unperturbed solution (see Figure 5.39), the convergence time T_{cnv} is defined when the difference between perturbed and unperturbed solution does not exceed a given value for a given number of points.
- The next perturbation is carried out for $\dot{\phi}_0 = \dot{\phi}_{Ui} + 2\Delta\dot{\phi}$, keeping the rest of the initial conditions the same. The procedure is repeated for $3\Delta\dot{\phi}$, $4\Delta\dot{\phi}$…, until the capsizing is observed as shown in Figure 5.39 for $\dot{\phi}_0 = \dot{\phi}_{Ui} + m\Delta\dot{\phi}$, where m is the number of iterations.

- Once capsizing is observed for $\dot{\phi}_0 = \dot{\phi}_{Ui} + m\Delta\dot{\phi}$, the critical roll rate is computed as $\dot{\phi}_{Ci} = \dot{\phi}_{Ui} + (m-1)\Delta\dot{\phi}$, convergence time T_{cnv} for the penultimate iteration is recorded for further use in the declustering procedure.
- Metric for the *i*-th upcrossing is computed with formula (5.41).

As demonstrated in Belenky et al (2018, 2018a, 2019a, 2019b), the independent large values of the metric (5.41) can be approximated with an exponential tail. As the upcrossings of a level usually comes in groups, the metric values are clustered, meaning that the metric values within a same cluster may be dependent.

A de-clustering procedure is used to ensure independence of the collected metric values. The cluster is defined as a group of the metric values y_i, corresponding to upcrossings that are closer than respective convergence time durations $\{y_i\}_{i=b_j}^{i=e_j}$, where b_j and e_j are indexes of the beginning and end of *j*-th cluster.

Once the clusters are defined, the declustered values are determined as maximum value within each cluster:

$$x_j = \max\left(\{y_i\}_{i=b_j}^{i=e_j}\right), j = 1 \ldots N \tag{5.43}$$

Fitting a tail involves finding a threshold, after which the exponential approximation is applicable. Two options are described below: one is the prediction error criterion (Mager 2015) and the other is the goodness-of-fit test (Stephens, 1974).

To use the prediction error technique, the data needs to be sorted in descending order. A mean squares prediction error function is defined as (Mager 2015):

$$\hat{\Gamma}(k) = \frac{1}{\hat{\gamma}_k^2}\sum_{j=1}^{k}\left(\frac{k+1}{j} - 1\right)^{-1}\left(x_j - x_k + \hat{\gamma}_k \log\left(\frac{j}{k+1}\right)\right)^2 + \frac{2}{k}\sum_{j=1}^{k}\left(\frac{k+1}{j} - 1\right)^{-1}\left(\log\left(\frac{j}{k+1}\right)\right)^2 - 1 \tag{5.44}$$

Where: *k* is an index corresponding to a candidate threshold, while $\hat{\gamma}_k$ is exponential distribution parameter estimated on the subset of the data points indexes from 1 to *k*.

$$k \in [\min(40, 0.02N); 0.2N] \tag{5.45}$$

$$\hat{\gamma}_k = \frac{1}{k}\sum_{j=1}^{k}(x_j - x_k) \tag{5.46}$$

The resulting threshold *u* (not to be confused with intermediate threshold *a*, used earlier) is found where the mean squares prediction error function experiences a global minimum.

To use the goodness-of-fit technique, the data needs to be sorted in ascending order. The candidate threshold *u* is searched for the data point indexes *k* within the following range:

$$k \in [0.7N; N - 10] \tag{5.47}$$

For a candidate threshold *u,* there are *n* points available for fitting ranging from 10 to 0.3*N*. The data points v_j above the candidate threshold are *u* defined as:

$$v_j = x_j - u; \;\; j = 1, \ldots, n \tag{5.48}$$

The exponential distribution parameter, $\hat{\gamma}_u$, estimated for the candidate threshold *u*

$$\hat{\gamma}_u = \frac{1}{n}\sum_{j=1}^{n} v_j \tag{5.49}$$

The test statistic for the null hypothesis is defined as

$$D^* = \left(D - \frac{0.2}{n}\right)\left(\sqrt{n} + 0.26 + \frac{0.5}{\sqrt{n}}\right) \tag{5.50}$$

Where $D = \max\{D^+, D^-\}$ with

$$D^+ = \max_{j=1,\ldots,n} \left|\frac{j}{n} - z_j\right| \tag{5.51}$$

$$D^- = \max_{j=1,\ldots,n} \left|z_j - \frac{j-1}{n}\right| \tag{5.52}$$

$$z_j = 1 - e^{-\frac{v_j}{\hat{\gamma}u}} \tag{5.53}$$

The critical values for the test statistic D^* were tabulated by Stephens (1974) and placed in Table 5.11. For a range of candidate thresholds, the test statistic D^* could then be computed and a p-value of the test for the exponential distribution be calculated. Since Stephens (1974) tabulated critical values for only a few significance levels, the p-value can be taken as the significance level whose critical value is the largest but still smaller than D^*. A final threshold can be selected as the largest u above which the thresholds have their associated p-value larger than certain significance level. A significance level of 5% seems reasonable but it has been found that for the extrapolation to work, it should be larger, say 10% or above.

Table 5.11. Critical Values for Goodness-of Fit Method

Level of significance, p	0.01	0.025	0.05	0.10	0.15	0.20	0.25	0.30	0.35	0.40	0.45	0.50
D*	1.308	1.190	1.094	0.990	0.926	0.880	0.835	0.795	0.766	0.736	0.710	0.685

The extrapolated estimate of the capsizing rate is computed as (see equation 5.42):

$$\hat{\lambda} = \hat{\lambda}(u)\exp\left(-\frac{1-u}{\hat{\gamma}}\right) \tag{5.54}$$

Where the estimate of the parameter $\hat{\gamma}$ corresponds to the chosen threshold u, $\hat{\lambda}(u)$ is the rate of upcrossing of threshold u, estimated through the direct counting procedure with its confidence interval, as described in the subsection 5.2.10 of this report.

The confidence interval for the extrapolated value is computed assuming a normal distribution for the estimate of the parameter $\hat{\gamma}$. Its variance estimate is expressed as:

$$\widehat{Var}(\hat{\gamma}) = \frac{\widehat{Var}(x-u)}{n} \tag{5.55}$$

Where $\widehat{Var}(x-u)$ is the variance, estimated for the points above the threshold u while n is the volume of sample above the threshold u.

The boundaries of the confidence interval of the estimate are:

$$\hat{\gamma}_{up,low} = \hat{\gamma} \pm K_\beta \sqrt{\widehat{Var}(\hat{\gamma})} \tag{5.56}$$

where K_β is a half of a non-dimensional confidence interval computed as a normal quantile of $0.5(1+\beta_2)$, where β_2 is the confidence probability for the parameter, computed as $\beta_2 = \sqrt{\beta}$, while is the confidence interval accepted for the entire extrapolated estimate. Boundaries for the

extrapolated estimate are computed through the lower and upper boundaries of the upcrossing rate estimate $\hat{\lambda}_{low,up}(u)$ and the parameter estimate $\hat{\gamma}_{up,low}$:

$$\begin{cases} \hat{\lambda}_{low}(c) = \hat{\lambda}_{low}(u)\exp\left(-\frac{1-u}{\hat{\gamma}_{low}}\right) \\ \hat{\lambda}_{up}(c) = \hat{\lambda}_{up}(u)\exp\left(-\frac{1-u}{\hat{\gamma}_{up}}\right) \end{cases} \tag{5.57}$$

where $\hat{\lambda}_{low}(u)$ and $\hat{\lambda}_{up}(u)$ are boundarues of the confidence interval of the upcrossing rated estimated with direct counting as described in paragraph 5.4 of Annex 1 of SDC 6 /WP.6.

The extrapolation procedure is demonstrating using ONR tumblehome topside configuration (Bishop, et al 2005). Principle dimensions are placed to Table 5.5. The only difference is that the KG was decreased to 7.5 m making GM=2.21 m. Example calculation were carried out for irregular waves with significant wave height 9 m and modal period of 14s. The extrapolation data sample consists from 80 half-hour records, produced with volume-based simulation tool (Weems, et al 2018). The maximum observed roll angle over 40 hours of simulation was 39.4 degrees. The intermediate threshold was chosen at 12 degrees, resulting in 527 upcrossing over 80 records. The de-clustering procedure produced 321 independent values of the metric, ranging from 0.344 rad/s to 0.767 rad/s.

For the choice of the threshold with the Prediction Error Criterion, the mean squares prediction error function is shown in Fig. 5.39; other intermediate numerical results are given in Table 5.12. Intermediate results for fitting the exponential tail with goodness-of-fit test is also placed in Table 5.12 for five levels of significance, ranging from 0.1 to 0.5. The final extrapolation results for both methods of fitting is shown in Fig. 5.40.

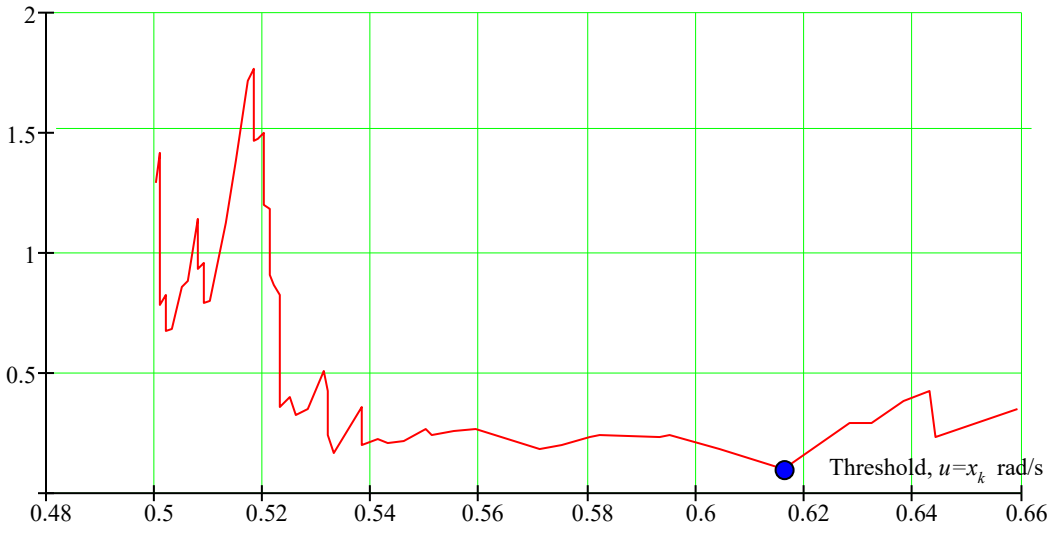

Figure 5.39. Mean Squares Prediction Error Function

Table 5.12. Intermediate Results of Fitting Exponential Tail

Method	Prediction Error Function	Goodness-of-Fit Test				
		p=0.1	p=0.2	p=0.3	p=0.4	p=0.5
Threshold, u	0.616	0.515	0.518	0.518	0.604	0.604
Available points	13	49	45	45	13	13
Parameter $\hat{\gamma}$ rad/s	0.058	0.062	0.064	0.064	0.07	0.07
Variance of $\hat{\gamma}$ (rad/s)^2	1.777E-4	9.409E-5	9.409E-5	1.039E-4	1.925E-4	1.925E-4
$\hat{P}(y > 1)$	1.38E-3	3.861E-4	5.126E-4	5.126E-4	3.476E-3	3.476E-3
Capsizing rate $\hat{\lambda}$, s^{-1}	1.267E-7	1.336E-7	1.629E-7	1.629E-7	3.191E-7	3.191E-7

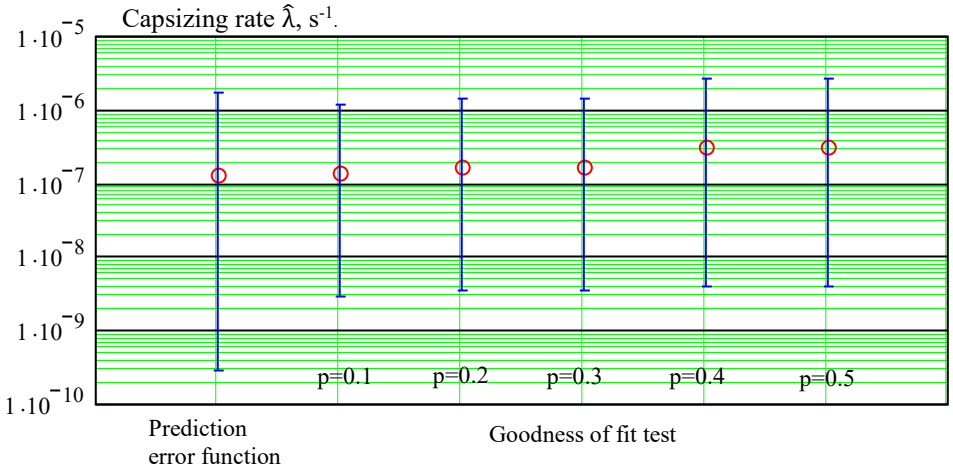

Figure 5.40. Results of Extrapolation for Capsizing Rate

5.3.6 Sample Calculations for Full Probabilistic Assessment

The full probabilistic assessment using extrapolation procedures is demonstrating using ONR tumblehome topside configuration (Bishop, et al., 2005). Principle dimensions are placed to Table 5.5. The only difference is that the KG was decreased to 7.5 m making GM = 2.21 m. Two extrapolation methods were used in these sample calculations. Envelope Peak-over-Threshold (EPOT) was applied for estimating the exceedance rate over 40° with additional targets of 30 and 50°. Split-time method (also known as Motion-perturbation method (MPM)) was employed for estimating a capsizing rate.

For computational speed, ship motions were evaluated with 3-DoF-volume based code (Weems et al. 2018). The code uses body-nonlinear formulation for Froude-Krylov and hydrostatic forces. Speed varied from 0 to 10 kn, assuming that high speeds will not be practical in high sea states and lower sea states do not make a significant contribution towards the final results. The course varied from 45 to 315° (due to limitations of current split-time implementation, a full set of heading needed to be evaluated). The technique of modeling following seas with 1 degree heading and head seas with 179° heading has not been tested yet for pure loss of stability with volume based code, so simulations were not run for exact head and following seas and the corresponding rate of events were taken as zeros.

As a sample study, the present calculations were carried out for 15 sea states. The waves were long-crested, with the conditions defined in wave scatter table from IACS recommendation 34 and as incorporated into the draft consolidated Interim Guidelines. As the primary focus of this sample application was on the pure loss of stability failure mode, wind considerations were not included in the simulation. There were total of 40 hr (80 records of 30 minute durations) of simulation time histories generated for each combination of speed and heading.

Sample results of a single sea state with significant wave height of Hs= 7.5 m and mean zero-crossing period TZ = 8.5 s are shown in Table 5.13 and in Table 5.14. Note that extrapolation methods do not produce zero-results, as both Pareto and exponential distributions, fitted for a tail, do extend to infinity. Also, one should expect symmetry (relative to heading angle) in results for EPOT exceedance rate; to check the robustness of calculations, this symmetricity was not assumed and full calculations were carried out for all the headings.

The results for each sailing conditions are further averaged to produce figures for each seas states. The results of averaging is summarized in Tables 5.15 and 5.16 for exceedance rates and capsizing rates, respectively.

Table 5.13. EPOT Extrapolation for Wave Height 7.5 m and Mean Zero-Crossing Period 8.5 s

Spd, kn	Heading, °	Target 30°			Target 40°			Target 50°		
		estimate	upper	lower	estimate	upper	lower	estimate	upper	lower
0	45	2.05E-05	4.91E-05	5.26E-06	6.67E-06	2.00E-05	1.17E-06	2.79E-06	1.00E-05	3.65E-07
	90	6.25E-08	2.02E-07	1.47E-08	2.48E-09	1.11E-08	3.88E-10	2.03E-10	1.17E-09	2.31E-11
	135	5.81E-10	1.41E-08	2.29E-12	2.53E-12	2.02E-10	1.20E-15	3.72E-14	7.48E-12	3.43E-18
	225	5.81E-10	1.41E-08	2.29E-12	2.53E-12	2.02E-10	1.20E-15	3.72E-14	7.48E-12	3.43E-18
	270	6.25E-08	2.02E-07	1.47E-08	2.48E-09	1.11E-08	3.88E-10	2.03E-10	1.17E-09	2.31E-11
	315	2.05E-05	4.91E-05	5.26E-06	6.67E-06	2.00E-05	1.17E-06	2.79E-06	1.00E-05	3.65E-07
5	45	4.06E-06	1.58E-05	3.33E-07	7.29E-07	4.35E-06	2.55E-08	1.92E-07	1.60E-06	3.48E-09
	90	6.25E-08	2.02E-07	1.47E-08	2.48E-09	1.11E-08	3.88E-10	2.03E-10	1.17E-09	2.31E-11
	135	3.80E-11	1.40E-09	9.40E-14	2.21E-13	2.36E-11	9.00E-17	4.08E-15	9.91E-13	4.10E-19
	225	3.77E-11	1.39E-09	9.29E-14	2.19E-13	2.34E-11	8.87E-17	4.03E-15	9.81E-13	4.03E-19
	270	6.27E-08	2.03E-07	1.47E-08	2.49E-09	1.11E-08	3.89E-10	2.04E-10	1.17E-09	2.33E-11
	315	4.06E-06	1.58E-05	3.33E-07	7.28E-07	4.35E-06	2.55E-08	1.92E-07	1.60E-06	3.48E-09
10	45	4.76E-06	1.20E-05	1.38E-06	3.20E-07	1.17E-06	5.53E-08	3.94E-08	1.93E-07	4.56E-09
	90	6.25E-08	2.02E-07	1.47E-08	2.48E-09	1.11E-08	3.88E-10	2.03E-10	1.17E-09	2.31E-11
	135	2.31E-13	4.71E-11	1.08E-17	7.97E-16	6.30E-13	2.81E-21	9.83E-18	2.22E-14	4.63E-24
	225	2.32E-13	4.72E-11	1.09E-17	8.03E-16	6.33E-13	2.83E-21	9.90E-18	2.23E-14	4.68E-24
	270	6.26E-08	2.02E-07	1.47E-08	2.48E-09	1.11E-08	3.88E-10	2.03E-10	1.17E-09	2.32E-11
	315	4.76E-06	1.20E-05	1.38E-06	3.20E-07	1.17E-06	5.53E-08	3.94E-08	1.93E-07	4.56E-09

Table 5.14. Split-Time Extrapolation for Capsizing Rate for Wave Height 7.5 m and Mean Zero-crossing Period 8.5 s

Spd, kn	Head. °	Prediction Error Function			Goodness of Fit with p=0.1			Goodness of Fit with p=0.2		
		Estimate	Upper	Lower	Upper	Lower	Upper	Upper	Lower	Upper
0	45	3.12E-10	3.70E-07	1.00E-30	1.75E-08	2.83E-06	1.00E-30	1.75E-08	2.83E-06	1.00E-30
	90	5.77E-10	1.55E-08	1.70E-12	5.09E-09	4.67E-08	1.84E-10	2.09E-09	2.75E-08	3.56E-11
	135	1.94E-31	1.96E-23	2.17E-50	1.11E-21	3.80E-18	1.86E-27	1.11E-21	3.80E-18	1.86E-27
	225	1.55E-13	1.78E-10	6.87E-22	1.41E-10	1.15E-09	8.99E-12	2.86E-11	5.99E-10	3.11E-13
	270	1.74E-25	1.82E-19	6.47E-39	4.68E-17	4.33E-15	8.65E-20	1.14E-21	2.18E-17	8.44E-30
	315	1.42E-06	6.06E-06	1.28E-07	2.62E-07	4.49E-06	1.49E-12	2.62E-07	4.49E-06	1.49E-12
5	45	3.39E-09	5.50E-07	2.47E-33	1.12E-10	1.19E-07	1.32E-72	1.12E-10	1.19E-07	1.32E-72
	90	5.77E-10	1.55E-08	1.70E-12	3.31E-09	3.67E-08	8.09E-11	3.31E-09	3.67E-08	8.09E-11
	135	1.00E-30	1.00E-29	1.00E-31	1.00E-30	1.00E-29	1.00E-31	1.00E-30	1.00E-29	1.00E-31
	225	3.63E-22	6.23E-17	3.08E-34	3.60E-30	1.72E-18	1.0E-146	3.60E-30	1.72E-18	1.0E-146
	270	1.74E-25	1.82E-19	6.47E-39	5.35E-17	4.86E-15	1.03E-19	7.91E-22	1.77E-17	3.84E-30
	315	2.51E-07	2.21E-06	2.83E-09	5.94E-08	4.59E-07	2.25E-09	4.91E-07	3.03E-06	1.82E-08
10	45	1.22E-12	1.21E-09	1.12E-22	1.94E-14	6.59E-13	1.58E-16	6.20E-16	9.76E-12	8.36E-30
	90	5.77E-10	1.55E-08	1.70E-12	3.31E-09	3.67E-08	8.09E-11	3.31E-09	3.67E-08	8.09E-11
	135	1.00E-30	1.00E-29	1.00E-31	1.00E-30	1.00E-29	1.00E-31	1.00E-30	1.00E-29	1.00E-31
	225	1.77E-14	2.70E-12	4.52E-18	5.99E-22	6.90E-13	1.00E-30	5.99E-22	6.90E-13	1.00E-30
	270	1.74E-25	1.82E-19	6.47E-39	4.70E-16	2.15E-14	2.79E-18	7.91E-22	1.77E-17	3.84E-30
	315	2.59E-09	3.13E-08	5.28E-11	1.74E-08	7.58E-08	2.58E-09	1.31E-08	6.42E-08	1.61E-09

Table 5.14. Split-Time Extrapolation for Capsizing Rate for Wave Height 7.5 m and Mean Zero-crossing Period 8.5 s (cont.)

HS	TZ	Goodness of Fit with p=0.3			Goodness of Fit with p=0.4			Goodness of Fit with p=0.5		
		Estimate	Upper	Lower	Upper	Lower	Upper	Upper	Lower	Upper
0	45	1.75E-08	2.83E-06	1.00E-30	1.75E-08	2.83E-06	1.00E-30	1.75E-08	2.83E-06	1.00E-30
	90	1.19E-10	9.07E-09	1.02E-14	1.11E-10	1.45E-08	3.78E-16	1.11E-10	1.45E-08	3.78E-16
	135	1.66E-33	6.74E-23	1.76E-71	1.66E-33	6.74E-23	1.76E-71	1.66E-33	6.74E-23	1.76E-71
	225	7.74E-16	1.34E-10	2.14E-71	7.74E-16	1.34E-10	2.14E-71	7.74E-16	1.34E-10	2.14E-71
	270	1.14E-21	2.18E-17	8.44E-30	1.14E-21	2.18E-17	8.44E-30	1.14E-21	2.18E-17	8.44E-30
	315	7.01E-07	7.53E-06	7.17E-11	7.01E-07	7.53E-06	7.17E-11	7.01E-07	7.53E-06	7.17E-11
5	45	1.12E-10	1.19E-07	1.32E-72	1.12E-10	1.19E-07	1.32E-72	1.12E-10	1.19E-07	1.32E-72
	90	1.62E-09	2.40E-08	2.11E-11	1.06E-10	1.42E-08	3.22E-16	1.06E-10	1.42E-08	3.22E-16
	135	1.00E-30	1.00E-29	1.00E-31	1.00E-30	1.00E-29	1.00E-31	1.00E-30	1.00E-29	1.00E-31
	225	3.60E-30	1.72E-18	1.0E-146	3.60E-30	1.72E-18	1.3E-146	3.60E-30	1.72E-18	1.3E-146
	270	7.91E-22	1.77E-17	3.84E-30	7.91E-22	1.77E-17	3.84E-30	7.91E-22	1.77E-17	3.84E-30
	315	4.91E-07	3.03E-06	1.82E-08	1.01E-07	1.61E-06	4.35E-11	1.01E-07	1.61E-06	4.35E-11
10	45	6.20E-16	9.76E-12	8.36E-30	8.07E-15	5.01E-11	2.52E-27	8.07E-15	5.01E-11	2.52E-27
	90	1.62E-09	2.40E-08	2.11E-11	1.06E-10	1.42E-08	3.22E-16	1.06E-10	1.42E-08	3.22E-16
	135	1.00E-30	1.00E-29	1.00E-31	1.00E-30	1.00E-29	1.00E-31	1.00E-30	1.00E-29	1.00E-31
	225	5.99E-22	6.90E-13	1.00E-30	5.99E-22	6.90E-13	1.00E-30	5.99E-22	6.90E-13	1.00E-30
	270	7.91E-22	1.77E-17	3.84E-30	7.91E-22	1.77E-17	3.84E-30	7.91E-22	1.77E-17	3.84E-30
	315	7.84E-10	3.77E-08	1.08E-13	7.84E-10	3.77E-08	1.08E-13	3.42E-10	2.54E-08	8.06E-15

Table 5.15. Summary of EPOT Calculations: Estimate of Rate 1/s

HS	TZ	Target 30°			Target 40°			Target 50°		
		Estimate	Upper	Lower	Estimate	Upper	Lower	Estimate	Upper	Lower
3.5	6.5	2.79E-10	2.00E-09	2.03E-11	1.96E-11	2.03E-10	8.63E-13	2.50E-12	3.46E-11	7.45E-14
4.5	6.5	4.47E-09	1.87E-08	7.31E-10	3.91E-10	2.14E-09	4.71E-11	6.05E-11	4.03E-10	5.92E-12
5.5	6.5	3.25E-08	1.58E-07	3.39E-09	4.57E-09	3.14E-08	2.67E-10	1.14E-09	1.00E-08	4.46E-11
5.5	8.5	6.01E-08	2.14E-07	1.07E-08	5.66E-09	2.82E-08	6.15E-10	9.06E-10	5.89E-09	6.70E-11
7.5	8.5	2.46E-06	6.46E-06	5.85E-07	6.44E-07	2.13E-06	1.04E-07	2.52E-07	9.83E-07	3.11E-08
9.5	8.5	5.84E-05	9.37E-05	3.15E-05	2.10E-05	3.98E-05	9.26E-06	9.67E-06	2.06E-05	3.73E-06
13.5	8.5	0.00136	0.00142	0.00144	0.000551	0.000657	0.000454	0.000328	0.000402	0.000264
5.5	10.5	1.58E-08	8.29E-08	1.36E-09	1.25E-09	1.01E-08	5.53E-11	1.76E-10	1.98E-09	4.62E-12
7.5	10.5	2.08E-07	7.64E-07	3.31E-08	1.24E-08	7.43E-08	9.24E-10	1.40E-09	1.24E-08	5.80E-11
9.5	10.5	7.09E-06	1.45E-05	3.03E-06	1.08E-06	2.67E-06	3.94E-07	2.92E-07	7.83E-07	9.97E-08
13.5	10.5	0.000397	0.000474	0.000325	0.000147	0.000189	0.000111	7.52E-05	0.000103	5.21E-05
5.5	12.5	3.59E-09	2.07E-08	3.08E-10	3.41E-10	2.79E-09	1.74E-11	5.52E-11	5.97E-10	1.88E-12
7.5	12.5	1.34E-07	4.94E-07	2.36E-08	1.56E-08	8.02E-08	1.69E-09	2.94E-09	1.97E-08	2.20E-10
9.5	12.5	7.20E-07	2.75E-06	6.64E-08	4.82E-08	3.81E-07	1.03E-09	5.97E-09	8.37E-08	4.18E-11
13.5	12.5	6.56E-05	9.36E-05	4.39E-05	1.87E-05	3.11E-05	9.78E-06	7.30E-06	1.38E-05	3.25E-06

While clustering were used for parametric roll (see Table 5.9), another scheme of data extension was tried here: spline interpolation was used between the cells and linear extrapolation for the outside points. The calculations were not performed for the cells with zero statistical weight.

The results of these data extension approach for EPOT are shown in Table 5.16 (an estimated rate for exceedance of 40 degrees) and 5.17 (upper boundaries if the estimates). The split-time results are shown in Table 5.18 (estimates for capsizing rate) and Table 5.19 (upper boundaries of the estimates). Goodness of fit test with p=0.2 was used to fit the exponential tail for split-time metrics. The sea states where simulation was performed are highlighted with yellow in Tables 5.16 through 5.19. These were the nodes for spline interpolation (some of these points had to be removed to avoid oscillation of splines). While the applied data extension technique is “ad hoc”, it has revealed a known fact that a long –term probability of pure loss of stability is governed by a few cells of scatter table with steep waves. These cells are highlighted by light red.

Table 5.16. Summary of Split-Time Calculations: Estimate of Capsizing Rate 1/s

HS	TZ	Prediction Error Function			Goodness of fit with p=0.1			Goodness of fit with p=0.2		
		Estimate	Upper	Lower	Upper	Lower	Upper	Upper	Lower	Upper
3.5	6.5	5.98E-19	2.71E-15	2.04E-26	2.06E-21	1.04E-16	4.01E-25	3.09E-22	1.14E-16	2.53E-30
4.5	6.5	1.20E-11	2.42E-09	1.91E-19	1.12E-14	1.40E-11	6.31E-18	3.22E-13	3.45E-10	1.56E-22
5.5	6.5	6.07E-08	3.41E-07	4.02E-09	1.46E-08	3.32E-07	1.49E-10	3.47E-08	4.48E-07	9.64E-10
5.5	8.5	3.39E-13	8.92E-11	2.32E-18	1.37E-12	2.00E-10	2.35E-14	2.83E-11	1.38E-08	5.49E-15
7.5	8.5	6.99E-08	3.86E-07	5.47E-09	1.53E-08	3.37E-07	2.16E-10	3.30E-08	4.43E-07	8.35E-10
9.5	8.5	1.26E-06	4.55E-06	1.79E-07	2.20E-06	5.43E-06	7.08E-07	1.45E-06	4.93E-06	1.69E-07
13.5	8.5	0.000111	0.000147	7.80E-05	0.000111	0.000148	7.82E-05	0.000111	0.000148	7.79E-05
5.5	10.5	5.01E-16	2.11E-13	9.26E-21	9.86E-15	2.15E-13	2.34E-16	1.15E-15	1.86E-12	1.09E-17
7.5	10.5	3.92E-10	2.56E-08	7.30E-14	8.70E-10	4.49E-08	8.88E-11	6.81E-10	4.43E-08	4.90E-11
9.5	10.5	2.74E-07	1.18E-06	1.72E-08	2.07E-07	9.98E-07	1.60E-08	1.85E-07	9.82E-07	9.28E-09
13.5	10.5	1.90E-05	3.16E-05	8.22E-06	1.90E-05	3.18E-05	8.25E-06	1.90E-05	3.18E-05	8.23E-06
5.5	12.5	4.48E-17	5.25E-14	2.42E-23	6.87E-15	2.28E-13	4.92E-17	2.16E-15	1.80E-13	7.68E-18
7.5	12.5	2.81E-11	5.78E-10	2.07E-13	6.39E-11	3.15E-10	8.83E-12	3.49E-11	1.15E-09	3.55E-14
9.5	12.5	3.88E-09	3.42E-08	1.16E-10	6.34E-09	2.10E-08	1.42E-09	6.97E-10	1.99E-08	6.26E-13
13.5	12.5	7.28E-07	2.59E-06	1.18E-07	1.27E-06	3.31E-06	3.58E-07	8.61E-07	2.80E-06	2.18E-07

Table 5.16. Summary of Split-Time Calculations: Estimate of Capsizing Rate 1/s (cont.)

HS	TZ	Goodness of Fit with p=0.3			Goodness of Fit with p=0.4			Goodness of Fit with p=0.5		
		Estimate	Upper	Lower	Upper	Lower	Upper	Upper	Lower	Upper
3.5	6.5	1.15E-21	1.52E-16	2.E-30	2.37E-21	2.26E-16	2.89E-31	2.37E-21	2.26E-16	4.89E-32
4.5	6.5	3.22E-13	3.45E-10	1.56E-22	1.42E-12	5.66E-10	2.97E-18	3.17E-12	1.30E-09	2.97E-18
5.5	6.5	4.78E-08	5.55E-07	5.60E-10	3.42E-08	5.06E-07	4.80E-12	3.42E-08	5.07E-07	4.80E-12
5.5	8.5	2.82E-11	1.38E-08	2.53E-16	2.81E-11	1.38E-08	6.32E-17	2.80E-11	1.38E-08	1.79E-17
7.5	8.5	5.06E-08	5.67E-07	7.64E-10	3.42E-08	5.07E-07	4.81E-12	3.42E-08	5.06E-07	4.80E-12
9.5	8.5	1.41E-06	5.03E-06	1.42E-07	1.36E-06	5.18E-06	9.10E-08	1.45E-06	5.60E-06	6.19E-08
13.5	8.5	0.000111	0.000148	7.79E-05	0.000111	0.000148	7.79E-05	0.000111	0.000147	7.79E-05
5.5	10.5	2.25E-16	1.96E-12	2.22E-19	1.46E-16	1.95E-12	7.85E-20	1.43E-16	2.67E-12	1.43E-23
7.5	10.5	3.14E-10	4.62E-08	1.62E-12	2.60E-10	4.69E-08	1.90E-16	2.60E-10	4.69E-08	1.90E-16
9.5	10.5	1.37E-07	1.01E-06	2.39E-09	1.35E-07	1.00E-06	2.38E-09	2.53E-07	1.23E-06	1.65E-08
13.5	10.5	1.89E-05	3.17E-05	8.22E-06	1.89E-05	3.17E-05	8.22E-06	1.89E-05	3.17E-05	8.22E-06
5.5	12.5	1.91E-18	1.04E-13	1.04E-28	1.91E-18	1.04E-13	3.42E-30	1.91E-18	1.04E-13	3.16E-30
7.5	12.5	1.95E-11	8.48E-10	8.56E-15	1.97E-11	1.21E-09	8.56E-15	1.97E-11	1.21E-09	8.56E-15
9.5	12.5	6.85E-10	2.01E-08	3.41E-13	5.86E-10	2.50E-08	1.03E-13	6.47E-09	8.62E-08	1.35E-11
13.5	12.5	7.14E-07	2.60E-06	1.47E-07	5.34E-07	2.49E-06	3.27E-08	5.26E-07	2.47E-06	3.21E-08

Table 5.17. Estimates of Exceedance Rate for 40 degrees, 1/s (columns are mean zero-crossing period in seconds, rows are significant wave heights in meters)

Hs \ TZ	3.5	4.5	5.5	6.5	7.5	8.5	9.5	10.5
0.5	5.05E-10	2.38E-10	1.12E-10	5.25E-11	2.47E-11	1.16E-11	5.46E-12	2.57E-12
1.5	0	8.19E-10	3.85E-10	1.81E-10	8.52E-11	4.01E-11	1.88E-11	8.86E-12
2.5	0	2.82E-09	1.33E-09	6.24E-10	2.94E-10	1.38E-10	6.49E-11	3.05E-11
3.5	0	9.74E-09	4.58E-09	2.15E-09	1.01E-09	4.76E-10	2.24E-10	1.05E-10
4.5	0	0	1.58E-08	7.42E-09	3.49E-09	1.64E-09	7.72E-10	3.63E-10
5.5	0	0	5.44E-08	2.56E-08	1.20E-08	5.66E-09	2.66E-09	1.25E-09
6.5	0	0	1.29E-06	4.61E-07	1.65E-07	5.90E-08	2.11E-08	7.56E-09
7.5	0	0	0	6.88E-06	1.94E-06	5.49E-07	1.55E-07	4.37E-08
8.5	0	0	0	7.04E-05	1.69E-05	4.04E-06	9.69E-07	2.32E-07
9.5	0	0	0	0.000408	9.27E-05	2.10E-05	4.77E-06	1.08E-06
10.5	0	0	0	0	0.000291	7.14E-05	1.75E-05	4.30E-06
11.5	0	0	0	0	0.000579	0.000171	5.07E-05	1.50E-05
12.5	0	0	0	0	0.000848	0.000326	0.000125	4.80E-05
13.5	0	0	0	0	0	0.000551	0.000285	0.000147
14.5	0	0	0	0	0	0.000694	0.000358	0.000185
15.5	0	0	0	0	0	0	0.000451	0.000233
16.5	0	0	0	0	0	0	0	0.000293

Table 5.17. Estimates of Exceedance Rate for 40°, 1/s (Columns are Mean Zero-Crossing Period in Seconds, Rows are Significant Wave Heights in Meters, cont.)

Hs \ TZ	11.5	12.5	13.5	14.5	15.5	16.5	17.5	18.5
0.5	1.34E-12	7.00E-13	0	0	0	0	0	0
1.5	4.62E-12	2.41E-12	1.26E-12	6.58E-13	3.44E-13	0	0	0
2.5	1.59E-11	8.32E-12	4.35E-12	2.27E-12	1.18E-12	6.18E-13	0	0
3.5	5.50E-11	2.87E-11	1.50E-11	7.82E-12	4.08E-12	2.13E-12	1.11E-12	0
4.5	1.89E-10	9.89E-11	5.16E-11	2.70E-11	1.41E-11	7.35E-12	3.84E-12	0
5.5	6.53E-10	3.41E-10	1.78E-10	9.29E-11	4.85E-11	2.53E-11	1.32E-11	6.91E-12
6.5	2.89E-09	1.11E-09	4.24E-10	1.62E-10	6.21E-11	2.38E-11	9.11E-12	3.49E-12
7.5	1.27E-08	3.69E-09	1.07E-09	3.10E-10	9.01E-11	2.62E-11	7.59E-12	2.20E-12
8.5	5.46E-08	1.29E-08	3.03E-09	7.12E-10	1.68E-10	3.94E-11	9.28E-12	2.18E-12
9.5	2.28E-07	4.82E-08	1.02E-08	2.14E-09	4.52E-10	9.55E-11	2.01E-11	4.25E-12
10.5	9.20E-07	1.97E-07	4.21E-08	9.01E-09	1.93E-09	4.12E-10	8.82E-11	1.89E-11
11.5	3.60E-06	8.63E-07	2.07E-07	4.97E-08	1.19E-08	2.86E-09	6.86E-10	1.65E-10
12.5	1.38E-05	3.97E-06	1.14E-06	3.29E-07	9.46E-08	2.72E-08	7.83E-09	0
13.5	5.24E-05	1.87E-05	6.67E-06	2.38E-06	8.49E-07	3.03E-07	1.08E-07	0
14.5	6.60E-05	2.36E-05	8.40E-06	3.00E-06	1.07E-06	3.81E-07	0	0
15.5	8.31E-05	2.97E-05	1.06E-05	3.77E-06	1.35E-06	4.80E-07	0	0
16.5	0.000105	3.73E-05	1.33E-05	4.75E-06	1.69E-06	0	0	0

Table 5.18. Upper Boundaries of Exceedance Rate for 40°, 1/s (Columns are Mean Zero-Crossing Period in Seconds, Rows are Significant Wave Heights in Meters)

Hs \ TZ	3.5	4.5	5.5	6.5	7.5	8.5	9.5	10.5
0.5	7.89E-10	4.72E-10	2.82E-10	1.69E-10	1.01E-10	6.05E-11	3.62E-11	2.16E-11
1.5	0	1.61E-09	9.65E-10	5.77E-10	3.45E-10	2.07E-10	1.24E-10	7.40E-11
2.5	0	5.51E-09	3.30E-09	1.97E-09	1.18E-09	7.06E-10	4.22E-10	2.53E-10
3.5	0	1.88E-08	1.13E-08	6.74E-09	4.03E-09	2.41E-09	1.44E-09	8.64E-10
4.5	0	0	3.85E-08	2.30E-08	1.38E-08	8.25E-09	4.93E-09	2.95E-09
5.5	0	0	1.32E-07	7.88E-08	4.71E-08	2.82E-08	1.69E-08	1.01E-08
6.5	0	0	2.58E-06	1.14E-06	5.07E-07	2.24E-07	9.93E-08	4.40E-08
7.5	0	0	0	1.39E-05	4.73E-06	1.61E-06	5.46E-07	1.86E-07
8.5	0	0	0	0.000119	3.33E-05	9.35E-06	2.63E-06	7.37E-07
9.5	0	0	0	0.000594	0.000154	3.98E-05	1.03E-05	2.67E-06
10.5	0	0	0	0	0.000423	0.000116	3.16E-05	8.63E-06
11.5	0	0	0	0	0.000763	0.000245	7.90E-05	2.54E-05
12.5	0	0	0	0	0.00104	0.000423	0.000173	7.04E-05
13.5	0	0	0	0	0	0.000657	0.000353	0.000189
14.5	0	0	0	0	0	0.000828	0.000444	0.000238
15.5	0	0	0	0	0	0	0.000559	0.0003
16.5	0	0	0	0	0	0	0	0.000378

Table 5.18. Upper Boundaries of Exceedance Rate for 40°, 1/s (Columns are Mean Zero-Crossing Period in Seconds, Rows are Significant Wave Heights in Meters, Cont.)

Hs \ TZ	11.5	12.5	13.5	14.5	15.5	16.5	17.5	18.5
0.5	1.14E-11	5.99E-12	0	0	0	0	0	0
1.5	3.89E-11	2.05E-11	1.08E-11	5.67E-12	2.98E-12	0	0	0
2.5	1.33E-10	7.00E-11	3.68E-11	1.94E-11	1.02E-11	5.36E-12	0	0
3.5	4.54E-10	2.39E-10	1.26E-10	6.62E-11	3.48E-11	1.83E-11	9.64E-12	0
4.5	1.55E-09	8.17E-10	4.30E-10	2.26E-10	1.19E-10	6.26E-11	3.30E-11	0
5.5	5.31E-09	2.79E-09	1.47E-09	7.73E-10	4.07E-10	2.14E-10	1.13E-10	5.93E-11
6.5	2.08E-08	9.84E-09	4.65E-09	2.20E-09	1.04E-09	4.93E-10	2.33E-10	1.10E-10
7.5	7.97E-08	3.42E-08	1.47E-08	6.31E-09	2.71E-09	1.16E-09	4.99E-10	2.14E-10
8.5	2.93E-07	1.16E-07	4.62E-08	1.83E-08	7.28E-09	2.89E-09	1.15E-09	4.56E-10
9.5	1.01E-06	3.81E-07	1.44E-07	5.44E-08	2.05E-08	7.76E-09	2.93E-09	1.11E-09
10.5	3.21E-06	1.19E-06	4.45E-07	1.65E-07	6.16E-08	2.29E-08	8.52E-09	3.17E-09
11.5	9.59E-06	3.61E-06	1.36E-06	5.14E-07	1.94E-07	7.30E-08	2.75E-08	1.04E-08
12.5	2.74E-05	1.07E-05	4.15E-06	1.62E-06	6.29E-07	2.45E-07	9.53E-08	0
13.5	7.68E-05	3.11E-05	1.26E-05	5.12E-06	2.08E-06	8.43E-07	3.42E-07	0
14.5	9.66E-05	3.92E-05	1.59E-05	6.45E-06	2.62E-06	1.06E-06	0	0
15.5	0.000122	4.94E-05	2.00E-05	8.12E-06	3.29E-06	1.34E-06	0	0
16.5	0.000153	6.21E-05	2.52E-05	1.02E-05	4.15E-06	0	0	0

Table 5.19. Estimates of Capsizing Rate, 1/s (Columns are Mean Zero-Crossing Period in Seconds, Rows are Significant Wave Heights in Meters)

Hs\TZ	3.5	4.5	5.5	6.5	7.5	8.5	9.5	10.5
0.5	1.52E-08	2.18E-09	3.13E-10	4.49E-11	6.44E-12	9.25E-13	1.33E-13	1.91E-14
1.5	0	9.73E-09	1.40E-09	2.01E-10	2.88E-11	4.14E-12	5.94E-13	8.53E-14
2.5	0	4.35E-08	6.25E-09	8.97E-10	1.29E-10	1.85E-11	2.66E-12	3.81E-13
3.5	0	1.95E-07	2.79E-08	4.01E-09	5.76E-10	8.27E-11	1.19E-11	1.70E-12
4.5	0	0	1.25E-07	1.79E-08	2.57E-09	3.70E-10	5.31E-11	7.62E-12
5.5	0	0	5.58E-07	8.01E-08	1.15E-08	1.65E-09	2.37E-10	3.41E-11
6.5	0	0	2.50E-06	3.58E-07	5.14E-08	7.39E-09	1.06E-09	1.52E-10
7.5	0	0	0	1.60E-06	2.30E-07	3.30E-08	4.74E-09	6.81E-10
8.5	0	0	0	4.24E-06	1.01E-06	2.42E-07	5.78E-08	1.38E-08
9.5	0	0	0	1.13E-05	4.05E-06	1.45E-06	5.18E-07	1.85E-07
10.5	0	0	0	0	1.37E-05	6.09E-06	2.72E-06	1.21E-06
11.5	0	0	0	0	4.00E-05	1.90E-05	9.00E-06	4.27E-06
12.5	0	0	0	0	0.000106	4.83E-05	2.20E-05	9.98E-06
13.5	0	0	0	0	0	0.000111	4.59E-05	1.90E-05
14.5	0	0	0	0	0	0.00014	5.78E-05	2.39E-05
15.5	0	0	0	0	0	0	7.28E-05	3.01E-05
16.5	0	0	0	0	0	0	0	3.79E-05

Table 5.19. Estimates of Capsizing Rate, 1/s (Columns are Mean Zero-Crossing Period in Seconds, Rows are Significant Wave Heights in Meters, Cont.)

Hs\TZ	11.5	12.5	13.5	14.5	15.5	16.5	17.5	18.5
0.5	4.32E-15	9.78E-16	0	0	0	0	0	0
1.5	1.93E-14	4.37E-15	9.89E-16	2.24E-16	5.07E-17	0	0	0
2.5	8.63E-14	1.95E-14	4.42E-15	1.00E-15	2.27E-16	5.13E-17	0	0
3.5	3.86E-13	8.74E-14	1.98E-14	4.48E-15	1.01E-15	2.29E-16	5.19E-17	0
4.5	1.73E-12	3.91E-13	8.84E-14	2.00E-14	4.53E-15	1.03E-15	2.32E-16	0
5.5	7.71E-12	1.75E-12	3.95E-13	8.95E-14	2.03E-14	4.59E-15	1.04E-15	2.35E-16
6.5	3.45E-11	7.81E-12	1.77E-12	4.00E-13	9.06E-14	2.05E-14	4.64E-15	1.05E-15
7.5	1.54E-10	3.49E-11	7.90E-12	1.79E-12	4.05E-13	9.17E-14	2.07E-14	4.70E-15
8.5	1.44E-09	1.51E-10	1.57E-11	1.64E-12	1.72E-13	1.79E-14	1.88E-15	1.96E-16
9.5	1.14E-08	6.97E-10	4.28E-11	2.63E-12	1.61E-13	9.89E-15	6.07E-16	3.72E-17
10.5	6.65E-08	3.65E-09	2.01E-10	1.10E-11	6.06E-13	3.33E-14	1.83E-15	1.00E-16
11.5	3.01E-07	2.13E-08	1.50E-09	1.06E-10	7.49E-12	5.28E-13	3.73E-14	2.63E-15
12.5	1.15E-06	1.33E-07	1.53E-08	1.77E-09	2.04E-10	2.36E-11	2.72E-12	0
13.5	4.04E-06	8.61E-07	1.83E-07	3.90E-08	8.30E-09	1.77E-09	3.76E-10	0
14.5	5.09E-06	1.08E-06	2.31E-07	4.91E-08	1.05E-08	2.23E-09	0	0
15.5	6.41E-06	1.36E-06	2.90E-07	6.18E-08	1.32E-08	2.80E-09	0	0
16.5	8.07E-06	1.72E-06	3.66E-07	7.78E-08	1.66E-08	0	0	0

Table 5.20. Upper Boundaries of Capsizing Rate, 1/s (Columns are Mean Zero-Crossing Period in Seconds, Rows are Significant Wave Heights in Meters)

Hs\TZ	3.5	4.5	5.5	6.5	7.5	8.5	9.5	10.5
0.5	3.04E-08	9.60E-09	3.04E-09	9.61E-10	3.04E-10	9.61E-11	3.04E-11	9.62E-12
1.5	0	3.20E-08	1.01E-08	3.21E-09	1.01E-09	3.21E-10	1.01E-10	3.21E-11
2.5	0	1.07E-07	3.38E-08	1.07E-08	3.38E-09	1.07E-09	3.39E-10	1.07E-10
3.5	0	3.57E-07	1.13E-07	3.57E-08	1.13E-08	3.57E-09	1.13E-09	3.57E-10
4.5	0	0	3.77E-07	1.19E-07	3.77E-08	1.19E-08	3.77E-09	1.19E-09
5.5	0	0	1.26E-06	3.98E-07	1.26E-07	3.98E-08	1.26E-08	3.98E-09
6.5	0	0	4.19E-06	1.33E-06	4.20E-07	1.33E-07	4.20E-08	1.33E-08
7.5	0	0	0	4.43E-06	1.40E-06	4.43E-07	1.40E-07	4.43E-08
8.5	0	0	0	1.05E-05	4.03E-06	1.55E-06	5.93E-07	2.27E-07
9.5	0	0	0	2.48E-05	1.11E-05	4.93E-06	2.20E-06	9.82E-07
10.5	0	0	0	0	2.79E-05	1.35E-05	6.52E-06	3.16E-06
11.5	0	0	0	0	6.53E-05	3.22E-05	1.59E-05	7.85E-06
12.5	0	0	0	0	0.000146	7.06E-05	3.41E-05	1.65E-05
13.5	0	0	0	0	0	0.000148	6.85E-05	3.18E-05
14.5	0	0	0	0	0	0.000186	8.63E-05	4.00E-05
15.5	0	0	0	0	0	0	0.000109	5.04E-05
16.5	0	0	0	0	0	0	0	6.34E-05

Table 5.20. Upper Boundaries of Capsizing 1/s (Columns are Mean Zero-Crossing Period in Seconds, Rows are Significant Wave Heights in Meters, Cont.)

Hs\TZ	11.5	12.5	13.5	14.5	15.5	16.5	17.5	18.5
0.5	1.55E-12	2.50E-13	0	0	0	0	0	0
1.5	5.18E-12	8.35E-13	1.35E-13	2.17E-14	3.51E-15	0	0	0
2.5	1.73E-11	2.79E-12	4.50E-13	7.26E-14	1.17E-14	1.89E-15	0	0
3.5	5.77E-11	9.30E-12	1.50E-12	2.42E-13	3.91E-14	6.30E-15	1.02E-15	0
4.5	1.92E-10	3.10E-11	5.01E-12	8.08E-13	1.30E-13	2.10E-14	3.39E-15	0
5.5	6.42E-10	1.04E-10	1.67E-11	2.70E-12	4.35E-13	7.02E-14	1.13E-14	1.83E-15
6.5	2.14E-09	3.46E-10	5.58E-11	9.00E-12	1.45E-12	2.34E-13	3.78E-14	6.10E-15
7.5	7.15E-09	1.15E-09	1.86E-10	3.00E-11	4.84E-12	7.82E-13	1.26E-13	2.03E-14
8.5	3.34E-08	4.91E-09	7.21E-10	1.06E-10	1.56E-11	2.29E-12	3.36E-13	4.94E-14
9.5	1.40E-07	1.99E-08	2.83E-09	4.03E-10	5.74E-11	8.17E-12	1.16E-12	1.66E-13
10.5	4.85E-07	7.44E-08	1.14E-08	1.75E-09	2.70E-10	4.14E-11	6.36E-12	9.76E-13
11.5	1.43E-06	2.59E-07	4.71E-08	8.56E-09	1.56E-09	2.83E-10	5.14E-11	9.33E-12
12.5	3.77E-06	8.62E-07	1.97E-07	4.51E-08	1.03E-08	2.36E-09	5.39E-10	0
13.5	9.43E-06	2.80E-06	8.30E-07	2.46E-07	7.31E-08	2.17E-08	6.44E-09	0
14.5	1.19E-05	3.52E-06	1.05E-06	3.10E-07	9.20E-08	2.73E-08	0	0
15.5	1.49E-05	4.43E-06	1.32E-06	3.90E-07	1.16E-07	3.44E-08	0	0
16.5	1.88E-05	5.58E-06	1.66E-06	4.92E-07	1.46E-07	0	0	0

Results of long-term EPOT and Split-time extrapolations are summarized in Table 5.21 and 5.22. The data extension technique has failed for low boundary of capsizing rate estimate twice, which is noted in the Table 5.20. No noticeable data extension technique failures has been

spotted in Table 5.20. The reason for the failure in both cases is believed to be oscillation of spline.

Table 5.21. Results of Long-Term EPOT Extrapolation

Exceedance rate	Target 30 deg	Target 40 deg	Target 50 deg
Estimate, s^{-1}	$3.937\ 10^{-7}$	$1.160\ 10^{-7}$	$0.534\ 10^{-7}$
Upper boundary, s^{-1}	$6.680\ 10^{-7}$	$2.094\ 10^{-7}$	$0.988\ 10^{-7}$
Lower boundary, s^{-1}	$2.329\ 10^{-7}$	$0.634\ 10^{-7}$	$0.283\ 10^{-7}$

Table 5.22. Results of Long-Term Split-time Extrapolation

Rate of capsizing	Prediction error function	Goodness-of-Fit Test	
		p=0.1	p=0.2
Estimate, s^{-1}	$2.088\ 10^{-8}$	$1.790\ 10^{-8}$	$1.456\ 10^{-8}$
Upper boundary, s^{-1}	$4.593\ 10^{-8}$	$4.122\ 10^{-8}$	$4.408\ 10^{-8}$
Lower boundary, s^{-1}	failure	$0.86\ 10^{-8}$	$0.350\ 10^{-8}$
Rate of capsizing	Goodness-of-Fit Test		
	p=0.3	p=0.4	p=0.5
Estimate, s^{-1}	$1.507\ 10^{-8}$	$1.414\ 10^{-8}$	$1.778\ 10^{-8}$
Upper boundary, s^{-1}	$5.207\ 10^{-8}$	$4.770\ 10^{-8}$	$5.192\ 10^{-8}$
Lower boundary, s^{-1}	$0.326\ 10^{-8}$	$0.913\ 10^{-8}$	failure

Estimate of exceedance rates both for short-term and long-term formulation are consistent between the different targets, where rate of exceedance of lower target is always higher (see tables 5.12, 5.14 and 5.20). This is expected due to consistent application of Pareto distribution (equation 5.30). Averaging with the same weights, indeed, does not change this tendency.

Estimates of capsizing rate seem to be lower than the exceedance rates. While it could be expected from general point of view, there are some details, as the mathematical models behind EPOT and split-time do not guarantee such consistency. EPOT looks into with a peak exceedance event. A "peak" means a ship was heeled and then came back, EPOT ignores events when ship did not come back, i.e. capsized. Thus, a probability of exceedance of a peak near the vanishing stability angle should be lower than probability of capsizing. EPOT with Pareto distribution is not applicable for this situation, as Pareto models heavy tails for the roll peak, while actual tail becomes light near capsizing, see (Belenky et al., 2019). EPOT with Pareto distribution has a limit of applicability in the vicinity of the angle of vanishing stability. However, in case of the inconsistency between the capsizing and exceedance rate, the first suspicion falls on the failure of the data extension technique.

Upper boundary of both exceedance rate of 40° angle and capsizing rate are larger than the direct assessment standard for full probabilistic assessment $2.6\ 10^{-8}\ s^{-1}$ per paragraph 5.3.2.2 of Annex 1 of SDC6/WP.6.

5.3.7 Validation of Extrapolation Procedures: EPOT

Requirements for validation of extrapolation procedures are laid out in section 5.6 of Annex 1 SDC 6 /WP.6. An approach to statistical validation was described by Smith and Zuzick

(2015) with some details further corroborated in Weems *et al*. (2018). Per paragraph 5.6.2, the idea is to demonstrate that the extrapolated value is in reasonable statistical agreement with a direct counting result if a sample of such size would be available.

Per the recommendation in paragraph 5.6.3, a reduced order mathematical model in the form of volume-based 3-DOF calculations was applied as described in Weems *et al*. (2018). This fast code creates very large samples of data in which large roll angles associated with rare failures are observable. The observations estimates a "true value" from direct counting.

Following the guidance in paragraph 5.6.4 of Annex 1 SDC 6 /WP.6, a series of validation data sets was computed for the ONR tumblehome configuration (Bishop et al. 2005). Principle dimensions are in Table 5.5, however, KG = 7.5 m, resulting in GM = 2.2 m (same as in the example in subsection 5.3.6). Simulations were performed with independent pseudo-random realizations of a seaway by a Bretschneider spectrum with a significant wave height of 9 m and a modal period of 15 s. The ship speed was set to 6 kn. Other simulations parameters, including the total simulation time determined the true value, are presented in Table 5.23

Table 5.23. "True" Value Calculations for EPOT Validation

Heading Angles, °	Total Time, hr	Number of Targets	Largest Target	Number of Exceedances of Largest Target
15	570,000	5	20	14
22.5	200,000	7	27.5	16
30	200,000	13	45	9
37.5	200,000	15	60	7
45	690,000	15	70	8
60	600,000	15	70	12
90	690,000	9	37.5	12
135	690,000	3	20	6

The extrapolation procedure was applied to a series of small subsets of this large sample, and the extrapolated estimates were compared with the "true value." Figure 5.42 shows an example comparison for a 45° heading (stern quartering seas) and a target roll value of 45°. Fifty (50) extrapolation estimates are carried out, each computed from 100 hr of data, as recommended by paragraph 5.6.5 of Annex 1 SDC 6 /WP.6. The main index of performance is the passing rate, which indicates the percentage of successful extrapolations. An extrapolation is considered successful if the confidence interval of the extrapolated exceedance rate includes the "true value", as required by paragraph 5.6.6 of Annex 1 SDC 6 /WP.6. The example shown in Figure 8 has 45 successful extrapolations, resulting in a passing rate of 90 %, which exceeds 88 % established in paragraph 5.6.6 of Annex 1 SDC 6 /WP.6.

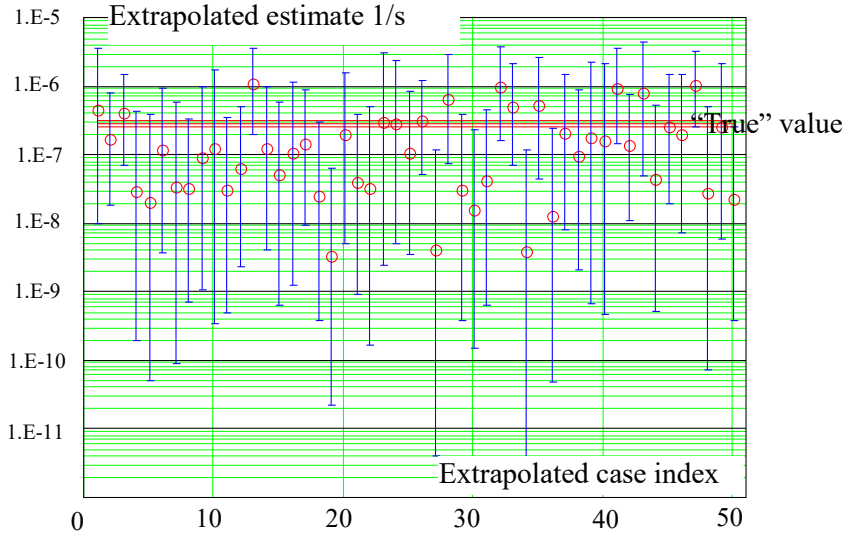

Figure 5.41. Example of Extrapolation Validation for a Heading of 45° and Target Value of 45°

In the three-tiered validation methodology of Smith and Zuzick (2015), the tiers are defined as:

- All extrapolations for a single target value,
- Extrapolations for all available target values, and
- Extrapolations for all available operational and environmental conditions.

The tier 1 validation is a set of comparisons of extrapolated estimates with the true value. Its example is shown in Figure 5.42.

The second tier of statistical validation considers all available target angles. The passing rates are shown in Fig. 5.43. An acceptable passing rate for 50 extrapolation data sets is from 0.88 to 1 (Smith, 2019, and paragraph 5.6.7 of Annex 1 of SDC 6 /WP.6 – and paragraph 3.5.6.7 of the Draft consolidated Interim Guidelines). This variation of the passing rate can be explained by the natural variability of the statistical estimates. The extrapolations are acceptable for all targets, excluding 50 and 60 degrees, for which the passing rates fell to 0.86. The average passing rate for the 45 degrees heading is 0.90, which is within the acceptable range.

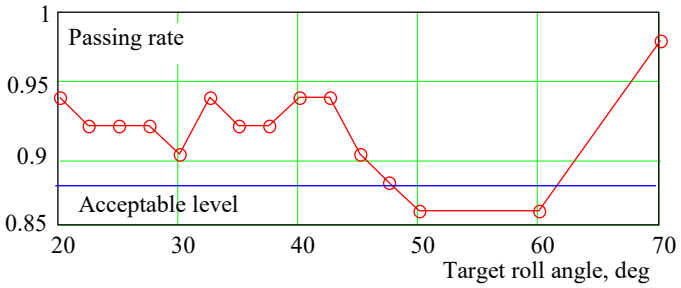

Figure 5.42. Passing Rate for Heading of 45°

The third tier of validation assesses the performance over all available conditions. The passing rates are shown in Fig. 5.43. Two lines are shown: one corresponds to an averaged passing rate over all target values, while the other corresponds to the smallest passing rate value encountered among all the target values. For a 45 degree heading, the latter corresponds to a minimum shown in Figure5.43. Obviously, the extrapolation did not work for the heading of 135 degrees.

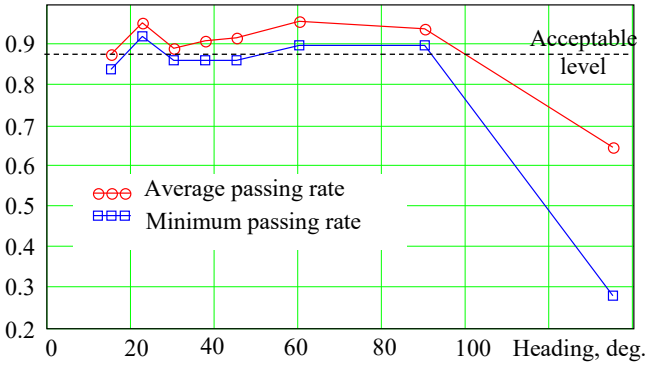

Figure 5.43. Passing Rate for all Headings

Belenky et al. (2018) looked into the reasons why the validation at the heading of 135 degrees failed, suggesting the reason is very likely to be insufficient data in the nonlinear region. The cited reference compared validation of 135 and 15 degrees heading. There angles were also small in the 15 degrees case, so the hypothesis was that the 15 degrees data are still nonlinear because of deterioration of stability in stern quartering seas.

Another hypotheses is that was not tested in (Belenky et al. 2018) is the influence of spectral width. The encounter wave spectrum in oblique seas (135 degrees heading) is significantly wider, compare to the encounter spectrum in stern seas (15 degrees heading). This leads to appearance of secondary wave peaks, generating the secondary peaks of roll motion. These secondary peaks may "confuse" envelope de-clustering, as shown in Fig. 5.31. To ensure that de-clustering algorithm provides statistically independent data, one may introduce an additional independence check, using decorrelation time as defined in the subsection 5.2.10 (Fig. 5.27) of this report. The may resolve the problem with validation of EPOT in oblique waves.

Meanwhile the lack of validation of EPOT in oblique waves does not have much influence on the present analysis. Belenky *et al*. (2018) reports that EPOT overestimates the target in oblique seas. In the case shown in Figure 5.44, the overestimation is about one order of magnitude, so inclusion of this data into averaging is conservative. At the same time, the exceedance rate data, seem to dominate by stern quartering seas, see Table 5.12. See the data for zero speed of 40° in Table 5.12: dropping the value from 2 10^{-12} s^{-1} to 10^{-13} s^{-1} seems to be inconsequential for the final result. Nevertheless validation of EPOT for oblique seas remains highly desirable.

Paragraph 5.6.5 requires validation to be performed for different sea states. Currently reported validation covers only one sea state with significant wave height of 9 m and modal period of 15 s. On this account, validation of EPOT can be recognized as partial at this time.

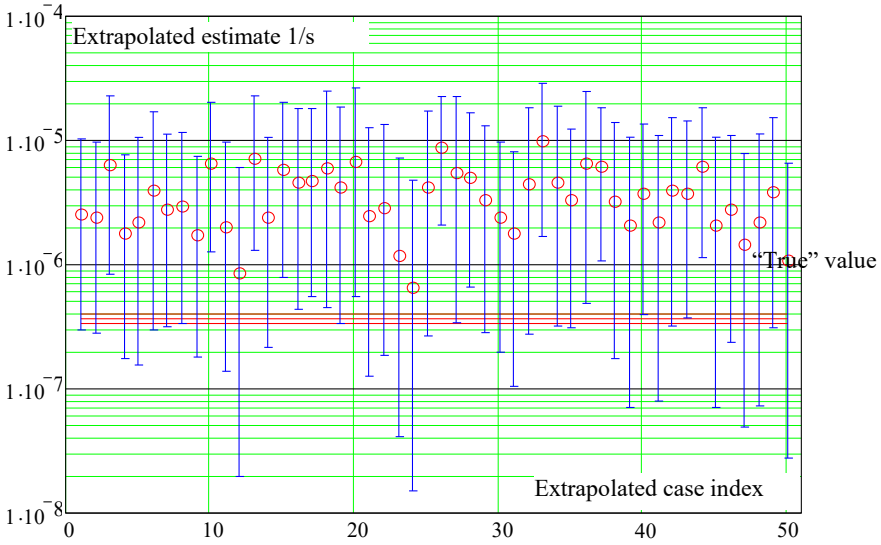

Figure 5.44. Extrapolations for a Heading 135° and Target Value 17.5° (Belenky *et al*. 2018)

5.3.8 Validation of Extrapolation Procedures: Split-time /Motion Perturbation Method

Requirements for validation of extrapolation procedures are available in section 5.6 of Annex 1 SDC 6 /WP.6. Per the recommendation in paragraph 5.6.3, a reduced order mathematical model in the form of volume-based 3-DOF calculations was applied as described in Weems et al. (2018). This fast code creates very large samples of data in which large roll angles associated with rare failures are observable. The observations estimates a "true value" from direct counting.

Following the guidance in paragraph 5.6.4 of Annex 1 SDC 6 /WP.6, a series of validation data sets was computed for the ONR tumblehome configuration (Bishop et al. 2005). Principle dimension are in Table 5.5, however, KG = 7.5 m, resulting in GM = 2.2 m (same as in the example in subsection 5.3.6). Simulations were performed with independent pseudo-random realizations of a seaway by a Bretschneider spectrum with a significant wave height of 9 m and a modal period of 14 s. The ship speed was set to 6 kn. Other simulations parameters, including the total simulation time determined the true value, are presented in Table 5.24.

Table 5.24. "True" Value Calculations for Split-Time Validation

Heading, °	Total Time, hr	"True" Estimate of Capsizing Rate, 1/s	Number of Capsizing's
35	720,000	4.71E-09	12
40	200,000	1.70E-08	12
45	200,000	7.20E-08	51
50	20,000	9.89E-08	7
55	60,000	3.25E-07	69
60	200,000	2.49E-07	176
65	200,000	1.13E-07	80
70	200,000	8.48E-09	6

The extrapolation procedure was applied to a series of small subsets of this large sample, and the extrapolated estimates were compared with the "true value." Fig. 5.45 shows an example comparison for a 45 degree heading (stern quartering seas) and a target roll value of 45 degrees. Fifty (50) extrapolation estimates were carried out, each computed from 100 hours of data. The main index of performance is the passing rate, which indicates the percentage of successful extrapolations. An extrapolation is considered successful if the confidence interval of the extrapolated exceedance rate includes the "true value." The example shown in Fig. 5.45 has 45 successful extrapolations, resulting in a passing rate of 98%. The exponential fit was done with the goodness-of-fit method while the significance level was taken equal to 0.2. Table 5.25 contains a summary for passing rates for other heading and methods of fitting the exponential tail.

Table 5.25. "True" Value Calculations for Split-Time Validation

Heading, °	Prediction Error Criterion	Goodness of Fit				
		p=0.1	p=0.2	p=0.3	p=0.4	p=0.5
35	0.94	1.00	1.00	1.00	1.00	1.00
40	0.98	0.92	0.98	1.00	1.00	0.98
45	0.98	0.98	0.98	0.96	0.98	0.98
50	1.00	0.98	1.00	1.00	1.00	1.00
55	1.00	0.98	0.98	0.98	0.98	0.98
60	0.98	0.92	0.98	0.96	0.96	0.96
65	0.90	0.92	0.98	1.00	0.96	0.96
70	0.98	0.86	0.96	0.98	1.00	0.98

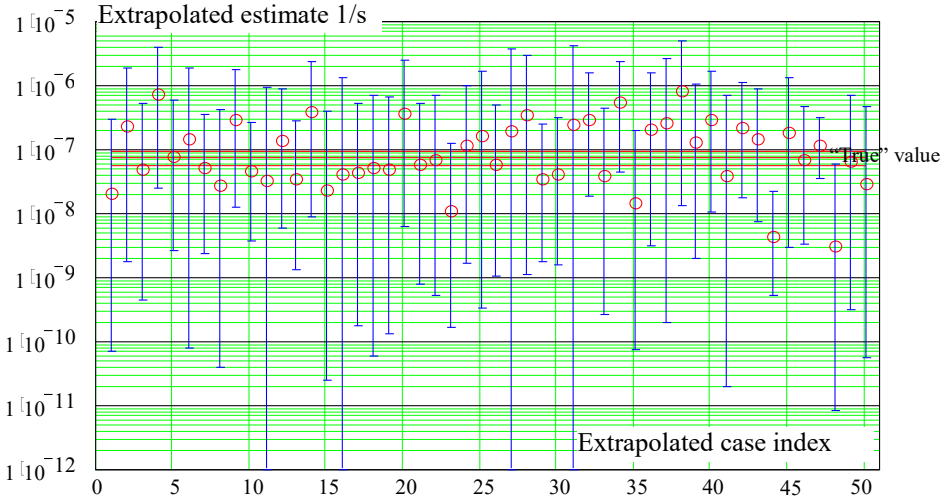

Figure 5.45. Validation of Capsizing Metric for the 45° Heading; Passing Rate is 0.98. Goodness-of-Fit Method with the Significance Level 0.2 was Used

The validity of the split-time method, can be characterized as acceptable. The passing rate falls short of the required 0.88 for a single case, but only by a minor amount - 0.02. However, paragraph 5.6.5 requires validation to be performed for different sea states. Currently reported validation covers only one sea state with significant wave height of 9 m and modal period of 12 seconds. On this account, validation of Split-time can be recognized as partial at this time.

5.3.9 Validation of Extrapolation Procedures: On the Required "Success Rate"

To determine the number of required datasets consider the confidence interval of the passing rate, assume an extrapolation method with ideal performance. That means that the percentage of failures related to random reason and tends to confidence probability P_β in infinity. If one uses the same confidence probability to assess the uncertainty of the passing rate, its boundaries are expressed as:

$$P_{low} = \frac{Qb\left(0.5\left(1-P_\beta\right);P_\beta,N_{Ex}\right)}{N_{Ex}} \tag{5.58}$$

$$P_{low} = \frac{Qb\left(0.5\left(1+P_\beta\right);P_\beta,N_{Ex}\right)}{N_{Ex}} \tag{5.59}$$

Where N_{ex} is the number of extrapolation datasets, i.e. the number of Bernoulli trials, while Qb is the quantile of binomial distribution.

The results are shown in Figure 5.46 for a number of extrapolation data set from 2 to 200. One can see that for the commonly used confidence probability of 0.95, $N_{ex} = 50$ provides a small-enough confidence interval for the statistical validation to be robust, the passing rate must be between 0.88 and 1.00. Other useful values can be found in Table 5.26.

It may make sense to add an additional accuracy allowance to make the boundaries a little wide to reflect approximations, inevitable in the extrapolation methods. Setting this allowance, however requires more practical experience with statistical validation and should be attempted later.

Table 5.26. Selected Values for Acceptable Boundaries for Passing Rates

Number of sets	50	60	70	80	90	100
Upper acceptable boundary of passing rate	0.88	0.883	0.9	0.9	0.9	0.9
Lower acceptable boundary for passing rate	1.0	1.0	1.0	0.988	0.989	0.99

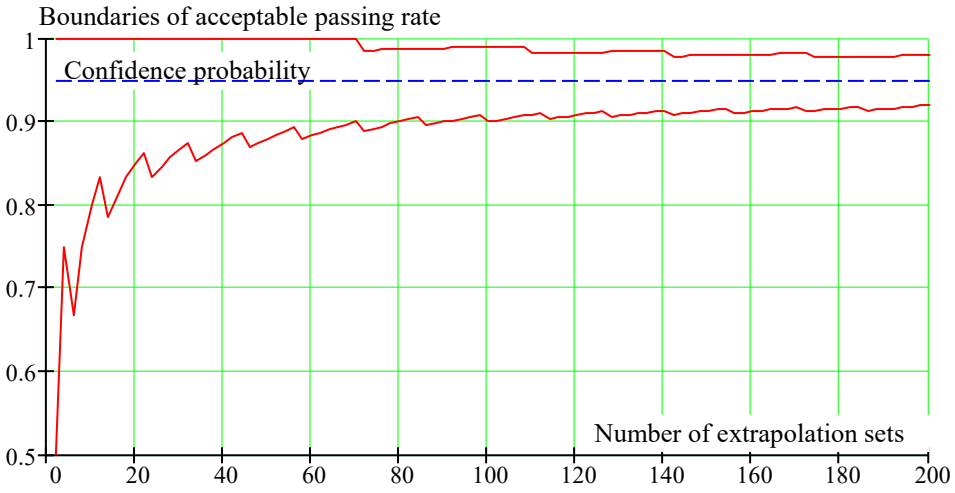

Figure 5.46. Boundaries of Acceptable Passing Rate

6. OPERATIONAL GUIDANCE AND OPERATIONAL LIMITATIONS

6.1 Effectiveness of Operational Guidance

For all failure modes, with the exception of the dead-ship condition, direct-stability assessment, and Level 2 vulnerability assessment, produce ship specific information about behavior in waves. When the information is presented to the master in an appropriate format, the results from these assessments of dynamic stability-failures may be used to improve safety. Recommendations for developing operational guidance and operational limitations are part of the second-generation intact-stability criteria and are included in Annex 2 of SDC6/WP.6.

Effectiveness of a proper operational guidance can be demonstrated with the example of a full probabilistic assessment, described in Subsection 5.3.6. The final results of this assessment are shown in Table 5.20 for exceedance of 40° roll and Table 5.21 for capsizing. Following requirements in paragraph 5.3.2.2 of Annex 1 of SDC 6/WP.6, these results were compared with the standard 2.6×10^{-8} s^{-1}, instead of the standard 2.6×10^{-3} $year^{-1}$, described in paragraph 1.2. The results from Table 5.20 and Table 5.21 to $year^{-1}$ may be recalculated by assuming 250 days at sea with reference to Table 5.17 (which is applicable for an exceedance of 40° and a capsizing rate with goodness of fit test with $p = 0.2$). Note that a uniform distribution was assumed for speeds and heading for calculations in Section 5.3.6, so the results may be considered as "without guidance". These resulst are summarized in Table 6.1.

Table 6.1. Long-Term Failure Rates without Assumed Guidance

Estimate	1/s	1/year
Estimate of exceedance rate of 40°	1.16E-7	2.505
Upper boundary of exceedance rate of 40°	2.094E-7	4.522
Estimate of capsizing rate	1.456E-8	0.315
Upper boundary of capsizing rate	4.408E-8	0.952

Such large values could be expected because: 1) the ONR tumblehome configuration is known for its vulnerability for pure loss of stability; and 2) assuming equal probability for all speeds and headings leads to very significant overestimations of the probability of failure because the realistic operator behavior was not taken into account (e.g. de Kat, et al 2002, Boonstra, *et al* 2004, ter Bekke, et al, 2006, van Daalen, et al 2005). The inclusion of a simple operator model was used to provide operational realism by the avoidance of beam and stern-quartering seas. The long-term results are in Table 6.2, while short term results are in the references for **Error! Reference source not found.** through **Error! Reference source not found.**.

Table 6.2. Long-Term Failure Rates with Assumed Guidance

Estimate	1/s	1/year
Estimate of exceedance rate of 40°	1.163E-10	2.51E-3
Upper boundary of exceedance rate of 40°	4.269E-10	9.22E-3
Estimate of capsizing rate	2.263E-11	4.89E-4
Upper boundary of capsizing rate	1.051E-10	2.27E-3

Table 6.3. Estimates of Exceedance Rate for 40°, 1/s (Columns are Mean Zero-Crossing Period in Seconds, Rows are Significant Wave Heights in Meters) with Assumed Guidance

Hs \ TZ	3.5	4.5	5.5	6.5	7.5	8.5	9.5	10.5
0.5	2.99E-13	4.70E-13	7.39E-13	1.16E-12	1.83E-12	2.88E-12	4.53E-12	7.13E-12
1.5	0	5.63E-13	8.86E-13	1.39E-12	2.19E-12	3.45E-12	5.43E-12	8.54E-12
2.5	0	6.75E-13	1.06E-12	1.67E-12	2.63E-12	4.13E-12	6.50E-12	1.02E-11
3.5	0	8.08E-13	1.27E-12	2.00E-12	3.15E-12	4.95E-12	7.79E-12	1.23E-11
4.5	0	0	1.52E-12	2.40E-12	3.77E-12	5.93E-12	9.33E-12	1.47E-11
5.5	0	0	1.83E-12	2.87E-12	4.52E-12	7.11E-12	1.12E-11	1.76E-11
6.5	0	0	1.27E-12	2.05E-12	3.29E-12	5.28E-12	8.48E-12	1.36E-11
7.5	0	0	0	2.09E-12	3.27E-12	5.12E-12	8.02E-12	1.26E-11
8.5	0	0	0	4.34E-12	6.06E-12	8.45E-12	1.18E-11	1.64E-11
9.5	0	0	0	2.64E-11	2.86E-11	3.09E-11	3.35E-11	3.63E-11
10.5	0	0	0	0	4.23E-10	3.01E-10	2.14E-10	1.52E-10
11.5	0	0	0	0	1.59E-08	6.49E-09	2.64E-09	1.07E-09
12.5	0	0	0	0	1.12E-06	2.38E-07	5.07E-08	1.08E-08
13.5	0	0	0	0	0	1.14E-05	1.21E-06	1.29E-07
14.5	0	0	0	0	0	1.44E-05	1.53E-06	1.62E-07
15.5	0	0	0	0	0	0	1.92E-06	2.04E-07
16.5	0	0	0	0	0	0	0	2.57E-07

Table 6.3 Estimates of Exceedance Rate for 40°, 1/s (Columns are Mean Zero-Crossing Period in Seconds, Rows are Significant Wave Heights in Meters) with Assumed Guidance, Cont.

Hs \ TZ	11.5	12.5	13.5	14.5	15.5	16.5	17.5	18.5
0.5	4.69E-13	3.08E-14	0	0	0	0	0	0
1.5	5.62E-13	3.70E-14	2.43E-15	1.60E-16	1.05E-17	0	0	0
2.5	6.73E-13	4.43E-14	2.91E-15	1.92E-16	1.26E-17	8.30E-19	0	0
3.5	8.06E-13	5.31E-14	3.49E-15	2.30E-16	1.51E-17	9.94E-19	6.54E-20	0
4.5	9.66E-13	6.36E-14	4.18E-15	2.75E-16	1.81E-17	1.19E-18	7.84E-20	0
5.5	1.16E-12	7.62E-14	5.01E-15	3.30E-16	2.17E-17	1.43E-18	9.39E-20	6.18E-21
6.5	1.25E-12	1.15E-13	1.05E-14	9.68E-16	8.88E-17	8.15E-18	7.49E-19	6.87E-20
7.5	1.60E-12	2.05E-13	2.61E-14	3.34E-15	4.26E-16	5.44E-17	6.94E-18	8.86E-19
8.5	2.90E-12	5.11E-13	9.00E-14	1.59E-14	2.80E-15	4.93E-16	8.70E-17	1.53E-17
9.5	8.74E-12	2.11E-12	5.08E-13	1.22E-13	2.95E-14	7.12E-15	1.72E-15	4.14E-16
10.5	4.94E-11	1.61E-11	5.24E-12	1.71E-12	5.56E-13	1.81E-13	5.89E-14	1.92E-14
11.5	4.68E-10	2.04E-10	8.86E-11	3.85E-11	1.68E-11	7.30E-12	3.18E-12	1.38E-12
12.5	6.23E-09	3.60E-09	2.08E-09	1.20E-09	6.95E-10	4.01E-10	2.32E-10	0
13.5	9.84E-08	7.53E-08	5.76E-08	4.40E-08	3.37E-08	2.58E-08	1.97E-08	0
14.5	1.24E-07	9.48E-08	7.25E-08	5.54E-08	4.24E-08	3.24E-08	0	0
15.5	1.56E-07	1.19E-07	9.13E-08	6.98E-08	5.34E-08	4.08E-08	0	0
16.5	1.96E-07	1.50E-07	1.15E-07	8.79E-08	6.72E-08	0	0	0

Table 6.4. Upper Boundaries of Exceedance Rate for 40°, 1/s (Columns are Mean Zero-Crossing Period in Seconds, Rows are Significant Wave Heights in Meters) with Assumed Guidance

Hs \ TZ	3.5	4.5	5.5	6.5	7.5	8.5	9.5	10.5
0.5	1.28E-10	1.21E-10	1.14E-10	1.08E-10	1.02E-10	9.61E-11	9.07E-11	8.57E-11
1.5	0	1.41E-10	1.33E-10	1.26E-10	1.19E-10	1.12E-10	1.06E-10	9.98E-11
2.5	0	1.64E-10	1.55E-10	1.46E-10	1.38E-10	1.31E-10	1.23E-10	1.16E-10
3.5	0	1.91E-10	1.81E-10	1.71E-10	1.61E-10	1.52E-10	1.44E-10	1.36E-10
4.5	0	0	2.11E-10	1.99E-10	1.88E-10	1.77E-10	1.67E-10	1.58E-10
5.5	0	0	2.46E-10	2.32E-10	2.19E-10	2.07E-10	1.95E-10	1.84E-10
6.5	0	0	9.05E-11	1.03E-10	1.16E-10	1.32E-10	1.50E-10	1.70E-10
7.5	0	0	0	6.46E-11	8.33E-11	1.07E-10	1.38E-10	1.78E-10
8.5	0	0	0	8.23E-11	1.08E-10	1.41E-10	1.85E-10	2.42E-10
9.5	0	0	0	3.01E-10	3.39E-10	3.81E-10	4.29E-10	4.83E-10
10.5	0	0	0	0	3.16E-09	2.49E-09	1.96E-09	1.54E-09
11.5	0	0	0	0	7.16E-08	3.34E-08	1.56E-08	7.27E-09
12.5	0	0	0	0	2.94E-06	7.26E-07	1.79E-07	4.43E-08
13.5	0	0	0	0	0	2.00E-05	2.48E-06	3.07E-07
14.5	0	0	0	0	0	2.52E-05	3.12E-06	3.86E-07
15.5	0	0	0	0	0	0	3.93E-06	4.86E-07
16.5	0	0	0	0	0	0	0	6.12E-07

Table 6.4. Upper Boundaries of Exceedance Rate for 40°, 1/s (Columns are Mean Zero-Crossing Period in Seconds, Rows are Significant Wave Heights in Meters) with Assumed Guidance, Cont.

Hs \ TZ	11.5	12.5	13.5	14.5	15.5	16.5	17.5	18.5
0.5	1.27E-11	1.88E-12	0	0	0	0	0	0
1.5	1.48E-11	2.19E-12	3.25E-13	4.81E-14	7.13E-15	0	0	0
2.5	1.72E-11	2.56E-12	3.79E-13	5.61E-14	8.31E-15	1.23E-15	0	0
3.5	2.01E-11	2.98E-12	4.41E-13	6.54E-14	9.69E-15	1.44E-15	2.13E-16	0
4.5	2.34E-11	3.47E-12	5.14E-13	7.62E-14	1.13E-14	1.67E-15	2.48E-16	0
5.5	2.73E-11	4.05E-12	5.99E-13	8.88E-14	1.32E-14	1.95E-15	2.89E-16	4.28E-17
6.5	3.74E-11	8.22E-12	1.81E-12	3.97E-13	8.74E-14	1.92E-14	4.23E-15	9.30E-16
7.5	5.70E-11	1.83E-11	5.84E-12	1.87E-12	5.99E-13	1.92E-13	6.13E-14	1.96E-14
8.5	1.08E-10	4.85E-11	2.17E-11	9.74E-12	4.36E-12	1.95E-12	8.76E-13	3.92E-13
9.5	2.85E-10	1.69E-10	9.98E-11	5.90E-11	3.49E-11	2.06E-11	1.22E-11	7.22E-12
10.5	1.12E-09	8.16E-10	5.93E-10	4.31E-10	3.13E-10	2.27E-10	1.65E-10	1.20E-10
11.5	6.13E-09	5.16E-09	4.34E-09	3.66E-09	3.08E-09	2.60E-09	2.19E-09	1.84E-09
12.5	4.16E-08	3.90E-08	3.66E-08	3.44E-08	3.23E-08	3.03E-08	2.84E-08	0
13.5	3.15E-07	3.23E-07	3.31E-07	3.40E-07	3.49E-07	3.58E-07	3.67E-07	0
14.5	3.96E-07	4.07E-07	4.17E-07	4.28E-07	4.39E-07	4.51E-07	0	0
15.5	4.99E-07	5.12E-07	5.25E-07	5.39E-07	5.53E-07	5.67E-07	0	0
16.5	6.28E-07	6.45E-07	6.61E-07	6.78E-07	6.96E-07	0	0	0

Table 6.5. Estimates of Capsizing Rate, 1/s (Columns are Mean Zero-Crossing Period in Seconds, Rows are Significant Wave Heights in Meters) with Assumed Guidance

Hs \ TZ	3.5	4.5	5.5	6.5	7.5	8.5	9.5	10.5
0.5	2.00E-08	4.73E-10	1.12E-11	2.66E-13	6.30E-15	1.49E-16	3.54E-18	8.39E-20
1.5	0	1.71E-09	4.05E-11	9.60E-13	2.27E-14	5.39E-16	1.28E-17	3.03E-19
2.5	0	6.17E-09	1.46E-10	3.46E-12	8.21E-14	1.95E-15	4.61E-17	1.09E-18
3.5	0	2.23E-08	5.28E-10	1.25E-11	2.96E-13	7.02E-15	1.66E-16	3.95E-18
4.5	0	0	1.90E-09	4.51E-11	1.07E-12	2.54E-14	6.01E-16	1.42E-17
5.5	0	0	6.87E-09	1.63E-10	3.86E-12	9.15E-14	2.17E-15	5.14E-17
6.5	0	0	2.48E-08	5.88E-10	1.39E-11	3.30E-13	7.83E-15	1.86E-16
7.5	0	0	0	2.12E-09	5.03E-11	1.19E-12	2.83E-14	6.70E-16
8.5	0	0	0	1.09E-09	6.27E-11	3.61E-12	2.08E-13	1.20E-14
9.5	0	0	0	1.08E-09	1.29E-10	1.55E-11	1.87E-12	2.24E-13
10.5	0	0	0	0	6.43E-10	1.23E-10	2.36E-11	4.53E-12
11.5	0	0	0	0	6.81E-09	1.66E-09	4.02E-10	9.78E-11
12.5	0	0	0	0	1.19E-07	3.15E-08	8.34E-09	2.21E-09
13.5	0	0	0	0	0	7.15E-07	1.91E-07	5.09E-08
14.5	0	0	0	0	0	9.01E-07	2.40E-07	6.41E-08
15.5	0	0	0	0	0	0	3.02E-07	8.06E-08
16.5	0	0	0	0	0	0	0	1.02E-07

Table 6.5 Estimates of Capsizing Rate, 1/s (Columns are Mean Zero-Crossing Period in Seconds, Rows are Significant Wave Heights in Meters) with Assumed Guidance, Cont.

Hs \ TZ	11.5	12.5	13.5	14.5	15.5	16.5	17.5	18.5
0.5	4.54E-20	2.46E-20	0	0	0	0	0	0
1.5	1.64E-19	8.88E-20	4.81E-20	2.61E-20	1.41E-20	0	0	0
2.5	5.92E-19	3.21E-19	1.74E-19	9.41E-20	5.10E-20	2.76E-20	0	0
3.5	2.14E-18	1.16E-18	6.27E-19	3.40E-19	1.84E-19	9.97E-20	5.40E-20	0
4.5	7.72E-18	4.18E-18	2.26E-18	1.23E-18	6.64E-19	3.60E-19	1.95E-19	0
5.5	2.78E-17	1.51E-17	8.17E-18	4.43E-18	2.40E-18	1.30E-18	7.03E-19	3.81E-19
6.5	1.01E-16	5.45E-17	2.95E-17	1.60E-17	8.65E-18	4.69E-18	2.54E-18	1.38E-18
7.5	3.63E-16	1.97E-16	1.06E-16	5.77E-17	3.12E-17	1.69E-17	9.17E-18	4.96E-18
8.5	1.92E-14	3.07E-14	4.91E-14	7.85E-14	1.25E-13	2.01E-13	3.21E-13	5.13E-13
9.5	7.51E-13	2.51E-12	8.41E-12	2.82E-11	9.42E-11	3.15E-10	1.06E-09	3.53E-09
10.5	1.74E-11	6.67E-11	2.56E-10	9.80E-10	3.76E-09	1.44E-08	5.53E-08	2.12E-07
11.5	2.57E-10	6.73E-10	1.76E-09	4.62E-09	1.21E-08	3.18E-08	8.33E-08	2.18E-07
12.5	2.80E-09	3.56E-09	4.52E-09	5.75E-09	7.30E-09	9.27E-09	1.18E-08	0
13.5	2.64E-08	1.37E-08	7.08E-09	3.67E-09	1.90E-09	9.86E-10	5.11E-10	0
14.5	3.32E-08	1.72E-08	8.91E-09	4.62E-09	2.39E-09	1.24E-09	0	0
15.5	4.18E-08	2.17E-08	1.12E-08	5.82E-09	3.01E-09	1.56E-09	0	0
16.5	5.26E-08	2.73E-08	1.41E-08	7.32E-09	3.79E-09	0	0	0

Table 6.6. Upper Boundaries of Capsizing Rate, 1/s (Columns are Mean Zero-Crossing Period in Seconds, Rows are Significant Wave Heights in Meters) with Assumed Guidance

Hs \ TZ	3.5	4.5	5.5	6.5	7.5	8.5	9.5	10.5
0.5	7.57E-11	3.80E-12	1.91E-13	9.59E-15	4.81E-16	2.42E-17	1.21E-18	6.10E-20
1.5	0	2.75E-11	1.38E-12	6.93E-14	3.48E-15	1.75E-16	8.78E-18	4.41E-19
2.5	0	1.99E-10	9.98E-12	5.01E-13	2.52E-14	1.26E-15	6.35E-17	3.19E-18
3.5	0	1.44E-09	7.22E-11	3.62E-12	1.82E-13	9.14E-15	4.59E-16	2.31E-17
4.5	0	0	5.22E-10	2.62E-11	1.32E-12	6.61E-14	3.32E-15	1.67E-16
5.5	0	0	3.77E-09	1.90E-10	9.52E-12	4.78E-13	2.40E-14	1.21E-15
6.5	0	0	2.73E-08	1.37E-09	6.88E-11	3.46E-12	1.74E-13	8.72E-15
7.5	0	0	0	9.91E-09	4.98E-10	2.50E-11	1.26E-12	6.30E-14
8.5	0	0	0	4.86E-08	2.97E-09	1.82E-10	1.11E-11	6.80E-13
9.5	0	0	0	2.23E-07	1.71E-08	1.31E-09	1.00E-10	7.67E-12
10.5	0	0	0	0	9.11E-08	9.18E-09	9.25E-10	9.31E-11
11.5	0	0	0	0	4.58E-07	6.32E-08	8.74E-09	1.21E-09
12.5	0	0	0	0	2.21E-06	4.30E-07	8.38E-08	1.63E-08
13.5	0	0	0	0	0	2.91E-06	8.10E-07	2.26E-07
14.5	0	0	0	0	0	3.66E-06	1.02E-06	2.84E-07
15.5	0	0	0	0	0	0	1.28E-06	3.58E-07
16.5	0	0	0	0	0	0	0	4.50E-07

Table 6.6 Upper Boundaries of Capsizing Rate, 1/s (Columns are Mean Zero-Crossing Period in Seconds, Rows are Significant Wave Heights in Meters) with Assumed Guidance, Cont.

Hs \ TZ	11.5	12.5	13.5	14.5	15.5	16.5	17.5	18.5
0.5	3.80E-20	2.37E-20	0	0	0	0	0	0
1.5	2.75E-19	1.72E-19	1.07E-19	6.69E-20	4.17E-20	0	0	0
2.5	1.99E-18	1.24E-18	7.75E-19	4.84E-19	3.02E-19	1.88E-19	0	0
3.5	1.44E-17	8.98E-18	5.60E-18	3.50E-18	2.18E-18	1.36E-18	8.50E-19	0
4.5	1.04E-16	6.49E-17	4.05E-17	2.53E-17	1.58E-17	9.85E-18	6.14E-18	0
5.5	7.52E-16	4.69E-16	2.93E-16	1.83E-16	1.14E-16	7.12E-17	4.44E-17	2.77E-17
6.5	5.44E-15	3.39E-15	2.12E-15	1.32E-15	8.25E-16	5.15E-16	3.21E-16	2.01E-16
7.5	3.93E-14	2.45E-14	1.53E-14	9.56E-15	5.97E-15	3.72E-15	2.32E-15	1.45E-15
8.5	9.81E-13	1.41E-12	2.04E-12	2.94E-12	4.23E-12	6.10E-12	8.79E-12	1.27E-11
9.5	1.95E-11	4.95E-11	1.26E-10	3.20E-10	8.13E-10	2.07E-09	5.25E-09	1.33E-08
10.5	2.60E-10	7.27E-10	2.03E-09	5.68E-09	1.59E-08	4.44E-08	1.24E-07	3.46E-07
11.5	2.47E-09	5.07E-09	1.04E-08	2.13E-08	4.37E-08	8.95E-08	1.83E-07	3.76E-07
12.5	1.87E-08	2.15E-08	2.47E-08	2.83E-08	3.25E-08	3.73E-08	4.28E-08	0
13.5	1.27E-07	7.12E-08	4.00E-08	2.24E-08	1.26E-08	7.08E-09	3.98E-09	0
14.5	1.60E-07	8.96E-08	5.03E-08	2.83E-08	1.59E-08	8.91E-09	0	0
15.5	2.01E-07	1.13E-07	6.34E-08	3.56E-08	2.00E-08	1.12E-08	0	0
16.5	2.53E-07	1.42E-07	7.98E-08	4.48E-08	2.52E-08	0	0	0

The upper boundary of the exceedance rate of 40° in Table 6.2 is still larger than the proposed standard value of 2.6×10^{-3} year^{-1}. The most probable reason for this outcome is that EPOT assumes a heavy tail. Consequently, EPOT may overestimate the crossing rate in oblique

seas, (see Belenky et al. 2018 and discussion in Section 5.3.8). An additional check for independence of the collected data for extrapolation (such as decorrelation time between the data points) may resolve this overestimation problem.

This example also provides an estimate of approximately two of orders of magnitude, which highlights the importance of the operator model for overall probabilistic assessment of stability failure. This estimate can be extended to an assessment of the effectiveness of operational guidance for the cases of when the crew does not have sufficient experience in handling dynamic stability issues, or new phenomena arising with a specific vessel type (such as parametric roll with a modern containership).

6.2 General Considerations for Development of Operational Guidance

6.2.1 Format

Paragraph 6.3.3 of Annex 2 of SDC 6 WP.6 contains a recommendation concerning the format of operational guidance in the form of a polar diagram. This paragraph provides a complete description of the format of the polar diagram; however, several clarifications provided in the following paragraphs may be useful.

For a polar diagram displayed onboard of a ship, the direction "up" (i.e. head seas) should normally be associated with a 0° heading to be consistent with other navigational aids.

While traditional media for operational limitations or operational guidance is paper, use of digital media such as a shipboard computer or a mobile device that replicates the information available on traditional media may be preferred. When properly configured, digital media can help to reduce user error and provide a consistent interface for user inputs. Inputs required include the ship's loading condition data, environmental conditions, speed, and heading. Use of a properly configured digital media can also allow a user to quickly access information available for a specific stability failure mode.

Paragraph 6.3.3 of Annex 2 of SDC 6 WP.6 provides specific guidance for a polar plot format for operational guidance, but implies that a polar plot format is not appropriate for presentation of operational limitations in Level 2 vulnerability assessments. The Level 2 vulnerability assessment does provide ship-specific information, whereas MSC.Circ 1228 does not. Additionally, information in MSC.Circ 1228 is provided in the form of polar diagram. As ship-specific operational information is deemed superior to generic consideration, one should find a way to present Level 2 results in a form of a polar plot. See further discussion of this subject in subsections 6.2.4 and 6.3.2.

6.2.2 Environmental Condition Data

Paragraph 6.1.2 provides general guidance on environmental conditions to be applied in preparation of operational limitations. No specific recommendations are given on the specifications of environmental conditions for development operational guidance. Since the operational guidance should be based on information produced by a direct stability assessment, the requirements for the specification of environmental conditions for direct stability assessments in Section 5.3 of Annex 1 of SDC 6 WP.6 should be applicable.

Paragraph 5.3.2.1 of Annex 1 of SDC 6 WP. 6 formulates requirements for environmental conditions for full probabilistic assessment as "all relevant seas states". This is interpreted as the entire scatter table, which is shown in two examples of full probabilistic assessment as described

in Section 5 of this report. However, the scatter table is limited by two parameters only: significant wave height and zero crossing period, which provide a very coarse description.

There are a number of environmental parameters that can influence ship dynamics in waves. Waves in a particular geographic location may be influenced by several surrounding weather systems. Also, a swell wave may exist hours after a weather system has dissipated. Most of the weather routing systems contain data for waves generated by the two most predominant weather systems, so two wave spectra are available in addition to wind data. A typical data set may include:

- Primary significant wave height
- Primary mean zero crossing (or modal) period
- Primary wave system spread (information on direction of different wave components of the primary wave system)
- Primary wave spectrum bandwidth (important information to distinguish wave winds from a swell; the latter usually has fairly narrowband spectrum)
- Secondary significant wave height
- Secondary mean zero crossing (or modal) period
- Secondary spread
- Secondary wave spectrum bandwidth
- Angle between the general direction of primary and secondary waves systems
- Mean wind speed
- Angle between the general direction of primary wave system and wind direction

This information is usually a result of numerical simulation of waves that is based on measured or computed wind speed.

Since the performance of a full probabilistic assessment and development of operational guidance that includes all possible combinations of environmental parameters is not feasible, a correlation between these parameters needs to be applied to decrease the number of parameters. A correlation between these parameters is available or can be determined from hindcast wave and wind data for the typical routes of the applicable ship. Note that ships for which a direct stability assessment may be performed typically have well-established routes.

For a given primary significant wave height, there are corresponding most probable secondary significant wave height, primary spread, secondary spread, and mean wind speed. However, as ship dynamics are particularly sensitive to wave period and frequency parameters, five or seven mean zero-crossings or modal periods should be used for the same primary significant wave height. For each primary-mean zero-crossing (or modal period), the following most probable parameters need determining:

- Secondary mean zero-crossing (or modal wave period)
- Angles between the primary wave system and secondary wave systems
- An angle between the general direction of primary wave-system and wind direction
- Primary and secondary spectral bandwidth values

Environmental information onboard a ship will be available from weather routing. The information provided by a weather routing service may include all or a subset of the 11

parameters listed above. To be useful, a polar plot from operational guidance will need to be related to the actual weather conditions described by these parameters.

6.2.3 Development of Operational Guidance from a Direct Stability Assessment

Section 6.4 of Annex 2 SDC 6/WP.6 describes probabilistic operational guidance, where sailing conditions are considered unsafe if the rate of failure exceeds 10^{-6} s^{-1}. To present this information on a polar plot, a number of levels for each roll angle are obtained from around the standard value of 40° as established in paragraph 2.1.1 of Annex 1 of ADC 6/WP.6. Similarly, a number of levels for lateral accelerations are taken near the standard value of 9.81 m/s^2 as required in 2.1.1 of Annex 1 of ADC 6/WP.6.

As the ship motion data is available, rates of exceedances for each of these levels are estimated by either direct counting or extrapolation. The upper boundary of the exceedance rate is compared with threshold value of 10^{-6} s^{-1}. If the upper value of the exceedance rates is greater than the threshold value and the standard level is less 40° or 9.81 m/s^2. The sailing condition is marked by the color yellow/amber. If the level is greater than or equal to 40° or 9.81 m/s^2, the color red is applied. The shade of red should become darker for each level above the standard value. For the levels below the standard value, the color to be selected should be yellow and become brighter with each level below the standard. See the example for parametric roll in the subsection 6.3.1 of this report.

6.2.4 Obtaining Operational Guidance from a Level 2 Vulnerability Assessment

While the outcomes of a direct stability assessment are expected to produce information that is more precise in terms of ship dynamics, the results of the Level 2 vulnerability assessment also offers ship-specific data, which is comparable or probably superior to the generic ship-independent guidance given in MSC.1/CIRC.1228. However, direct stability-assessments are unlikely to be performed frequently due to the significant effort required for assessment. Thus, the ship-specific information produced as a result of a Level 2 vulnerability assessment is expected to be generally more available. Below, some general recommendations are proposed in regards to the approach for development of a polar plot based on data available from a Level 2 vulnerability assessment.

The intermediate outcomes of the Level 2 vulnerability assessment for pure loss of stability consists of a set of GZ curves for waves with a length equal to the ship length and wave steepness ranging from 0.01 to 0.1. The second criterion uses a heeling lever that depends on the service speed. Performing additional calculations for reduced speeds allows the polar diagram to show speed dependence. To account for a decreasing variation of stability in waves with the increase of the heading, the effective wave height for the joint distribution can be corrected using the cosine of the heading angle. If the angle of heel under this heeling lever exceeds the level of R_{PL2}, the combination of speed and heading should be shown with the shade of red color. Exceeding a level a few degrees less than of R_{PL2} should be shown in shades of yellow. A similar approach should be used with criterion 1 for all speeds.

The intermediate outcomes of the Level 2 vulnerability assessment for parametric roll consists of a table of roll amplitudes computed for different speeds and wave heights. A sea state (significant wave height and mean zero-crossing period) is associated with a wave height for the grim effective wave. The amplitudes for a particular sea state can be found by interpolation. Each speed is associated with an encounter frequency, so the information for a particular sea

state is a set of roll amplitudes defined for a grid of encounter frequencies. As each combination of speed and heading is also associated with encounter frequency, the amplitudes can be mapped to the polar diagram. To account for a decrease of stability variation when the heading differs from exact following or head seas, the wave height may be decreased by multiplying by the cosine of the heading angle and interpolating from the table data, or simply excluding the beam seas sector. See subsection 6.3.2 for detailed consideration and example.

The intermediate outcomes of Level 2 vulnerability assessment for surf-riding/broaching consists of a table of critical speeds depending on wave steepness and the ratio between the wave length and the ship length. Each critical speed has a statistical weight computed from joint distribution of wave steepness and length ratio. This data is sufficient for the estimation of the probability distribution of critical speeds leading to surf-riding. All the speeds where the probability exceeds the level of significance can be shown with shades of red. Probabilities below the level of significance, for example from 0.01 to 0.04, can be shown as shades of yellow. To account for decreasing surging wave forces with the increase of the heading, the significant wave-height for the joint distribution can be corrected using the cosine of heading angle. These estimated operational limitations are conservative since surf-riding in irregular waves does not always lead to broaching because of changes in the wave field.

The intermediate outcomes of a Level 2 vulnerability assessment for excessive acceleration consist of a table of standard deviations of lateral accelerations depending on significant wave height and mean zero-crossing period. Each cell of this table contains the standard deviation for a specific sea state, beam seas, and speeds. To account for decreasing wave excitation for non-beam seas heading, the correction equal to absolute value of the sine of the heading angle may be implemented. To account for the changing encounter frequency, another correction may be implemented by the appropriate shifting of the mean zero-crossing period. The values of standard deviation for non-beam seas heading can be found by interpolation of the table. The coloring of the polar diagram is performed similarly to that for the direct assessment case assuming a normal distribution for the accelerations

6.3 An Example of Operational Guidance and Operational Limitations for Parametric Roll

6.3.1 Operational Guidance from Direct Assessment

An example for development of operational guidance for a C11 class containers ship is shown in Table 2.3. In this table, the principle dimensions are given with the exception of mean draft = 11.5 m, KG = 18.95, leading to GM = 1.4 m with no trim specified. Simulation data set #1 from Table 5.6 (significant wave height 9 m, modal period 14 s, mean zero-crossing period 9.94 s) was used for the sample operational guidance.

The first step in the development of the operational guidance is to estimate the exceedance rate for a series of angles: 25, 30, 35, 45, and 50° in addition to 40°, as available from Table 5.7. The exceedance rate is estimated based on the direct-counting procedure as described in the subsection 5.2.10. The results of these calculations are placed in Table 6.7.

Table 6.7. Upper Boundary of Exceedance Rate (s^{-1})

Speed, kn	Heading °	Exceedance level, °					
		25	30	35	40	45	50
0	0	3.96E-03	3.96E-03	3.96E-03	3.64E-03	3.43E-03	3.32E-03
	15	5.76E-03	5.28E-03	5.08E-03	4.69E-03	3.59E-03	3.49E-03
	30	4.65E-03	4.47E-03	4.28E-03	3.91E-03	3.17E-03	2.54E-03
	45	3.06E-03	2.83E-03	2.52E-03	2.28E-03	1.77E-03	1.12E-03
	60	1.72E-03	1.44E-03	1.12E-03	5.86E-04	2.18E-04	8.13E-05
	75	0	0	0	0	0	0
	90	0	0	0	0	0	0
	105	0	0	0	0	0	0
	120	1.41E-03	8.90E-04	6.89E-04	3.35E-04	8.13E-05	8.13E-05
	135	1.65E-03	1.58E-03	1.48E-03	1.41E-03	1.20E-03	7.40E-04
	150	4.07E-03	3.80E-03	3.63E-03	3.58E-03	2.97E-03	2.46E-03
	165	3.50E-03	3.50E-03	3.43E-03	3.22E-03	2.94E-03	2.58E-03
	180	4.28E-03	4.18E-03	4.09E-03	3.91E-03	3.63E-03	3.44E-03
5	0	6.25E-03	5.81E-03	5.59E-03	5.04E-03	4.48E-03	4.26E-03
	15	4.93E-03	4.48E-03	4.26E-03	4.03E-03	3.92E-03	3.58E-03
	30	6.29E-03	5.96E-03	5.55E-03	4.98E-03	4.40E-03	3.73E-03
	45	5.03E-03	4.31E-03	3.73E-03	3.23E-03	2.45E-03	1.65E-03
	60	1.72E-03	1.28E-03	9.89E-04	4.81E-04	2.97E-04	1.31E-04
	75	0	0	0	0	0	0
	90	0	0	0	0	0	0
	105	0	0	0	0	0	0
	120	8.90E-04	4.09E-04	1.31E-04	8.13E-05	0	0
	135	2.22E-03	1.89E-03	1.55E-03	8.50E-04	4.40E-04	1.89E-04
	150	2.53E-03	2.18E-03	1.87E-03	1.51E-03	9.48E-04	3.44E-04
	165	2.75E-03	2.59E-03	2.34E-03	2.04E-03	1.45E-03	1.05E-03
	180	2.78E-03	2.66E-03	2.38E-03	2.05E-03	1.65E-03	9.30E-04
10	0	1.68E-03	1.57E-03	1.33E-03	8.85E-04	6.75E-04	5.45E-04
	15	3.24E-03	2.70E-03	2.08E-03	1.55E-03	1.05E-03	7.75E-04
	30	2.00E-03	1.84E-03	1.72E-03	1.44E-03	1.24E-03	9.88E-04
	45	2.48E-03	2.12E-03	1.86E-03	1.42E-03	1.08E-03	6.01E-04
	60	1.34E-03	6.21E-04	2.58E-04	0	0	0
	75	0	0	0	0	0	0
	90	0	0	0	0	0	0
	105	0	0	0	0	0	0
	120	1.31E-04	0	0	0	0	0
	135	6.21E-04	2.18E-04	8.13E-05	0	0	0
	150	1.12E-03	4.45E-04	1.31E-04	0	0	0
	165	1.31E-03	7.57E-04	2.97E-04	8.13E-05	8.13E-05	8.13E-05
	180	1.31E-03	8.24E-04	2.97E-04	1.31E-04	0	0

Table 6.7 Upper Boundary of Exceedance Rate (s^{-1}) Cont.

Speed, kn	Heading °	Exceedance level, °					
		25	30	35	40	45	50
15	0	0	0	0	0	0	0
	15	8.13E-05	0	0	0	0	0
	30	8.13E-05	0	0	0	0	0
	45	1.60E-03	1.46E-03	1.11E-03	6.75E-04	4.84E-04	2.80E-04
	60	7.23E-04	3.72E-04	8.13E-05	0	0	0
	75	0	0	0	0	0	0
	90	0	0	0	0	0	0
	105	0	0	0	0	0	0
	120	0	0	0	0	0	0
	135	0	0	0	0	0	0
	150	1.76E-04	8.13E-05	8.13E-05	0	0	0
	165	8.13E-05	0	0	0	0	0
	180	8.13E-05	0	0	0	0	0
20	0	5.86E-04	5.86E-04	4.45E-04	4.09E-04	2.58E-04	1.31E-04
	15	8.57E-04	4.45E-04	2.97E-04	1.76E-04	8.13E-05	0
	30	1.76E-04	0	0	0	0	0
	45	0	0	0	0	0	0
	60	2.97E-04	8.13E-05	0	0	0	0
	75	0	0	0	0	0	0
	90	0	0	0	0	0	0
	105	0	0	0	0	0	0
	120	0	0	0	0	0	0
	135	0	0	0	0	0	0
	150	0	0	0	0	0	0
	165	0	0	0	0	0	0
	180	0	0	0	0	0	0

The second step in the development of the operational guidance is to relate the upper boundary of the exceedance rate with the exceedance level based on the criterion of 10^{-6} s^{-1} as defined in paragraph 6.4.2 of Annex 2 SDC 6/WP.6. Each row of the Table 6.7 shows the angle corresponding to the upper boundary of the exceedance rate relative to 10^{-6} s^{-1}. For example for the first row of Table 6.7 (speed = 0 kn, heading 0°) none of these exceedances rates are below 10^{-6} s^{-1}, so 50° is selected. For the sixth row (speed = 0 kn heading 75°) all rates are zeros, so the angle is set to 0°. For the speed of 5 kn at heading 120°, the upper boundary for the exceedance rate of 40° is 8.13×10^{-5}, while for 45°, the exceedance rate is 0, so the angle is set to 40°. The results are summarized in Table 6.8.

Table 6.8 contains sufficient input information for creation of a polar plot, shown in Figure 6.1. The figure was created with special utility Polar-Plot, included in the LAMP system.

Table 6.8. Roll Angle Levels for Polar Plot

Speed 0 kn		Speed 5 kn		Speed 10 kn		Speed 15 kn		Speed 20 kn	
Heading, °	Angle, °	Heading, °	Angle, °	Heading, °	Angle, °	Heading, °	Angle, °	Heading, °	Angle, °
0	50	0	50	0	50	0	0	0	50
15	50	15	50	15	50	15	25	15	45
30	50	30	50	30	50	30	25	30	25
45	50	45	50	45	50	45	50	45	0
60	50	60	50	60	35	60	35	60	30
75	0	75	0	75	0	75	0	75	0
90	0	90	0	90	0	90	0	90	0
105	0	105	0	105	0	105	0	105	0
120	50	120	40	120	25	120	0	120	0
135	50	135	50	135	35	135	0	135	0
150	50	150	50	150	35	150	35	150	0
165	50	165	50	165	50	165	25	165	0
180	50	180	50	180	40	180	25	180	0

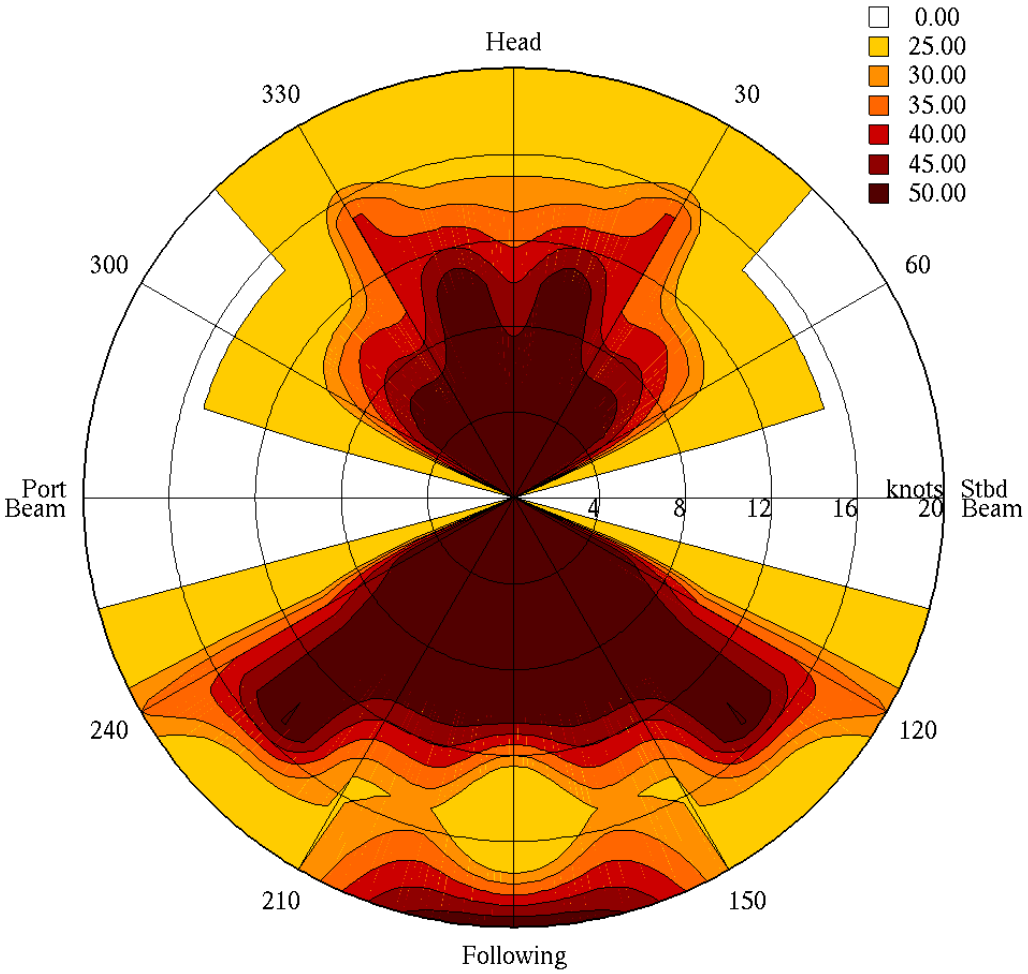

Figure 6.1. Sample Polar Plot for C11-Class Containership; Significant Wave Height 9 m, Modal Period 14 s, Mean Zero-Crossing Period 9.94 s Draft 11.5 m KG = 18.95, GM = 1.4

6.3.2 Operational Guidance from Level 2 Vulnerability Assessment

A polar plot for operational limitation based the Level 2 vulnerability assessment which is then based on the data available is described in an example in subsection 7.3.3. To facilitate comparisons with the polar plot based on more accurate LAMP calculations shown in Figure 6.1, the same sea state is applied where: significant wave height of 9 m and modal period of 14 s (mean zero-crossing period of 9.94). This sea state corresponds to the cell of scatter table of IACS Recommendation 34 with significant wave height of 9.5 m and mean zero-crossing period 9.5 s. Table 7.16 provides a value of a Grim-effective wave of 6.9 m and amplitude of 3.45 m

As calculations of amplitude of a parametric roll response for check 2 of the level 2 vulnerability assessment for speeds V_{mi} in Table 7.15 may be associated with encounter frequencies given by:

$$\omega_e = \omega_w - k_w V_{mi} \tag{6.1}$$

where ω_w is a frequency and k_w is a wave number of Grim effective wave respectively.

Since the length of Grim effective wave equals to ship length, these quantities are determined as:

$$k_w = \frac{2\pi}{L}; \quad \omega_w = \sqrt{k_w g} \tag{6.2}$$

where g = 9.81 m/s^2 is gravity acceleration and L is length of a ship.

Using linear interpolation for wave amplitude in Table 7.15 and equation (6.1), the amplitude of parametric roll response as a function of encounter frequency can be obtained with results shown in Figure 6.2. The encounter frequencies for the polar plot are computed from the polar plot scale with 12 headings (β: from 1 to 180°) and 5 speeds (Vs: from 0 to 20 kn) using the standard formula:

$$\omega 1_e = \omega_w - k_w V_s \cos(\beta) \tag{6.3}$$

The encounter frequencies $\omega 1_e$ are used to compute angles in the polar plot based on linear interpolation of the parametric roll response amplitudes from Figure 6.2. The numerical results are shown in Table 6.10, while polar plot is shown in Figure 6.3.

Table 6.9. Roll Angle Levels for Polar Plot Based on Vulnerability Assessment

Heading, °	Speed 0 kn		Speed 5 kn		Speed 10		Speed 15 kn		Speed 20	
	$\omega 1_e$	Level	$\omega 1_e$	Level	$\omega 1_e$	Level	$\omega 1_e$	Level	$\omega 1_e$	Level
0	0.485	50	0.4234	50	0.3617	28	0.3	0	0.2383	18
15	0.485	50	0.4255	50	0.3659	30	0.3063	0	0.2467	0
30	0.485	50	0.4316	50	0.3782	35	0.3248	13	0.2714	0
45	0.485	50	0.4414	50	0.3978	45	0.3542	25	0.3106	0
60	0.485	50	0.4542	50	0.4234	50	0.3925	42	0.3617	28
75	0.485	0	0.4691	0	0.4531	0	0.4371	0	0.4212	0
90	0.485	0	0.485	0	0.485	0	0.485	0	0.485	0
105	0.485	0	0.501	0	0.517	0	0.5329	0	0.5489	0
120	0.485	50	0.5159	34	0.5467	24	0.5776	14	0.6084	0
135	0.485	50	0.5287	29	0.5723	16	0.6159	0	0.6595	0
150	0.485	50	0.5385	26	0.5919	0	0.6453	0	0.6987	0
165	0.485	50	0.5446	25	0.6042	0	0.6638	0	0.7234	0
180	0.485	50	0.5467	24	0.6084	0	0.6701	0	0.7318	0

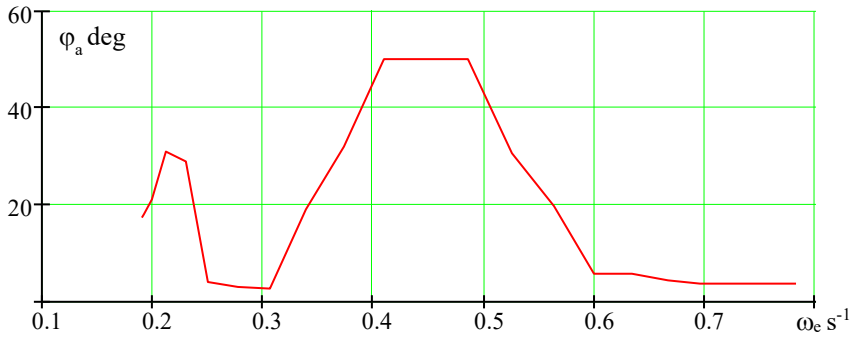

Figure 6.2. Amplitude of Parametric Roll Response for Wave Amplitude 3.45 m

The decrease of variation of stability in beam seas was modeled forcing zero response to 30° sector: from 75 to 105°.

Comparison of polar plots in Figure 6.1and Figure 6.1 shows that the topology of the both plots are similar. Note that both plots show possible parametric roll response in both head and following seas. Both plots show some indication of a large roll response in high speed in following seas (see also Figure 6.2). The physical background of this response is probably due to the fundamental parametric resonance, which occurs near the natural roll frequency (0.21 s^{-1}).

The polar plot based on the vulnerability criterion under predicts the area of large-amplitude of parametric roll compared to the polar plot computed from the direct stability assessment. This under prediction is likely due to the effect of pitch and heave dynamics on parametric roll that are not included in the Level 2 check 2 vulnerability criteria (where the GZ curve in waves used for the vulnerability criteria is computed with balancing in heave and pitch).

This influence can be revealed when comparing a response curve computed with a single DOF equation and roll with GZ curve variation (i.e. mathematical model, used in the check 2, Level 2 vulnerability criterion) with the results from 3-DOF volume-based calculations, (where dynamics of heave and pitch are included), see Weems et al. (2018). As shown in Figure 6.4 below, these response curves are computed for a C11 class container ship with draft = 12.7 m, and KG = 19 m leading to GM = 1.29 m. While the single-DOF model finds the largest roll angle correctly, the range, where parametric roll exists is under predicted.

To compensate these, the amplitude of effective wave can be increased. See Figure 6.5 that shows how the range where parametric roll exists, increases when the amplitude of wave.

As it can be seen in Figure 6.5, doubling the wave amplitude provides quite conservative compensation for the effect of heave and pitch dynamic. Also noticeable is that the effect is more pronounced for higher frequencies, (i.e. for head waves), which is consistent with the difference between polar plot in Figure 6.1 and Figure 6.3.

Calculations for the polar plot repeated using 6.55 m for the amplitude of the Grim effective wave. The results are placed in Table 6.10 and the polar plot is shown in Figure 6.6.

As expected the read area in head seas increased and the indication of fundamental parametric roll is more pronounced. In general, the polar plot in Figure 6.6 is a bit more conservative than the plot in Figure 6.1 and may be considered as a candidate to represent the operational limitation for the sea state.

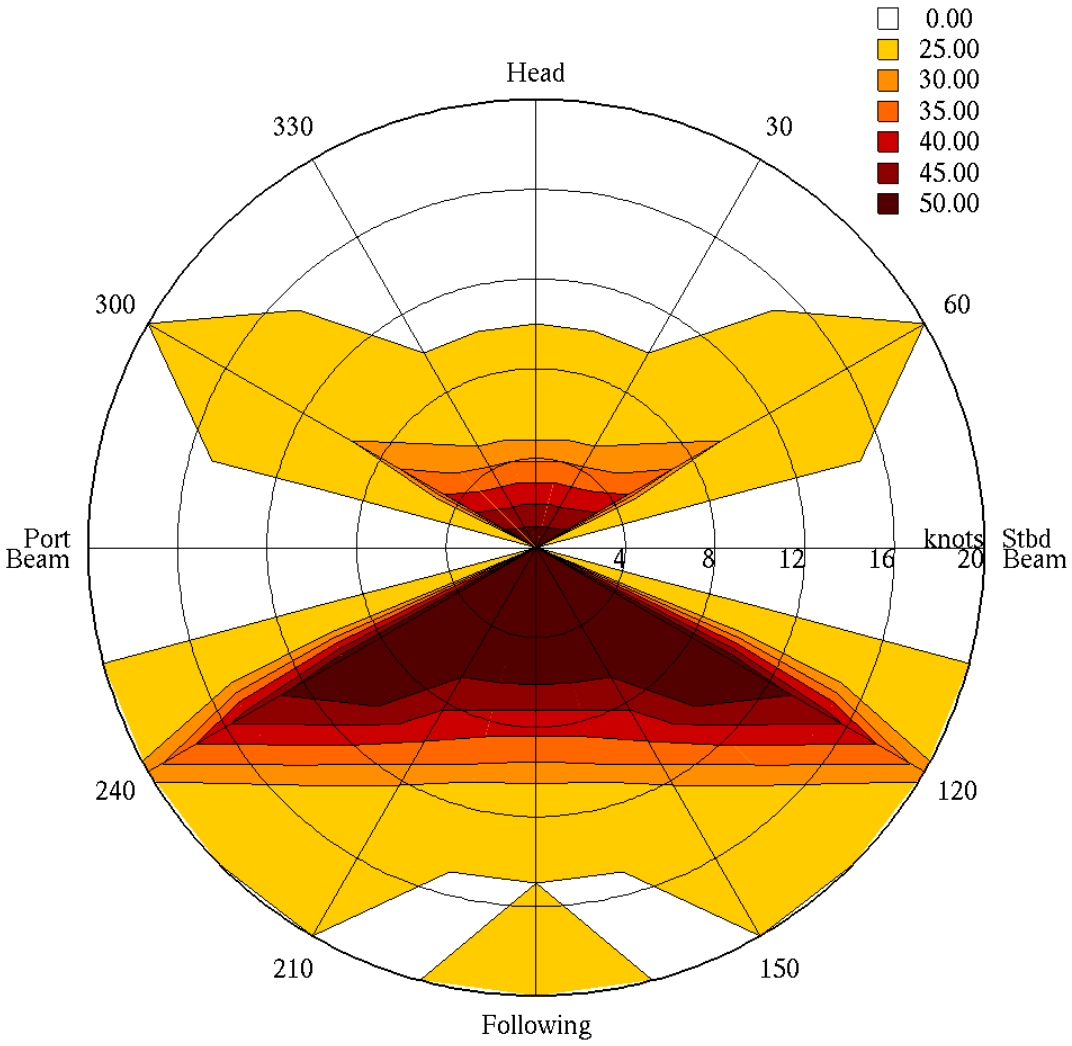

Figure 6.3. . Sample Polar Plot for C11-class Containership Based on Level 2 Vulnerability Assessment Effective Wave Amplitude 3.45 m

Subsection 6.2.4 also mentions usage of a cosine function to model the decrease of stability variation within near beam seas. Figure 6.7 shows a polar plot computed using this option. It appears to underestimate the parametric roll-response in following seas as compared to the polar plot in Figure 6.1.

Since conservatism is an objective when setting operational limitations, the option with simple exclusion of the 30° sector around beam seas appears to be preferable. The polar plot representation of the operational limitation for parametric roll formulated in the subsection 6.2.4 generally works if a 100 % correction is introduced for the amplitude of Grim effective waves.

Polar plot presentations for other modes of failure may be applicable, but a comparison to the polar plot developed from direct stability assessment must be present in a careful approach for the development of operational limitations.

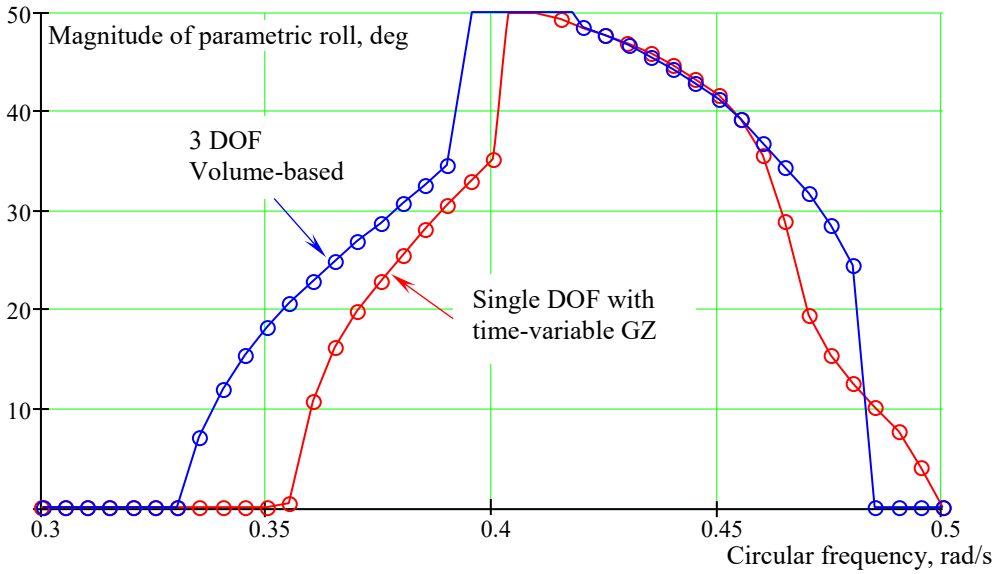

Figure 6.4. Parametric Roll Response Curves for Single DOF (red) and 3 DOF (blue) Cases. C11-Class Containership, d = 12.7, KG = 19 m, GM = 1.29 m Wave Amplitude 2 m

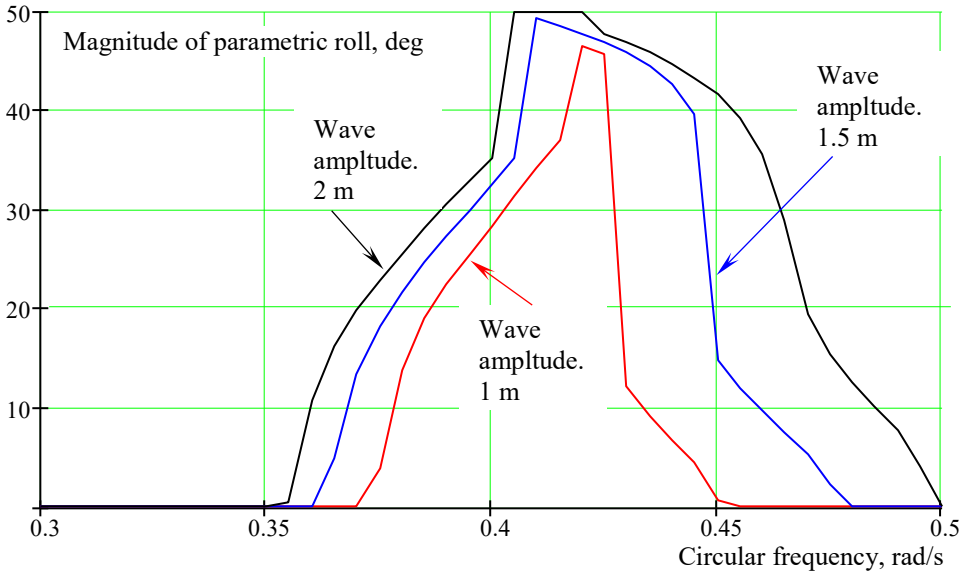

Figure 6.5. Effect of Wave Amplitude on Parametric Roll Range for a 1-DOF Mathematical Model: C11-Class Containership, d = 12.7, KG = 19 m, GM = 1.29 m

Table 6.10. Roll Angle Levels for Polar Plot Based on Vulnerability Assessment with Increased Wave Amplitude

Heading, deg	Speed 0 kn		Speed 5 kn		Speed 10		Speed 15 kn		Speed 20	
	$\omega 1_e$	Level	$\omega 1_e$	Level	$\omega 1_e$	Level	$\omega 1_e$	Level	$\omega 1_e$	Level
0	0.485	50	0.4234	50	0.3617	40	0.3	0	0.2383	50
15	0.485	50	0.4255	50	0.3659	44	0.3063	0	0.2467	50
30	0.485	50	0.4316	50	0.3782	50	0.3248	12	0.2714	12
45	0.485	50	0.4414	50	0.3978	50	0.3542	33	0.3106	0
60	0.485	50	0.4542	50	0.4234	50	0.3925	50	0.3617	40
75	0.485	0	0.4691	0	0.4531	0	0.4371	0	0.4212	0
90	0.485	0	0.485	0	0.485	0	0.485	0	0.485	0
105	0.485	0	0.501	0	0.517	0	0.5329	0	0.5489	0
120	0.485	50	0.5159	50	0.5467	50	0.5776	50	0.6084	50
135	0.485	50	0.5287	50	0.5723	50	0.6159	50	0.6595	24
150	0.485	50	0.5385	50	0.5919	50	0.6453	38	0.6987	11
165	0.485	50	0.5446	50	0.6042	50	0.6638	20	0.7234	0
180	0.485	50	0.5467	50	0.6084	50	0.6701	17	0.7318	0

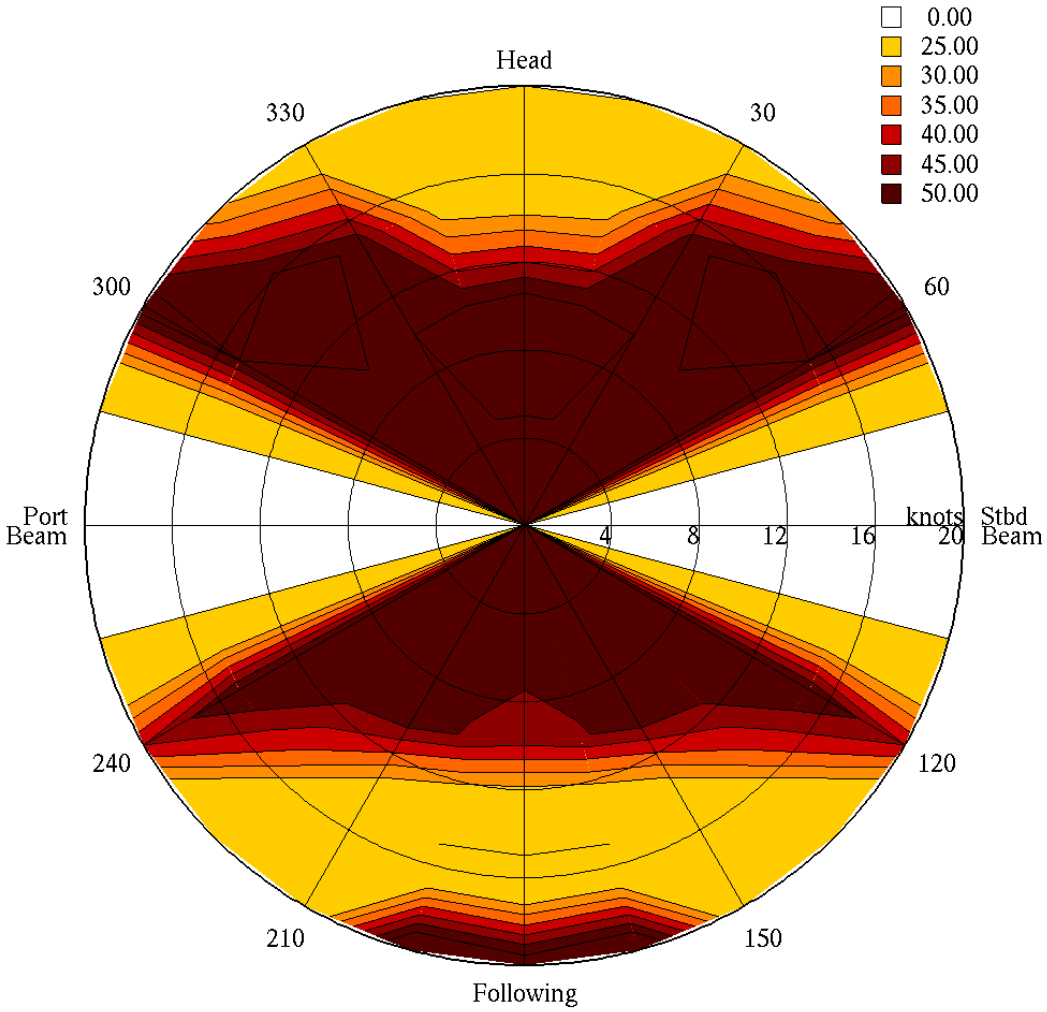

Figure 6.6. Sample Polar Plot for C11-Class Containership Based on Level 2 Vulnerability Assessment Effective Wave Amplitude 6.55 m

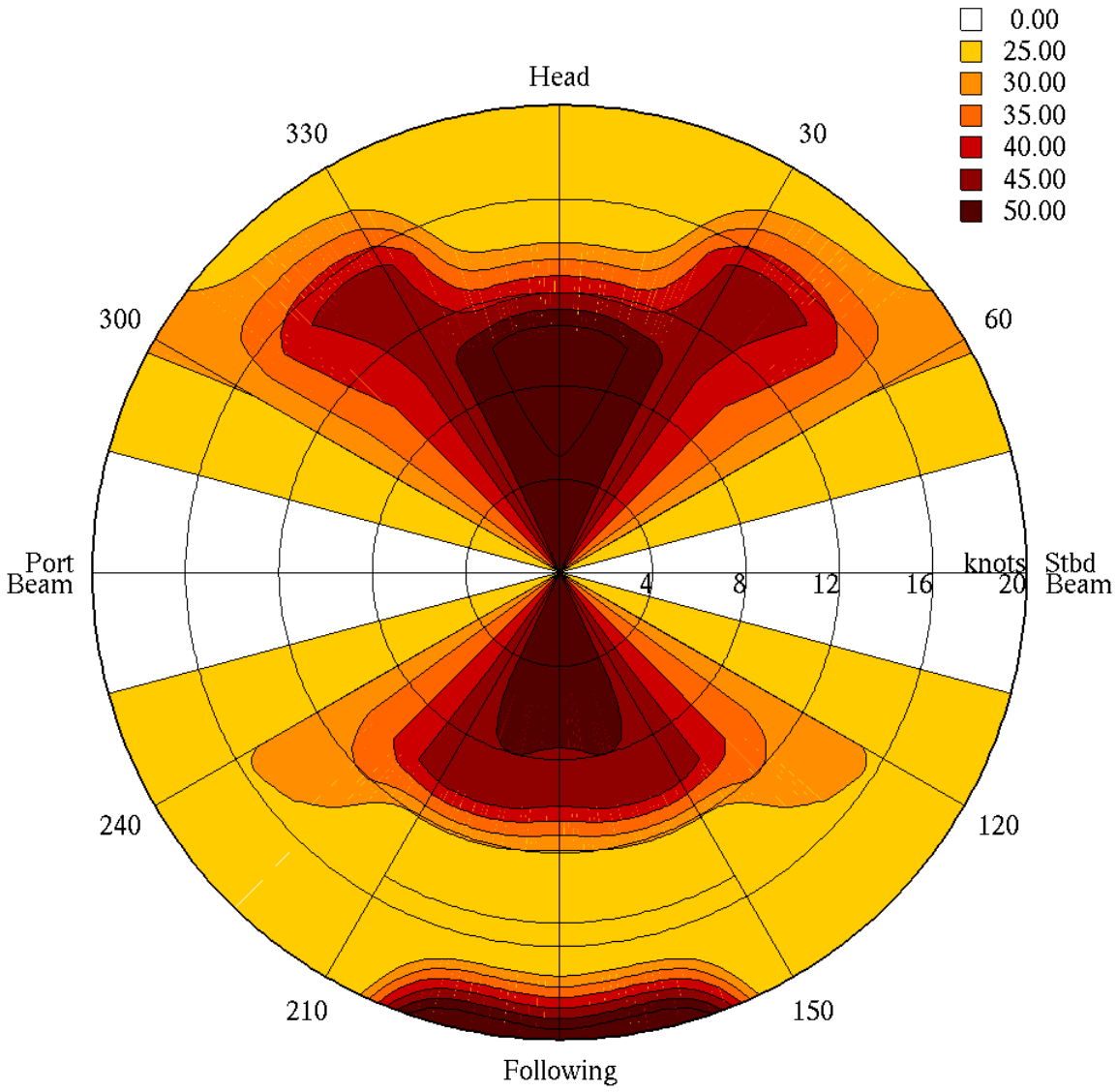

Figure 6.7. Sample Polar Plot for C11-Class Containership Based on Level 2 Vulnerability Assessment Effective Wave Amplitude 6.55 m. Cosine Function is Used to Model a Decrease of Stability Variation in Beam Seas

7. REFINEMENT OF EXPLANATORY NOTES

7.1 Calculation of Roll Damping with Simplified Ikeda's Method

7.1.1 General

An estimation of roll damping is required to complete calculations for the level 2 of the vulnerability criteria for:

- Parametric roll, see Appendix 4 of Annex 2 of SDC-4/5/1Add.1
- Dead ship condition, see paragraph 3.4.1.2 in Annex 4 of SDC-4/5/1Add.3
- Excessive accelerations, see paragraph 3.1.1 in Annex 5 of SDC-4/5/1Add.4

The method itself is described Appendix 4 of Annex 2 of SDC-4/5/1Add.1. The method is based on a regression analysis of a large number of model tests. This method is commonly referred as Simplified Ikeda's Method; its description and studies of different aspects of its applicability is covered in a large number of sources. One of the relatively recent descriptions is available from Kawahara, *et al*. (2012). The method is also included in the current ITTC procedure 7.5-02-07-04.

The description of Appendix 4 of Annex 2 of SDC-4/5/1Add.1 involves a large number of bulky formulae, in particular for wave, eddy, and bilge keel components. Transforming these formulae into a tabular form will make the application of the roll damping estimation method easier and improve readability of the documents. Subsections 7.1.2 through 7.1.4 contain a proposal for new forms of the empirical formulae for wave eddy-making and bilge keel components. Subsections 7.1.5 and 7.1.6 describe the lift and frictional components. Finally, subsection 7.1.7 focuses on verification.

7.1.2 Wave Component of Roll Damping

The wave component at zero forward speed is given by the following equation

$$\hat{B}_W = \frac{A_1}{\hat{\omega}} \cdot \exp\left(-0.6944 A_2 \left(\log(\hat{\omega}) - A_3\right)^2\right) \tag{7.1}$$

where $\hat{\omega}$ undimensional frequency

$$\hat{\omega} = \omega_W \sqrt{\frac{B}{2g}} \tag{7.2}$$

ω_W wave frequency, B ship breadth, g gravity acceleration

$$x_1 = B/d \; ; \quad x_2 = C_b \; ; \quad x_3 = C_m \; ; \quad x_4 = 1 - OG/d \tag{7.3}$$

$$A_1 = AA_1 \cdot \sum_{i=1}^{3} \sum_{j=1}^{4} \sum_{k=1}^{5} Q1_{j+4i,k} \, x_1^{5-k} x_2^{4-j} x_4^{3-i} \tag{7.4}$$

$$AA_1 = 1.0 + (1 - x_4) \cdot \sum_{i=1}^{2} \sum_{j=1}^{4} \sum_{k=1}^{5} Q1_{j+4i+12,k} \, x_1^{5-k} x_2^{3-j} x_3^{2-i} \tag{7.5}$$

$$A_2 = \sum_{i=1}^{5} Q2_i \, x_4^{5-i} \tag{7.6}$$

$$A_3 = AA_3 + \sum_{i=1}^{7} \sum_{j=1}^{7} Q3_{i,j} \, x_2^{7-j} x_4^{7-i} \tag{7.7}$$

$$AA_3 = \sum_{i=1}^{4} Q4_{1,i} \, x_1^{4-i} \cdot \sum_{j=1}^{2} \sum_{k=1}^{4} Q4_{2+j,k} \, x_2^{3-k} x_4^{2-j} \cdot \left(\prod_{i=1}^{10} \left(x_4 - \sum_{j=1}^{4} Q4_{4,j} \, x_1^{4-j} \right)^{10-i} + \sum_{i=1}^{3} Q5_{i+9} \, x_1^{3-i} \right) \tag{7.8}$$

Factors Q1 and Q2 are available in Table 7.1. The first index of the factor Q1 refers to the line number in Table 7.1 while the second index of the factor Q1 refers to the column number in Table 7.1.

Factors Q3 are placed in Table 7.2. The first index of the factor Q3, *i*, refers to the line number in Table 7.2, while the second index of the factor Q3, *j*, refers to the column number in Table 7.2. Factors Q4 and Q5 are available from Table 7.3. The first index of the factor Q4 refers to the line number in Table 7.3, while the second index of the factor Q4 refers to the column number in Table 7.3. The index for the factor Q5 is located above the values in Table 7.3.

Table 7.1. Factors Q1 and Q2

Factor Q1					
	1	**2**	**3**	**4**	**5**
1	0.00000	0.00000	0.00000	0.00000	0.00000
2	0.00000	-0.00222	0.04087	-0.28687	0.59942
3	0.00000	0.01019	-0.16118	0.90499	-1.64139
4	0.00000	-0.01542	0.22037	-1.08499	1.83417
5	-0.06287	0.49893	0.52735	-10.79187	16.61633
6	0.11407	-0.81090	-2.21868	25.12697	-37.77298
7	-0.05893	0.26397	3.19497	-21.81266	31.41135
8	0.01077	0.00187	-1.24941	6.94279	-10.20190
9	0.00000	0.19221	-2.78746	12.50785	-14.76486
10	0.00000	-0.35056	5.22235	-23.97485	29.00785
11	0.00000	0.23710	-3.53506	16.36838	-20.53991
12	0.00000	-0.06712	0.96636	-4.40754	5.89470
13	0.00000	17.945	-166.294	489.799	-493.142
14	0.00000	-25.507	236.275	-698.683	701.494
15	0.00000	9.077	-84.332	249.983	-250.787
16	0.00000	-16.872	156.399	-460.689	463.848
17	0.00000	24.015	-222.507	658.027	-660.665
18	0.00000	-8.56	79.549	-235.827	236.579
Factor Q2					
	0.00000	-1.402	7.189	-10.993	9.45

Table 7.2. Factor Q3

Factor Q3				
	1	**2**	**3**	**4**
1	-7686.0287	30131.5678	-49048.9664	42480.7709
2	61639.9103	-241201.0598	392579.5937	-340629.4699
3	-130677.4903	507996.2604	-826728.7127	722677.104
4	-110034.6584	446051.22	-724186.4643	599411.9264
5	709672.0656	-2803850.2395	4553780.5017	-3888378.9905
6	-822735.9289	3238899.7308	-5256636.5472	4500543.147
7	299122.8727	-1175773.1606	1907356.1357	-1634256.8172
Factor Q3				
	5	**6**	**7**	
1	-20665.147	5355.2035	-577.8827	
2	166348.6917	-43358.7938	4714.7918	
3	-358360.7392	95501.4948	-10682.8619	
4	-264294.7189	58039.7328	-4774.6414	
5	1839829.259	-457313.6939	46600.823	
6	-2143487.3508	538548.1194	-55751.1528	
7	780020.9393	-196679.7143	20467.0904	

Table 7.3. Factors Q4 and Q5

Factor Q4				
	1	**2**	**3**	**4**
1	-0.3767	3.39	-10.356	11.588
2	-17.109	41.495	-33.234	8.8007
3	36.566	-89.203	71.8	-18.108
4	0	-0.0727	0.7	-1.2818
Factor Q5				
Index	**1**	**2**	**3**	**4**
Q5	-1.05584	12.688	-63.70534	172.84571
Index	**5**	**6**	**7**	**8**
Q5	-274.05701	257.68705	-141.40915	44.13177
Index	**9**	**10**	**11**	**12**
Q5	-7.1654	-0.0495	0.4518	-0.61655

7.1.3 Eddy-making component

The eddy component at zero forward speed is given by the following equation

$$\hat{B}_E = \frac{4\,\hat{\omega}\,\varphi_a}{3\,\pi\,x_2 \cdot {x_1}^3} C_R \tag{7.9}$$

where φ_a is roll angle in radians, while other values are:

$$x_1 = B/d \;;\; x_2 = C_b \;;\; x_3 = C_m \tag{7.10}$$

where d draft, C_b block coefficient, C_m midshipsection coefficient

$$C_R = A_E \cdot \exp\left(B_{E1} + B_{E2} \cdot {x_3}^{B_{E3}}\right) \tag{7.11}$$

$$A_E = (-0.0182x_2 + 0.0155)\cdot(x_1 - 1.8)^3 + \sum_{i=1}^{5} Q6_{1,i}\, x_2^{5-i} \tag{7.12}$$

$$B_{E1} = (-0.2x_1 + 1.6)\cdot(3.98x_2 - 5.1525) \cdot \frac{OG}{d}\cdot\left(\frac{OG}{d}\sum_{i=1}^{3} Q6_{2,i}\, x_2^{3-i} + \sum_{i=1}^{2} Q6_{2,i+3}\, x_2^{2-i}\right) \tag{7.13}$$

$$B_{E2} = (0.25x_4 + 0.95)\cdot x_4 + \sum_{i=1}^{5} Q6_{2,i}\, x_2^{5-i} \tag{7.14}$$

$$B_{E3} = (46.5 - 15x_1)\cdot x_2 + 11.2x_1 - 28.6 \tag{7.15}$$

Factors Q6 are placed in Table 7.4. The first index of the factor Q6 refers to the line number in Table 7.4, while the second index of the factor Q6 refers to the column number in Table 7.4.

Table 7.4. Factors Q6

Factor Q6					
	1	**2**	**3**	**4**	**5**
1	-79.414	215.695	-215.883	93.894	-14.848
2	0.9717	-1.55	0.723	0.04567	0.9408
3	0	-219.2	443.7	-283.3	59.6

7.1.4 Bilge-Keel Component

The bilge keel component at zero forward speed is given by the following equation

$$\hat{B}_{BK} = A_{BK}\cdot\hat{\omega}\cdot\exp\left(B_{BK1} + B_{BK2}\cdot x_3^{B_{BK3}}\right) \tag{7.16}$$

Where

$$x_1 = B/d\ ; \quad x_2 = C_b\ ; \quad x_3 = C_m \tag{7.17}$$

$$x_6 = \phi_a\ (\text{deg})\ ; \quad x_7 = b_{BK}/B\ ; \quad x_8 = l_{BK}/L_{BP} \tag{7.18}$$

$$A_{BK} = f_1\cdot f_2\cdot f_3 \tag{7.19}$$

$$f_1 = (x_1 - 2.83)^2\sum_{i=1}^{3} Q7_{1,i}\, x_2^{3-i} + \sum_{i=1}^{3} Q7_{2,i}\, x_2^{3-i} \tag{7.20}$$

$$f_2 = \sum_{i=1}^{3} Q7_{3,i}\, x_6^{3-i} \tag{7.21}$$

$$f_3 = \sum_{i=1}^{2}\sum_{j=1}^{3} Q7_{4+i,j}\, x_7^{3-j} x_8^{3-i} \tag{7.22}$$

$$B_{BK1} = x_4\cdot\left(5x_7 + 0.3x_1 - 0.2x_8 + \sum_{i=1}^{3} Q7_{6,i}\, x_6^{3-i}\right) \tag{7.23}$$

$$B_{BK2} = -15\,x_7 + 1.2\,x_2 - 0.1x_1 + \sum_{i=1}^{3} Q7_{7,i}\left(\frac{OG}{d}\right)^{3-i} \tag{7.24}$$

$$B_{BK3} = 2.5\frac{OG}{d} + 15.75 \tag{7.25}$$

Factors Q6 are placed in Table 7.5. The first index of the factor Q7 refers to the line number in Table 7.5 while the second index of the factor Q7 refers to the column number in Table 7.5.

Table 7.5. Factors Q7

Factor Q7			
	1	**2**	**3**
1	0	-0.3651	0.3907
2	0	-2.21	2.632
3	0.00255	0.122	0.4794
4	-0.8913	-0.0733	0
5	5.2857	-0.01185	0.00189
6	0.00125	-0.0425	-1.86
7	-0.0657	0.0586	1.6164

7.1.5 Lift Component

No changes were proposed for lift component. The formulae for the lift component are include for the sake of completeness and verification.

$$\hat{B}_L = \frac{S_L K_n l_0 l_R V_{ms}}{2\nabla B^2}\left(1 - 1.4\frac{OG}{l_R} + 0.7\frac{OG^2}{l_0 l_R}\right)\sqrt{\frac{B}{2g}} \tag{7.26}$$

where,∇ is volumetric displacement, V_{ms} is forward speed in m/s, other quantities are defined as:

$$K_n = \frac{2\pi d}{L_{BP}} + \kappa\left(4.1\frac{B}{L_{BP}} - 0.045\right) \tag{7.27}$$

$$S_L = L_{BP}d \tag{7.28}$$

$$l_0 = 0.3d \tag{7.29}$$

$$l_R = 0.5d \tag{7.30}$$

$$\kappa = \begin{cases} 0 & C_m \le 0.92 \\ 0.1 & 0.92 < C_m \le 0.97 \\ 0.3 & 0.97 < C_m \end{cases} \tag{7.31}$$

7.1.6 Frictional Component

The formulae for the frictional component are as follows:

$$\hat{B}_F = \frac{B_F}{\rho\nabla B^2}\sqrt{\frac{B}{2g}} \tag{7.32}$$

$$B_F = \frac{4}{3\pi}\rho s_f r_f^3 \varphi_a \omega_w c_f \tag{7.33}$$

where φ_a is roll angle in radians, ω_w is wave frequency, other values are:

$$s_f = L_{BP}(1.7d + C_B B) \tag{7.34}$$

$$r_f = \frac{1}{\pi}\left\{(0.887 + 0.145C_B)(1.7d + C_B B) - 2\overline{OG}\right\} \tag{7.35}$$

$$cf = 1.328\left(\frac{3.22 r_f^2 \varphi_a^2}{T_w v}\right)^{-0.5} \tag{7.36}$$

where T_w is the wave period

$$T_w = \frac{2\pi}{\omega_w} \tag{7.37}$$

7.1.7 Complete Formula and Verification

The compile formula for the non-dimensional roll damping is a function of a wave frequency ω_w and a roll amplitude φ_a:

$$\hat{B}_{44}(\omega_w, \varphi_a) = \hat{B}_F + \hat{B}_W + \hat{B}_{BK} + \hat{B}_E + \hat{B}_L \tag{7.38}$$

where:

$\hat{B}_F$ is the frictional component of roll damping, see equation (7.32)

$\hat{B}_W$ is the wave component of roll damping, see equation (7.1)

$\hat{B}_E$ is the eddy-making component of roll damping, see equation (7.9)

$\hat{B}_{BK}$ is the bilge keel component of roll damping, see equation (7.32)

$\hat{B}_L$ is the bilge keel component of roll damping, see equation (7.26)

The verification of the calculations made in and performed by a comparison against a FORTRAN code "Roll_Damping.for" that was developed by Y. Ikeda, Y. Kawahara, and K. Maekawa of the Osaka Prefecture University and made available at http://www.marine.osakafu-u.ac.jp/~lab15/roll_damping.html. Table 7.6 contains an excerpt of the program output; names of the mot variables are kept as they are in the program for easy references. To the left of each intermediate result is a corresponding number of equation for the reference in the text.

Table 7.6. Verification Data

L_{BP}, m	262	Friction component			Wave component			Bilge Keel Component		
L_{BP}/B	6.55	RF	17.69516	7.35	A2	4.585643	7.6	FBK1	1.471423	7.20
B/d	3.478	SF	11147.19	7.34	AA3	9.53E-02	7.8	FBK2	1.9544	7.21
C_b	0.5605	CF	8.09E-04	7.36	A3	0.565087	7.7	FBK3	6.02E-04	7.22
C_m	0.959	BF	237227.8	7.33	BWHAT	6.16E-03	7.1	ABK	1.73E-03	7.19
OG/d	-0.65	BFHAT	3.07E-05	7.32	Eddy component			BBK1	0.731268	7.23
φ_a,°	10	Wave component			AE	0.125915	7.12	BBK2	1.725352	7.24
T_w, s	10	X1	3.478	7.3	BE1	1.481782	7.13	BBK3	14.125	7.25
l_{BK}/L_{BP}	0.292137	X2	0.5605	7.3	BE2	1.093147	7.14	BBKHAT	8.38E-03	7.16
b_{BK}/B	1.00E-02	X3	0.959	7.3	BE3	7.175565	7.15			
Physical constants		X4	1.65	7.3	CR	1.245002	7.11			
RO[4]	102	AA1	1.001308	7.5	BEHAT	3.51E-03	7.9	Total Roll Damping		
KVC[5]	1.14E-06	A1	2.34E-02	7.4				B44HAT	1.81E-02	7.38

7.2 Example Data Set for Vulnerability Assessment

7.2.1 Input Data

The subject ship is the C11-class post-panamax containership. The input was based on the data made available to the Intact Stability Correspondence Group (ISCG) presented by ITTC and available at http://www.naoe.eng.osaka-u.ac.jp/imo/ssdp1.htm. The hull form is in Figure 2.11, while principal dimensions, basic hydrostatic data, and relevant input parameters are in Table 7.7. Note that the KG value adjusted to account for the free-surface correction, which results in an upright GM = 1.40 m. The GZ curve is shown in Figure 7.1.

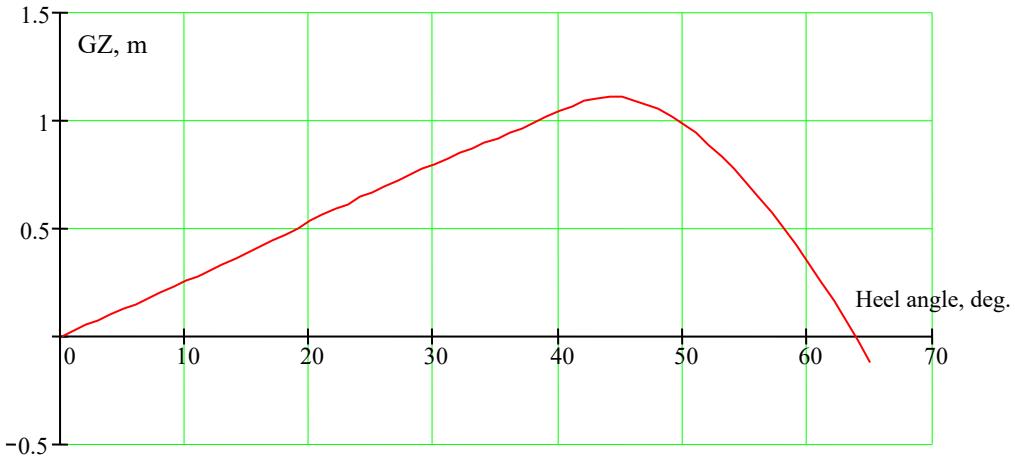

Figure 7.1. GZ curve computed for KG corresponding to GM = 1.4 m

[4] Units are not specified in the source code
[5] Kinematic Viscosity Coefficient, units are not specified in the source code

Table 7.7. Principal Dimensions, Basic Hydrostatic Data and Other Relevant Input Parameters

Length, bp, m	262.00	Bilge keel length ratio (l_{BK}/Lbp)		0.2921
Beam, m	40.00	Bilge keel height ratio (h_{BK}/B)		0.010
Draft amidships, m	11.50	Down flooding angle, °		50
Trim, °	0.0	Lateral windage area, m^2		7,887
KG, m	18.976	Height of centroid above WL, m		14.73
Volumetric displacement ,m^3	67,504	Wind heeling moment coefficient		1.17
Block coefficient	0.56	Natural roll period, s		30.35
Midship section coefficient	0.959	Natural frequency, s^{-1}		0.21
GM, m	1.40	Number of propellers		1
Diameter of propeller, m	8.4	Propeller developed area ratio		0.590
Propeller pitch ratio	0.743	Propeller number of blades		6
Location of excessive acceleration assessment		x=-50 m	y=20 m	Z=40 m

7.2.2 Pure Loss of Stability

Per paragraph 1.1.1 of Annex 3 of SDC 6/WP.6, vulnerability criteria for pure loss of stability are applicable to the subject ship, as her Froude number at service speed 24 kn is 0.244. Paragraph 1.1.1 of Annex 3 of SDC 6/WP.6 establishes the applicability of vulnerability criteria for pure loss of stability if the service-speed Froude-number exceeds 0.24.

The simplified formula in paragraph 1.2.2 for minimum GM yields the following value:

$$GM_{min} = -2.69\, m < R_{PLA} = 0.05 \tag{7.39}$$

The requirement for applicability of the simplified formula in paragraph 1.2.1 is satisfied:

$$\frac{\nabla_D - \nabla}{A_w(D-d)} = 1.176 > 1 \tag{7.40}$$

where ∇_Dvolumetric displacement at waterline is equal to depth D, ∇ is volumetric displacement at draft d, while A_W is area of waterplane at the draft d. Thus, the level 1 criterion indicated a possible vulnerability to pure loss of stability.

For the level 2 vulnerability assessment, GZ curve in waves was computed for 10 wave steepness's, while the wave length was equal to ship length, as directed in paragraph 1.3.2.1 of Annex 3 of SDC 6/WP.6. The calculations were performed for 21 positions of wave crest along the ship, while paragraph 1.3.2.1 requires only 11 positions. Sample GZ curves in waves are shown in Figure 7.1.

The angle of vanishing stability was found for each of these GZ curves (see Table 7.8) for preparation to apply C1 criterion as described in the paragraph 1.3.3. Then the angles of the heel under an external heeling moment was found (see Table 7.9) as described in the paragraph 1.3.4. The minimal angle of vanishing stability and maximum heel angle per wave pass are highlighted in Table 7.8 and Table 7.9, respectively.

Calculation of the criteria C1 and C2 is shown in Table 7.10. Figure 7.2 shows GZ curve in waves.

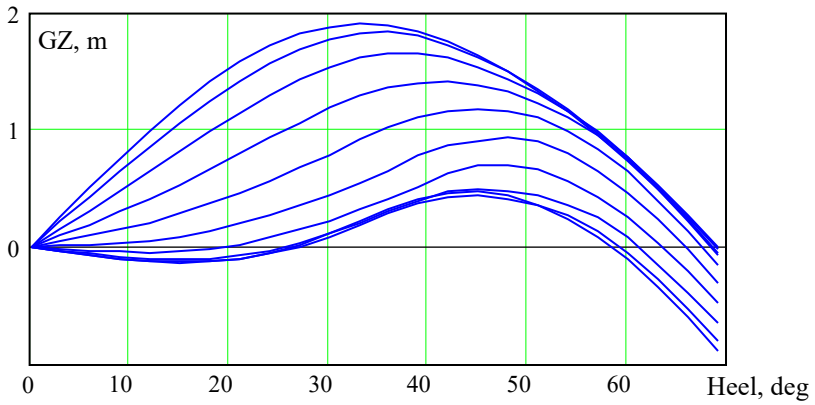

Figure 7.2. GZ Curve in Waves, Wave Height 10.48 m, Wave Length 262 m

Table 7.8. Angles of Vanishing Stability (in °) in Waves – for C1 Criterion

Position of wave crest, m	Wave height m									
	1.31	2.62	3.93	5.24	6.55	7.86	9.17	10.48	11.79	13.1
-131	67.47	67.79	68.10	68.21	68.24	68.28	68.30	68.27	68.28	68.28
-117.9	67.43	67.68	68.00	68.26	68.43	68.51	68.63	68.71	68.75	68.75
-104.8	67.36	67.53	67.81	68.11	68.27	68.50	68.80	68.92	69.01	69.06
-91.7	67.20	67.31	67.51	67.72	67.88	68.09	68.27	68.46	68.56	68.68
-78.6	67.06	66.98	67.07	67.13	67.20	67.26	67.33	67.37	67.38	67.35
-65.5	66.91	66.64	66.52	66.40	66.26	66.11	65.91	65.70	65.48	65.23
-52.4	66.74	66.42	65.89	65.50	65.06	64.56	64.02	63.41	62.80	62.16
-39.3	66.61	66.12	65.55	64.90	64.13	63.21	62.19	60.77	59.54	58.41
-26.2	66.49	65.88	65.14	64.31	63.32	61.94	60.49	59.10	57.53	55.84
-13.1	66.44	65.73	64.99	63.79	62.79	61.20	59.86	58.38	56.60	54.85
0	66.41	65.78	64.77	64.01	62.82	61.95	60.46	58.86	57.19	55.39
13.1	66.44	65.94	65.09	64.67	63.76	62.76	61.67	60.55	59.34	58.05
26.2	66.57	66.19	65.50	65.27	64.60	63.91	63.18	62.47	61.77	61.03
39.3	66.70	66.49	65.96	66.01	65.58	65.14	64.71	64.27	63.84	63.44
52.4	66.86	66.82	66.73	66.61	66.53	66.49	66.38	66.12	65.82	65.50
65.5	67.10	67.09	67.20	67.47	67.20	67.31	67.12	66.87	66.63	66.38
78.6	67.24	67.42	67.60	67.68	67.62	67.52	67.44	67.32	66.77	66.58
91.7	67.39	67.74	67.97	67.94	67.87	67.76	67.62	67.47	67.29	67.09
104.8	67.45	67.84	68.07	68.07	68.00	67.89	67.76	67.49	67.33	67.13
117.9	67.51	67.89	68.04	68.07	68.04	67.96	67.89	67.83	67.77	67.67
-131	67.47	67.79	68.10	68.21	68.24	68.28	68.30	68.27	68.28	68.28

Table 7.9. Angles of Heel (in °) in Waves – for C2 Criterion

Position of wave crest, m	Wave height m									
	1.31	2.62	3.93	5.24	6.55	7.86	9.17	10.48	11.79	13.1
-131	0.86	1.36	1.69	1.92	2.12	2.30	2.46	2.59	2.70	2.80
-117.9	0.92	1.56	2.00	2.36	2.60	2.79	2.94	3.05	3.14	3.21
-104.8	1.01	1.83	2.52	3.08	3.50	3.83	4.08	4.27	4.40	4.50
-91.7	1.13	2.24	3.30	4.26	5.09	5.79	6.35	6.80	7.13	7.35
-78.6	1.27	2.80	4.52	6.35	8.15	9.80	11.22	12.40	13.30	14.00
-65.5	1.41	3.53	6.50	10.12	13.77	17.01	19.67	21.88	23.64	25.03
-52.4	1.55	4.44	9.30	15.09	19.81	23.78	26.95	29.68	31.76	33.49
-39.3	1.66	5.31	12.10	18.69	23.98	27.87	31.03	33.28	35.23	38.48
-26.2	1.70	5.77	13.44	20.66	25.79	29.33	32.03	33.91	36.41	39.63
-13.1	1.67	5.56	13.43	20.55	25.57	28.91	31.31	32.92	34.89	37.25
0	1.58	4.77	11.18	18.17	23.26	26.97	29.36	31.20	32.56	34.68
13.1	1.43	3.80	7.76	13.24	18.37	22.33	25.25	27.45	29.52	31.01
26.2	1.25	2.83	4.86	7.34	10.18	13.38	16.63	19.51	21.94	23.96
39.3	1.09	2.13	3.01	3.70	4.36	5.05	5.80	6.64	7.58	8.64
52.4	0.98	1.65	2.03	2.42	2.81	3.21	3.61	4.01	4.44	4.87
65.5	0.88	1.36	1.68	2.03	2.36	2.68	2.99	3.29	3.58	3.88
78.6	0.82	1.22	1.53	1.84	2.13	2.40	2.65	2.88	3.11	3.33
91.7	0.79	1.16	1.46	1.74	2.00	2.23	2.43	2.62	2.80	2.95
104.8	0.79	1.17	1.44	1.71	1.94	2.15	2.33	2.48	2.61	2.73
117.9	0.81	1.24	1.50	1.74	1.97	2.16	2.32	2.46	2.58	2.68
-131	0.86	1.36	1.69	1.92	2.12	2.30	2.46	2.59	2.70	2.80

Table 7.10. Calculation of Criteria C1 and C2 for Pure Loss of Stability Assessment

Value	Wave height m									
	1.31	2.62	3.93	5.24	6.55	7.86	9.17	10.48	11.79	13.1
φ_{Vmin}	66.41	65.73	64.77	63.79	62.79	61.20	59.86	58.38	56.60	54.85
C1	0	0	0	0	0	0	0	0	0	0
φ_{Smax}	1.70	5.77	13.44	20.66	25.79	29.33	32.03	33.91	36.41	39.63
C2	0	0	0	0	1	1	1	1	1	1

The following requirements of paragraph 1.3.2.3 are related to how 3 % of the largest effective wave height were computed, as recommended in the explanatory notes, paragraph 3.4 of Annex 1 SDC 4/5/1 or 2.3.2.4 and section 7 of Annex 19 of SDC 5/INF.4/Add.1. The results are placed in Table 7.11.

Paragraph 1.3.2.2 of Annex 3 of SDC 6/WP.6 establishes use of a linear interpolation to compute the value of criteria C1 and C2 for each value of effective wave-height shown in Table 7.11. Then the result of linear interpolation is weight averaged as described in paragraph 1.3.2. Statistical weights are taken from IACS recommendation 34 scatter wave table.

Table 7.11. Grim Effective Wave Heights for Assessment of Pure Loss of Stability

Hs \ TZ	3.5	4.5	5.5	6.5	7.5	8.5	9.5	10.5
0.5	0.0	0.1	0.2	0.3	0.4	0.5	0.5	0.5
1.5	0.1	0.2	0.5	0.9	1.3	1.5	1.6	1.6
2.5	0.2	0.4	0.8	1.4	2.1	2.5	2.7	2.7
3.5	0.3	0.6	1.1	2.0	2.9	3.5	3.8	3.8
4.5	0.4	0.7	1.4	2.6	3.8	4.5	4.8	4.9
5.5	0.5	0.9	1.7	3.2	4.6	5.5	5.9	5.9
6.5	0.5	1.0	2.0	3.8	5.5	6.5	7.0	7.0
7.5	0.6	1.2	2.3	4.3	6.3	7.6	8.1	8.1
8.5	0.7	1.3	2.6	4.9	7.1	8.6	9.1	9.2
9.5	0.8	1.5	2.9	5.5	8.0	9.6	10.2	10.2
10.5	0.9	1.7	3.2	6.1	8.8	10.6	11.3	11.3
11.5	1.0	1.8	3.5	6.6	9.7	11.6	12.4	12.4
12.5	1.0	2.0	3.8	7.2	10.5	12.6	13.5	13.5
13.5	1.1	2.1	4.1	7.8	11.4	13.6	14.5	14.6
14.5	1.2	2.3	4.4	8.4	12.2	14.6	15.6	15.6
15.5	1.3	2.5	4.7	8.9	13.0	15.6	16.7	16.7
16.5	1.4	2.6	5.0	9.5	13.9	16.6	17.8	17.8

Table 7.11 Grim Effective Wave Heights for Assessment of Pure Loss of Stability (Cont.)

Hs \ TZ	11.5	12.5	13.5	14.5	15.5	16.5	17.5	18.5
0.5	0.5	0.5	0.5	0.4	0.4	0.4	0.3	0.3
1.5	1.6	1.5	1.4	1.3	1.2	1.1	1.0	0.9
2.5	2.6	2.4	2.3	2.1	1.9	1.8	1.6	1.5
3.5	3.6	3.4	3.2	2.9	2.7	2.5	2.3	2.1
4.5	4.7	4.4	4.1	3.8	3.5	3.2	2.9	2.7
5.5	5.7	5.4	5.0	4.6	4.2	3.9	3.6	3.3
6.5	6.8	6.4	5.9	5.5	5.0	4.6	4.2	3.9
7.5	7.8	7.3	6.8	6.3	5.8	5.3	4.9	4.5
8.5	8.8	8.3	7.7	7.1	6.6	6.0	5.5	5.1
9.5	9.9	9.3	8.7	8.0	7.3	6.7	6.2	5.7
10.5	10.9	10.3	9.6	8.8	8.1	7.4	6.8	6.3
11.5	12.0	11.3	10.5	9.7	8.9	8.1	7.5	6.9
12.5	13.0	12.2	11.4	10.5	9.7	8.9	8.1	7.4
13.5	14.0	13.2	12.3	11.3	10.4	9.6	8.8	8.0
14.5	15.1	14.2	13.2	12.2	11.2	10.3	9.4	8.6
15.5	16.1	15.2	14.1	13.0	12.0	11.0	10.1	9.2
16.5	17.2	16.2	15.0	13.9	12.7	11.7	10.7	9.8

The results of the weight averaging were as follows:

$$CR_1 = \sum_{i=1}^{NH} \sum_{j=1}^{NT} W_{i,j} C1_{i,j} = 0 < R_{PL0} = 0.06 \quad (7.41)$$

$$CR_2 = \sum_{i=1}^{NH} \sum_{j=1}^{NT} W_{i,j} C2_{i,j} = 0.126 > R_{PL0}=0.06 \quad (7.42)$$

where NH = 17 is the number of significant wave heights, while NT = 18 is the number of mean zero-crossing periods in the wave scatter table from IACS recommendation.

The subject ship was found to be vulnerable to pure loss of stability by the level 2 assessment. This result is expected after the study carried out in the section 2.2, as it was demonstrated how conservative the current vulnerability criterion is.

7.2.3 Pure Loss of Stability – Alternative Criterion

Following the description of alternative criterion, given in section 2.2.9 of this report, the level 1 assessment was done for the safety level 2 % leading to wave steepness close to 0.033, see Table 2.1. Wind pressure, associated with this safety level is 0.407 kPa, resulting in the heeling lever of 0.024 m. It was assumed that wind was acting at 20° to ship heading.

Heel angle under this heeling moment was computed using GZ curves in wave for all position of wave crest, see Figure 7.3. The largest heel angle was found when the wave crest position was 26.2 m aft from the midship section.

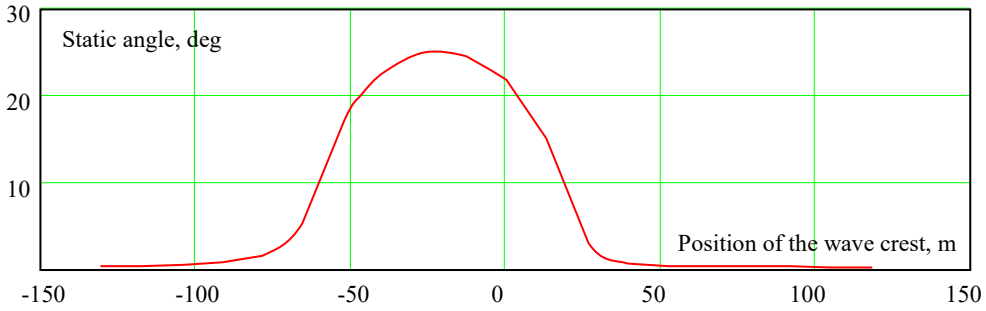

Figure 7.3. Heel Under Steady Wind, Wave Height 8.58 m, Wave Length 262 m, Wind pressure 0.407 kPa

The dynamic heling moment was applied afterwards. Similar to the weather criterion, the dynamic heeling moment is taken 50 % above the steady wind to account for gustiness. The dynamic heel angle was computed by equalizing area “a” and “b” as shown in Figure 2.21 for the GZ curve computed for the wave crest position 26.2 m aft from the midship section. The initial fragment of this GZ curve is shown in Figure 7.4.

The dynamic angle was found to be 38.3°, exceeding the standard 25° for non-passenger vessels. The subject ship was found vulnerable to the pure loss of stability by alternative level 1 criterion.

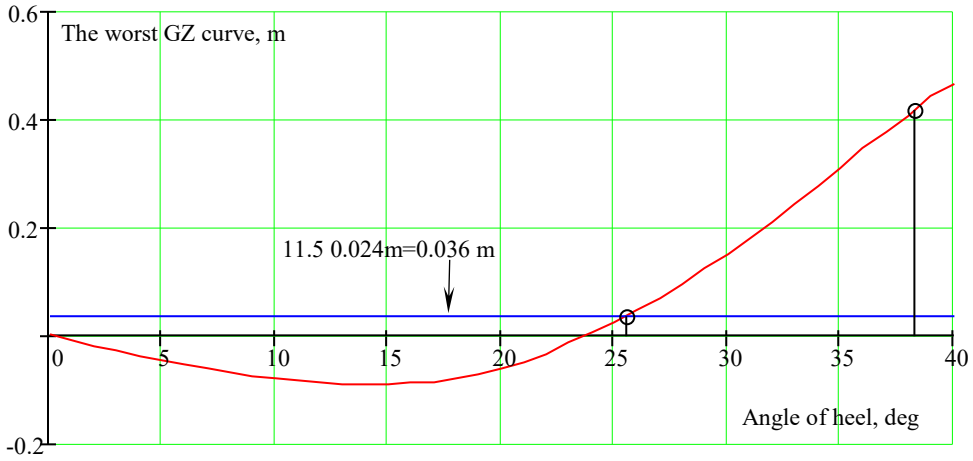

Figure 7.4. On Determination of Dynamic Heel Angle for Alternative Level 1 Vulnerability Criteria for Pure Loss of Stability

This result is also not surprising. The calculations were done for KG = 18.876 m. Column 6 of Table 2.8Table 2.8 contains ΔKG = -1.374 for this criterion. So the critical KG for alterative level 1 criterion $KGcr_{AL1}$ is:

$$KGcr_{AL1} = KGcr_{ISCode} + \Delta KG = 19.93 - 1.374 = 18.55\ m \tag{7.43}$$

where $KGcr_{ISCode}$ is critical KG per 2008 IS code (see Table 2.3).

To improve the accuracy of interpolation, 25 sets of GZ curves in waves were computed for the alternative level 1 assessment. Following the description in the subsection 2.2.10, the largest heel angles were computed, by numerical solution of equation (2.20) and (2.22) and placed in Table 7.12 and Table 7.13 respectively. Roll damping function $R_\varphi(\dot{\varphi})$ was taken as:

$$R_\varphi(\dot{\varphi}) = (I_x + A_{44}) \cdot \left(2\mu_\varphi \omega_\varphi \dot{\varphi} + \delta 2_\varphi \dot{\varphi}|\dot{\varphi}|\right) \tag{7.44}$$

where , I_x is the moment of inertia in roll; A_{44} is the added mass in the roll, ω_φ is the natural roll frequency; coefficients μ_φ and $\delta 2_\varphi$ were estimated using simplified Ikeda method for forward speed of 24 kn:

$$\mu_\varphi = 0.036\ ; \quad \delta 2_\varphi = 0.038 \tag{7.45}$$

Interpolation procedure for the level 2 alternative criteria is similar to the one described in the subsection 7.3.2. The only difference is that wind pressures are associated with significant wave heights through the equations (2.10) and (2.11). Thus each columns in Table 7.12 and Table 7.13 are also associated with a particular value of significant wave height, i.e. with the line in scatter table (see for example Table 1.3.2 in Annex 3 SDC 6/WP.6). Linear interpolation is used to compute the values of the short-term criterion C for different mean zero-crossing periods. The result of the weight averaging is as follows:

$$CR_{alt} = \sum_{i=1}^{NH} \sum_{j=1}^{NT} W_{i,j} C_{i,j} = 0.023 < R_{PL0} = 0.06 \tag{7.46}$$

As expected, the alternative level 2 criterion does not indicate vulnerability to pure loss of stability to the subject ship, which is consistent with existing operational experience.

Table 7.12. Maximum Roll Angle (°) Computed Without Surging

Wave height. m	Wind Pressure, kPa								
	0.01	0.04	0.09	0.14	0.19	0.25	0.32	0.38	0.45
0.3	0.1	0.3	0.6	1.0	1.4	1.8	2.2	2.7	3.2
0.5	0.1	0.3	0.7	1.0	1.4	1.9	2.4	2.8	3.4
0.8	0.1	0.4	0.7	1.1	1.5	2.0	2.5	3.0	3.5
1.0	0.1	0.4	0.7	1.1	1.6	2.1	2.6	3.2	3.8
1.3	0.1	0.4	0.8	1.2	1.7	2.2	2.8	3.4	4.0
1.6	0.1	0.4	0.8	1.3	1.8	2.4	3.0	3.6	4.3
1.8	0.1	0.5	0.9	1.4	2.0	2.6	3.2	3.9	4.6
2.1	0.1	0.5	1.0	1.5	2.1	2.8	3.5	4.2	4.9
2.4	0.1	0.5	1.0	1.6	2.3	3.0	3.7	4.5	5.3
2.6	0.1	0.6	1.1	1.8	2.5	3.2	4.0	4.8	5.7
2.9	0.1	0.6	1.2	1.9	2.6	3.4	4.3	5.2	6.1
3.1	0.1	0.6	1.3	2.0	2.8	3.6	4.5	5.5	6.5
3.4	0.2	0.7	1.4	2.1	3.0	3.9	4.8	5.8	6.9
3.7	0.2	0.7	1.5	2.3	3.2	4.1	5.1	6.2	7.3
3.9	0.2	0.8	1.5	2.4	3.4	4.4	5.4	6.6	7.7
4.2	0.2	0.8	1.6	2.5	3.6	4.6	5.8	6.9	8.1
4.5	0.2	0.9	1.7	2.7	3.7	4.9	6.1	7.3	8.6
4.7	0.2	0.9	1.8	2.8	3.9	5.1	6.4	7.7	9.0
5.0	0.2	1.0	1.9	2.9	4.1	5.4	6.7	8.0	9.4
5.2	0.2	1.0	2.0	3.1	4.3	5.6	7.0	8.4	9.8
6.8	0.3	1.3	2.5	3.9	5.4	7.0	8.7	10.5	12.3
8.4	0.3	1.5	2.9	4.5	6.3	8.2	10.2	12.3	14.4
10.0	0.4	1.6	3.2	5.1	7.1	9.2	11.5	13.8	16.1
11.5	0.4	1.8	3.5	5.5	7.6	10.0	12.4	14.9	17.4
13.1	0.4	1.9	3.7	5.8	8.1	10.5	13.0	15.6	18.2

Table 7.12 Maximum Roll Angle (°) Computed Without Surging (Cont.)

Wave height. m	Wind Pressure, kPa							
	0.53	0.60	0.68	0.76	0.84	0.93	1.01	1.10
0.3	3.7	4.2	4.8	5.4	5.9	6.5	7.1	7.7
0.5	3.9	4.4	5.0	5.6	6.2	6.8	7.4	8.1
0.8	4.1	4.7	5.3	5.9	6.5	7.1	7.8	8.4
1.0	4.4	5.0	5.6	6.2	6.9	7.5	8.2	8.9
1.3	4.6	5.3	6.0	6.6	7.3	8.0	8.7	9.4
1.6	4.9	5.6	6.3	7.1	7.8	8.5	9.3	10.0
1.8	5.3	6.0	6.8	7.6	8.3	9.1	9.9	10.7
2.1	5.7	6.5	7.3	8.1	8.9	9.8	10.6	11.4
2.4	6.1	6.9	7.8	8.6	9.5	10.4	11.3	12.2
2.6	6.5	7.4	8.3	9.3	10.2	11.1	12.0	13.0
2.9	7.0	8.0	8.9	9.9	10.9	11.8	12.8	13.8
3.1	7.5	8.5	9.5	10.5	11.6	12.6	13.6	14.6
3.4	7.9	9.0	10.1	11.2	12.3	13.4	14.4	15.5
3.7	8.4	9.5	10.7	11.8	13.0	14.1	15.2	16.3
3.9	8.9	10.1	11.3	12.5	13.7	14.9	16.0	17.2
4.2	9.4	10.6	11.9	13.1	14.4	15.6	16.8	18.0
4.5	9.9	11.2	12.5	13.8	15.1	16.4	17.7	18.9
4.7	10.4	11.7	13.1	14.4	15.8	17.1	18.4	19.7
5.0	10.9	12.3	13.7	15.1	16.5	17.9	19.2	20.5
5.2	11.3	12.8	14.3	15.8	17.2	18.6	20.0	21.3
6.8	14.1	15.9	17.7	19.5	21.2	22.8	24.3	25.8
8.4	16.5	18.6	20.6	22.6	24.5	26.3	27.9	29.4
10.0	18.5	20.7	22.9	25.0	26.9	28.8	30.5	32.0
11.5	19.9	22.3	24.6	26.7	28.7	30.5	32.3	33.8
13.1	20.8	23.3	25.6	27.8	29.9	31.7	33.5	35.1

Table 7.13. Maximum Roll Angle (°) Computed With Surging

Wave height. m	Wind Pressure, kPa								
	0.01	0.04	0.09	0.14	0.19	0.25	0.32	0.38	0.45
0.3	0.1	0.3	0.6	1.0	1.4	1.8	2.2	2.7	3.2
0.5	0.1	0.3	0.7	1.0	1.4	1.9	2.4	2.8	3.4
0.8	0.1	0.4	0.7	1.1	1.5	2.0	2.5	3.0	3.5
1.0	0.1	0.4	0.7	1.1	1.6	2.1	2.6	3.2	3.8
1.3	0.1	0.4	0.8	1.2	1.7	2.2	2.8	3.4	4.0
1.6	0.1	0.4	0.8	1.3	1.8	2.4	3.0	3.6	4.3
1.8	0.1	0.5	0.9	1.4	2.0	2.6	3.2	3.9	4.6
2.1	0.1	0.5	1.0	1.5	2.2	2.8	3.5	4.2	4.9
2.4	0.1	0.5	1.1	1.7	2.3	3.0	3.8	4.6	5.4
2.6	0.1	0.6	1.1	1.8	2.5	3.3	4.1	4.9	5.8
2.9	0.1	0.6	1.2	1.9	2.7	3.5	4.4	5.3	6.3
3.1	0.2	0.7	1.3	2.1	2.9	3.8	4.8	5.8	6.8
3.4	0.2	0.7	1.5	2.3	3.2	4.1	5.2	6.2	7.3
3.7	0.2	0.8	1.6	2.5	3.4	4.5	5.6	6.7	7.9
3.9	0.2	0.9	1.7	2.7	3.7	4.9	6.0	7.2	8.5
4.2	0.2	0.9	1.9	2.9	4.0	5.2	6.5	7.8	9.1
4.5	0.2	1.0	2.0	3.1	4.4	5.7	7.0	8.4	9.8
4.7	0.3	1.1	2.2	3.4	4.7	6.1	7.6	9.1	10.6
5.0	0.3	1.2	2.3	3.6	5.0	6.6	8.1	9.7	11.4
5.2	0.3	1.3	2.5	3.9	5.4	7.1	8.7	10.4	12.2
6.8	0.5	2.0	4.0	6.2	8.6	11.0	13.5	15.9	18.2
8.4	0.8	3.4	6.7	10.2	13.8	17.3	20.6	23.5	26.0
10.0	1.6	6.9	12.9	18.8	23.7	27.3	30.0	32.0	33.6
11.5	4.9	19.3	29.8	33.5	35.4	36.9	38.1	39.1	40.1
13.1	7.2	27.1	39.4	43.4	44.1	44.7	45.4	46.2	47.2

Table 7.13 Maximum Roll Angle (deg) Computed Without Surging (Cont.)

Wave height. m	Wind Pressure, kPa							
	0.53	0.60	0.68	0.76	0.84	0.93	1.01	1.10
0.3	3.7	4.2	4.8	5.4	5.9	6.5	7.1	7.7
0.5	3.9	4.4	5.0	5.6	6.2	6.8	7.4	8.1
0.8	4.1	4.7	5.3	5.9	6.5	7.1	7.8	8.4
1.0	4.3	5.0	5.6	6.2	6.8	7.5	8.2	8.9
1.3	4.6	5.3	5.9	6.6	7.3	8.0	8.7	9.4
1.6	4.9	5.6	6.4	7.1	7.8	8.5	9.3	10.0
1.8	5.3	6.0	6.8	7.6	8.4	9.2	9.9	10.7
2.1	5.7	6.5	7.3	8.1	9.0	9.8	10.7	11.5
2.4	6.2	7.0	7.9	8.8	9.7	10.5	11.4	12.3
2.6	6.7	7.6	8.5	9.5	10.4	11.3	12.3	13.2
2.9	7.2	8.2	9.2	10.2	11.2	12.2	13.1	14.1
3.1	7.8	8.9	9.9	11.0	12.0	13.1	14.1	15.1
3.4	8.4	9.5	10.7	11.8	12.9	14.0	15.1	16.1
3.7	9.1	10.3	11.5	12.7	13.8	15.0	16.1	17.2
3.9	9.7	11.0	12.3	13.6	14.8	16.0	17.2	18.3
4.2	10.5	11.8	13.2	14.5	15.8	17.0	18.2	19.4
4.5	11.3	12.7	14.1	15.5	16.8	18.1	19.4	20.6
4.7	12.1	13.6	15.1	16.5	17.9	19.2	20.5	21.7
5.0	13.0	14.6	16.1	17.6	19.0	20.4	21.7	22.9
5.2	13.9	15.5	17.1	18.7	20.2	21.6	22.9	24.1
6.8	20.3	22.3	24.1	25.8	27.3	28.7	30.0	31.1
8.4	28.1	29.9	31.4	32.7	33.9	35.0	35.9	36.7
10.0	35.0	36.2	37.2	38.2	39.1	39.9	40.6	41.4
11.5	41.0	41.9	42.7	43.6	44.4	45.3	46.2	47.2
13.1	48.3	49.6	51.5	57.3	71.8	98.3	102.2	100.7

7.2.4 Parametric Roll

The simplified formula in paragraph 2.2.1 for relative GM variation yields the following value:

$$\frac{\Delta GM}{GM} = 1.46 < R_{PR} = 0.413 \tag{7.47}$$

The requirement for applicability of the simplified formula in paragraph 2.2.1 is satisfied:

$$\frac{\nabla_D - \nabla}{A_W(D-d)} = 1.176 > 1 \tag{7.48}$$

where ∇_D volumetric displacement at waterline is equal to depth D, ∇ is volumetric displacement at draft d, while A_W is area of waterplane at the draft d. Thus, the level 1 criterion has indicated possible vulnerability to parametric roll.

As formulated in section 2.3 of Annex 3 SDC 6/WP.6, the level 2 assessment for parametric roll consists of two checks. The first check is involved GM in waves for 16 wave cases defined in the Table 2.3.2.3 of Annex 3 SDC 6/WP.6. Figure 7.5shows values of GM as a function of the wave crest position. As the waves are of different length each GM curve out of 16, has its own range. The curve for the wave length 442.7 m is shown in bright red for the reference.

Paragraph 2.3.2.1 contains a criterion to see which of these GM values have sufficient variation to start parametric resonance, applying

$$\frac{\Delta GM}{GM} < R_{PR} = 0.413 \tag{7.49}$$

where value of ΔGM is taken from direct calculations, shown in Figure 7.5.

The result of the assessment is shown in Figure 7.6. The requirement, described in paragraph 2.3.2 checks a if "reference" speed where parametric roll that is possible is within an achievable range. Results are shown in Figure 7.7. Numerical results are placed in Table 7.14. The first check of level 2 criteria for parametric roll has indicated possible vulnerability:

$$C1 = \sum_{i=1}^{Nc} W_i C_i = 0.437 < R_{PR0} = 0.06 \tag{7.50}$$

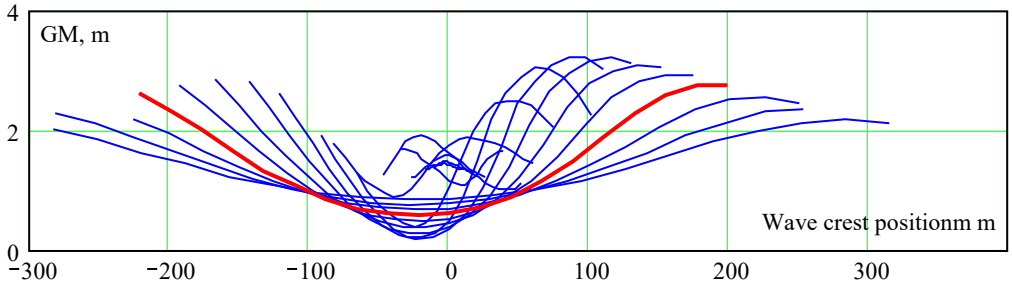

Figure 7.5. GM Values for the Wave Cases from Table 2.3.2.3 of Annex 3 SDC 6/WP.6

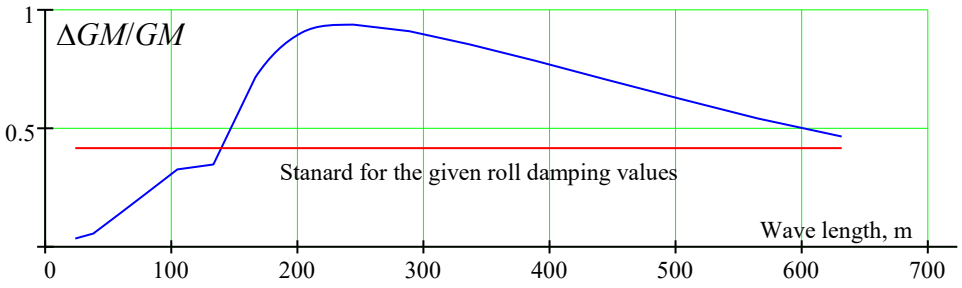

Figure 7.6. Assessment of Variation of GM in Waves

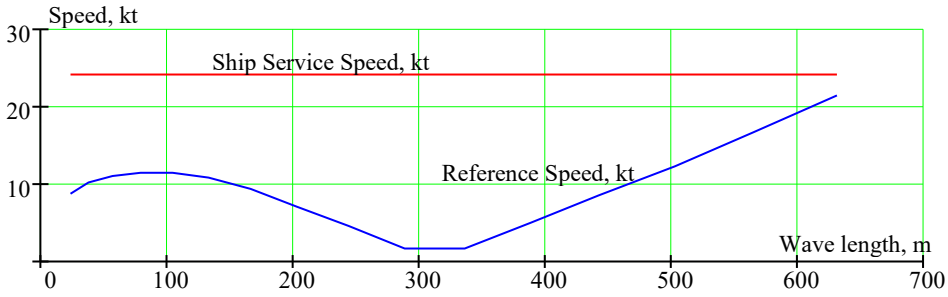

Figure 7.7. Assessment of Variation of GM in Waves

Table 7.14. Level 2 Check 1 Parametric Roll Assessment

Wave case number	1	2	3	4	5	6	7	8
Wave length, m	22.6	37.3	55.7	77.9	103.7	133.1	166.3	203.2
$\Delta GM/GM$	0.03	0.05	0.13	0.22	0.32	0.34	0.71	0.90
Reference speed, kn	8.65	10.06	11.00	11.42	11.28	10.71	9.36	7.01
Criterion C	0	0	0	0	0	0	1	1
Wave case number	9	10	11	12	13	14	15	16
Wave length, m	243.7	287.9	335.8	387.4	442.7	501.7	564.3	630.7
$\Delta GM/GM$	0.94	0.91	0.85	0.78	0.70	0.62	0.54	0.46
Reference speed, kn	4.42	1.59	1.49	4.82	8.41	12.21	16.49	21.29
Criterion C	1	1	1	1	1	1	1	1

Calculations needed for the second check of level 2 criteria for parametric roll is described in paragraph 2.3.3 and 2.3.4 of Annex 3 of SDC 6/ WP.6. These calculations require the same set of GZ curve in wave that level 2 pure loss vulnerability assessment described in section 7.2.3 and with example shown in Figure 7.2.

The calculation of the maximum roll angles was carried out for series of speeds as defined by speed factor in Table 2.3.3 of Annex 3 of SDC 6/ WP. Numerical technique is described in section 3.3 of Annex 19 of ADC 5/INF.4/Add.1 or in Appendix 3 to Annex 2 of SDC 4/5/1/Add.1. The results are summarized in Table 7.15.

Table 7.15. Roll Amplitudes

Wave amplitude, m	Speed factor, K												
	1.0	0.991	0.966	0.924	0.866	0.793	0.707	0.609	0.500	0.383	0.259	0.131	0
	Speed, m/s												
	12.35	12.24	11.93	11.41	10.69	9.80	8.73	7.52	6.17	4.72	3.20	1.61	0.00
0.66	2.7	2.4	2.8	4.1	2.6	2.7	2.7	2.5	2.6	3.8	28.7	28.3	3.2
1.31	1.5	2.8	8.0	26.3	3.3	2.6	2.3	2.3	1.7	16.7	180	39.9	9.7
1.97	9.0	9.3	17.0	28.6	7.1	2.8	2.5	2.4	4.6	22.5	180	180	30.4
2.62	13.8	15.3	20.4	29.2	9.7	3.0	2.2	2.4	16.6	27.4	180	180	36.0
3.28	16.7	17.5	20.7	24.7	26.7	4.2	2.5	2.3	20.3	31.8	180	180	180
3.93	18.3	19.1	21.4	180	35.5	3.4	4.0	3.1	15.1	31.6	180	180	180
4.59	20.4	14.8	23.9	180	180	16.8	4.2	3.2	23.5	32.2	180	180	180
5.24	21.8	24.6	24.2	180	180	21.9	3.9	3.0	17.9	180	180	180	180
5.90	13.9	26.1	24.5	180	180	26.4	3.8	3.3	18.5	180	180	180	180
6.55	16.1	16.4	17.7	180	180	180	4.1	3.5	16.5	180	180	180	180

Table 7.15 Roll Amplitudes (Cont.)

Wave amplitude, m	Speed factor, K											
	0.131	0.259	0.383	0.500	0.609	0.707	0.793	0.866	0.924	0.966	0.991	1.0
	Speed, m/s											
	-1.61	-3.20	-4.72	-6.17	-7.52	-8.73	-9.80	-10.69	-11.41	-11.93	-12.24	-12.35
0.66	3.3	3.2	3.1	3.1	3.0	3.0	3.0	2.9	3.0	2.9	3.0	2.9
1.31	3.8	3.8	3.6	3.3	3.2	3.1	3.2	3.2	3.1	3.1	3.1	3.1
1.97	12.9	6.0	4.0	3.8	3.4	3.4	3.3	3.3	3.3	3.3	3.3	3.2
2.62	21.8	6.7	5.0	4.2	3.5	3.5	3.6	3.4	3.3	3.4	3.3	3.4
3.28	29.3	17.9	3.6	5.2	4.1	3.6	3.7	3.6	3.4	3.6	3.5	3.6
3.93	34.0	25.3	12.0	7.0	4.4	3.8	3.7	3.7	3.5	3.6	3.6	3.5
4.59	180	29.2	21.6	6.4	6.5	4.5	4.0	3.8	4.1	3.8	3.7	3.5
5.24	180	180	26.2	17.5	9.8	5.1	4.3	4.2	2.9	4.0	3.8	4.1
5.90	180	180	180	21.6	16.9	4.0	4.6	4.6	4.5	4.2	3.9	4.2
6.55	180	180	180	180	18.2	12.6	5.8	5.1	4.6	4.1	4.1	4.5

Roll damping coefficients μ_φ and $\delta 2_\varphi$ were estimated using simplified Ikeda method for zero speed (for the sake of conservatism).

$$\mu_\varphi = 0.00365\ ;\quad \delta 2_\varphi = 0.038 \tag{7.51}$$

Computation of the value C2(Fn,β) is described in paragraph 2.3.3.1 as weighted average. Effective wave heights were computed, as recommended in the draft explanatory notes,

paragraph 3.8 of Annex 2 SDC 4/5/1 or 2.3.2.4 and section 3.2.2 of Annex 19 of SDC 5/INF.4/Add.1. The results are placed in Table 7.16.

Table 7.16. Grim Effective Wave Heights for Parametric Roll Assessment

Hs \ TZ	3.5	4.5	5.5	6.5	7.5	8.5	9.5	10.5
0.5	0.0	0.1	0.1	0.2	0.3	0.3	0.4	0.4
1.5	0.1	0.2	0.3	0.6	0.8	1.0	1.1	1.1
2.5	0.1	0.3	0.5	1.0	1.4	1.7	1.8	1.8
3.5	0.2	0.4	0.7	1.4	2.0	2.4	2.5	2.5
4.5	0.3	0.5	0.9	1.7	2.5	3.0	3.2	3.3
5.5	0.3	0.6	1.1	2.1	3.1	3.7	4.0	4.0
6.5	0.4	0.7	1.3	2.5	3.7	4.4	4.7	4.7
7.5	0.4	0.8	1.5	2.9	4.2	5.1	5.4	5.4
8.5	0.5	0.9	1.7	3.3	4.8	5.7	6.1	6.1
9.5	0.5	1.0	1.9	3.7	5.4	6.4	6.9	6.9
10.5	0.6	1.1	2.1	4.1	5.9	7.1	7.6	7.6
11.5	0.6	1.2	2.3	4.5	6.5	7.8	8.3	8.3
12.5	0.7	1.3	2.5	4.8	7.0	8.4	9.0	9.0
13.5	0.8	1.4	2.7	5.2	7.6	9.1	9.7	9.8
14.5	0.8	1.5	2.9	5.6	8.2	9.8	10.5	10.5
15.5	0.9	1.6	3.1	6.0	8.7	10.5	11.2	11.2
16.5	0.9	1.8	3.3	6.4	9.3	11.1	11.9	11.9

Table 7.16 Grim Effective Wave Heights for Parametric Roll Assessment (Cont.)

Hs \ TZ	11.5	12.5	13.5	14.5	15.5	16.5	17.5	18.5
0.5	0.3	0.3	0.3	0.3	0.3	0.2	0.2	0.2
1.5	1.0	1.0	0.9	0.8	0.8	0.7	0.7	0.6
2.5	1.7	1.6	1.5	1.4	1.3	1.2	1.1	1.0
3.5	2.4	2.3	2.1	2.0	1.8	1.7	1.5	1.4
4.5	3.1	3.0	2.7	2.5	2.3	2.1	2.0	1.8
5.5	3.8	3.6	3.4	3.1	2.8	2.6	2.4	2.2
6.5	4.5	4.3	4.0	3.7	3.4	3.1	2.8	2.6
7.5	5.2	4.9	4.6	4.2	3.9	3.6	3.3	3.0
8.5	5.9	5.6	5.2	4.8	4.4	4.0	3.7	3.4
9.5	6.6	6.2	5.8	5.4	4.9	4.5	4.1	3.8
10.5	7.3	6.9	6.4	5.9	5.4	5.0	4.6	4.2
11.5	8.0	7.6	7.0	6.5	6.0	5.5	5.0	4.6
12.5	8.7	8.2	7.6	7.0	6.5	5.9	5.4	5.0
13.5	9.4	8.9	8.2	7.6	7.0	6.4	5.9	5.4
14.5	10.1	9.5	8.9	8.2	7.5	6.9	6.3	5.8
15.5	10.8	10.2	9.5	8.7	8.0	7.4	6.7	6.2
16.5	11.5	10.8	10.1	9.3	8.5	7.8	7.2	6.6

Paragraph 2.3.4.2 of Annex 3 of SDC 6/WP.6 establishes use of a linear interpolation to compute the value of criterion C for each value of effective wave height shown in Table 7.16. Then the result of linear interpolation is a weight averaged as described in paragraph 2.3.3.1. Statistical weights are taken from IACS recommendation 34 scatter wave table. Finally the

criterion C2 is computed by averaging C2(Fn,β) over the all 25 speed/heading combinations as described in paragraph 2.3.3:

$$C2 = 0.104 < R_{PR1} = 0.025 \tag{7.52}$$

The second check of the level 2 criterion also indicated a vulnerability of the considered ship to parametric roll. Again, this result is expected, keeping in mind that a C11-class containership has been involved in dynamic stability accident, identified as parametric roll (France, 2003).

7.2.5 Surf-Riding / Broaching

Level 1 vulnerability criteria for surf-riding is described in paragraph 3.2.1 of Annex 3 of SDC 6/WP.6. Two conditions are checked: length below 200 m and Froude number above 0.3. The considered ship is not vulnerable: her length is 262 m > 200 m and Fn = 0.244 < 0.3. Nevertheless the assessment for level 2 surf-riding/broaching vulnerability criteria is carried out.

Paragraph 3.3.5.3 sets the requirements for approximation of calm-water resistance. Regression-based method by Holtrop and Mennen (1994) is used to compute a resistance curve, wake fraction, and thrust deduction. Thrust was modeled using propeller B-series (Oosterveld and van Oossanen, 1975). Numerical results are shown in Table 7.17.

Table 7.17. Resistance and Thrust in Calm Water

Speed kn	Speed, m/s	Resistance, kN	Wake fraction	Thrust deduction	Thrust, kN
0	0.00	0.00	0.07	0.10	7397
1	0.51	4.21	0.08	0.10	7258
2	1.03	15.83	0.08	0.10	7111
3	1.54	34.71	0.08	0.10	6956
4	2.06	60.84	0.08	0.10	6794
5	2.57	94.11	0.08	0.10	6623
6	3.09	134.30	0.08	0.10	6445
7	3.60	181.20	0.08	0.10	6259
8	4.12	234.30	0.08	0.10	6066
9	4.63	293.60	0.08	0.10	5866
10	5.14	358.60	0.08	0.10	5659
11	5.66	429.30	0.08	0.10	5445
12	6.17	505.50	0.08	0.10	5224

Table 7.17 Resistance and Thrust in Calm Water (Cont.)

Speed kn	Speed, m/s	Resistance, kN	Wake fraction	Thrust deduction	Thrust, kN
13	6.69	587.40	0.08	0.10	4996
14	7.20	675.30	0.08	0.10	4762
15	7.72	769.60	0.08	0.10	4522
16	8.23	871.10	0.08	0.10	4275
17	8.75	980.60	0.08	0.10	4022
18	9.26	1100.00	0.08	0.10	3764
19	9.77	1229.00	0.08	0.10	3499
20	10.29	1371.00	0.08	0.10	3229
21	10.80	1526.00	0.08	0.10	2953
22	11.32	1696.00	0.08	0.10	2671
23	11.83	1884.00	0.08	0.10	2385
24	12.35	2093.00	0.08	0.10	2093
25	12.86	2330.00	0.08	0.10	1796
26	13.38	2592.00	0.08	0.10	1495
27	13.89	2870.00	0.08	0.10	1188
28	14.40	3152.00	0.08	0.10	877
29	14.92	3433.00	0.08	0.10	562
30	15.43	3718.00	0.08	0.10	242
31	15.95	4022.00	0.08	0.10	-82
32	16.46	4364.00	0.08	0.10	-411
33	16.98	4760.00	0.08	0.10	-743
34	17.49	5228.00	0.08	0.10	-1079
35	18.01	5785.00	0.08	0.10	-1418
36	18.52	6446.00	0.08	0.10	-1761
37	19.03	7218.00	0.08	0.10	-2108
38	19.55	8107.00	0.08	0.10	-2458
39	20.06	9110.00	0.08	0.10	-2810
40	20.58	10380.00	0.08	0.10	-3166

Paragraph 3.3.5.3 of Annex 3 of SDC 6/WP.6 requires that polynomial approximation of resistance ensures its continuing increasing. For the most of practical cases a cubic parabola will provide sufficient accuracy if the fitting start from some intermediate speed rather than zero. Half of the service speed is used here as the initial point for fitting, see Figure 7.8. All the speed and range can be used to fit the thrust curve. The polynomials approximation used for resistance R and thrust T in calm water are below:

$$R(U) = \sum_{i=1}^{3} r_i U^i \;\; ; \;\; T(U,n) = \tau_0 n^2 + \tau_1 nU + \tau_2 U^2 \qquad (7.53)$$

where U is speed in m/s, n is number of revolutions 1/s, r and t are fitted coefficients, see Table 7.18.

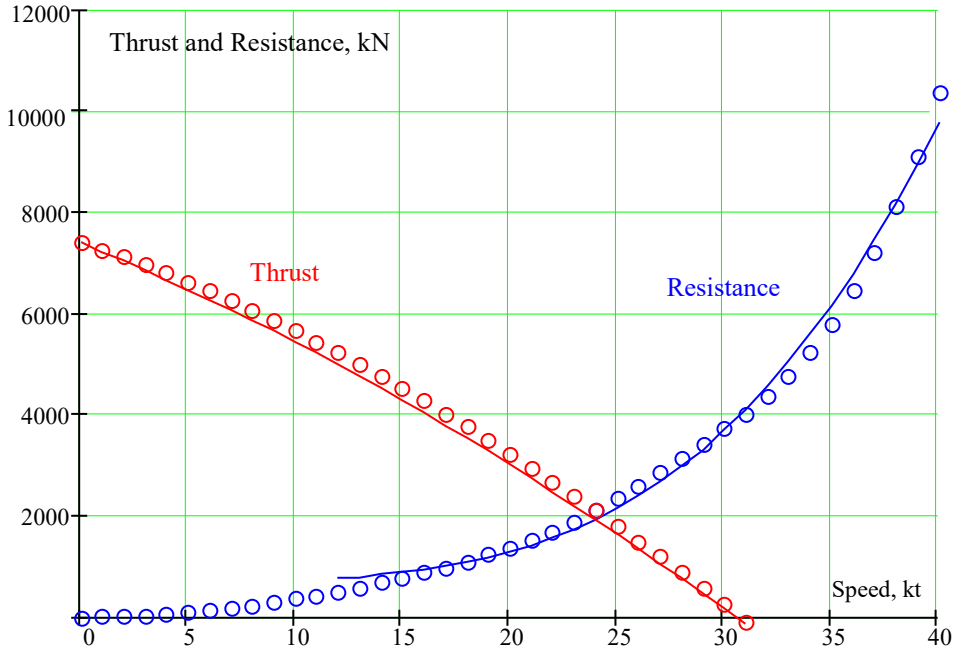

Figure 7.8. Polynomial Fit for Resistance and Thrust in Calm Water

Table 7.18. Fitted Coefficients

Coeff	Value	Coeff	Value
τ_0	1598	r_1	261.9
τ_1	-157.6	r_2	-36.91
τ_2	-8.439	r_3	2.295

The core of level 2 vulnerability criteria is determination of a critical number of propeller, corresponding to the second threshold of surf-riding as described in paragraph 3.3.5.6 of Annex 3 SDC 6/WP6. This critical number of revaluation is associated with zero-crossing of Melinkov function $M_v(n)$:

$$M_v(n) = 2\pi\left(\frac{rr(n)}{q} + \frac{4\,p_1(n)}{\pi} - 2p_2 + \frac{32p_3}{3\pi}\right) \tag{7.54}$$

All the coefficients $rr(n)$, $p_1(n)$, p_2 and p_3 depends on wave surging force, but coefficients $rr(n)$, $p_1(n$ are also dependent on thrust and resistance, thus are function of number of revolutions. Sample values of these coefficients are placed in Table 7.19 for a wave length 262 m and wave height 6.6 m.

Figure 7.9 shows Melnikov function for these wave condition. The function crosses 0 at 2.67 revolutions per second. It is the critical number of revolutions that was referred in paragraph 3.3.5.6 of Annex 3 SDC 6/WP6. As the number of revolutions corresponding to service speed of 24 kn is only 2.15 resolutions per second, the considered conditions are safe from possible surf-riding.

Table 7.19. Melnikov Function

n	rr(n)	$p_1(n)$	$M_v(n)$
0.00	-3.977E-03	0.231	-0.88
0.25	-4.197E-03	0.236	-0.96
0.50	-4.353E-03	0.241	-1.00
0.75	-4.447E-03	0.246	-1.01
1.00	-4.478E-03	0.250	-0.99
1.25	-4.446E-03	0.255	-0.94
1.50	-4.351E-03	0.260	-0.85
1.75	-4.193E-03	0.265	-0.73
2.00	-3.972E-03	0.269	-0.58
2.25	-3.688E-03	0.274	-0.39
2.50	-3.341E-03	0.279	-0.17
2.75	-2.932E-03	0.283	0.09
3.00	-2.460E-03	0.288	0.37
3.25	-1.924E-03	0.293	0.69
3.50	-1.326E-03	0.298	1.04
3.75	-6.649E-04	0.302	1.43
4.00	5.913E-05	0.307	1.85
p_2	6.06E-02	p_3	5.73E-03
λ, m	262	H, m	6.6

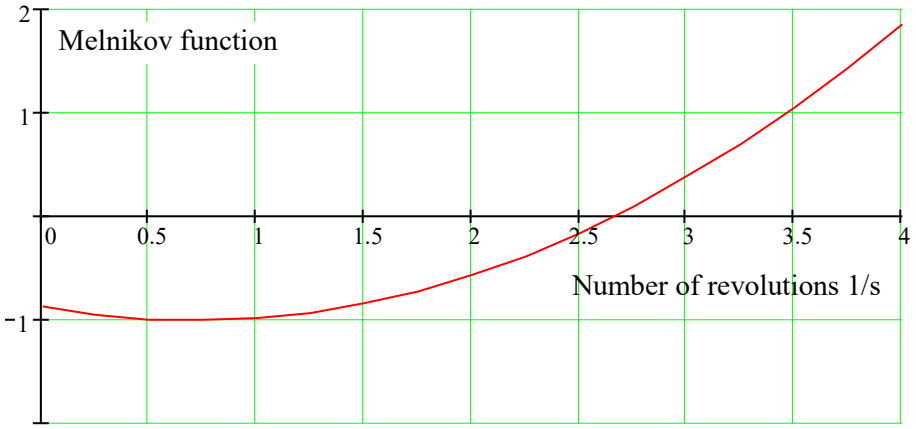

Figure 7.9. Example of Melnikov Function, Wave length 262 m wave height 6.6 m

The final result of level 2 vulnerability assessment for surf-riding/broaching as descried in paragraph 3.3.2 of Annex 3 SDC 6/WP6 is below:

$$C=1.573E\text{-}9 < R_{SR}=0.005 \qquad (7.55)$$

The result of level 2 vulnerability assessment is consistent with level 1 criterion and has indicated no vulnerability of the considered ship to surf-riding/broaching.

7.2.6 Dead Ship Condition

The subject ship was studied intensively in relation with vulnerability to the dead ship condition in Section 3 of this report. Section 3.4 contains a case study for the C11 class containership, with the main focus on different assumptions used for formulation of level 2 criteria for vulnerability to stability failure in the dead-ship condition. As a main approach of the study different possible options were considered and compared. The example in this subsection has a different objective: to report the results of calculations described in the section 4 of Annex 3 SDC 6/WP6.

The subject ship used in this section is slightly different from the one in the other section 3 and 4. There are two differences. First, the natural roll frequency was computed by approximation formula form 2008 IS Code. In this section, (as well as in the sections 2, 5, and 6) direct calculation were used, as the comparison with numerical simulation was important. As a result the period of roll used here is 30 s (Table 7.7) while 23 s was used in Table 3.5. The second difference is the GM value adjustment priority. There is always some difference between GM computed from the moment of inertia of the waterplane area and the value evaluated from the GZ curve. In sections 3 and 4 GZ curves was corrected to match the "waterplane" GM. In this section as well as in the section 2, 5, and 6, KG was adjusted to produce desirable GM through the GZ curve.

These two different approaches to GM and roll period make difficult direct comparison of the results of calculation in this subsection with other C11 calculation in section 3. This does undermine any previously reported results as the main focus of calculations in section 3 was understanding the tendencies and consequences of assumptions.

A level 1 vulnerability assessment in dead ship condition failure mode is described in section 4.2 of Annex 3 of SDC 5/WP.6. It is essentially weather criterion with the table of roll periods extended to 30 s. With this change in mind, following the guidance of paragraph 2.3, one gets the following results:

- Area a = 0.042
- Area b = 0.4
- Dynamic angle of heel 4.9°

These results clearly indicate that the subject ship is not vulnerable to a stability failure in dead ship condition.

A level 2 vulnerability assessment for stability failure in dead ship condition is described in section 4.3 of Annex 3 SDC 6/WP6. The calculation starts form computing the effective wave slope function as described in paragraph 4.3.2.4 of Annex 3 of SDC 5/ WP.6. The paragraph contains the description of "the standard" methodology, which was extensively analyzed in section 3.2. While there are issues with application of the "standard methodology", the paragraph 4.3.2.4 appears not to limit effective wave slope calculation by the "standard methodology" only. It calls for application of "a reliable method, based on computations", which indeed includes direct pressure integration described in subsection 3.2.2 of this report, which is used in further calculations.

The next step is the calculation of a standard deviation of roll motions under the action of wind and waves, as described in paragraph 4.3.2.3 of Annex 3 SDC 6/WP6. The expert group decided to keep relative motions for waves and absolute motions for wind, despite a clear

physical inconsistency (see section 3.3). Thus consistent use of standard deviation of roll motion in absolute coordinates is no longer an option. Table 7.20 contains a standard deviation of roll motion under the combined action of irregular waves and gusty wind.

Table 7.20. Standard Deviation of Roll Motion (rad) Under Waves and Wind

Hs, m	Mean zero-crossing period, s								
	1.5	2.5	3.5	4.5	5.5	6.5	7.5	8.5	9.5
0.5	9.47E-02	1.56E-02	7.68E-03	6.66E-03	5.95E-03	5.36E-03	4.92E-03	4.59E-03	4.33E-03
1.5	2.84E-01	4.76E-02	2.47E-02	2.19E-02	2.00E-02	1.84E-02	1.73E-02	1.64E-02	1.58E-02
2.5	4.74E-01	7.98E-02	4.23E-02	3.77E-02	3.46E-02	3.21E-02	3.03E-02	2.89E-02	2.79E-02
3.5	6.63E-01	1.12E-01	5.97E-02	5.34E-02	4.91E-02	4.57E-02	4.31E-02	4.13E-02	3.99E-02
4.5	8.53E-01	1.44E-01	7.70E-02	6.88E-02	6.33E-02	5.90E-02	5.57E-02	5.34E-02	5.16E-02
5.5	1.04E+00	1.76E-01	9.42E-02	8.42E-02	7.75E-02	7.22E-02	6.83E-02	6.54E-02	6.32E-02
6.5	1.23E+00	2.08E-01	1.11E-01	9.95E-02	9.16E-02	8.53E-02	8.07E-02	7.73E-02	7.47E-02
7.5	1.42E+00	2.40E-01	1.28E-01	1.14E-01	1.05E-01	9.78E-02	9.24E-02	8.85E-02	8.55E-02
8.5	1.61E+00	2.72E-01	1.44E-01	1.28E-01	1.18E-01	1.09E-01	1.03E-01	9.84E-02	9.50E-02
9.5	1.80E+00	3.03E-01	1.59E-01	1.42E-01	1.30E-01	1.20E-01	1.13E-01	1.08E-01	1.04E-01
10.5	1.99E+00	3.34E-01	1.75E-01	1.56E-01	1.43E-01	1.32E-01	1.24E-01	1.18E-01	1.14E-01
11.5	2.18E+00	3.66E-01	1.91E-01	1.70E-01	1.55E-01	1.43E-01	1.35E-01	1.28E-01	1.24E-01
12.5	2.37E+00	3.97E-01	2.07E-01	1.83E-01	1.67E-01	1.55E-01	1.45E-01	1.38E-01	1.33E-01
13.5	2.56E+00	4.28E-01	2.22E-01	1.96E-01	1.79E-01	1.65E-01	1.54E-01	1.46E-01	1.41E-01
14.5	2.75E+00	4.59E-01	2.37E-01	2.09E-01	1.91E-01	1.75E-01	1.64E-01	1.56E-01	1.49E-01
15.5	2.94E+00	4.90E-01	2.52E-01	2.23E-01	2.02E-01	1.86E-01	1.74E-01	1.65E-01	1.58E-01
16.5	3.13E+00	5.21E-01	2.67E-01	2.35E-01	2.13E-01	1.96E-01	1.83E-01	1.73E-01	1.66E-01

Table 7.20 Standard Deviation of Roll Motion (rad) Under Waves and Wind (Cont.)

Hs, m	Mean zero-crossing period, s								
	10.5	11.5	12.5	13.5	14.5	15.5	16.5	17.5	18.5
0.5	4.13E-03	3.98E-03	3.86E-03	3.84E-03	4.02E-03	4.46E-03	5.07E-03	5.68E-03	6.21E-03
1.5	1.53E-02	1.49E-02	1.46E-02	1.45E-02	1.47E-02	1.54E-02	1.64E-02	1.75E-02	1.85E-02
2.5	2.72E-02	2.66E-02	2.61E-02	2.59E-02	2.60E-02	2.66E-02	2.77E-02	2.90E-02	3.01E-02
3.5	3.89E-02	3.81E-02	3.74E-02	3.71E-02	3.72E-02	3.78E-02	3.89E-02	4.02E-02	4.14E-02
4.5	5.03E-02	4.92E-02	4.84E-02	4.80E-02	4.80E-02	4.85E-02	4.96E-02	5.09E-02	5.21E-02
5.5	6.16E-02	6.03E-02	5.93E-02	5.87E-02	5.86E-02	5.90E-02	6.00E-02	6.12E-02	6.24E-02
6.5	7.28E-02	7.13E-02	7.01E-02	6.93E-02	6.90E-02	6.93E-02	7.02E-02	7.13E-02	7.24E-02
7.5	8.32E-02	8.15E-02	8.01E-02	7.92E-02	7.88E-02	7.91E-02	7.98E-02	8.09E-02	8.19E-02
8.5	9.24E-02	9.04E-02	8.88E-02	8.78E-02	8.75E-02	8.78E-02	8.87E-02	8.98E-02	9.08E-02
9.5	1.01E-01	9.90E-02	9.73E-02	9.62E-02	9.58E-02	9.62E-02	9.72E-02	9.83E-02	9.93E-02
10.5	1.11E-01	1.08E-01	1.06E-01	1.05E-01	1.04E-01	1.05E-01	1.06E-01	1.07E-01	1.08E-01
11.5	1.20E-01	1.17E-01	1.15E-01	1.13E-01	1.13E-01	1.13E-01	1.14E-01	1.15E-01	1.16E-01
12.5	1.29E-01	1.26E-01	1.23E-01	1.22E-01	1.21E-01	1.21E-01	1.22E-01	1.23E-01	1.24E-01
13.5	1.36E-01	1.33E-01	1.30E-01	1.29E-01	1.28E-01	1.28E-01	1.29E-01	1.30E-01	1.31E-01
14.5	1.45E-01	1.41E-01	1.38E-01	1.36E-01	1.36E-01	1.36E-01	1.36E-01	1.37E-01	1.38E-01
15.5	1.53E-01	1.49E-01	1.46E-01	1.44E-01	1.43E-01	1.43E-01	1.44E-01	1.44E-01	1.45E-01
16.5	1.60E-01	1.56E-01	1.52E-01	1.50E-01	1.50E-01	1.50E-01	1.50E-01	1.51E-01	1.51E-01

Standard deviations of roll motions under the action of irregular waves is computed in relative coordinates, while the standard deviation of roll motions under the action of gusty wind is calculated in absolute coordinates. This inconsistency probably explains the very large values of the standard deviation of high and short waves (see the column for TZ = 1.5 s). Equivalent damping coefficients were computed with equivalent linearization and placed in Table 7.21 for each combination of significant wave height and mean-zero-crossing period.

Table 7.21. Values of Equivalent Damping

Hs, m	Mean zero-crossing period, s								
	1.5	2.5	3.5	4.5	5.5	6.5	7.5	8.5	9.5
0.5	1.09E-03	1.06E-03	1.07E-03	1.07E-03	1.07E-03	1.07E-03	1.07E-03	1.07E-03	1.07E-03
1.5	1.69E-03	1.64E-03	1.65E-03	1.65E-03	1.65E-03	1.65E-03	1.65E-03	1.65E-03	1.65E-03
2.5	2.35E-03	2.28E-03	2.28E-03	2.29E-03	2.29E-03	2.29E-03	2.29E-03	2.29E-03	2.29E-03
3.5	3.03E-03	2.92E-03	2.93E-03	2.94E-03	2.94E-03	2.94E-03	2.94E-03	2.94E-03	2.94E-03
4.5	3.70E-03	3.56E-03	3.57E-03	3.58E-03	3.58E-03	3.58E-03	3.58E-03	3.59E-03	3.59E-03
5.5	4.36E-03	4.19E-03	4.21E-03	4.22E-03	4.22E-03	4.22E-03	4.22E-03	4.22E-03	4.23E-03
6.5	5.01E-03	4.82E-03	4.84E-03	4.85E-03	4.85E-03	4.85E-03	4.85E-03	4.85E-03	4.86E-03
7.5	5.65E-03	5.42E-03	5.45E-03	5.46E-03	5.46E-03	5.46E-03	5.46E-03	5.46E-03	5.47E-03
8.5	6.27E-03	5.99E-03	6.02E-03	6.04E-03	6.04E-03	6.04E-03	6.04E-03	6.05E-03	6.05E-03
9.5	6.89E-03	6.55E-03	6.59E-03	6.61E-03	6.61E-03	6.61E-03	6.61E-03	6.62E-03	6.62E-03
10.5	7.49E-03	7.11E-03	7.15E-03	7.18E-03	7.18E-03	7.18E-03	7.18E-03	7.18E-03	7.19E-03
11.5	8.09E-03	7.66E-03	7.71E-03	7.73E-03	7.73E-03	7.73E-03	7.74E-03	7.74E-03	7.75E-03
12.5	8.67E-03	8.19E-03	8.24E-03	8.27E-03	8.27E-03	8.27E-03	8.28E-03	8.28E-03	8.29E-03
13.5	9.26E-03	8.70E-03	8.76E-03	8.79E-03	8.80E-03	8.80E-03	8.80E-03	8.80E-03	8.81E-03
14.5	9.83E-03	9.21E-03	9.27E-03	9.31E-03	9.32E-03	9.31E-03	9.32E-03	9.32E-03	9.33E-03
15.5	1.04E-02	9.71E-03	9.78E-03	9.82E-03	9.82E-03	9.82E-03	9.82E-03	9.83E-03	9.84E-03
16.5	1.10E-02	1.02E-02	1.03E-02	1.03E-02	1.03E-02	1.03E-02	1.03E-02	1.03E-02	1.03E-02

Table 7.21 Values of Equivalent Damping (Cont.)

Hs, m	Mean zero-crossing period, s								
	10.5	11.5	12.5	13.5	14.5	15.5	16.5	17.5	18.5
0.5	1.07E-03	1.07E-03	1.07E-03	1.08E-03	1.09E-03	1.13E-03	1.17E-03	1.21E-03	1.25E-03
1.5	1.65E-03	1.65E-03	1.65E-03	1.66E-03	1.69E-03	1.74E-03	1.82E-03	1.90E-03	1.97E-03
2.5	2.29E-03	2.29E-03	2.30E-03	2.31E-03	2.34E-03	2.40E-03	2.48E-03	2.58E-03	2.67E-03
3.5	2.95E-03	2.95E-03	2.95E-03	2.96E-03	3.00E-03	3.06E-03	3.16E-03	3.27E-03	3.37E-03
4.5	3.59E-03	3.59E-03	3.60E-03	3.61E-03	3.65E-03	3.72E-03	3.82E-03	3.94E-03	4.04E-03
5.5	4.23E-03	4.23E-03	4.24E-03	4.25E-03	4.29E-03	4.36E-03	4.46E-03	4.58E-03	4.69E-03
6.5	4.86E-03	4.86E-03	4.87E-03	4.88E-03	4.92E-03	4.99E-03	5.09E-03	5.20E-03	5.32E-03
7.5	5.47E-03	5.47E-03	5.48E-03	5.50E-03	5.54E-03	5.61E-03	5.71E-03	5.83E-03	5.95E-03
8.5	6.05E-03	6.06E-03	6.07E-03	6.09E-03	6.14E-03	6.23E-03	6.36E-03	6.50E-03	6.63E-03
9.5	6.63E-03	6.64E-03	6.65E-03	6.68E-03	6.74E-03	6.85E-03	7.00E-03	7.15E-03	7.29E-03
10.5	7.20E-03	7.21E-03	7.22E-03	7.25E-03	7.32E-03	7.44E-03	7.59E-03	7.75E-03	7.89E-03
11.5	7.75E-03	7.76E-03	7.78E-03	7.82E-03	7.89E-03	8.01E-03	8.16E-03	8.33E-03	8.47E-03
12.5	8.30E-03	8.31E-03	8.33E-03	8.37E-03	8.44E-03	8.57E-03	8.73E-03	8.89E-03	9.04E-03
13.5	8.82E-03	8.84E-03	8.87E-03	8.92E-03	9.02E-03	9.17E-03	9.36E-03	9.55E-03	9.70E-03
14.5	9.35E-03	9.36E-03	9.39E-03	9.45E-03	9.55E-03	9.71E-03	9.91E-03	1.01E-02	1.03E-02
15.5	9.86E-03	9.88E-03	9.91E-03	9.97E-03	1.01E-02	1.03E-02	1.05E-02	1.07E-02	1.08E-02
16.5	1.04E-02	1.04E-02	1.04E-02	1.05E-02	1.06E-02	1.08E-02	1.10E-02	1.13E-02	1.14E-02

The final formulation for the level 2 criterion for vulnerability to stability failure in dead ship condition is given in paragraphs 4.3.1 and 4.3.2 of Annex 3 of SDC 6/WP.6. The result of vulnerability assessment is as follows:

$$C = 0.00012 < R_{DS0} = 0.06 \tag{7.56}$$

The result of level 2 vulnerability assessment is consistent with level 1 criterion and has indicated no vulnerability of the considered ship to stability failure in dead ship condition.

7.2.7 Excessive Accelerations

Level 1 vulnerability assessment for excessive accelerations is described in section 5.2 of Annex 3 of SDC 5/ WP.6. The following are the results of the level 1 vulnerability assessment:

- Wave slope coefficient 0.93
- Amplitude of roll 7.56°
- Criterion value 1.49 m/s^2

The criterion value is below the boundary value $R_{EA1} = 4.64$ m/s^2, thus the subject ship is not vulnerable to a stability failure due to excessive acceleration at the considered loading condition. This is an expected result as the issues related to excessive acceleration are known to be occurring in high GM loading conditions.

Note that there is a difference between the numbers above and similar figures in Table 4.2. The discussion of the difference is in the beginning of the section 7.2.6. The difference for level 1 acceleration criterion and amplitude of roll is much less compare to the difference observed for dead ship condition vulnerability assessment.

Level 2 vulnerability criteria is described in section 5.3 of Annex 3 of SDC 5/WP.6. The criteria are based on linear-ship motion-calculations, which are described in paragraph 5.3.2.2. It allows computing the effective wave-slope with direct-pressure integration. The draft explanatory notes in SDC 4/5/1/Add.4 offers two options for equivalent damping: stochastic linearization or using equivalent roll damping for 15°. It makes sense also to consider the third option: using equivalent linearization from the level 2 for dead ship conditions.

First, computation of roll damping were performed with the Simplified Ikeda method, resulting in: $\mu = 0.002$, $\delta_2 = 0.624$ and $\delta_3 = 1.823$. Results for all three linearization options are presented in Table 7.22 and Table 7.23 for all the sea states from the wave scatter table of IACS recommendation 34. The equivalent damping coefficient for 15° is 0.0239296.

The long-term criteria and standard are defined in paragraph 5.3.1 and 5.3.2. The value of the long-term criterion *C* was 0 for all three damping options considered. The level 2 assessment was consistent with level 1 results and did not indicate any vulnerability to excessive accelerations for the considered ship in loading condition characterized by GM = 1.4 m.

No inconsistency between the levels has been observed for the considered case with excessive acceleration vulnerability criteria.

Table 7.22. Equivalent Damping by Stochastic Linearization

Hs, m	Mean zero-crossing period, s								
	1.5	2.5	3.5	4.5	5.5	6.5	7.5	8.5	9.5
0.5	2.09E-03	2.09E-03	2.14E-03	2.20E-03	2.24E-03	2.26E-03	2.27E-03	2.28E-03	2.30E-03
1.5	2.09E-03	2.09E-03	2.25E-03	2.44E-03	2.54E-03	2.60E-03	2.64E-03	2.68E-03	2.74E-03
2.5	2.09E-03	2.09E-03	2.35E-03	2.68E-03	2.85E-03	2.94E-03	3.02E-03	3.09E-03	3.17E-03
3.5	2.09E-03	2.10E-03	2.46E-03	2.91E-03	3.15E-03	3.29E-03	3.39E-03	3.49E-03	3.61E-03
4.5	2.09E-03	2.10E-03	2.57E-03	3.15E-03	3.46E-03	3.64E-03	3.77E-03	3.90E-03	4.06E-03
5.5	2.09E-03	2.10E-03	2.67E-03	3.39E-03	3.77E-03	3.99E-03	4.15E-03	4.31E-03	4.51E-03
6.5	2.09E-03	2.10E-03	2.78E-03	3.63E-03	4.09E-03	4.34E-03	4.54E-03	4.72E-03	4.96E-03
7.5	2.09E-03	2.11E-03	2.89E-03	3.88E-03	4.40E-03	4.70E-03	4.93E-03	5.14E-03	5.41E-03
8.5	2.09E-03	2.11E-03	3.00E-03	4.12E-03	4.72E-03	5.06E-03	5.31E-03	5.56E-03	5.87E-03
9.5	2.09E-03	2.11E-03	3.11E-03	4.36E-03	5.03E-03	5.42E-03	5.71E-03	5.99E-03	6.33E-03
10.5	2.09E-03	2.11E-03	3.22E-03	4.61E-03	5.35E-03	5.78E-03	6.10E-03	6.41E-03	6.79E-03
11.5	2.09E-03	2.12E-03	3.32E-03	4.85E-03	5.67E-03	6.14E-03	6.50E-03	6.84E-03	7.26E-03
12.5	2.09E-03	2.12E-03	3.43E-03	5.10E-03	6.00E-03	6.51E-03	6.90E-03	7.27E-03	7.73E-03
13.5	2.09E-03	2.12E-03	3.54E-03	5.35E-03	6.32E-03	6.88E-03	7.30E-03	7.71E-03	8.21E-03
14.5	2.09E-03	2.13E-03	3.65E-03	5.60E-03	6.65E-03	7.25E-03	7.71E-03	8.15E-03	8.68E-03
15.5	2.09E-03	2.13E-03	3.76E-03	5.85E-03	6.98E-03	7.63E-03	8.11E-03	8.59E-03	9.16E-03
16.5	2.09E-03	2.13E-03	3.87E-03	6.10E-03	7.31E-03	8.00E-03	8.53E-03	9.03E-03	9.65E-03

Table 7.22. Equivalent Damping by Stochastic Linearization (Cont.)

Hs, m	Mean zero-crossing period, s								
	10.5	11.5	12.5	13.5	14.5	15.5	16.5	17.5	18.5
0.5	2.35E-03	2.48E-03	2.67E-03	2.86E-03	3.01E-03	3.11E-03	3.16E-03	3.17E-03	3.16E-03
1.5	2.86E-03	3.20E-03	3.67E-03	4.11E-03	4.44E-03	4.65E-03	4.76E-03	4.79E-03	4.77E-03
2.5	3.38E-03	3.88E-03	4.56E-03	5.18E-03	5.63E-03	5.92E-03	6.07E-03	6.11E-03	6.08E-03
3.5	3.89E-03	4.52E-03	5.38E-03	6.14E-03	6.71E-03	7.06E-03	7.24E-03	7.28E-03	7.24E-03
4.5	4.39E-03	5.16E-03	6.15E-03	7.05E-03	7.70E-03	8.11E-03	8.31E-03	8.36E-03	8.30E-03
5.5	4.90E-03	5.78E-03	6.91E-03	7.91E-03	8.64E-03	9.10E-03	9.32E-03	9.37E-03	9.30E-03
6.5	5.42E-03	6.39E-03	7.63E-03	8.74E-03	9.54E-03	1.00E-02	1.03E-02	1.03E-02	1.02E-02
7.5	5.93E-03	6.99E-03	8.35E-03	9.55E-03	1.04E-02	1.09E-02	1.12E-02	1.12E-02	1.12E-02
8.5	6.45E-03	7.60E-03	9.05E-03	1.03E-02	1.13E-02	1.18E-02	1.21E-02	1.21E-02	1.20E-02
9.5	6.96E-03	8.20E-03	9.74E-03	1.11E-02	1.21E-02	1.27E-02	1.29E-02	1.30E-02	1.29E-02
10.5	7.48E-03	8.80E-03	1.04E-02	1.18E-02	1.29E-02	1.35E-02	1.38E-02	1.38E-02	1.37E-02
11.5	8.01E-03	9.40E-03	1.11E-02	1.26E-02	1.36E-02	1.43E-02	1.46E-02	1.46E-02	1.45E-02
12.5	8.53E-03	9.99E-03	1.18E-02	1.33E-02	1.44E-02	1.51E-02	1.54E-02	1.54E-02	1.52E-02
13.5	9.06E-03	1.06E-02	1.24E-02	1.40E-02	1.52E-02	1.58E-02	1.61E-02	1.62E-02	1.60E-02
14.5	9.59E-03	1.12E-02	1.31E-02	1.47E-02	1.59E-02	1.66E-02	1.69E-02	1.69E-02	1.67E-02
15.5	1.01E-02	1.18E-02	1.38E-02	1.54E-02	1.66E-02	1.73E-02	1.77E-02	1.77E-02	1.75E-02
16.5	1.07E-02	1.24E-02	1.44E-02	1.61E-02	1.74E-02	1.81E-02	1.84E-02	1.84E-02	1.82E-02

Table 7.23. Equivalent Damping Using Equivalent Linearization

Hs, m	Mean zero-crossing period, s								
	1.5	2.5	3.5	4.5	5.5	6.5	7.5	8.5	9.5
0.5	2.09E-03	2.09E-03	2.14E-03	2.20E-03	2.24E-03	2.26E-03	2.27E-03	2.28E-03	2.30E-03
1.5	2.09E-03	2.09E-03	2.25E-03	2.44E-03	2.54E-03	2.60E-03	2.64E-03	2.68E-03	2.74E-03
2.5	2.09E-03	2.09E-03	2.35E-03	2.67E-03	2.84E-03	2.94E-03	3.01E-03	3.08E-03	3.17E-03
3.5	2.09E-03	2.10E-03	2.46E-03	2.91E-03	3.15E-03	3.29E-03	3.39E-03	3.49E-03	3.61E-03
4.5	2.09E-03	2.10E-03	2.57E-03	3.15E-03	3.46E-03	3.64E-03	3.77E-03	3.90E-03	4.06E-03
5.5	2.09E-03	2.10E-03	2.67E-03	3.39E-03	3.77E-03	3.99E-03	4.15E-03	4.31E-03	4.51E-03
6.5	2.09E-03	2.10E-03	2.78E-03	3.63E-03	4.09E-03	4.34E-03	4.54E-03	4.73E-03	4.96E-03
7.5	2.09E-03	2.11E-03	2.89E-03	3.87E-03	4.40E-03	4.70E-03	4.93E-03	5.15E-03	5.42E-03
8.5	2.09E-03	2.11E-03	3.00E-03	4.12E-03	4.72E-03	5.06E-03	5.32E-03	5.57E-03	5.88E-03
9.5	2.09E-03	2.11E-03	3.11E-03	4.36E-03	5.04E-03	5.42E-03	5.71E-03	5.99E-03	6.34E-03
10.5	2.09E-03	2.11E-03	3.21E-03	4.61E-03	5.36E-03	5.79E-03	6.11E-03	6.42E-03	6.81E-03
11.5	2.09E-03	2.12E-03	3.32E-03	4.86E-03	5.68E-03	6.15E-03	6.51E-03	6.85E-03	7.28E-03
12.5	2.09E-03	2.12E-03	3.43E-03	5.10E-03	6.01E-03	6.52E-03	6.91E-03	7.29E-03	7.75E-03
13.5	2.09E-03	2.12E-03	3.54E-03	5.35E-03	6.33E-03	6.89E-03	7.32E-03	7.73E-03	8.23E-03
14.5	2.09E-03	2.13E-03	3.65E-03	5.61E-03	6.66E-03	7.27E-03	7.73E-03	8.17E-03	8.71E-03
15.5	2.09E-03	2.13E-03	3.76E-03	5.86E-03	6.99E-03	7.65E-03	8.14E-03	8.62E-03	9.20E-03
16.5	2.09E-03	2.13E-03	3.87E-03	6.11E-03	7.32E-03	8.02E-03	8.55E-03	9.07E-03	9.69E-03

Table 7.23 Equivalent Damping Using Equivalent Linearization (Cont.)

Hs, m	Mean zero-crossing period, s								
	10.5	11.5	12.5	13.5	14.5	15.5	16.5	17.5	18.5
0.5	2.35E-03	2.48E-03	2.67E-03	2.86E-03	3.01E-03	3.10E-03	3.15E-03	3.17E-03	3.16E-03
1.5	2.86E-03	3.20E-03	3.67E-03	4.11E-03	4.44E-03	4.65E-03	4.76E-03	4.79E-03	4.77E-03
2.5	3.37E-03	3.88E-03	4.56E-03	5.18E-03	5.64E-03	5.93E-03	6.07E-03	6.12E-03	6.08E-03
3.5	3.88E-03	4.52E-03	5.38E-03	6.15E-03	6.72E-03	7.07E-03	7.25E-03	7.29E-03	7.25E-03
4.5	4.40E-03	5.16E-03	6.16E-03	7.06E-03	7.72E-03	8.13E-03	8.33E-03	8.38E-03	8.32E-03
5.5	4.91E-03	5.78E-03	6.92E-03	7.93E-03	8.67E-03	9.12E-03	9.35E-03	9.40E-03	9.33E-03
6.5	5.42E-03	6.40E-03	7.65E-03	8.77E-03	9.57E-03	1.01E-02	1.03E-02	1.04E-02	1.03E-02
7.5	5.94E-03	7.01E-03	8.37E-03	9.58E-03	1.04E-02	1.10E-02	1.12E-02	1.13E-02	1.12E-02
8.5	6.46E-03	7.62E-03	9.08E-03	1.04E-02	1.13E-02	1.19E-02	1.21E-02	1.22E-02	1.21E-02
9.5	6.98E-03	8.22E-03	9.78E-03	1.11E-02	1.21E-02	1.27E-02	1.30E-02	1.30E-02	1.29E-02
10.5	7.50E-03	8.83E-03	1.05E-02	1.19E-02	1.29E-02	1.36E-02	1.38E-02	1.39E-02	1.37E-02
11.5	8.03E-03	9.43E-03	1.12E-02	1.27E-02	1.37E-02	1.44E-02	1.47E-02	1.47E-02	1.45E-02
12.5	8.56E-03	1.00E-02	1.18E-02	1.34E-02	1.45E-02	1.52E-02	1.55E-02	1.55E-02	1.53E-02
13.5	9.10E-03	1.06E-02	1.25E-02	1.41E-02	1.53E-02	1.59E-02	1.63E-02	1.63E-02	1.61E-02
14.5	9.63E-03	1.12E-02	1.32E-02	1.48E-02	1.60E-02	1.67E-02	1.70E-02	1.70E-02	1.68E-02
15.5	1.02E-02	1.19E-02	1.38E-02	1.56E-02	1.68E-02	1.75E-02	1.78E-02	1.78E-02	1.76E-02
16.5	1.07E-02	1.25E-02	1.45E-02	1.63E-02	1.75E-02	1.82E-02	1.85E-02	1.85E-02	1.83E-02

8. SUMMARY AND CONCLUSIONS

The objectives of this project were to review current issues related to finalization of the second-generation intact-stability criteria, test vulnerability criteria for dead ship condition and excessive acceleration, develop specifications for direct stability assessment and a methodology for developing operational guidance based on direct stability-assessment information. The objectives also included refinement of explanatory notes for the second generation of intact stability criteria.

One of the central technical problem was an inconsistency between the levels of vulnerability criteria. This problem manifests itself when the level criterion did not indicated vulnerability, while the level-2 criterion did. At the same time, the level 1 criterion is supposed to be more conservative that the level 2 criterion. Another focus area is the direct stability assessment and operational guidance, based on the information from direct stability assessment.

What was done and what was learned:

- Inconsistency between the levels of the vulnerability criteria for pure loss of stability (sections 1.2 and 1.3 of Annex 3 SDC6/WP.6) takes place because of two reasons. First, the level 1 criterion is deterministic and level 2 criteria is probabilistic. To assure consistency, probability of encounter environmental conditions for the level 1 should be less than the standard for the level 2. The second reason is physical: the level 1 criterion is based on GM, while the level 2 criterion is based on GZ curve. The GM value does not describe stability in large angles. To assure consistency the criteria need to be reformulated in terms of dynamic heel angle, like the weather criterion. The dynamic angle is computed on the worst GZ curve during the wave pass for the level 1 criterion. For the level 2 criterion, the dynamic angle is computed for a single wave pass and the realistic timing of a GZ variation is introduced. As the worst stability condition of a certain way exist for a finite duration of time, the level 1 criterion is more conservative than level 2 criterion. The dynamic angle approach also helps with distinguishing vulnerability to pure loss of stability from vulnerability to parametric roll as the latter requires several wave passes for the stability failure to develop. New formulation can be used as alternative criteria during the trial period of the second generation intact stability criteria (Subsection 2.2).
- Inconsistency between the levels of vulnerability criteria for parametric roll (sections 2.2 and 2.3 of Annex 3 SDC6/WP.6) can also be caused by two reasons, first, when roll damping is overestimated by an empirical formula in level 1 criterion. The second reason is approximation of stability variation in wave with a sine or cosine function, while actual variation of GM is not described by a sine or cosine function. More application experience is needed to propose a practical solution for the problem (Subsection 2.3).
- The method of calculation of effective wave-slope function for level 2 vulnerability criteria for dead-ship condition (paragraph 4.3.2.4 of Annex 3 SDC6/WP.6) has been studied. It was found that standard methodology when a station is substituted with a rectangle (section 3.6.3 of Annex 4 of SDC 4/5/1/Add.3) may lead to substantial errors, especially for ships with fine forms. Direct pressure integration over actual stations does require same computational efforts as the standard method and does not have associated

approximation problems. It is recommended to use direct pressure integration (Subsection 3.2).

- The current formulation for the standard deviation of roll motion in level 2 vulnerability criteria for dead ship condition (paragraph 4.3.2.3 of Annex 3 SDC6/WP.6) combines calculations in absolute and relative coordinates. This formulation is inconsistent and may lead to substantial errors. It is recommended to use calculations in absolute coordinates only (Subsections 3.3 through 3.5).
- Inconsistency between the levels of vulnerability criteria for dead ship condition (sections 4.2 and 4.3 of Annex 3 SDC6/WP.6) is caused by two circumstances. The first one is that different mathematical models are used to describe stability failure. To study this inconsistency, an alternative criterion was formulated for level 2 that uses the same. The second one is that the level 1 criterion is deterministic and level 2 criteria is probabilistic. It was found that the inconsistency cannot be completely removed, even with the alternative formulation of the level 2 criterion. However, the inconsistency can be controlled by setting a standard with certain allowable probability of inconsistency. A judgement, how practical this approach is can be made during the trial period of the second generation intact stability criteria (Subsection 3.6 and 3.7).
- The vulnerability criteria for excessive accelerations were examined and sample calculation were carried out. A theoretical inconsistency appears in the formulation of the vulnerability criterion level 2, but it did not lead to any noticeable errors. Three options for roll damping linearization were tested, and the results found to be very similar. It is recommended to choose one option that can be common for vulnerability assessment of all failure modes (Section 4).
- The practical aspect of the organization of direct stability assessment are considered, and existing experiences are reviewed. The recommendation on a possible organization of the process is given, having in mind the expertise level needed to perform the calculations and the cost associated with validation of the simulation tools (Subsection 5.1).
- An example of direct stability-assessment for parametric-roll failure-mode is described. The Large Amplitude Motion Program (LAMP) was used as ship motion simulation tool. The example includes a description of qualitative and partial quantitative validation, as well as the verification of stability failure. Direct counting procedure is used to estimate the failure rate. It was found that the direct counting procedure, as described in paragraph 5.4.3 of Annex 1 SDC 6/WP.6, may need to use censoring to handle records without failure. The direct counting procedure, described in paragraph 5.4.4 of Annex 1 SDC 6/WP.6, was found to have a limited applicability, when no more than one failure occurs per record and not all records contain a failure. To avoid the necessity of censoring and limited applicability an alternative procedure is described that does not suffer from these problems and is recommended to use. To alleviate high cost of quantitative validation, it is recommended to collect data for existing comparison of simulation tools to experimental data (Subsection 5.2).
- An example for a direct stability assessment for pure loss of stability is described using fast volume-based ship-motion calculations. Extrapolation methods were used to

estimate rate of failure. Peak over threshold method was used to estimate rate of exceedance of large roll angle, while the split-time method helped estimate the rate of capsizing events. The example includes description of validation of both extrapolation procedures. To alleviate the high volume of computations needed for the direct stability assessment, consider methods of optimal planning (Subsection 5.3).

- Note that the probability of encounter of a larger roll angle due to parametric roll is about 3-4 orders of magnitude higher than due to pure loss of stability, for ships with known vulnerabilities for these failure mode. Also note how the probabilistic approach allows for the comparison of stability performance of different ships against different modes of failure.
- The methodology and an example of development of operational guidance from the information produced by direct stability assessment for parametric roll mode of failure is described. The result is presented in a form of plot in accordance with paragraph 6.3.3 of Annex 2 of SDC 6/WP.6. Having in mind the high cost of direct stability assessment, a methodology is described on how to build a polar plot using an output of the level 2 vulnerability assessment. Such a polar plot can be used as a form of operational limitation, complementing those described in section 6.1 and 6.2 of Annex 2 of SDC 6/WP.6 (Subsection 6.2 and 6.3).
- To facilitate finalization of explanatory notes for the second generation intact stability criteria, verification of the formulae for the simplified Ikeda method from Annex 19 of SDC 5/INF 4 has been carried out and some minor editing has been done. Also a data set of sample vulnerability assessment has been developed; it includes input, output, and some intermediate data for easy reference (Section 7).

9. REFERENCES

ABS, 2019 “Guide for the Assessment of Parametric Roll Resonance in the Design of Container Carriers”, Houston, TX, 70 p

ABS, 2008 "ABS Awards First Containership Parametric Roll Notation", *Activities*, ABS, May. 2008, pp. 10-11.

Andrew, W. 2012. Report of the Commission of Inquiry into the sinking of Rabaul Queen 28 June 2012, www.mvrabaulqueen.com or www.coi.gov.pg/rabaulqueen.html

Anastopoulos, P.A., Spyrou, K.J., Bassler, C.C. and V. Belenky. 2015. “Towards an Improved Critical Wave Groups Method for the Probabilistic Assessment of Large Ship Motions in Irregular Sea,” *Probabilistic Engineering Mechanics* Vol. 44, 2015, pp 18-27

Beck, R. F. and A. M. Reed (2001). “Modern Computational Methods for Ships in a Seaway”. *SNAME Trans.* Vol. 109, pp. 1–51.

Beirlant, J., Y. Goegebeur, J. Teugels, and J. Segers (2004). *Statistics of Extremes*, Wiley Series in Probability and Statistics. John Wiley & Sons, Ltd., Chichester.

Belenky, V.L. (1995) “Analysis of probabilistic balance of IMO stability regulation by piece-wise linear method”, *Marine Technology Trans.*, Polish Academy of Sciences, Branch in Gdansk, Vol. 6, pp. 5-55.

Belenky, V.L. and N.B. Sevastianov (2007) *Stability and Safety of Ships: Risk of Capsizing.* Second edition SNAME, Jersey City, ISBN 0-939773-61-9.

Belenky, V. and K.M. Weems (2008) “Probabilistic Qualities of Stability Change in Waves”, *Proc. 10th International Ship Stability Workshop*, Daejon, Korea, pp. 95-108

Belenky, V. L., Weems, K. M., and Lin, W.-M., (2008), “Numerical Procedure for Evaluation of Capsizing Probability with Split Time Method”, *Proc. 27th Symposium Naval Hydrodynamics*, Seoul, Korea

Belenky, V.L., Weems, K.M., Lin. W.M. and Spyrou, K.J. 2010. “Numerical Evaluation of Capsizing Probability in Quartering Seas with Split Time Method” *Proc. 28th Symposium Naval Hydrodynamics,* Pasadena, California, pp.

Belenky, V.L. (2011) “On Self-Repeating Effect in Reconstruction of Irregular Waves”, Chapter 33 of “*Contemporary Ideas on Ship Stability*”, Neves, M.A.S., Belenky, V., de Kat, J.O., Spyrou, K. and N. Umeda, eds., Springer, ISBN 978-94-007-1481-6, pp. 589-598

Belenky, V., and B. Campbell (2011). *Evaluation of the Exceedance Rate of a Stationary Stochastic Process by Statistical Extrapolation Using the Envelope Peaks over Threshold (EPOT) Method*. Naval Surface Warfare Center Carderock Division Report NSWCCD-50-TR-2011/032, 216 p. (Approved for public release, distribution unlimited).

Belenky, V., Bassler, C.C. and K.J. Spyrou (2011) *Development of Second Generation Intact Stability Criteria*, Naval Surface Warfare Center Carderock Division Report NSWCCD-50-TR-2011/065, 174 p. (Approved for public release, distribution unlimited)

Belenky, V. and K.M. Weems (2012) "Probabilistic Properties of Parametric Roll", Chapter 6 of *Parametric Resonance in Dynamical Systems*, Fossen, T. I. and H. Nijmeijer, eds., Springer, ISBN 978-1-4614-10423-0, pp.129-146

Belenky, V., Spyrou, J., Weems, K.M. and W.-M. Lin (2013) "Split-time Method for the Probabilistic Characterization of Stability Failures in Quartering Waves", *International Shipbuilding Progress,* Vol. 60, No. 1-4, pp. 579-612

Belenky, V.L., Spyrou, K.J. Weems, K.M., (2016) "On Probabilistic Properties of Surf-Riding and Broaching-to in Irregular Waves" *Proc. 31st Symposium Naval Hydrodynamics,* Monterey, California, USA, pp.

Belenky, V., Weems, K. and W.M. Lin. 2016a. "Split-time Method for Estimation of Probability of Capsizing Caused by Pure Loss of Stability" in *Ocean Engineering*, Vol. 122, pp. 333-343.

Belenky, V., D. Glotzer, V. Pipiras, and T. Sapsis. 2016b. "On the Tail of Nonlinear Roll Motions". *Proc.* 15th Intl. Ship Stability Workshop, Stockholm (ISSW2016), Sweden, pp. 109-114.

Belenky, V., Weems, K., Pipiras, V., Glotzer, D., and T. Sapsis (2018) "Tail Structure of Roll and Metric of Capsizing in Irregular Waves" *Proc. 32nd Symposium Naval Hydrodynamics,* Hamburg, Germany

Belenky, V., Weems, K., Pipiras, V., and D. Glotzer. 2018a. "Extreme-Value Properties of the Split-Time Metric", *Proc. 13th International Conference on Stability of Ships and Ocean Vehicles STAB 2018*, Kobe, Japan

Belenky, V., Spyrou, K., and K. M. Weems. 2019. "Modeling of Surf-Riding in Irregular Waves", Chapter B2.2 of *Contemporary Ideas on Ship Stability. Risk of Capsizing*, Belenky, V., Spyrou, K., van Walree F., Neves, M.A.S., and N. Umeda, eds., Springer, ISBN 978-3-030-00514-6

Belenky, V., D. Glotzer, V. Pipiras, and T. Sapsis. 2019a. "Distribution tail structure and extreme value analysis of constrained piecewise linear oscillators". *Probabilistic Engineering Mechanics*. Vol. 57, pp 1-13.

Belenky, V., Weems, K. M., Pipiras, V., Sapsis, T. (2019b) "Metric of Ship Capsizing of Random Seas", *Proc. 8th International Conference Computational Stochastic Mechanics (CSM 8)*, Deodatis, G. and P. D. Spanos, eds., Paros, Greece, (to appear)

Belenky, V., Spyrou, K., van Walree F., Neves, M.A.S., and N. Umeda, Ed. 2019c. *Contemporary Ideas on Ship Stability. Risk of Capsizing*, Springer, Series Fluid Mechanics and Its Application Vol. 119 ISBN 978-3-030-00514-6.

Bishop, R. C., W. Belknap, C. Turner, B. Simon, and J. H. Kim (2005). "Parametric Investigation on the Influence of GM, Roll damping, and Above-Water Form on the Roll Response of Model 5613", Report NSWCCD-50-TR-2005/027.

Boonstra, H., de Jongh, M.P., & L. Palazzi (2004) "Safety Assessment of Small Container Feeders", Proc. of PRADS 2004, Lübeck-Travemünde, Germany.

BSU, 2009 Fatal Accident on Board the CMV CHICAGO EXPRESS during Typhoon "HAGUPIT" on 24 September 2008 of the coast of Hong Kong Investigation Report 510/08, 1 November 2009.

BSU, 2011. Fatal Accident on Board the CMV CCNI GUAYAS during Typhoon "KOPPU" on 15 September 2009 in the sea area off Hong Kong. Investigation Report 391/09. 1 June 2011

Campbell, B. and Belenky, V., 2010, "Assessment of Short-Term Risk with Monte-Carlo Method", *Proc. 11th Intl. Ship Stability Workshop*, Wageningen, Netherlands, pp. 85-92.

Campbell, B., Belenky, V., and V. Pipiras. 2016. "Application of the Envelope Peaks over Threshold (EPOT) Method for Probabilistic Assessment of Dynamic Stability, in *Ocean Engineering,* Vol. 120, pp. 298-304.

Coles, S. 2001. *An Introduction to Statistical Modeling of Extreme Values*. Springer, London.

Danish Maritime Accident Investigation Board. 2014. Marine Accident Report Svendborg Maersk Heavy Weather Damage on 14 February 2014

De Kat, J. O. and J. R. Paulling. 1989. "The Simulation of Ship Motions and Capsizing in Severe Seas". In: *Transactions of SNAME*. Vol. 97. Jersey City, NJ: Society of Naval Architects and Marine Engineers, pp. 139–168.

de Kat, J.O., Pinkster, D.J. & K. McTaggart (2002) Random waves and capsize probability based on large amplitude motion analysis, Proc. 21st International Conference on Offshore Mechanics and Arctic Engineering OMAE 2002, J.V. Wehausen Symposium on Water Waves, Oslo, Norway.

Degtyarev, A.B., Reed, A.M., and I. Gankevich. 2019. "Modeling of Incident Waves near the Ship's Hull (Application of Autoregressive Approach in Problems of Simulation of Rough Seas)" Chapter 2 of *Contemporary Ideas on Ship Stability. Risk of Capsizing*, Belenky, V., Spyrou, K., van Walree F., Neves, M.A.S., and N. Umeda, eds., Springer, ISBN 978-3-030-00514-6, pp. 25-35.

Degtyarev, A.B. and I. Gankevich. 2019. "Evaluation of Hydrodynamic Pressures for Autoregressive Model of Irregular Waves" Chapter 3 of *Contemporary Ideas on Ship Stability. Risk of Capsizing*, Belenky, V., Spyrou, K., van Walree F., Neves, M.A.S., and N. Umeda, eds., Springer, ISBN 978-3-030-00514-6, pp. 37-47.

Dudziak, J., Buczkowski, A. 1978. "Probability of ship capsizing under the action of the beam wind and sea as a background of stability criteria", Polish Register of Ships, Prace Studialno-Roswojowe, and Zeszyt No. 13, Gdansk.

Dupuis, D. J., and M.-P. Victoria-Feser (2006). "A robust prediction error criterion for Pareto modelling of upper tails," *Canadian Journal of Statistics*, Vol. 34, 2006, pp. 639–658.

IACS Recommendation No. 34 Standard Wave Data, November 2001

IMO International Code on Intact Stability, 2008, IMO, London, 2009.

IMO MSC.1/Circ.1200 Interim Guidelines for Alternative Assessment of the Weather Criterion, London, 2006.

IMO MSC.1/Circ. 1228 Revised Guidance for Avoiding Dangerous Situations in Adverse Weather and Sea Conditions, London, 2007.

IMO MSC.267(85) Adoption of the International Code on Intact Stability, 2008 (2008 IS Code), London, 2008.

IMO SDC 1/5/4 Proposal of working version of explanatory notes on the vulnerability of ships to the broaching stability failure mode. Submitted by Japan, London, November, 2013

IMO SDC 1/INF.6. Vulnerability assessment for dead-ship stability failure mode. Submitted by Italy and Japan London, November, 2013.

IMO SDC 1/INF.8. Development of Second Generation Intact Stability Criteria. Information collected by the intersessional correspondence group. Submitted by Japan London, November, 2013.

IMO SDC 2/INF.10. Development of Second Generation Intact Stability Criteria. Information collected by the intersessional correspondence group. Submitted by Japan London, November, 2014.

IMO SDC 2/WP.4. Development of the Second generation Intact Stability Criteria. Report of the Working Group (part 1). London, February, 2015.

IMO SDC 3/6/2 Further validation of some draft second generation intact stability criteria. . Submitted by Germany, London, October, 2015.

IMO SDC 3/6/4 Comments on pure loss of stability failure mode for a vessel with extended low weather deck. Submitted by Japan, London, November, 2015.

IMO SDC 3/6/8 Comments on the outcome of SDC 2 on the proposed amendments to 2008 IS Code on second-generation intact stability criteria. Submitted by Norway, London, November, 2015.

IMO SDC 3/6/9 Comments on vulnerability criteria for pure loss of stability and parametric roll failure modes. Submitted by Japan, London, November, 2015.

IMO SDC 3/INF.10Finalization of Second Generation Intact Stability Criteria. Information collected by the intersessional correspondence group. Submitted by Japan, London, November, 2015.

IMO SDC 3/INF.12. Probabilistic direct stability assessment and operational guidance, Submitted by Germany, London, November, 2015

IMO SDC 3/INF.15. Material relevant to operational guidance and operational limitations, Submitted by Germany, Italy and Sweden, London, November, 2015

IMO SDC 3/WP.5 Finalization of the Second generation Intact Stability Criteria. Report of the Working Group (part 1). London, January, 2016.

IMO SDC 4/5/1 Finalization of the Second generation Intact Stability Criteria. Report of correspondence group (part 1 through 7). Submitted by Japan, London, November 2016.

IMO SDC 4/5/6 Draft consolidated explanatory notes for the second generation intact stability criteria London, November 2016.

IMO SDC 4/5/12 Comments on document SDC 4/5/1. Submitted by Germany. London December, 2016.

IMO SDC 4/INF.4. Finalization of Second Generation Intact Stability Criteria. Information collected by the intersessional correspondence group on Intact Stability (parts 1 through 3). Submitted by Japan, London, December, 2016

IMO SDC 4/INF.7. Sample ship calculations outcome. Submitted by United States, London, December, 2016

IMO SDC 4/INF.8, Direct stability assessment – information for further discussion. Submitted by Germany,. London, December, 2016.

IMO SDC 4/INF.9. Sample ship calculations results. Submitted by Denmark, London, December, 2016

IMO SDC 4/INF.10 Additional sample calculation results obtained by using the modified effective wave slope coefficient estimation procedure, Submitted by Japan, London, December, 2016

IMO SDC 4/WP.4 Finalization of the Second generation Intact Stability Criteria. Report of the Working Group (part 1). London, February, 2017.

IMO SDC 5/6/5 Proposal on improving consistency of pure loss of stability vulnerability criteria. Submitted by China. London, November, 2017

IMO SDC 5/6/14 Comments on document SDC 5/6. Submitted by Finland and Sweden. London, November, 2017.

IMO SDC 5/INF.4 Finalization of Second Generation Intact Stability Criteria. Information collected by the intersessional correspondence group on Intact Stability. Submitted by Japan, London, November, 2017.

IMO SDC 5/INF.7 Application examples of direct stability assessment for pure loss of stability, parametric rolling and dead ship condition failure modes. Submitted by Japan, London, December, 2017.

IMO SDC 5/INF.8 Sample calculations and validations of the direct stability assessment of parametric roll. Submitted by China, London, November, 2017.

IMO SDC 5/INF.12 Sample ship calculation results. Submitted by Brazil London, November, 2017.

IMO SDC 5/WP.1 Report to maritime safety committee, London, January, 2018.

IMO SDC 6/5 Finalization of the Second generation Intact Stability Criteria. Report of the Correspondence Group parts 1 and 2. Submitted by Japan. London, November, 2018.

IMO SDC 6/5/6 Proposal for finalization of second generation intact stability criteria. Submitted by Japan. London, November 2018.

IMO SDC 6/INF.4 Finalization of Second Generation Intact Stability Criteria. Information collected by the intersessional correspondence group on Intact Stability. Submitted by Japan, London, November, 2018.

IMO SDC 6/WP.6 Finalization of the Second generation Intact Stability Criteria. Report of the Experts' Group on Intact Stability. London, February, 2019.

IMO SLF 50/4/4, Framework for the Development of New Generation Criteria for Intact tability, submitted by Japan, the Netherlands and the United States, London, 2007.

IMO SLF 53/3/6 Comments on the report of the working group at SLF 52 (part 2). Submitted by Poland, Nove,ber 2010

IMO SLF 53/WP.4 Development of the Second generation Intact Stability Criteria. Report of the Working Group (part 1). London, January, 2011.

IMO SLF 54/3/1 Development of Second Generation Intact Stability Criteria. Report of the Working Group at SLF 53 (part 2), Submitted by the Chairman of the Working Group, London, August 2011.

IMO SLF 54/3/3 Summary of research into Stability failure modes and associated criteria development. Submitted by the United States, London, 2011.

IMO SLF 54/3/6 Evaluation of Ikeda's simplified method for prediction of roll damping. Submitted by Sweden, Londin, November 2011

IMO SLF 54/INF.4 Research into Stability failure modes and associated criteria development. Submitted by the United States, London, November, 2011

IMO SLF 54/INF.12. Development of Second Generation Intact Stability Criteria. Information collected by the intersessional correspondence group. Submitted by Japan London, November, 2011

IMO SLF 54/WP.3 Development of the Second generation Intact Stability Criteria. Report of the Working Group (part 1). London, January, 2012.

IMO SLF 54/INF.14. Verification of the draft Levels 1 and 2 vulnerability criteria for parametric rolling and pure loss of stability. Submitted by IACS. London, December 2012.

IMO SLF 55/INF.15. Development of Second Generation Intact Stability Criteria. Information collected by the intersessional correspondence group. Submitted by Japan London, December, 2012.

IMO SLF 55/WP.3 Development of the Second generation Intact Stability Criteria. Report of the Working Group (part 1). London, Febuary , 2013.

IMO SLF 55/3/1 Development of Second Generation Intact Stability Criteria. Report of the Correspondnece Group Ppart 1: Second Generation Intact Stability Criteria), Submitted by Japan, London, December 2012.

IMO SLF 55/3/15 Comments and proposal for further steps with regard to second generation intact stability criteria. Submitted byPoland, London, January 2013.

IMO Resolution A.167(ES.IV) Recommendation on intact stability for passenger and cargo ships under 100 meters in length. Lonon, November 1968.

IMO Resolution A.749(18) Code on intact stability for all ships covered by IMO instruments. London, November 1993.

ITTC 7.5-02-07-04.5 Numerical Estimation of Roll Damping. ITTC – Recommended Procedures, International Towing Tank Conference, Revision 00, 2011.

ITTC 7.5-02-07-04.3 Predicting the Occurance and Magnitude of Parametric Rolling Recommended Procedures, International Towing Tank Conference, Revision 02, 2017.

France, W. M, M. Levadou, T. W. Treakle, J. R. Paulling, K. Michel & C. Moore. 2003. An Investigation of Head-Sea Parametric Rolling and its Influence on Container Lashing Systems. *Marine Tech.*¸ 40(1):1–19.

Hashimoto, H., N. Umeda & A. Matsuda. 2011. "Broaching prediction of a wave-piercing tumblehome vessel with twin screws and twin rudders". *J. Marine Sci. & Tech.* Vol. 16, Issue 4, pp 448-451.

Hayter, A. J. (2012) *Probability and Statistics for Engineers and Scientists*, 4th Edition. Brooks/Cole Cengage learning, Boston, ISBN-13: 978-1111827045

Holtrop, J. and Mennen, G.G.J. 1984. "A Statistical Re-Analysis of Resistance and Propulsion Data", Int. Shipbuilding Progress, Vol 31, No 363, pp. 272-276

Maritime New Zealand. 2007. Incident Report Heavy Weather/Cargo Shift Aratere 3 March 2006. Maritime New Zealand Investigation Report 06-201, vi+57 p.

Newman, J. N. 1977. "Marine hydrodynamics", Massachusetts Institute of Technology Press. Cambridge.

Kawahara, Y., Maekawa, K., Ikeda, Y. 2012. "A Simple Prediction Formula of Roll Damping of Conventional Cargo Ships on the Basis of Ikeda's Method and Its Limitation" *Journal of Shipping and Ocean Engineering*, Vol. 2, pp. 201-210.

Kim, D.H., Belenky, V., Campbell, B. L., and A. W. Troesch. 2014. "Statistical Estimation of Extreme Roll in Head Seas" *Proc. of 33rd Intlernational Conference on Ocean, Offshore and Arctic Engineering OMAE 2014*, San-Francisco, USA,

Kobylinski, L. K. and Kastner S. 2003. "Stability and Safety of Ships. Volume 1: Regulation and Operation", Elsevier Ocean Engineering Book Series, Vol. 9. Elsevier, Amsterdam.

Kontolefas, I. and K. Spyrou. 2018. Predict, ing the Probability of Ship High-Runs form Phase Space Data, *Proc. 32nd Symposium Naval Hydrodynamics,* Hamburg, Germany.

Leadbetter, M.R., Rychlik, I. and K. Stambaugh. 2011. "Estimating Dynamic Stability Event Probabilities from Simulation and Wave Modeling Methods" *Proc. 12th Intl. Ship Stability Workshop*. Washington, D.C., USA. pp. 147-153.

Leadbetter, M.R., Rychlik, I. and K. Stambaugh. 2019. "Estimating Dynamic Stability Event Probabilities from Simulation and Wave Modeling Methods" Chapter 22 of *Contemporary Ideas on Ship Stability. Risk of Capsizing*, Belenky, V., Spyrou, K., van Walree F., Neves, M.A.S., and N. Umeda, *eds*., Springer, ISBN 978-3-030-00514-6, pp. 381-391.

Lin, W. M. and D. K. P. Yue. 1990. Numerical Solutions for Large Amplitude Ship Motions in the Time-Domain. *Proc. 18th Symposium of Naval Hydro*., Ann Arbor, MI, pp. 41–66.

Mager, J. 2015. "Automatic threshold selection of the peaks over threshold method", Master's Thesis, Technische Universitat Munchen.

Meeker, W. O. & L. A. Escobar. 1998. Statistical Methods for Reliability Data. Wiley, New York, p. 680.

Newman, J. N. 1977. Marine Hydrodynamics, MIT Press. Boston, MA.

Oosterveld, M. W. C. and P. van Oossanen. 1975. "Further Computer-Analyzed Data of the Wageningen B-Screw Series," *Intl. Shipbuilding Progress*, pp. 251-262.

Paulling, J. R. 1961. "The Transverse Stability of a Ship in a Longitudinal Seaway." *J. Ship Research*, 4(4):37–49.

Paulling, J. R., O. H. Oakley & P. D. Wood. 1975. “Ship Capsizing in Heavy Seas: The Correlation of Theory and Experiments.” *Proc. 1st International. Conference on Stability of Ships and Ocean Vehicles*, Glasgow.

Perrault, D. 2015. “Exploration of the Probabilities of Extreme Roll of Naval Vessels”, *Proc. 12th International. Conference on Stability of Ships and Ocean Vehicles STAB 2015*, Glasgow, UK, pp. 855-868.

Peters, W., Belenky, V., Bassler C., Spyrou, K., Umeda, N., Bulian, G., and B. Altmayer. 2011. “The Second Generation of Intact Stability Criteria An Overview of Development”, *SNAME Trans.* 119**.** pp. 225-264.

Peters, W.S., Belenky, V., and A.M. Reed. 2019. “On Regulatory Framework of Direct Stability Assessment” Chapter 40 of *Contemporary Ideas on Ship Stability. Risk of Capsizing*, Belenky, V., Spyrou, K., van Walree F., Neves, M.A.S., and N. Umeda, eds., Springer, ISBN 978-3-030-00514-6, pp. 689-706.

Pickands, J. 1975. “Statistical Inference Using Extreme Order Statistics,” The Annals of Statistics, Vol. 3, No. 1, pp. 119-131.

Pollard, J. & A. Dudebout. 1892. Theorie du Navire, Tome III. Dynamique du Navire: Mouvement de Roulis sur Houle, Mouvement Rectiligne Horizontal Direct (Résistance des Carènes) Paris: Gauthier-Villars et Fils.

Rahola, Y. 1939. The Judging of the Stability of Ships and the Determination of the Minimum Amount of Stability, Ph.D. Thesis, Helsinki.

Reed, A.M. 2011. “26th ITTC Parametric Roll Benchmark Study”, *Proc. 12th Intl. Ship Stability Workshop*, Washington D.C., USA, pp. 195-204.

Reed, A.M., Belknap, W.F., Smith, T.C., and B. L. Campbell. 2019. "Model Characteristics and Validation Approach for a Simulation Tool Supporting Direct Stability Assessment" Chapter 33 of *Contemporary Ideas on Ship Stability. Risk of Capsizing*, Belenky, V., Spyrou, K., van Walree F., Neves, M.A.S., and N. Umeda, eds., Springer, ISBN 978-3-030-00514-6, pp. 557-572.

Reed, A.M. 2019 “26th ITTC Parametric Roll Benchmark Study” Chapter 37 of *Contemporary Ideas on Ship Stability. Risk of Capsizing*, Belenky, V., Spyrou, K., van Walree F., Neves, M.A.S., and N. Umeda, *eds*., Springer, ISBN 978-3-030-00514-6, pp. 619-636.

Reed, A.M., Beck, R.F. 2016 “Advances in the Predictive Capability for Ship Dynamics in Extreme Waves”, *SNAME Trans,* Vol. 124, pp.

Reed, A.M., Zuzick, A.V. 2015 "Direct Assessment Will Require Accreditation – What This Mean", *Proc. 12th Intl. Conf. on Stability of Ships and Ocean Vehicles STAB 2015*, Glasgow, UK.

Sevastianov, N. B. 1963 “On probabilistic approach to stability standards” *Transactions of Kaliningrad Institute of Technology*, Vol. 18, Kaliningrad, pp. 3-12 (in Russian).

Sevastianov, N. B. 1978. “On possibility of practical implementation of probabilistic stability regulations”, *Sudostroenie* No 1, Leningrad, pp.13-17, (in Russian).

Sevastianov, N. B. 1982. "Probabilistic stability regulation as a problem of reliability theory", *Transactions of Russian Register Shipping*, Vol. 12, Leningrad, pp. 94-100, (in Russian).

Sevastianov, N. B. 1994. "An algorithm of probabilistic stability assessment and standards" *Proc. of STAB'94: 5th International Conference on Stability of Ships and Ocean Vehicles*, Vol. 5, Melbourne, Florida.

Shigunov, V., Themelis, N., and K. Spyrou. 2012. "Critical wave groups vs. Direct Monte-Carlo simulations for typical stability failure modes of a container ship" *Proc. 11th International Conference on the Stability of Ships and Ocean Vehicle STAB2012,* Athens, Greece.

Shin, Y.S, Belenky, V.L., Lin, W.M., Weems, K.M., and A. H. Engle. 2003. "Nonlinear time domain simulation technology for seakeeping and wave-load analysis for modern ship design" *SNAME Trans*. Vol. 111, pp. 557-578.

Shin, Y.S, Belenky, V.L., Paulling, J.R., Weems, K.M., and W.M. Lin. 2004. "Criteria for Parametric Roll of Large Containerships in Longitudinal Seas", *SNAME Trans.* Vol. 112, pp. 14-47.

Smith, T.C. 2012. "Approaches to Ship Motion Simulation Acceptance Criteria*" Proc. of 11th Intl Conference of the Stability of Ships and Ocean* Vehicles, Athens, Greece. pp. 101-114.

Smith, T., Zuzick, A.V. 2015. "Validation of Statistical Extrapolation Methods for Large Motion Prediction" *Proc. 12th Intl. Conf. on Stability of Ships and Ocean Vehicles STAB 2015*, Glasgow, UK.

Smith, T.C. 2019. "Validation Approach for Statistical Extrapolation"*,* Chapter 34 of *Contemporary Ideas on Ship Stability*, Belenky, V., Neves, M., Spyrou, K., Umeda, N., van Walree, F., eds., Springer, ISBN 978-3-030-00514-6, pp. 573-589.

Söding, H. 1982. Leckstabilität im Seegang. Report No. 429, Institut für Schiffbau, Hamburg, Germany. p. 69.

Spanos, P. D. 1983. ARMA Algorithms for Ocean Wave Modeling*. Journal Energy Resources Technology,* Trans. ASME, Vol. 105 pp. 300–309.

Spyrou, K.J., Belenky, V., Reed, A., Weems, K., Themelis, N. & I. Kontolefas. 2014. "Split-Time Method for Pure Loss of Stability and Broaching-To" *Proc. 30th Symp. Naval Hydrodynamics,* Hobart, Tasmania, Australia.

Spyrou, K.J., Tigkas, I., Scanferla, G., Pallikaropoullos, N., and N. Themelis. 2008. "Prediction potential of the parametric rolling behaviour of a post-panamax containership", *Ocean Engineering*, Vol. 35, 1235-1244.

Stephens, M. A. 1974. "Pdf statistics for goodness of *t* and some comparisons", Journal of the American Statistical Association", *Journal of the American Statistical Association,* Vol. 69, No. 347, pp. 730-737.

Swedish Accident Investigation. 2008. Loss of m/s Finnbirch between Oland and Gotland 1 November 2006, Report RS 2008:03e, Case S-130/06

ter Bekke, E. C. A., Willeboordse, E.J., van Dallen, E.F.G., Boonstra, H., Keizer, E.W.H., & B. Ale. 2006. "Integrated safety assessment of small container ship", *Proc of 8th International.*

Conference on Probabilistic *Safety Assessment and Management*, ASME, New Orleans, Louisiana, USA.

Thompson, J.M.T. and Stewart, H.B. 1986. Nonlinear Dynamics and Chaos, John Wiley, Chichester.

Umeda, N., Usada, S., Mizumoto, K., Matsuda, A. 2016. "Broaching probability for a ship in irregular stern-quartering waves: theoretical prediction and experimental validation", *Journal of Marine Science and Technology* Vol. 21, pp 23–37.

van Daalen, E. F. G., Boonstra, H., & J. J. Blok. 2005. "Capsize probability analysis for a small container vessel" *Proc. of 6th International Ship Stability Workshop*, Istanbul, Turkey.

van Walree, F. and P. de Jong. 2019. "Deterministic Validation of a Time Domain Panel Code for Parametric Roll" Chapter 36 of *Contemporary Ideas on Ship Stability. Risk of Capsizing*, Belenky, V., Neves, M., Spyrou, K., Umeda, N., van Walree, F., eds., Springer, ISBN 978-3-030-00514-6, pp. 605-617

Weems, K., Reed, A.M., Degtyarev, A.B., Gankevich, I. 2016. "Implementation of an Autoregressive Wave Model in a Numerical Simulation Code," *Proc. 31st Symp. on Naval Hydrodynamics*, Monterey, California, USA.

Weems, K., V. . Belenky, and K. Spyrou. 2018. "Numerical Simulations for Validating Models of Extreme Ship Motions in Irregular Waves" *Proc. 32nd Symposium of Naval Hydrodynamics,* Hamburg, Germany.

Ypma, E., Harmsen, E., 2012. Development of a new methodology to predict the capsize risk of ships, *11th International Conference on the Stability of Ships and Ocean Vehicle STAB2012,* Athens, Greece.

THIS PAGE INTENTIONALLY LEFT BLANK

Distribution

	#	#
Naval Surface Warfare Center Carderock Division 9500 MacArthur Blvd West Bethesda, MD 20817		
Defense Technical Information Center 8725 John J. Kingman Road Ft. Belvoir, VA 22060-6218		1

NSWC, CARDEROCK DIVISION
INTERNAL DISTRIBUTION

Code	Name		
809	D. Intolubbe	1	1
83	Technical Data Library	1	1
1033	TIC - SCRIBE		1


NAVSEA
WARFARE CENTERS
Carderock